National Library
of Canada

Acquisitions and
Bibliographic Services Branch

395 Wellington Street
Ottawa, Ontario
K1A 0N4

Bibliothèque nationale
du Canada

Direction des acquisitions et
des services bibliographiques

395, rue Wellington
Ottawa (Ontario)
K1A 0N4

Your file Votre référence

Our file Notre référence

NOTICE

The quality of this microform is heavily dependent upon the quality of the original thesis submitted for microfilming. Every effort has been made to ensure the highest quality of reproduction possible.

If pages are missing, contact the university which granted the degree.

Some pages may have indistinct print especially if the original pages were typed with a poor typewriter ribbon or if the university sent us an inferior photocopy.

Reproduction in full or in part of this microform is governed by the Canadian Copyright Act, R.S.C. 1970, c. C-30, and subsequent amendments.

AVIS

La qualité de cette microforme dépend grandement de la qualité de la thèse soumise au microfilmage. Nous avons tout fait pour assurer une qualité supérieure de reproduction.

S'il manque des pages, veuillez communiquer avec l'université qui a conféré le grade.

La qualité d'impression de certaines pages peut laisser à désirer, surtout si les pages originales ont été dactylographiées à l'aide d'un ruban usé ou si l'université nous a fait parvenir une photocopie de qualité inférieure.

La reproduction, même partielle, de cette microforme est soumise à la Loi canadienne sur le droit d'auteur, SRC 1970, c. C-30, et ses amendements subséquents.

Canada

UNIVERSITY OF ALBERTA

Studies on the Origin of Indirect UV Detection in Liquid Chromatography

BY

Laura Luisa Maria Glavina ©

A thesis submitted to the Faculty of Graduate Studies and Research in partial fulfillment of the requirements for the degree of **Doctor of Philosophy**.

DEPARTMENT OF CHEMISTRY

EDMONTON, ALBERTA
FALL 1993

National Library
of Canada

Acquisitions and
Bibliographic Services Branch

395 Wellington Street
Ottawa, Ontario
K1A 0N4

Bibliothèque nationale
du Canada

Direction des acquisitions et
des services bibliographiques

395, rue Wellington
Ottawa (Ontario)
K1A 0N4

Your file Votre référence

Our file Notre référence

The author has granted an irrevocable non-exclusive licence allowing the National Library of Canada to reproduce, loan, distribute or sell copies of his/her thesis by any means and in any form or format, making this thesis available to interested persons.

L'auteur a accordé une licence irrévocable et non exclusive permettant à la Bibliothèque nationale du Canada de reproduire, prêter, distribuer ou vendre des copies de sa thèse de quelque manière et sous quelque forme que ce soit pour mettre des exemplaires de cette thèse à la disposition des personnes intéressées.

The author retains ownership of the copyright in his/her thesis. Neither the thesis nor substantial extracts from it may be printed or otherwise reproduced without his/her permission.

L'auteur conserve la propriété du droit d'auteur qui protège sa thèse. Ni la thèse ni des extraits substantiels de celle-ci ne doivent être imprimés ou autrement reproduits sans son autorisation.

ISBN 0-315-88233-6

Canada

UNIVERSITY OF ALBERTA

RELEASE FORM

NAME OF AUTHOR: **Laura L. M. Glavina**

TITLE OF THESIS: **Studies on the Origin of Indirect UV Detection in Liquid Chromatography**

DEGREE: **Doctor of Philosophy**

YEAR THIS DEGREE GRANTED: **1993**

Permission is hereby granted to the University of Alberta Library to reproduce single copies of this thesis and to lend or sell such copies for private, scholarly or scientific research purposes only.

The author reserves all other publication and other rights in association with the copyright in the thesis, and except as hereinbefore provided neither the thesis nor any substantial portion thereof may be printed or otherwise reproduced in any material form whatever without the author's written permission.

AUTHOR'S SIGNATURE: Laura Glavina

PERMANENT ADDRESS: **2207 15 Avenue South**
Lethbridge, Alberta
T1K 0X5

DATE: September 21, 1993

UNIVERSITY OF ALBERTA

FACULTY OF GRADUATE STUDIES AND RESEARCH

The undersigned certify that they have read, and recommend to the Faculty of Graduate Studies and Research for acceptance, a thesis entitled **Studies on the Origin of Indirect UV Detection in Liquid Chromatography** submitted by **Laura L. M. Glavina** in partial fulfillment of the requirements for the degree of **Doctor of Philosophy**.

Frederick F. Cantwell

Dr. F. F. Cantwell, Supervisor

Dr. N. J. Dovichi

Dr. L. Li

John E. Bertie

Dr. J. E. Bertie

Peter Sporns

Dr. P. Sporns

Dr. S. G. Weber, External Reader
University of Pittsburgh

DATE: September 20, 1993

This thesis is dedicated to my loving parents.

Thank you for the opportunity, for the support and for instilling in me
the qualities that made this all possible.

ABSTRACT

In indirect UV detection, non-UV absorbing sample species are injected onto a column which has come to equilibrium with a mobile phase containing a UV absorbing compound (probe). The change in sorption of the probe in the injected sample zone is responsible for the indirect detection phenomenon.

The main studies in this thesis were concerned with determining how a particular sample type affects probe sorption. Column equilibration experiments were performed in which a solution containing sample and/or probe was pumped through a small column packed with Partisil-10 ODS-3 in order to study their simultaneous sorption. Two specific cases were investigated. In the first case, the origin of indirect UV detection of the neutral sample butanol was determined using the anionic probe naphthalene-2-sulfonate(NS^-). From elution chromatography results, it is known that butanol decreases NS^- probe sorption. By studying the effect of sample on probe sorption and *vice versa*, a competition for space between the two was found to be primarily responsible for the decrease in probe sorption.

In the second case, the origin of indirect UV detection of a cationic sample, tetra-*n*-butyl ammonium ion (TBA^+) using a cationic probe ion, 4-nitrobenzyltrimethylammonium ($NBTA^+$) was studied. The sample TBA^+ also decreases $NBTA^+$ probe sorption in this case. Since both sample and probe are ionic, electrostatic effects play a significant role. Sorption of $NBTA^+$ probe was studied by the column equilibration technique as a function of TBA^+ sample concentration and ionic strength. Simultaneous sorption of the two cations was found to give rise to two separate charge surfaces in the compact layer, one for each ion. A modified version of the Stern Gouy Chapman theory of the electrical double layer was used to determine the potentials at each charge surface. The simultaneous sorption data were then evaluated in terms of a derived model which includes both a competition for space and an electrostatic potential effect. Under the conditions used in this

study, an electrostatic potential effect was mainly responsible for the decrease in probe sorption when sample is present. However, there was evidence that sorption of TBA^+ sample also alters the space available for sorption of $NBTA^+$ probe.

Acknowledgement

I would like to thank my excellent research supervisor, Dr. Cantwell, for his guidance and help throughout the research presented in this thesis and for always managing to find the time to be available. His optimism and enthusiasm were wonderful and a source of encouragement. Graduate school has been a fantastic learning experience and he has been an excellent teacher.

Throughout my student years, I have been fortunate to have received several awards. I am grateful for all the awards that I have received and I would particularly like to thank the Natural Sciences and Engineering Research Council of Canada (NSERC) for their financial support.

I would also like to thank Chandra S. Angle of Energy, Mines and Resouces Canada for the BET measurement of Partisil-10 ODS-3.

Finally, to A. D. C. C., thank you for your support, understanding and encouragement. Also, thanks for providing a little extra special incentive. The future is now ours!

Table of Contents

Chapter 1 Introduction

1.1 Background to Indirect UV Detection 1

1.2 Principles of Indirect UV Detection 8

  1.2.1 Principles of Indirect UV Detection Elution Chromatography 8

  1.2.2 Principles of Indirect UV Detection Frontal Chromatography 14

1.3 Principles of the Column Equilibration Technique 19

1.4 Scope of the Present Work 24

Chapter 2 Experimental

2.1 Introduction 27

2.2 The ODS Packing 27

2.3 Chemicals, Reagents and Solvents 32

2.4 Indirect UV Detection Elution and Frontal Chromatography 34

  2.4.1 Apparatus and Procedure 34

  2.4.2 Mobile Phase and Sample Solutions 37

2.5 Column Equilibration Technique 39

  2.5.1 Precolumns 39

  2.5.2 Column Equilibration Apparatus and Procedure 40

  2.5.3 Procedure and Solutions for Case I: Neutral Sample (Butanol) and Ionic Probe (NS^-) 43

  2.5.4 Procedure and Solutions for Case II: Cationic Sample (TBA^+) and Cationic Probe ($NBTA^+$) 45

  2.5.5 Holdup Volume Measurement 48

    2.5.5.1 Apparatus and Procedure 48

    2.5.5.2 Gas Chromatography 49

2.5.6 Calibration....49

2.6 Gas Chromatography for Off-Line Determination of Butanol....51

2.6.1 Apparatus and Procedure....51

2.6.2 Standard Solutions....52

2.7 Solvent Extraction / Flow Injection Analysis (SE/FIA) for Off-Line Determination of TBA$^+$....54

2.7.1 Principles of SE/FIA....54

2.7.2 Apparatus and Procedure....55

2.7.3 Reagent and Standard Solutions....57

Chapter 3 Indirect UV Detection Elution and Frontal Chromatography

3.1 Introduction....58

3.2 Theory....60

3.2.1 Sorption Isotherms....60

3.2.2 Rate of Travel of Sample Molecules and of Probe Concentration Pulses...64

3.3 Results and Discussion....68

3.3.1 Probe Breakthrough....68

3.3.2 Temperature Effect....71

3.3.3 Sample Injections....76

3.3.3.1 Injection of Mobile Phase Without Probe as a Sample....76

3.3.3.2 Injection of Probe as a Sample....77

3.3.3.3 Injection of Inert Electrolyte Samples....79

3.3.3.4 Injection of Water as a Sample....81

3.3.3.5 Injection of Cationic, Anionic and Neutral Sample Species.......83

3.3.3.6 Magnitude of Indirect Detection Response....83

3.3.4 Frontal Chromatography....85

3.4 Conclusions....94

Chapter 4 Origin of Indirect UV Detection of the Neutral Sample Butanol Using the Anionic Probe Naphthalene-2-Sulfonate

4.1 Introduction 95
4.2 Theory 97
  4.2.1 Competition for Space 97
  4.2.2 Extended Solubility Parameter Theory 99
4.3 Results and Discussion 102
  4.3.1 Determination of Column Equilibration Conditions 102
    4.3.1.1 Precolumn Holdup Volumes 102
    4.3.1.2 Loading and Elution Volumes for NS^- 102
    4.3.1.3 Loading and Elution Volumes for NS^- and Butanol Together .. 107
  4.3.2 Effect of NS^- Probe on Butanol Sample Sorption 113
  4.3.3 Effect of Butanol Sample on NS^- Probe Sorption 122
  4.3.4 Langmuir Isotherm Behaviour 131
  4.3.5 Changing Eluent and Sorbent Strength 138
  4.3.6 Adsorption *versus* Partitioning 140
4.4 Conclusions 142

Chapter 5 Origin of Indirect UV Detection of the Cationic Sample Tetrabutylammonium Ion Using the Cationic Probe 4-Nitrobenzyltrimethylammonium Ion

5.1 Introduction 143
5.2 Theory 147
  5.2.1 SGC Theory of the Electrical Double Layer 147
  5.2.2 Modified SGC Theory for Simultaneous Sorption of Different Ions of the Same Charge 156
  5.2.3 Sorption of $NBTA^+$ Probe Ion 164

5.2.3.1 Coion Exclusion of NBTA$^+$ 165

5.2.3.2 Adsorption Distribution Coefficient of NBTA$^+$.......... 166

5.2.3.3 Adsorption of NBTA$^+$.......... 168

5.2.4 Adsorption of TBA$^+$.......... 170

5.3 Results and Discussion 171

5.3.1 Determination of Column Equilibration Conditions.......... 171

5.3.1.1 Precolumn Holdup Volume.......... 171

5.3.1.2 Loading and Elution Volumes for NBTA$^+$.......... 171

5.3.1.3 Loading and Elution Volumes for NBTA$^+$ and TBA$^+$ Together 172

5.3.2 Sorption of NBTA$^+$ Alone 181

5.3.3 Sorption of Both NBTA$^+$ and TBA$^+$. 189

5.3.4 Effect of TBA$^+$ on NBTA$^+$ Sorption 199

5.3.4.1 Coion Exclusion of NBTA$^+$ and of TBA$^+$.......... 202

5.3.4.2 Testing of the Competition for Space and Electrical Potential Effect Model.......... 203

5.3.4.3 Indirect Detection Chromatography.......... 214

5.4 Conclusions.......... 217

Chapter 6 Conclusions

6.1 Summary of Results 219

6.2 Directions for Future Work 221

6.2.1 Sample and Probe with Opposite Charge.......... 221

6.2.2 Role of the Compact Layer.......... 221

Bibliography.......... 223

Appendix A Tables and Figures for Chapter Four 232

Appendix B Tables and Figures for Chapter Five 255

Appendix C Calculation of Γ_+ 279

List of Tables

Table

1.1 Response pattern for indirect UV detection 7

2.1 Experimental parameters for indirect UV detection elution and frontal chromatography 38

2.2 Description of precolumns used in column equilibration experiments 41

2.3 Experimental parameters for the determination of loading and elution volumes in column equilibration experiments for $NBTA^+$ and TBA^+ 46

2.4 GC parameters for the determination of water in the measurement of the precolumn holdup volumes 50

2.5 GC parameters for the determination of butanol 53

3.1 Plateau absorbance *versus* column temperature data 75

3.2 Results for the injection of buffer and NS^- probe concentration pulses on Partisil-10 ODS-3 78

3.3 Results for the injection of inert electrolyte and water samples on Partisil-10 ODS-3 80

3.4 Results for the injection of cationic, anionic and neutral samples on Partisil-10 ODS-3 84

3.5 Response magnitude for hexanesulfonate sample on Partisil-10 ODS-3 87

3.6 Frontal chromatography on Partisil-10 ODS-3 for two different butanol concentrations 91

4.1 Precolumn holdup volumes for column equilibration studies dealing with NS^- and butanol 103

4.2 Sorption data for the effect of NS^- probe on butanol sample sorption on Partisil-10 ODS-3 using precolumn #3 117

4.3 Change in weight of packing in precolumn #3 for the study of the effect of NS^- probe on butanol sample sorption 118

4.4 NS^- sorption isotherm data on Partisil-10 ODS-3 without and with butanol present in solution from pH 2 aqueous solutions using precolumn #2 124

4.5 Standard data used to determine the effective weight of packing in precolumn #2 for the NS^- sorption isotherm without and with butanol present in solution 125

4.6 Sorption data for the effect of butanol sample on NS^- probe sorption on Partisil-10 ODS-3 using precolumn #3 127

4.7 Change in weight of packing in precolumn #3 for the study of the effect of butanol sample on NS^- probe sorption 128

5.1 Interference of $NBTA^+$ - picrate on the determination of TBA^+ - picrate by SE/FIA 178

5.2 SGC behavior of $NBTA^+$ on Partisil-10 ODS-3 from linear plots of σ_o^{-1} *versus* $c^{-1/2}[(ZF\Psi_{OHP}/2RT)^{-1} \sinh (ZF\Psi_{OHP}/2RT)]^{-1}$ at five activities of $NBTA^+$ in solution 188

5.3 Amounts of $NBTA^+$ and of TBA^+ sorbed in the electrical double layer (n_{NBTA},n_{TBA}), excluded from the diffuse part of the electrical double layer ($n_{NBTA,DL}$,$n_{TBA,DL}$) and adsorbed in the compact part of the electrical double layer ($n_{NBTA,ADS}$,$n_{TBA,ADS}$) at a constant activity of $NBTA^+ = 1.50 \times 10^{-3}$ mol/L and five different activities of TBA^+ 193

5.4 SGC behavior of $NBTA^+$ and TBA^+ on Partisil-10 ODS-3 from linear plots of σ_T^{-1} *versus* $c^{-1/2}[(ZF\Psi_{OHP}/2RT)^{-1} \sinh (ZF\Psi_{OHP}/2RT)]^{-1}$ at a constant $NBTA^+$ activity and five activities of TBA^+ in solution 194

5.5 Values for $(d\sigma_{TBA}/d\sigma_T)$ at a constant $a_{NBTA} = 1.50 \times 10^{-3}$ mol/L and five activities of TBA^+ from Figure 5.15 196

5.6 Calculation of potentials at $NBTA^+$ charge surface at five ionic strengths and a constant $a_{NBTA} = 1.50 \times 10^{-3}$ mol/L 200

5.7 Results of the linear plots in Figure 5.18 for a potential effect only at five ionic strengths 206

5.8 Nonlinear curve fitting of equation 5.54 to fit the constants $\overline{A}'_{TBA}$ and *m* at five ionic strengths 208

5.9 Results of the linear plots in Figure 5.19 for a competition for space and an electrostatic potential effect at five ionic strengths 210

5.10 Values of the competition for space term, A_S, and the electrostatic potential effect term, $\exp(-Z_+F\Psi_I/RT)$, in equation 5.54 at five ionic strengths 212

A.1 GC calibration curve data for the determination of the holdup volumes for precolumns #1, #2 and #3 233

A.2 NS^- calibration curve data for the determination of the amount of NS^- sorbed on the precolumn 235

A.3 NS^- loading curve data for 1.01×10^{-4} mol/L NS^- in pH 2 buffer pumped through precolumn #1 for various volumes and at various flow rates 237

A.4 NS^- loading curve data for 4.08×10^{-4} mol/L NS^- in pH 2 buffer pumped through precolumn #1 for various volumes 238

A.5 NS^- elution data for a solution of 1.02×10^{-4} mol/L NS^- in pH 2 buffer loaded onto precolumn #1 for a volume of 30 mL 239

A.6 NS^- and butanol loading curve data using precolumn #1 240

A.7 NS^- and butanol elution data using precolumn #1 241

A.8 NS^- loading curve data with butanol present using precolumn #2 242

A.9 NS^- elution data with butanol present using precolumn #2 243

A.10 Butanol sorption isotherm data on Partisil-10 ODS-3 from pH 2 aqueous solutions 244

A.11 Butanol calibration curve data for the determination of the butanol sorption isotherm at low concentrations of butanol in the solution pumped through the precolumn (2.18×10^{-4} to 2.18×10^{-2} mol/L) 245

A.12 Butanol calibration curve data for the determination of the butanol sorption isotherm at high concentrations of butanol in the solution pumped through the precolumn (7.63×10^{-2} to 0.654 mol/L) 247

A.13 Butanol calibration curve data for the determination of the amount of butanol sorbed on precolumn #3 in the study of the effect of butanol sample on NS^- probe sorption at low concentrations of butanol in the solution pumped through the precolumn (2.18×10^{-4} to 1.09×10^{-3} mol/L) 249

A.14 Butanol calibration curve data for the determination of the amount of butanol sorbed on precolumn #3 in the study of the effect of butanol sample on NS^- probe sorption at high concentrations of butanol in the solution pumped through the precolumn (5.45×10^{-3} to 4.36×10^{-2} mol/L) 251

A.15 NS^- sorption isotherm data on Partisil-10 ODS-3 from pH 2 aqueous solutions with 1.09×10^{-3} mol/L butanol present 253

A.16 Solvent effect of butanol on NS^- sorption using solubility parameter theory ... 254

B.1 GC calibration curve data for the determination of the holdup volume of precolumn #4 256

B.2 $NBTA^+$ calibration curve data for the determination of the amount of $NBTA^+$ sorbed on precolumn #4 258

B.3 $NBTA^+$ loading curve data for 1.97×10^{-4} mol/L $NBTA^+$ in 0.050 mol/L NaCl and pH 5 buffer pumped through precolumn #4 for various volumes 260

B.4 $NBTA^+$ loading curve data for 2.09×10^{-4} mol/L $NBTA^+$ in 0.500 mol/L NaCl and pH 5 buffer pumped through precolumn #4 for various volumes 261

B.5 $NBTA^+$ elution data for the solution in Table B.3 loaded onto precolumn #4 for a volume of 60 mL 262

B.6 $NBTA^+$ elution data for the solution in Table B.4 loaded onto precolumn #4 for a volume of 60 mL 263

B.7 TBA^+ calibration curve data for the determination of the amount of TBA^+ sorbed on precolumn #4 264

B.8 $NBTA^+$ and TBA^+ loading curve data for a solution of 9.87×10^{-4} mol/L $NBTA^+$ and 1.00×10^{-5} mol/L TBA^+ in 0.050 mol/L NaCl and pH 5 buffer pumped through precolumn #4 for various volumes 266

B.9 $NBTA^+$ and TBA^+ loading curve data for a solution of 9.31×10^{-4} mol/L $NBTA^+$ and 1.00×10^{-5} mol/L TBA^+ in 0.500 mol/L NaCl and pH 5 buffer pumped through precolumn #4 for various volumes 267

B.10 $NBTA^+$ and TBA^+ elution data for the solution in Table B.8 loaded onto precolumn #4 for 150 mL........ 268

B.11 $NBTA^+$ and TBA^+ elution data for the solution in Table B.9 loaded onto precolumn #4 for 150 mL........ 269

B.12 $NBTA^+$ sorption isotherm data on Partisil-10 ODS-3 from pH 5 aqueous solutions at five different concentrations of NaCl in solution........ 270

B.13 Data for plot of σ_0^{-1} *versus* $c^{-1/2}[(ZF\Psi_{OHP}/2RT)^{-1} \sinh (ZF\Psi_{OHP}/2RT)]^{-1}$ for five constant activities of $NBTA^+$........ 271

B.14 Sorption data for $NBTA^+$ and TBA^+ on Partisil-10 ODS-3 from pH 5 aqueous solutions at five concentrations of NaCl in solution 272

B.15 Data for plot of σ_T^{-1} *versus* $c^{-1/2}[(ZF\Psi_{OHP}/2RT)^{-1} \sinh (ZF\Psi_{OHP}/2RT)]^{-1}$ for $NBTA^+$ and TBA^+ at a constant $NBTA^+$ activity = 1.50×10^{-3} mol/L and a constant TBA^+ activity = 3.84×10^{-6} mol/L........ 273

B.16 Data for plot of σ_T^{-1} *versus* $c^{-1/2}[(ZF\Psi_{OHP}/2RT)^{-1} \sinh (ZF\Psi_{OHP}/2RT)]^{-1}$ for $NBTA^+$ and TBA^+ at a constant $NBTA^+$ activity = 1.50×10^{-3} mol/L and a constant TBA^+ activity = 7.68×10^{-6} mol/L........ 274

B.17 Data for plot of σ_T^{-1} *versus* $c^{-1/2}[(ZF\Psi_{OHP}/2RT)^{-1} \sinh (ZF\Psi_{OHP}/2RT)]^{-1}$ for $NBTA^+$ and TBA^+ at a constant $NBTA^+$ activity = 1.50×10^{-3} mol/L and a constant TBA^+ activity = 3.84×10^{-5} mol/L........ 275

B.18 Data for plot of σ_T^{-1} *versus* $c^{-1/2}[(ZF\Psi_{OHP}/2RT)^{-1} \sinh (ZF\Psi_{OHP}/2RT)]^{-1}$ for $NBTA^+$ and TBA^+ at a constant $NBTA^+$ activity = 1.50×10^{-3} mol/L and a constant TBA^+ activity = 7.68×10^{-5} mol/L..276

B.19 Data for plot of σ_T^{-1} *versus* $c^{-1/2}[(ZF\Psi_{OHP}/2RT)^{-1} \sinh (ZF\Psi_{OHP}/2RT)]^{-1}$ for $NBTA^+$ and TBA^+ at a constant $NBTA^+$ activity = 1.50×10^{-3} mol/L and a constant TBA^+ activity = 3.84×10^{-4} mol/L..277

B.20 Data for plots in Figures 5.18 and 5.19..278

List of Figures

Figure

1.1 Direct detection chromatogram of a sample solution containing toluene and ethylbenzene on Partisil-10 ODS-3 using a methanol:water (80:20) mobile phase and a 254 nm detection wavelength.. 3

1.2 Indirect UV detection chromatogram of a hexanesulfonate sample on Partisil-10 ODS-3 using a mobile phase composed of 2.00 x 10^{-4} mol/L naphthalene-2-sulfonate in 0.04 mol/L H_3PO_4/0.03 mol/L NaH_2PO_4 (pH = 2) 5

1.3 Magnitude of indirect detection response as a function of sample type (*i.e.* sign of charge) and sample capacity factor (k'_{smp}) versus probe capacity factor (k'_{sys}) for the case of an anionic probe.. 9

1.4 Indirect UV detection elution chromatography. (a) Hypothetical breakthrough curve for probe on column. (b) Indirect UV detection elution chromatogram obtained from a sample injection after establishment of probe breakthrough.....10

1.5 Processes occurring within the column during an indirect UV detection elution chromatogram for the case of a sample which decreases probe sorption and for which $k'_{smp} < k'_{sys}$..12

1.6 Processes occurring within the column during an indirect UV detection elution chromatogram for the case of a sample which decreases probe sorption and for which $k'_{smp} > k'_{sys}$..15

1.7 Processes occurring within the column during an indirect UV detection elution chromatogram for the case of a sample which increases probe sorption and for which $k'_{smp} < k'_{sys}$..16

1.8 Processes occurring within the column during an indirect UV detection elution chromatogram for the case of a sample which increases probe sorption and for which $k'_{smp} > k'_{sys}$..17

1.9 Frontal chromatogram of a sample containing three components. 18

1.10 Indirect UV detection frontal chromatograms for $k'_{smp} < k'_{sys}$. (a) Sample decreases probe sorption. (b) Sample increases probe sorption. 20

1.11 Column equilibration technique for studying the simultaneous sorption of a sample and a probe...21

1.12 Hypothetical loading curve for a single component on precolumn.................23

2.1 Synthesis of octadecylsilyl (ODS) reversed phase bonded phases (RPBPs) 29-31

2.2 Indirect UV detection elution and frontal chromatography apparatus..............35

2.3 Column jacket design for thermostatting the analytical column....................36

2.4 Column equilibration apparatus 42

2.5 Solvent extraction/flow injection analysis system for the determination of TBA^+...56

3.1 Hypothetical sorption isotherm for a solute *i*.... 61

3.2 Common isotherm shapes in chromatography.......................................63

3.3 Rate of travel of sample molecules and of probe concentration pulses injected onto a column...65

3.4 Calculation of the distribution coefficient for a probe concentration pulse. 67

3.5 Absorption spectrum of 2.00×10^{-4} mol/L NS^- probe in 0.04 mol/L H_3PO_4/0.03 mol/L NaH_2PO_4 (pH = 2) *versus* 0.04 mol/L H_3PO_4/0.03 mol/L NaH_2PO_4. . .69

3.6 NS^- probe breakthrough curve on Partisil-10 ODS-3 analytical column. 70

3.7 Absorbance *versus* volume of solution passed through column with changing temperature...73

3.8 Plateau absorbance *versus* column temperature....................................74

3.9 Indirect UV detection elution chromatogram on Partisil-10 ODS-3 for the injection of water as a sample. 82

3.10 Magnitude of the indirect UV detection response for hexanesulfonate sample. . .86

3.11 Frontal chromatograms for the low butanol concentration case 89

3.12 Frontal chromatograms for the high butanol concentration case....................90

4.1 NS^- loading curve for 1.01×10^{-4} mol/L NS^- in pH 2 buffer on precolumn #1 at various flow rates 105

4.2 NS^- loading curve for 4.08×10^{-4} mol/L NS^- in pH 2 buffer on precolumn #1 106

4.3 NS^- elution curve for a solution of 1.02×10^{-4} mol/L NS^- in pH 2 buffer which was loaded onto precolumn #1 for 10 minutes at a flow rate of 3.0 mL/min. . . 108

4.4 NS^- and butanol loading curves for a solution of 2.00×10^{-4} mol/L NS^- and 2.18×10^{-4} mol/L butanol in pH 2 buffer pumped through precolumn #1 for various volumes. 109

4.5 NS^- and butanol elution curves for the solution in Figure 4.4 loaded onto precolumn #1 for 2 hours at 3 mL/min 111

4.6 NS^- loading curve with butanol present for a solution of 1.00×10^{-4} mol/L NS^- and 2.18×10^{-2} mol/L butanol in pH 2 buffer pumped through precolumn #2 for various volumes.. 112

4.7 NS^- elution curve with butanol present in solution for the solution in Figure 4.6 loaded onto precolumn #2 for 20 minutes at 3.0 mL/min and then for 100 minutes at 1.0 mL/min.. 114

4.8 Butanol sorption isotherm on Partisil-10 ODS-3 from pH 2 aqueous solutions 115

4.9 Change in the effective weight of packing in precolumn #3 for column equilibration experiments dealing with the effect of NS^- probe on butanol sample sorption.. 120

4.10 Effect of NS^- probe on butanol sample sorption on Partisil-10 ODS-3 using precolumn #3 121

4.11 NS^- sorption isotherms on Partisil-10 ODS-3 from pH 2 aqueous solutions without and with butanol present using precolumn #2 123

4.12 Change in the effective weight of packing in precolumn #3 for the column equilibration experiments dealing with the effect of butanol sample on NS^- probe sorption 129

4.13 Effect of butanol sample on NS^- probe sorption on Partisil-10 ODS-3 using precolumn #3 130

4.14 Double reciprocal plot of the butanol sorption isotherm shown as curve a in Figure 4.8 according to equation 3.3. 133

4.15 Expansion of the lower left hand corner of the plot in Figure 4.14 134

4.16 NS^- sorption isotherm on Partisil-10 ODS-3 from pH 2 aqueous solutions with 1.09×10^{-3} mol /L butanol present using precolumn #3. 136

4.17 Double reciprocal plot of the NS^- sorption isotherm shown in Figure 4.16 according to equation 3.3. 137

4.18 Solubility parameter plot of the data in Figure 4.13 based on equation 4.13 to test if a solvent effect is responsible for the decrease in NS^- sorption when butanol is present in solution 139

5.1 Electrical double layer for the sorption of a single potential producing ion 148

5.2 Electrical double layer for the sorption of two different potential producing ions 157

5.3 $NBTA^+$ loading curve for 1.97×10^{-4} mol/L $NBTA^+$ in 0.050 mol/L NaCl and pH 5 buffer 173

5.4 $NBTA^+$ loading curve for 2.09×10^{-4} mol/L $NBTA^+$ in 0.500 mol/L NaCl and pH 5 buffer 174

5.5 $NBTA^+$ elution curve for the solution in Figure 5.3 loaded onto precolumn #4 for 30 minutes at a flow rate of 2.0 mL /min 175

5.6 $NBTA^+$ elution curve for the solution in Figure 5.4 loaded onto precolumn #4 for 30 minutes at a flow rate of 2.0 mL /min 176

5.7 NBTA$^+$ and TBA$^+$ loading curves for a solution of 9.87×10^{-4} mol/L NBTA$^+$ and 1.00×10^{-5} mol/L TBA$^+$ in 0.050 mol/L NaCl and pH 5 buffer 179

5.8 NBTA$^+$ and TBA$^+$ loading curves for a solution of 9.31×10^{-4} mol/L NBTA$^+$ and 1.00×10^{-5} mol/L TBA$^+$ in 0.500 mol/L NaCl and pH 5 buffer 180

5.9 NBTA$^+$ and TBA$^+$ elution curves for the solution in Figure 5.7 loaded onto precolumn #4 for 75 minutes at 2.0 mL/min 182

5.10 NBTA$^+$ and TBA$^+$ elution curves for the solution in Figure 5.8 loaded onto precolumn #4 for 75 minutes at 2.0 mL/min 183

5.11 NBTA$^+$ sorption isotherms on Partisil-10 ODS-3 from pH 5 aqueous solutions at five concentrations of NaCl in solution 184

5.12 Plots of data from Figure 5.11 for NBTA$^+$ at five activities of NBTA$^+$ according to equation 5.12 to show SGC behavior. 187

5.13 Surface excess of NBTA$^+$ plus TBA$^+$, Γ_+, on Partisil-10 ODS-3 from pH 5 aqueous solutions at five concentrations of NaCl in solution 190

5.14 Plots of data from Figure 5.13 for the sum of NBTA$^+$ plus TBA$^+$ at a constant activity of NBTA$^+$ (1.50×10^{-3} mol/L) and five activities of TBA$^+$ according to equation 5.25, to show SGC behavior 191

5.15 TBA$^+$ charge density *versus* total charge density at a constant activity of NBTA$^+$ (1.50×10^{-3} mol/L) and five activities of TBA$^+$ 195

5.16 Reciprocal compact layer differential capacitance from the intercept of the straight line plots in Figure 5.14 *versus* the slopes of the straight line plots in Figure 5.15 197

5.17 Surface excess of NBTA$^+$ as a function of TBA$^+$ concentration and NaCl concentration (*i.e.* ionic strength) in solution 201

5.18 Plots according to equation 5.48 for a potential effect only at five concentrations of NaCl in solution (*i.e.* ionic strength) 205

5.19 Plots according to equation 5.55 for a competition for space and an electrostatic potential effect at five ionic strengths 209

A.1 GC calibration curve for the determination of the holdup volume for precolumns #1, #2 and #3 234

A.2 NS^- calibration curve for the determination of the amount of NS^- sorbed on the precolumn 236

A.3 Butanol calibration curve for the determination of the butanol sorption isotherm at low butanol concentrations in the solution pumped through the precolumn (2.18×10^{-4} to 2.18×10^{-2} mol/L) 246

A.4 Butanol calibration curve for the determination of the butanol sorption isotherm at high butanol concentrations in the solution pumped through the precolumn (7.63×10^{-4} to 0.654 mol/L) 248

A.5 Butanol calibration curve for the determination of the amount of butanol sorbed on precolumn #3 in the study of the effect of butanol sample on NS^- probe sorption for the following range of butanol concentrations in solution: 2.18×10^{-4} to 1.09×10^{-3} mol/L 250

A.6 Butanol calibration curve for the determination of the amount of butanol sorbed on precolumn #3 in the study of the effect of butanol sample on NS^- probe sorption for the following range of butanol concentrations in solution: 5.45×10^{-3} to 4.36×10^{-2} mol/L 252

B.1 GC calibration curve for the determination of the holdup volume of precolumn #4 257

B.2 $NBTA^+$ calibration curve for the determination of the amount of $NBTA^+$ sorbed on precolumn #4 259

B.3 TBA$^+$ calibration curve for the determination of the amount of TBA$^+$ sorbed on precolumn #4 265

List of Symbols

a_i	activity of component i (mol/L)
A_{260}	absorbance at 260 nm
A_{276}	absorbance at 276 nm
$\overline{A}_i$	space occupied per mole of component i in its own charge plane (cm^2)
$\overline{A}'_{TBA}$	effective space occupied per mole of TBA$^+$ in NBTA$^+$ charge plane (cm^2)
A_S	space available for sorption (cm^2)
$A_{S,i}$	space occupied by component i (cm^2)
A_T	total space available for sorption (cm^2)
c	ionic strength (mol/L)
$C_{e,i}$	concentration of component i in column effluent (mol/L)
$C_{m,i}$	concentration of component i in the mobile phase (mol/L)
$C_{s,i}$	concentration of component i in the stationary phase (mol/kg)
$C_{s,i,max}$	maximum concentration of component i in the stationary phase (mol/kg)
C_1	differential capacitance of the compact part of the electrical double layer (Farad/cm^2)
C_2	differential capacitance of the diffuse part of the electrical double layer (Farad/cm^2)
d	arbitrary thickness in the bonded phase (cm)
δ	compact layer thickness (cm)
δ_{inner}	thickness of the inner region of the compact layer (cm)
δ_{outer}	thickness of the outer region of the compact layer (cm)
δ_i	solubility parameter of component i (cal$^{1/2}$/cm$^{3/2}$)
δ_m	solubility parameter of a two component mixture (cal$^{1/2}$/cm$^{3/2}$)
δ_{MP}	solubility parameter of the mobile phase (cal$^{1/2}$/cm$^{3/2}$)
δ_{SP}	solubility parameter of the stationary phase (cal$^{1/2}$/cm$^{3/2}$)

ε	permittivity of solution (Coulomb/Volt·cm)
E_i	cohesive energy density of component i (cal/mol)
γ_i	ionic activity coefficient of component i
$\gamma_{i,\mathrm{ADS}}$	nonionic activity coefficient of component i on the bonded phase
$\gamma_{i,\mathrm{MP}}$	activity coefficient of component i in the mobile phase
$\gamma_{i,\mathrm{SP}}$	activity coefficient of component i in the stationary phase
Γ_i	surface excess of component i in the entire electrical double layer (mol/cm^2)
Γ_+	surface excess due to all positively charged ions in the entire electrical double layer (mol/cm^2)
Γ_i^{AD}	surface excess of component i due to adsorption (mol/cm^2)
Γ_+^{AD}	surface excess due to all positive ions adsorbed (mol/cm^2)
Γ_i^{DL}	surface excess of component i excluded from the diffuse part of the electrical double layer (mol/cm^2)
Γ_+^{DL}	surface excess of all positively charged ions excluded from the diffuse part of the electrical double layer (mol/cm^2)
$[i]$	molar concentration of component i (mol/L)
K_C	integral capacitance of compact layer (Farad/cm^2)
K_{inner}	integral capacitance of inner region of compact layer (Farad/cm^2)
K_{outer}	integral capacitance of outer region of compact layer (Farad/cm^2)
$K_{D,i}$	distribution coefficient of component i (L/kg) or (L/cm^2)
k'_{smp}	capacity factor of sample peak
k'_{sys}	capacity factor of system peak
$K_{i,\mathrm{IEX}}$	selectivity constant for ion i over coion of swamping electrolyte
$K_{\mathrm{NBTA,ADS}}$	adsorption distribution coefficient for NBTA$^+$ (L/cm^2)
$K'_{\mathrm{NBTA,ADS}}$	adsorption equilibrium constant for NBTA$^+$
$1/\kappa$	thickness of the diffuse part of the electrical double layer (cm)

$\mu^{\circ}_{NBTAADS}$	standard chemical potential for the transfer of $NBTA^+$ from bulk solution to its charge plane in the bonded phase when the potential is zero (J/mol)
$\mu_{NBTA,ADS}$	chemical potential for the transfer of $NBTA^+$ from bulk solution to its charge plane in the bonded phase
n_i	moles of component *i* sorbed on packing or in entire electrical double layer (mol)
$n_{T,i}$	total moles of component *i* eluted from precolumn (mol)
$n_{NS,t}$	moles of NS^- sorbed on packing from standard solution at time t (mol)
$n_{NS,o}$	moles of NS^- sorbed on packing from standard solution on a freshly packed precolumn (mol)
$n_{max,i}$	maximum number of moles of component *i* sorbed on packing (mol)
$n_{i,ADS}$	moles of component *i* adsorbed in its charge plane in the bonded phase (mol)
$n_{i,DL}$	moles of component *i* excluded from diffuse part of electrical double layer (mol)
Ψ_I	electrical potential at outer charge surface (Volts)
Ψ_o	electrical potential at charge surface for one potential producing ion or electrical potential at inner charge surface for two potential producing ions (Volts)
Ψ_{OHP}	electrical potential at Outer Helmholtz Plane (Volts)
R	ideal gas constant (8.314 J/mol·K, 8.314 Coulomb·V/mol·K, 1.987 cal/mol·K)
S	specific surface area of stationary phase (cm^2/g)
σ_o	charge density of charge surface due to presence of one type of potential producing ion ($Coulomb/cm^2$)
σ_{NBTA}	charge density at $NBTA^+$ charge surface ($Coulomb/cm^2$)
σ_{TBA}	charge density at TBA^+ charge surface ($Coulomb/cm^2$)

σ_T	total charge density due to all potential producing ions (Coulomb/cm^2)
σ'_T	effective charge density (Coulomb/cm^2)
σ_{DL}	charge density in the diffuse part of the electrical double layer (Coulomb/cm^2)
T	temperature (K)
v_m	rate of travel of sample molecules (cm/sec)
v_{MP}	rate of travel of the mobile phase (cm/sec)
v_p	rate of travel of a probe concentration pulse (cm/sec)
$V_{R,i}$	retention volume of component *i* (mL)
V_m	holdup volume of precolumn (L)
V'_m	void volume of column (L)
$\overline{V}_i$	molar volume of component *i* (cm^3/mol)
V_{MP}	volume of mobile phase in column (L)
W_{eff}	effective weight of packing in precolumn, *i.e.* $W_{S,t}$ (g)
W_S	weight of packing in precolumn (g)
$W_{S,t}$	corrected weight of packing, *i.e.* W_{eff} (g)
$W_{S,o}$	actual weight of packing in freshly packed precolumn (g)
W_{SP}	weight of stationary phase in column (kg)

Chapter 1

Introduction

1.1 Background to Indirect UV Detection

The most popular means of detection in high performance liquid chromatography (HPLC) is based on absorption of ultraviolet (UV) light [1]. Although many compounds have this property, there are several types of compounds which do not, with the result that they cannot be detected in the usual mode. This is an inherent disadvantage to UV detection. Several classes of compounds fall in this category such as inorganic cations and anions and organic compounds which lack a suitable chromophore. Pre- or post- column derivitization with a UV absorbing species are two methods that are used to overcome this problem [2,3]. However, these methods complicate the chromatographic system and they have their own disadvantages. A more universal detector, such as a differential refractometer, is another alternative, but this detector has undesirable properties such as low sensitivity, temperature dependence and the inability to be used with gradient elution [1].

In the early 1980s, Schill pioneered the technique of indirect UV detection to facilitate the detection of non-UV absorbing samples [4-6]. Indirect UV detection HPLC is similar to ion pair solvent extraction where detection of a non-UV absorbing sample ion is possible by extraction as an ion pair with a UV absorbing counter ion from an aqueous phase to an organic phase [7]. By measuring the absorbance of the organic phase, the ion pair, and thus the sample ion, can be detected and quantitated due to the inherent absorbance of the counter ion. Initially this principle was applied to liquid-liquid (partitioning) chromatography (LLC) where the UV absorbing counter ion is present in an aqueous stationary phase and a non-UV absorbing sample ion with opposite charge is injected into an organic mobile phase and migrates down the column as an ion pair with the counter ion [8,9]. Upon exiting the column, the ion pair passes through a detector where its absorbance is measured.

Today, most HPLC and indirect UV detection HPLC are performed on reversed phase bonded phases (RPBPs) in which an alkyl group is covalently bound to the surface of silica gel [10,11]. The most widely used RPBP is octadecylsilyl (ODS or C-18) in which octadecane is the bound group. Initially, bonded phases were viewed as being equivalent to a "mechanically-held liquid phase" [12] having properties resembling, though not identical to, those of a bulk liquid [13-17]. As a result there is a debate as to whether retention on bonded phases is due to partitioning or adsorption [12,18,19]. In this thesis the term "adsorption" will be used in a more general sense to refer to the situation in which solute has been sorbed into or onto the bonded phase itself (*i.e.* adsorption/partitioning). "Sorption" is a more general term that is commonly used to indicate all types of retention processes such as adsorption, partitioning, ion exchange and electrolyte exclusion. It will be used when it is not necessary to make a distinction between "adsorption" and other types of retention processes such as electrolyte exclusion.

The mobile phase that is used with RPBPs is usually aqueous with or without an organic modifier present (e.g. methanol, acetonitrile, tetrahydrofuran). Chromatography performed with these types of bonded phases is thus referred to as reversed phase liquid chromatography (RPLC) since the stationary phase is less polar than the mobile phase.

In a typical RPLC separation, there is a low baseline/background absorbance (*i.e.* mobile phase absorbance). When a UV absorbing sample is injected into such a system, it is directly detected since a peak in the positive direction (relative to the baseline absorbance) appears in the chromatogram as the sample passes through the detector. This is illustrated in Figure 1.1. Using the elution chromatography apparatus described in Chapter 2 and a detection wavelength of 254 nm, toluene and ethylbenzene are easily separated and detected using an ODS bonded phase and a methanol:water (80:20) mobile phase (both have a molar

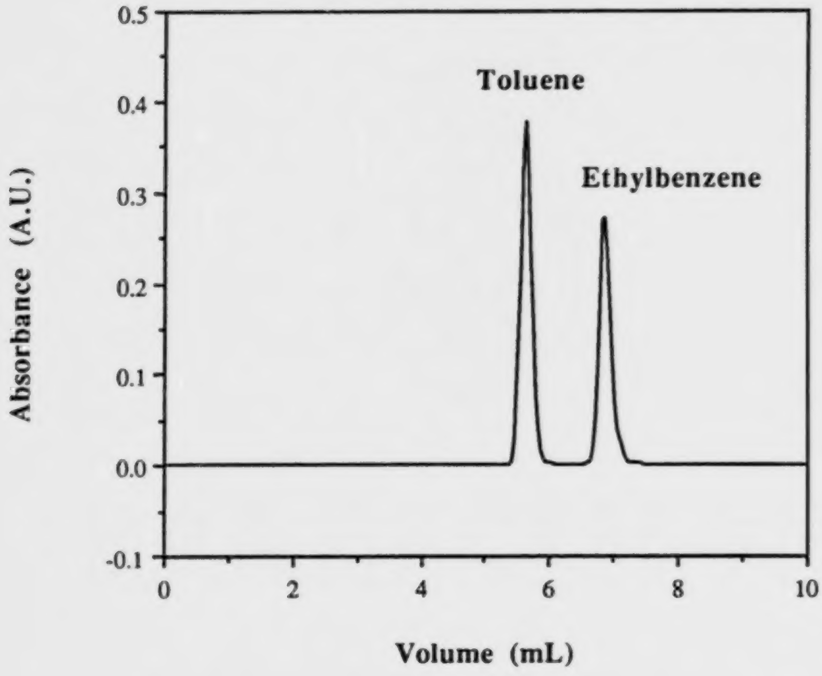

Figure 1.1 Direct detection chromatogram of a sample solution containing toluene and ethylbenzene on Partisil-10 ODS-3 using a methanol:water (80:20) mobile phase and a 254 nm detection wavelength. Flow rate is 1.0 mL/min.

absorptivity of 163 L/(mol·cm) at 254 nm).

Compared to RPLC in the usual mode, the key to performing indirect UV detection is the addition of a UV absorbing species as a component of the mobile phase [4-6]. This UV absorbing compound is usually referred to as the probe. Before a sample can be injected, the probe must distribute itself between the mobile phase and the stationary phase until equilibrium is established. In the case of indirect UV detection there is now a high background absorbance due to the addition of the probe to the mobile phase. When a sample is injected, the initial probe equilibrium is disturbed by the presence of the sample which brings about the indirect detection of the sample. Shown in Figure 1.2 is an example of an indirect UV detection chromatogram which was obtained according to the procedure described in Chapter 2. The sample is hexanesulfonate which has no UV absorbance and the probe is naphthalene-2-sulfonate.

Figure 1.2 reveals two unique characteristics of indirect UV detection chromatograms compared to typical HPLC chromatograms. First, the most obvious difference is that the peaks in the chromatogram appear in both a positive direction and a negative direction relative to the baseline absorbance. Second, besides a peak appearing in the chromatogram at the retention volume of the sample hexanesulfonate ($V_R = 44$ mL), there is an additional peak present which appears at the probe retention volume ($V_R = 61$ mL). For a particular chromatographic system, the probe peak always occurs at the same retention volume regardless of the sample injected and is characteristic of the system [20,21]. Hence, it is referred to as the system peak.

It is important to realize that the sample and system peaks arise from local changes in the probe concentration since it is only the probe which absorbs UV light. Depending upon how the sample affects the probe equilibrium and the capacity factor of the sample, k'_{smp}, relative to the capacity factor of the probe, k'_{sys}, a peak in either the positive direction or in the negative direction (relative to the baseline) will be observed at the sample retention volume [4,5,20-24]. That is, the presence of the sample may increase or decrease

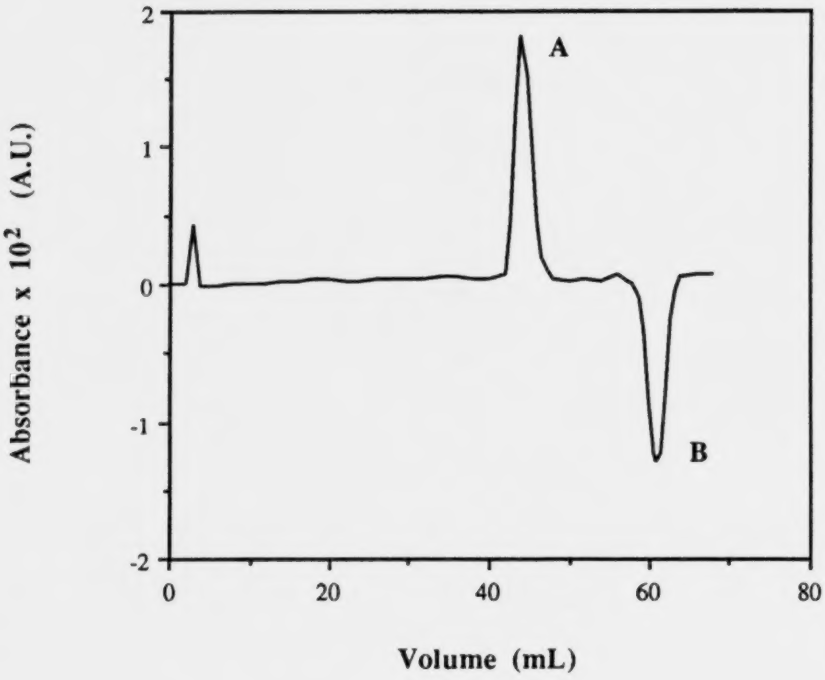

Figure 1.2 Indirect UV detection chromatogram of a hexanesulfonate sample on Partisil-10 ODS-3 using a mobile phase composed of 2.00 x 10^{-4} mol/L naphthalene-2-sulfonate in 0.04 mol/L H_3PO_4 / 0.03 mol/L NaH_2PO_4 (pH = 2). The detection wavelength is 276 nm and the flow rate is 1.0 mL/min. Peak A is the hexanesulfonate sample peak. Peak B is the naphthalene-2-sulfonate probe system peak.

the local sorption of the probe in the sample zone, which gives rise to a zone that has a different composition compared to when no sample is present. Zones in which there is a higher probe concentration produce positive peaks while zones in which there is a lower probe concentration produce negative peaks.

In order to re-establish the initial probe equilibrium after a sample has been injected, an equivalent amount of probe must desorb or resorb depending upon how the sample initially affected probe sorption. If the sample decreases probe sorption, then probe will resorb, but if the sample increases probe sorption, then probe will desorb. This produces another zone in which the probe concentration is different compared to when no sample is present and it gives rise to a system peak whose direction is opposite to that of the sample peak.

Compounds which have been used as probes to perform indirect UV detection are neutral, anionic, or cationic, but ionic probes are most commonly used. Similarly, the samples injected may be neutral or ionic. It is generally observed that when the probe is ionic, sample species which have a sign of charge opposite to that of the probe increase the sorption of the probe while sample species which have the same sign of charge as the probe or have no charge decrease the sorption of the probe [4,5,20-24]. The pattern of sample and system peaks that result is given in Table 1.1 and can be summarized as follows [4,5,20,21,23]. When probe sorption is decreased by the presence of the sample, the sample peak will be positive and the system peak will be negative if the sample elutes before the probe (*i.e.* $k'_{smp} < k'_{sys}$). However, if the sample elutes after the probe (*i.e.* $k'_{smp} > k'_{sys}$), then the system peak will be positive and the sample peak will be negative. On the other hand, when probe sorption is increased, rather than decreased, by the presence of the sample, then the above patterns will be reversed.

Other unique features of indirect detection chromatography which should be mentioned are that when ionic probes and samples are used rather than neutral samples and probes, the indirect detection response observed is larger (*i.e.* larger peak areas)

Table 1.1 Response pattern for indirect UV detection.

Probe	Sample	$k'_{smp} < k'_{sys}$		$k'_{smp} > k'_{sys}$	
		Sample Peak	System Peak	Sample Peak	System Peak
Cationic	Cationic	Positive	Negative	Negative	Positive
	Anionic	Negative	Positive	Positive	Negative
	Neutral	Positive	Negative	Negative	Positive
Anionic	Cationic	Negative	Positive	Positive	Negative
	Anionic	Positive	Negative	Negative	Positive
	Neutral	Positive	Negative	Negative	Positive

[5,20,21,25]. In addition, when the sample elutes before the probe, the response increases as k'_{smp} approaches k'_{sys} and the response is largest when $k'_{smp} \cong k'_{sys}$. On the other hand, when the sample elutes after the probe, the response decreases and approaches a constant value as the sample elutes further away from the probe. This variation in the magnitude of the response is illustrated in Figure 1.3 [20,21,26].

1.2 Principles of Indirect UV Detection

In the next two sections, the principles and experimental aspects for both indirect UV detection elution and frontal chromatography are discussed in greater detail.

1.2.1 Principles of Indirect UV Detection Elution Chromatography

To perform indirect UV detection, the mobile phase must have a high background absorbance which is achieved by adding a UV absorbing compound (probe) to the mobile phase. The probe should have a high molar absorptivity in order to obtain a large indirect detection response [27]. It should also be hydrophobic so that it has some degree of retention. The mobile phase is typically aqueous with or without an organic modifier present and it usually also contains hydrophilic buffer components which have little or no retention [27].

Before a sample can be injected onto the column, the probe must establish equilibrium between the mobile phase and the stationary phase. This is achieved by pumping the mobile phase through the column until complete breakthrough occurs, as demonstrated by monitoring the absorbance of the effluent from the column and recording a "breakthrough curve" for the probe on the column. Figure 1.4a shows a typical breakthrough curve. If the column is previously equilibrated with the solvent only (*i.e.* no probe present), then when the mobile phase containing probe is introduced into the column,

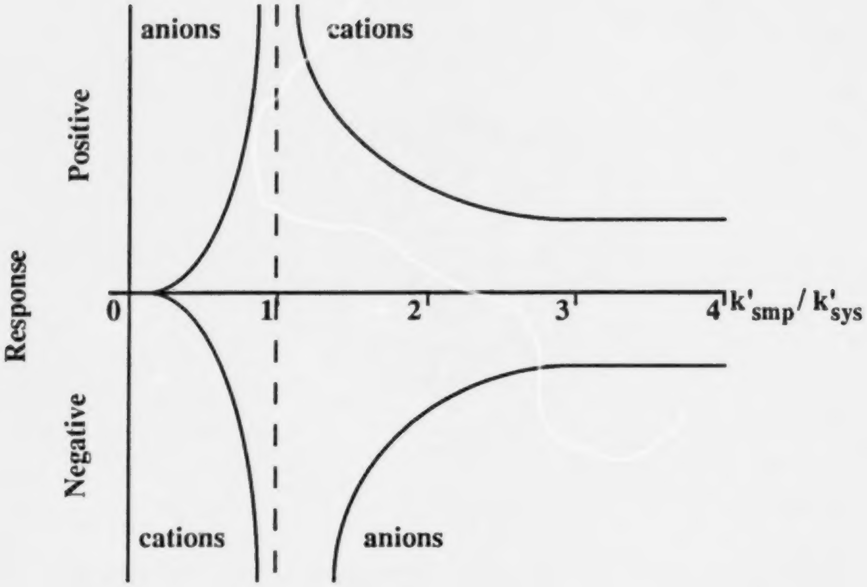

Figure 1.3 Magnitude of indirect detection response as a function of sample type (*i.e.* sign of charge) and sample capacity factor (k'_{smp}) versus probe capacity factor (k'_{sys}) for the case of an anionic probe. The figure is based on references 20 and 21.

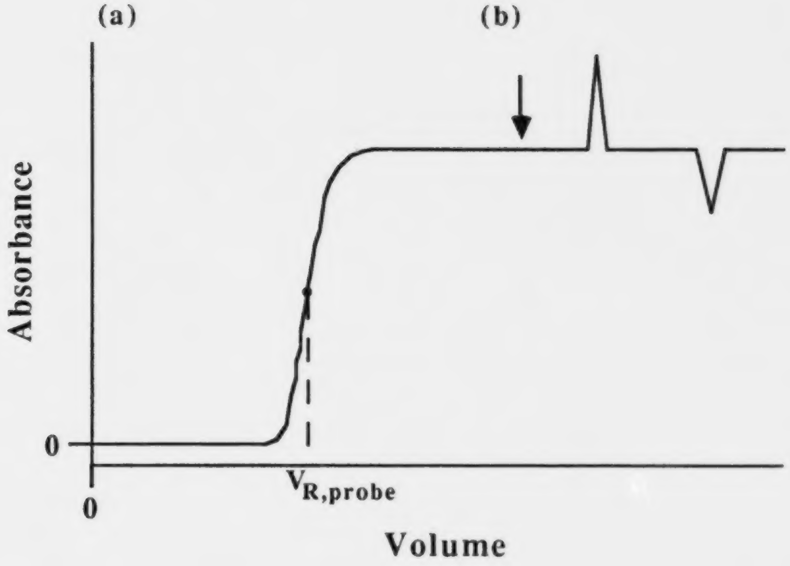

Figure 1.4 Indirect UV detection elution chromatography. (a) Hypothetical breakthrough curve for probe on column. (b) Indirect UV detection elution chromatogram obtained from a sample injection (arrow) after establishment of probe breakthrough.

the probe migrates at a slower rate than the solvent since it is retained. In the initial plateau region of the breakthrough curve where the absorbance is equal to zero, probe is sorbing into the stationary phase and only the solvent is eluting from the column, which accounts for the low absorbance in this region. When the probe starts to emerge from the column outlet, the absorbance rises and reaches another plateau region, indicating that complete breakthrough of the probe on the column has been achieved. On this plateau, the concentration of the probe exiting the column is the same as the concentration of the probe entering the column. Note that the plateau has a high absorbance due to the probe. This plateau constitutes the background signal or baseline for indirect UV detection elution chromatography. The retention volume of the probe, $V_{R,probe}$, is the volume of solution that must be pumped through the column in order for the probe to emerge at the column outlet.

After establishment of the probe equilibrium, samples may be injected onto the column. When a sample is injected, the initial probe equilibrium is disrupted with the result that more or less probe is sorbed in the presence of the sample. Relative to the high background absorbance, peaks of positive absorbance or of negative absorbance are observed in the chromatogram. This is illustrated in Figure 1.4b which shows an example of an indirect UV detection elution chromatogram for a single component sample superimposed upon the high background absorbance. There are two peaks of opposite direction in the chromatogram. One peak occurs at the sample retention volume and the other peak occurs at the probe retention volume (the system peak). Since the changes in the amount of probe sorbed due to sample injection are very small (typically 0.02 A.U.), very sensitive detector ranges must be used, and as a result, the high background absorbance is usually electronically offset to a value close to 0 A.U.

A particular pattern of sample and system peaks is observed depending upon k'_{smp} relative to k'_{sys} and how the sample affects probe sorption [23]. Figure 1.5 illustrates the case of a sample which decreases probe sorption and for which $k'_{smp} < k'_{sys}$. Before a

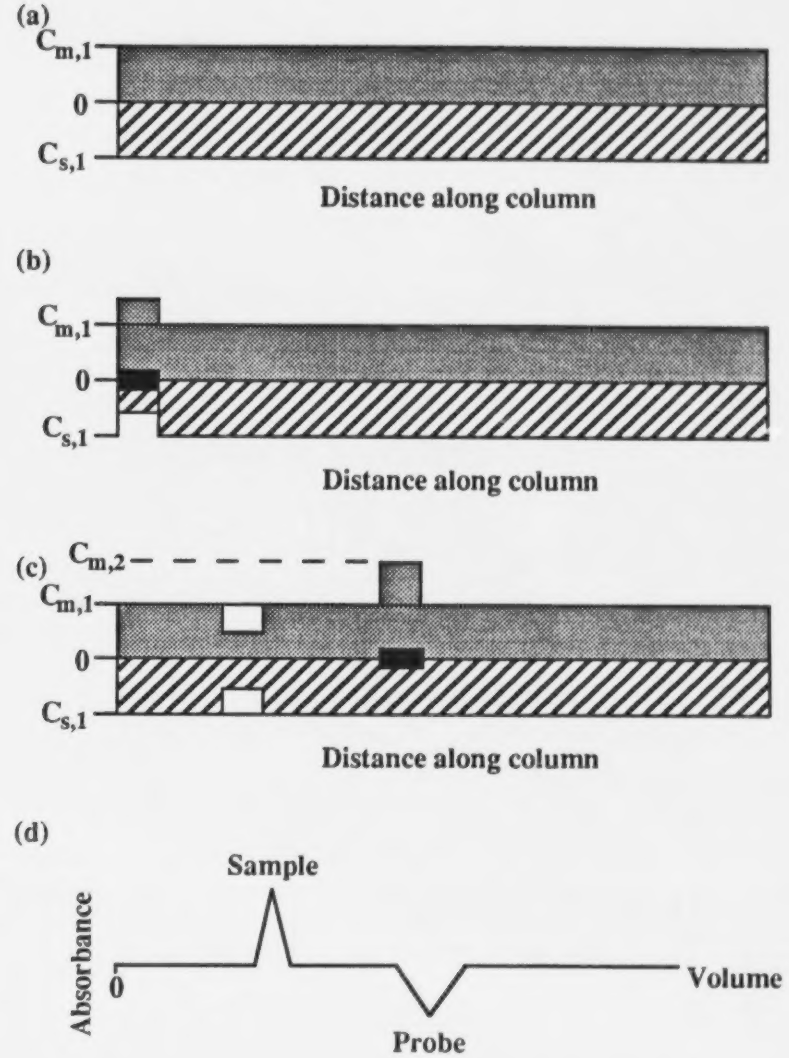
(a)
$C_{m,1}$
0
$C_{s,1}$
Distance along column
(b)
$C_{m,1}$
0
$C_{s,1}$
Distance along column
(c)
$C_{m,2}$
$C_{m,1}$
0
$C_{s,1}$
Distance along column
(d)
Sample
Absorbance
0
Volume
Probe

Figure 1.5 Processes occurring within the column during an indirect UV detection elution chromatogram for the case of a sample which decreases probe sorption and for which $k'_{smp} < k'_{sys}$. (a) Equilibrium concentrations of probe in the mobile phase ($C_{m,1}$) and stationary phase ($C_{s,1}$). (b) Injection of sample (black rectangle). (c) Sample and system zones that develop in the column. $C_{m,2}$ is the new equilibrium probe concentration in the mobile phase in the sample zone. (d) Resulting indirect UV detection elution chromatogram.

sample is injected, there are constant concentrations of probe in the mobile ($C_{m,1}$) and stationary ($C_{s,1}$) phases, as determined by equilibrium (Figure 1.5a). The ratio $C_{s,1}/C_{m,1}$ is the distribution coefficient for the probe on the column of stationary phase ($K_{D,1}$). When the sample is injected at the top of the column (Figure 1.5b), some probe desorbs from the stationary phase into the mobile phase creating an excess of probe in the mobile phase and a deficiency of probe in the stationary phase. The sample zone will travel down the column continuing to desorb probe from fresh stationary phase that it encounters, until the concentration of probe in the mobile phase in the sample zone is at equilibrium with the concentration $C_{s,1}$ in the stationary phase. The new equilibrium concentration of probe in the mobile phase is $C_{m,2}$. The ratio $C_{s,1}/C_{m,2}$ is the distribution coefficient of the probe in the presence of sample, $K_{D,2}$. After this equilibrium is established in the sample zone, probe will no longer be desorbed from the fresh stationary phase that is encountered by the sample zone as it migrates down the column. The situation after this equilibrium in the sample zone has been established is illustrated in Figure 1.5c. Since the probe distribution coefficient is smaller in the sample zone compared to when no sample is present (Figure 1.5a), there is an excess of probe in the mobile phase compared to the original equilibrium amount. When the sample zone elutes from the column, the excess probe gives rise to a positive peak in the chromatogram at the sample retention volume.

The system peak arises in the following way. As the sample zone migrates down the column and desorbs probe from the stationary phase, a deficiency of probe is created in the stationary phase. In order to bring the entire column back to equilibrium, probe from the mobile phase sorbs into the stationary phase to fill this deficiency as shown in the system zone of Figure 1.5c. Note that no sample is present in this zone. The amount of probe which sorbs is such that in the system zone the ratio of the probe concentration in the stationary phase to that in the mobile phase is equal to $K_{D,1}$. This is necessary in order to give a probe distribution coefficient which has the same value as when no sample is present (Figure 1.5a). As a result, when the system zone elutes from the column, the deficiency of probe yields a negative peak in the chromatogram at the probe retention volume. Since there is no sample in this zone, the system zone propagates as a negative probe concentration pulse. Propagation of probe concentration pulses is discussed in Chapter 3. The chromatogram which results is shown in Figure 1.5d in which there is a positive sample peak followed by a negative system peak.

In the case where the sample decreases probe sorption and $k'_{smp} > k'_{sys}$ (Figure 1.6), the situation is similar to the case discussed above and shown in Figure 1.5. The opposite behaviour is observed when the sample increases the sorption of the probe. This is illustrated in Figure 1.7 for $k'_{smp} < k'_{sys}$ and in Figure 1.8 for $k'_{smp} > k'_{sys}$.

1.2.2 Principles of Indirect UV Detection Frontal Chromatography

In frontal chromatography, the sample components are present as constituents of the mobile phase [28,29]. The mobile phase is continually pumped through the column and the UV absorbance of the column effluent is monitored.

First, consider the typical case in which there is no probe in the mobile phase and the sample components are UV absorbing. When the mobile phase containing the sample components is pumped through the column, each component will migrate down the column at its own characteristic rate and a breakthrough curve will be recorded for each sample component. This is illustrated in Figure 1.9 for the case of a sample containing three components. In Figure 1.9, the rate of migration is 1 > 2 > 3. At point A there is complete breakthrough of component 1, at point B there is complete breakthrough of component 2 and at point C there is complete breakthrough of component 3. The retention volumes of components 1, 2 and 3 are noted in Figure 1.9.

When frontal chromatography is done using indirect UV detection, the mobile phase containing the UV absorbing probe is pumped through the column until complete breakthrough is achieved (Figure 1.4a). The mobile phase is then changed to one which

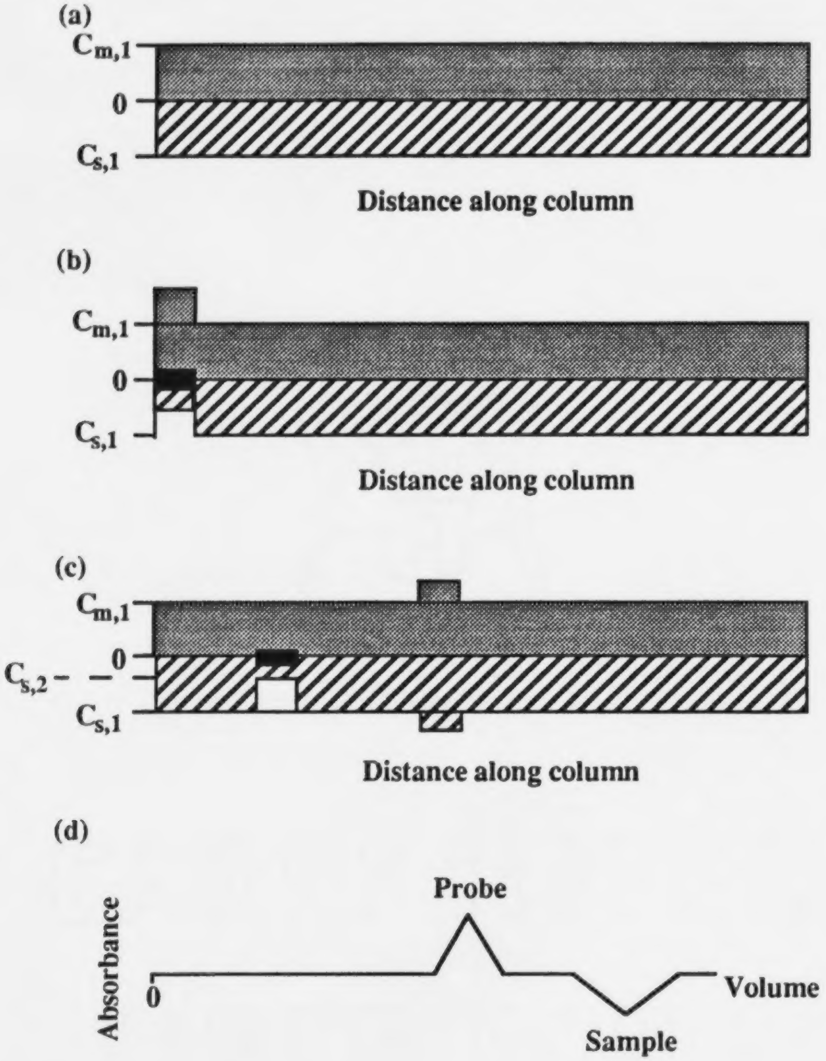
(a)
Cm,1
0
Cs,1
Distance along column
(b)
Cm,1
0
Cs,1
Distance along column
(c)
Cm,1
0
Cs,2
Cs,1
Distance along column
(d)
Probe
Absorbance
0
Volume
Sample

Figure 1.6 Processes occurring within the column during an indirect UV detection elution chromatogram for the case of a sample which decreases probe sorption and for which $k'_{smp} > k'_{sys}$. Panels (a) to (d) are the same as in Figure 1.5. $C_{s,2}$ is the new equilibrium probe concentration in the stationary phase in the sample zone.

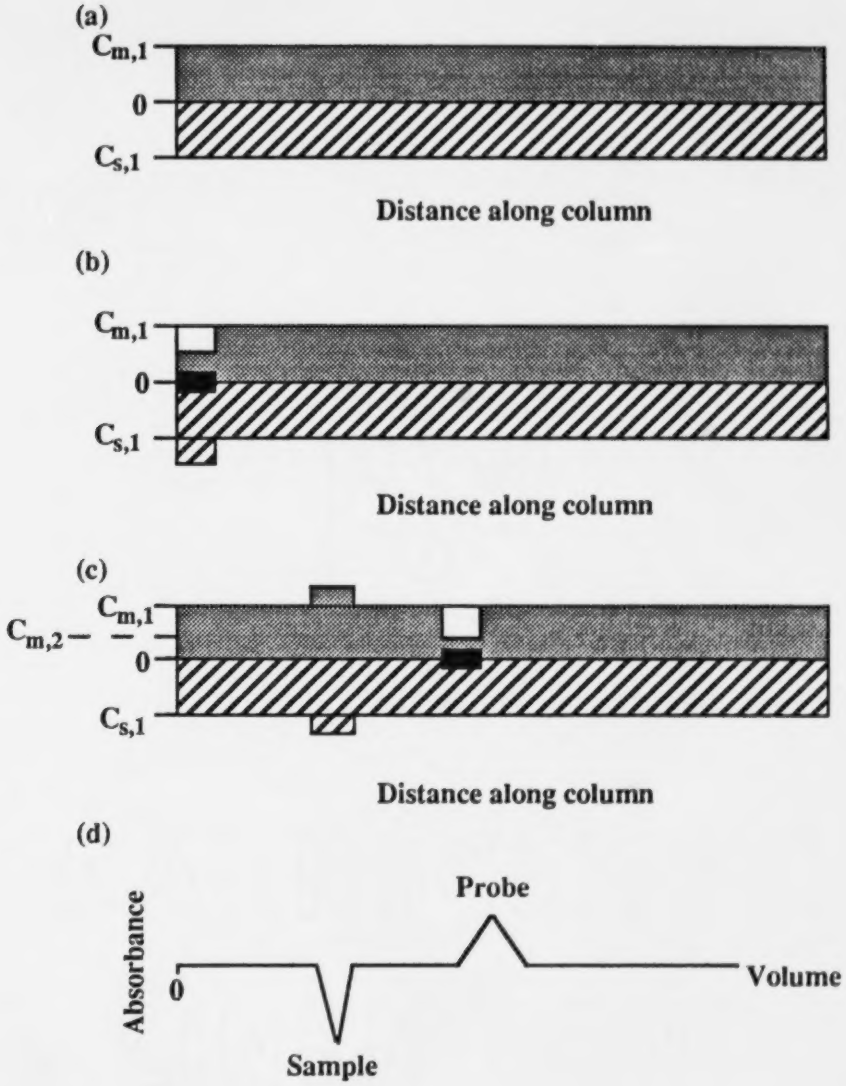
(a)
$C_{m,1}$
0
$C_{s,1}$
Distance along column
(b)
$C_{m,1}$
0
$C_{s,1}$
Distance along column
(c)
$C_{m,1}$
$C_{m,2}$
0
$C_{s,1}$
Distance along column
(d)
Absorbance
0
Probe
Volume
Sample

Figure 1.7 Processes occurring within the column during an indirect UV detection elution chromatogram for the case of a sample which increases probe sorption and for which $k'_{smp} < k'_{sys}$. Panels (a) to (d) are the same as in Figure 1.5. $C_{m,2}$ is the new equilibrium probe concentration in the mobile phase in the sample zone.

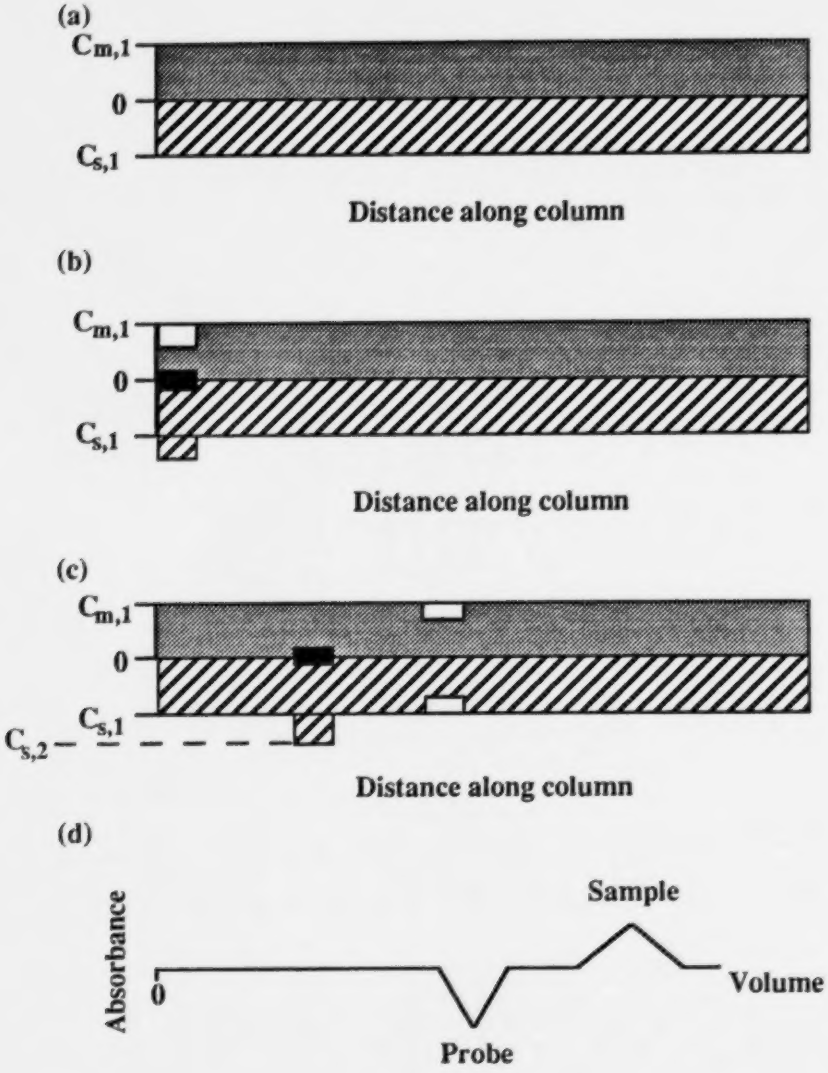
(a)
$C_{m,1}$
0
$C_{s,1}$
Distance along column
(b)
$C_{m,1}$
0
$C_{s,1}$
Distance along column
(c)
$C_{m,1}$
0
$C_{s,1}$
$C_{s,2}$
Distance along column
(d)
Absorbance
Sample
0
Volume
Probe

Figure 1.8 Processes occurring within the column during an indirect UV detection elution chromatogram for the case of a sample which increases probe sorption and for which $k'_{smp} > k'_{sys}$. Panels (a) to (d) are the same as in Figure 1.5. $C_{s,2}$ is the new equilibrium probe concentration in the stationary phase in the sample zone.

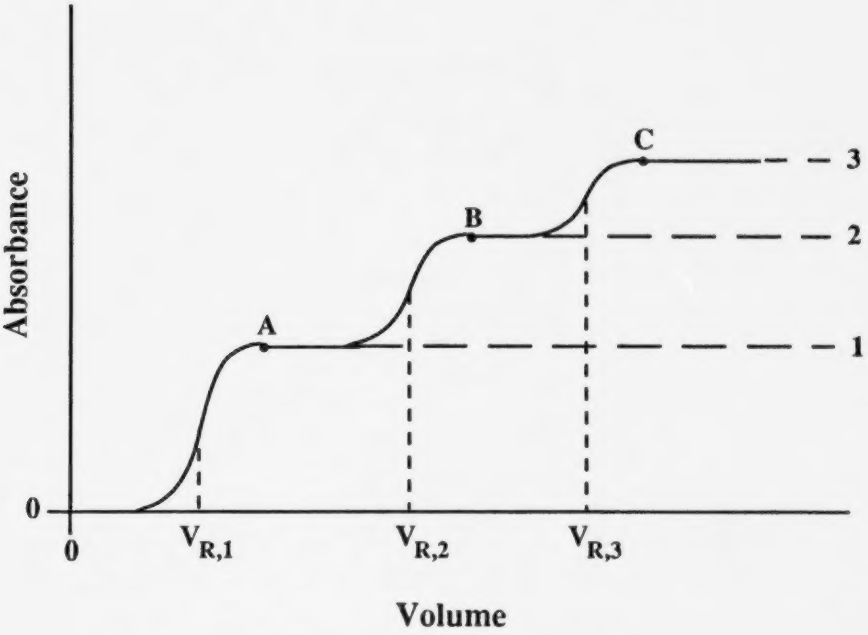

Figure 1.9 Frontal chromatogram of a sample containing three components.

has the same composition as the initial mobile phase except that a certain concentration of sample is also present. If $k'_{smp} < k'_{sys}$ and the sample decreases the sorption of the probe, then the frontal chromatogram shown in Figure 1.10a will be recorded. The initial ascending front occurs at the retention volume of the sample indicating breakthrough of the sample while the descending portion at the rear of the chromatogram occurs at the retention volume of the probe. The descending portion appears in this case indicating that the new equilibrium conditions have been established along the entire length of the column. The baseline thus returns to the original value since the concentration of the probe in the mobile phase without and with sample present is the same.

If $k'_{smp} < k'_{sys}$ and the sample increases probe sorption, then the frontal chromatogram shown in Figure 1.10b will be recorded. The initial descending front occurs at the sample retention volume while the ascending portion at the rear of the chromatogram occurs at the probe retention volume.

1.3 Principles of the Column Equilibration Technique

The basic principles behind the column equilibration technique [30,31] are the same as those discussed in Section 1.2.1 for probe breakthrough curves. This section will expand on those principles as they apply to the column equilibration technique. The main difference is that rather than using a large analytical column, a small column (*i.e.* precolumn) is packed with a known weight of stationary phase, W_S, through which a solution is pumped. Chromatography is not performed. Instead, the amount of each component sorbed on the stationary phase at equilibrium is measured.

In the column equilibration studies, a solution containing two components (probe and sample) is pumped through the precolumn until both components have achieved equilibrium between the solution and the ODS packing. This is illustrated in Figure 1.11a. Assuming that the two components do not interact with one another, then when the solution

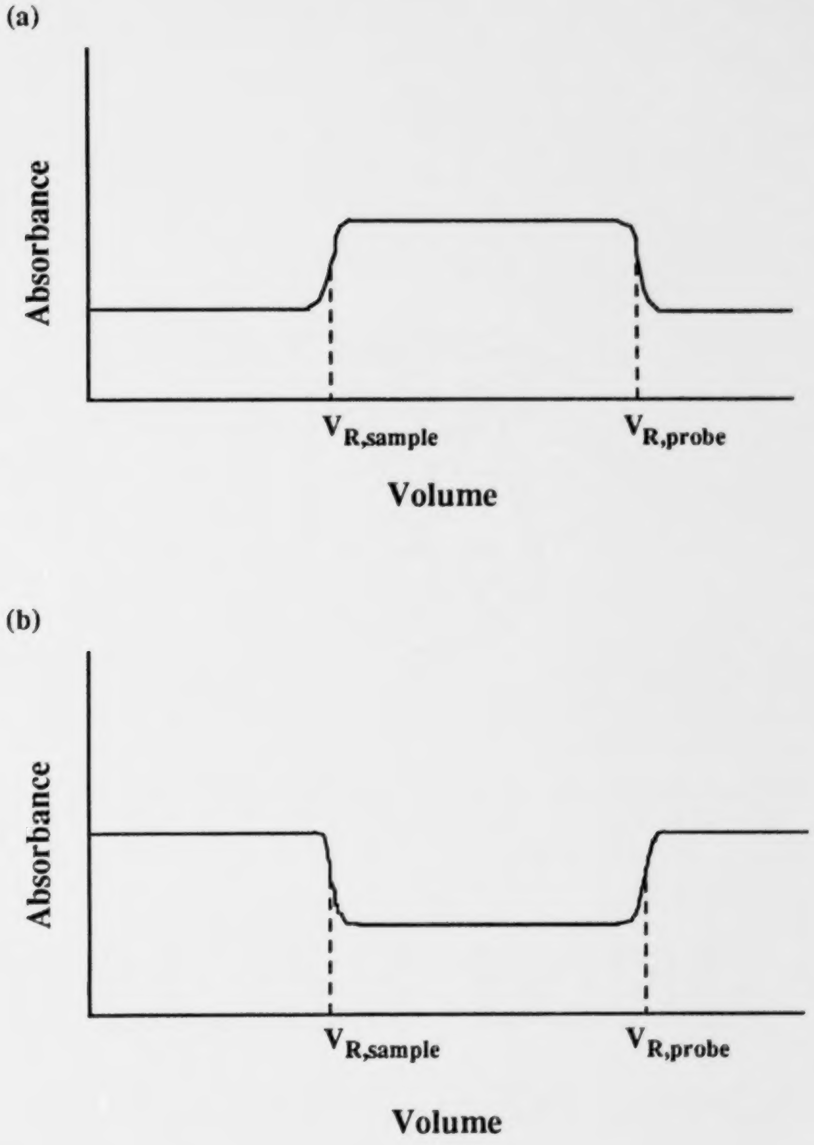
(a)
Absorbance
V_R,sample
V_R,probe
Volume
(b)
Absorbance
V_R,sample
V_R,probe
Volume

Figure 1.10 Indirect UV detection frontal chromatograms for $k'_{smp} < k'_{sys}$. (a) Sample decreases probe sorption. (b) Sample increases probe sorption.

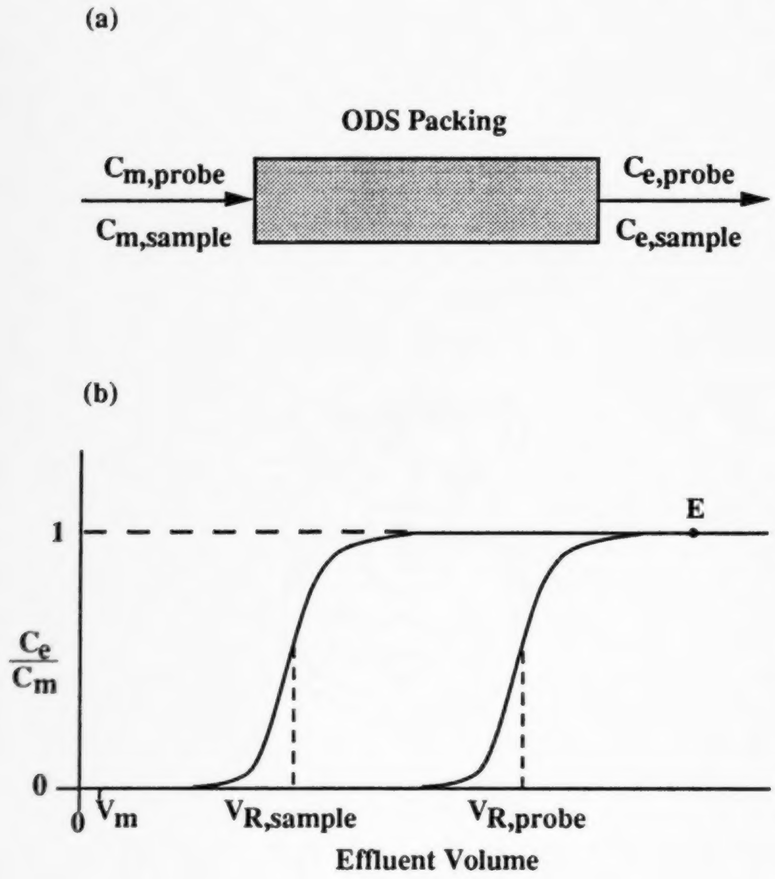
(a)
ODS Packing
$C_{m,probe}$
$C_{m,sample}$
$C_{e,probe}$
$C_{e,sample}$
(b)
E
1
$\frac{C_e}{C_m}$
0
0
V_m
$V_{R,sample}$
$V_{R,probe}$
Effluent Volume

Figure 1.11 Column equilibration technique for studying the simultaneous sorption of a sample and a probe. (a) Small column (precolumn) packed with ODS packing through which a solution containing a probe and a sample is pumped. $C_{m,i}$ is the concentration of sample or probe in the solution pumped through the precolumn. $C_{e,i}$ is the concentration of sample or probe in the column effluent. (b) Hypothetical breakthrough curves for sample and probe on the precolumn assuming that there is no interaction between the two components. At point E both sample and probe have achieved equilibrium.

is introduced into the precolumn, each component will migrate at its own characteristic rate and produce its own breakthrough curve as shown in Figure 1.11b. The retention volume of each component, $V_{R,i}$, is the volume of solution that is pumped through the column in order for its zone to emerge at the outlet of the column. The breakthrough curves in Figure 1.11b are identical to those which would be obtained if a solution of either probe or sample alone is pumped through the precolumn.

It is important to recall that in indirect detection, the sorption of the probe is influenced by the sample and *vice versa*. The breakthrough curves shown in Figure 1.11b do not illustrate this. They are simply drawn to point out the fact that in the column equilibration experiment for two components in solution, measurements are made for the amount of each component sorbed when *both* components have achieved equilibrium. That is, both breakthrough curves have reached a plateau. This is indicated by point E in Figure 1.11b.

The establishment of equilibrium can be expressed as a breakthrough curve or as a loading curve. A loading curve is a plot of the amount of component sorbed *versus* the volume of solution pumped through the precolumn. An example is shown in Figure 1.12. It is obtained by pumping various volumes of solution through the precolumn and determining the amount of component sorbed for each volume. When two components are present in solution, a loading curve is obtained for each component to determine when complete equilibrium is achieved. When both curves have reached a plateau, equilibrium for both components has been achieved.

The amount of each component sorbed, n_i, on the packing at equilibrium is calculated by the following equation:

$$n_i = n_{T,i} - V_m C_{m,i} \tag{1.1}$$

where $n_{T,i}$ is the total number of moles of component i eluted from the precolumn,

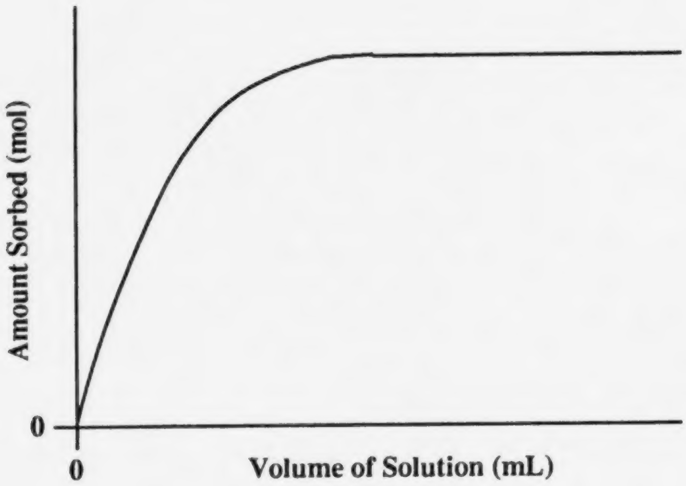

Figure 1.12 Hypothetical loading curve for a single component on precolumn.

including that in the holdup volume, V_m is the holdup volume of the precolumn or the retention volume of an unretained component and $C_{m,i}$ is the concentration of component *i* in the solution that is being pumped through the precolumn. The concentration of the component in the stationary phase, $C_{s,i}$, is obtained from the following equation:

$$C_{s,i} = \frac{n_i}{W_s} \tag{1.2}$$

A sorption isotherm is a plot of $C_{s,i}$ *versus* $C_{m,i}$ and is obtained by repeating the experiment at several $C_{m,i}$.

1.4 Scope of the Present Work

The goal of the present thesis is to determine *via* the column equilibration technique why a particular sample type (*i.e.* sign of charge) produces the observed increase or decrease in probe sorption. By determining how various sample types affect probe sorption, a better understanding of the processes which give rise to the indirect detection phenomenon can be achieved.

Two specific cases are investigated. In both cases, the probe is ionic. In the first case, the effect of a neutral sample on probe sorption is examined while in the second case, the effect of an ionic sample on the sorption of a probe with the same charge is examined. Based on the discussion above, there is a decrease in probe sorption in the presence of the sample in both cases.

Generally speaking, there are three possible ways that a sample can affect probe sorption:

(i) The sample alters the solvent strength of the mobile phase.

(ii) The sample competes with the probe for space in the stationary phase.

(iii) The sample alters the sorbent strength of the stationary phase.

The purpose of the studies in this thesis is to determine which reason(s) is/are responsible for the decreased probe sorption in the presence of the sample for the two cases investigated.

Electrical double layer models have been formulated to explain the sorption of ionic species on RPBPs [32-45]. These models have primarily been developed to explain ion pair RPLC (IP-RPLC) in which a large hydrophobic pairing ion is added to the mobile phase in order to enhance the retention of oppositely charged sample ions. In the first case studied in this thesis, that of a neutral sample, the interpretation of how the sample affects probe sorption is simplified since electrostatic effects are not important, as the sample has no charge. The second case, however, where both the probe and the sample have the same sign of charge, is potentially more complicated than the neutral sample case since electrostatic effects can now play a significant role. The electrical double layer models that have been described in the literature to explain IP-RPLC are applicable in this case. However, these models usually consider only the contribution to the electrical double layer that is due to sorption of the probe/pairing ion [35,37,39,40]. Since the sample is usually present at "trace conditions" in IP-RPLC its contribution to the electrical double layer is ignored. In indirect detection of an ionic sample using an ionic probe, the sample is also usually present at "trace conditions". However, this does not mean that sorption of the sample ion makes no contribution to the potential - only that it causes a small change in potential which may produce a consequent small change in the sorption of the probe [46]. From the discussion in Section 1.2.1, it is important to note that, under conditions typically used in indirect detection elution chromatography, sample and system peaks correspond to a change in the sorption of only a small fraction of the probe. The treatment of the second case is therefore more complex since the contribution of both probe and sample sorption to the electrical double layer is considered. In determining how the sample affects probe sorption, a greater understanding of the electrical double layer that is created by the sorption of two different ions of the same charge on a RPBP is achieved.

A brief description of each chapter in this thesis is given below.

In Chapter 2, the details and procedures of the indirect UV detection elution and frontal chromatography experiments and the column equilibration experiments are presented. The RPBP used in all experiments is also described.

In Chapter 3, indirect UV detection elution chromatography is performed on an analytical column to achieve familiarity with the technique and to confirm literature results on the particular RPBP used throughout this thesis. In addition, some indirect UV detection frontal chromatography results are presented for the case of a neutral sample and an ionic probe.

In Chapter 4, the results of the column equilibration study for the case of a neutral sample and an ionic probe are presented. The simultaneous sorption of the probe and sample is measured and the effect of the probe on sample sorption and *vice versa* is shown. Sorption isotherms for both the probe and the sample are given.

In Chapter 5, the results of the column equilibration study for the case of a cationic probe and a cationic sample are presented. There are two main sections to this chapter. In the first section, sorption isotherms for the probe are measured as a function of ionic strength and are quantitatively described by the Stern Gouy Chapman (SGC) model of the electrical double layer. Simultaneous sorption of sample and probe is measured as a function of sample concentration and ionic strength while the probe concentration is kept constant. The data are treated in terms of SGC theory and the role of the compact part of the electrical double layer is investigated. In the second section, the simultaneous sorption data are examined in order to determine how the sample affects probe sorption and the origin of indirect detection. The sorption of the probe is evaluated in terms of a derived model which includes both a competition for space and an electrical potential effect.

In Chapter 6, conclusions are made from the two column equilibration studies, neutral/ionic and ionic/ionic, as they apply to indirect UV detection HPLC. Possibilities for future work are also discussed.

Chapter 2

Experimental

2.1 Introduction

In this chapter, the details for all the experiments that were done are presented. Two basic types of experiments were performed. First, elution chromatography and frontal chromatography were performed on an analytical column using indirect UV detection in which naphthalene-2-sulfonate (NS^-) was the ionic probe. Second, the column equilibration technique was used to measure the simultaneous equilibrium sorption of probe and sample in order to determine the origin of indirect detection of the neutral sample butanol using NS^- as the ionic probe and to determine the origin of indirect detection of the cationic sample tetrabutylammonium ion (TBA^+) using the cationic probe 4-nitrobenzyltrimethylammonium ion ($NBTA^+$). Experimental details for the gas chromatographic determination of butanol and the solvent extraction/flow injection analysis (SE/FIA) determination of TBA^+ are described separately. The octadecylsilyl (ODS) packing used as the stationary phase throughout this work is also described.

2.2 The ODS Packing

The ODS packing used as the stationary phase in all experiments is Whatman Partisil-10 ODS-3. It is a reversed phase bonded phase packing (RPBP) with a 10 µm particle diameter. It is described by the manufacturer as being "highly end-capped".

RPBPs are the most commonly used stationary phases in liquid chromatography today [10,47]. Their popularity is due to their applicability to a wide variety of separation problems and to their high efficiency. They are prepared by covalently bonding an alkyl group (typically ODS) to the surface silanol groups of silica gel. The reactions commonly used for synthesizing RPBPs are shown in Figure 2.1a-c [10,11,48-50]. The alkyl group used as the example in Figure 2.1 is ODS.

The starting materials used in the synthesis reactions are typically chloro- and alkoxy-silanes. Depending upon the degree of substitution of the silane and reaction conditions, either a monomeric or polymeric RPBP is produced. Monofunctional silanes react with only one silanol group on the silica gel surface (Figure 2.1a) to give a single bond linkage between each molecule and the silica. The product is a monomeric RPBP since the silica gel surface is covered with a monomolecular layer of ODS groups. In the absence of water, di- or tri-functional silanes also produce monomeric RPBPs (Figure 2.1b). On the other hand, in the presence of water, di- or tri-functional silanes can react with more than one silanol group and can also undergo polymerization reactions to produce a cross linked layer which is referred to as a polymeric RPBP (Figure 2.1c).

It is generally agreed that the surface silanol concentration on most forms of silica is about 8 $\mu mol/m^2$ (or 4.8 $silanols/nm^2$) [10,11,50]. Due to steric constraints, only about half of these silanols undergo reaction [50-53]. It is desirable to reduce the number of unreacted silanol groups since their presence can lead to severe problems when chromatography is performed, such as peak tailing and low linear sample capacities [10,49,54,55]. In order to reduce the number of unreacted silanols, a further reaction is carried out with a smaller silane which can react with the less accessible silanol groups [10,49]. Trimethylchlorosilane is most commonly used for this purpose. This procedure is referred to as "end-capping". Depending upon the end-capping procedure, there still may be some residual silanol groups present.

In addition to the synthesis reaction and the type of alkyl group bound to the silica gel surface, RPBPs are also characterized by the number of alkyl groups bound to the surface. This can be expressed as either the carbon loading or the surface coverage [10,48-

(a)

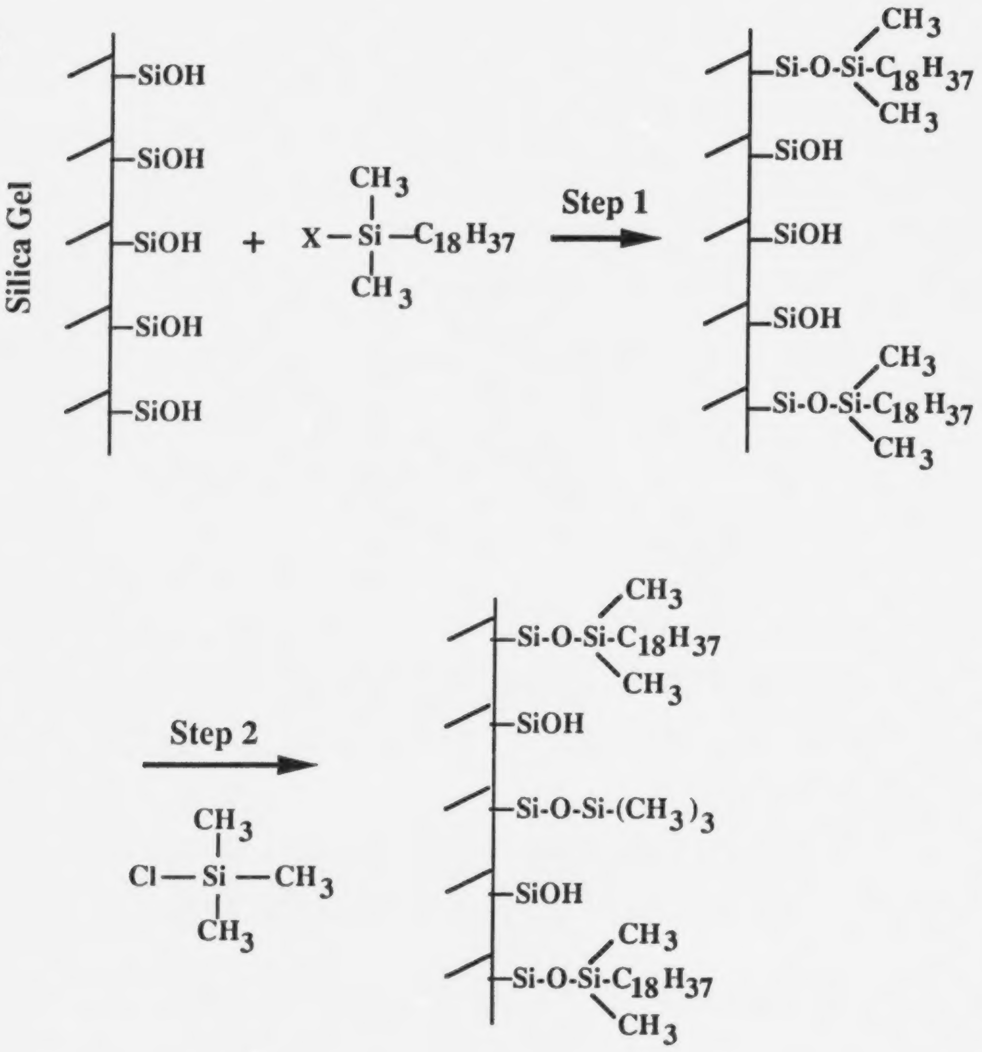
Silica Gel
SiOH
SiOH
SiOH
SiOH
SiOH
+
$X-Si(CH_3)_2-C_{18}H_{37}$
Step 1
$Si-O-Si(CH_3)_2-C_{18}H_{37}$
SiOH
SiOH
SiOH
$Si-O-Si(CH_3)_2-C_{18}H_{37}$
Step 2
$Cl-Si(CH_3)_3$
$Si-O-Si(CH_3)_2-C_{18}H_{37}$
SiOH
$Si-O-Si-(CH_3)_3$
SiOH
$Si-O-Si(CH_3)_2-C_{18}H_{37}$

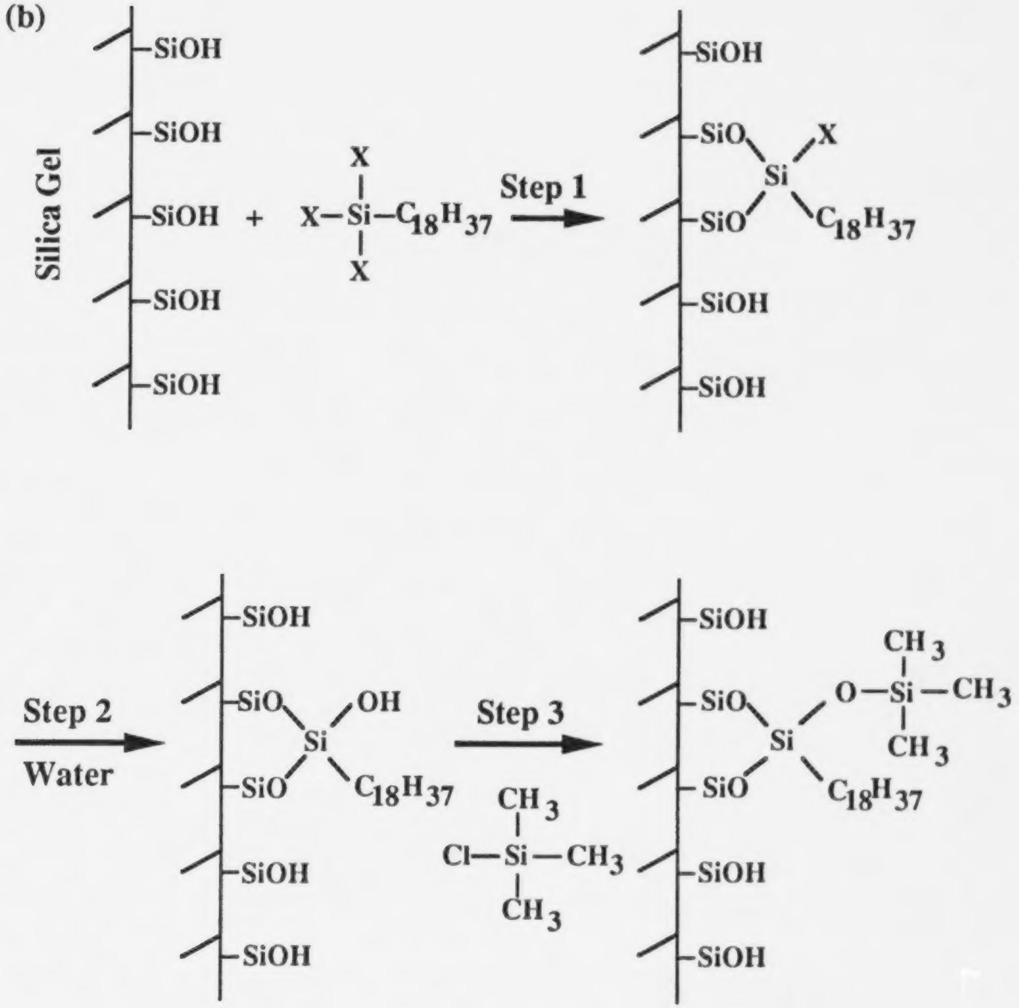
(b)
Silica Gel
SiOH
X
X—Si—C18H37
X
Step 1
SiO
Si
X
C18H37
Step 2
Water
OH
Step 3
CH3
Cl—Si—CH3
CH3
O—Si—CH3
CH3
CH3

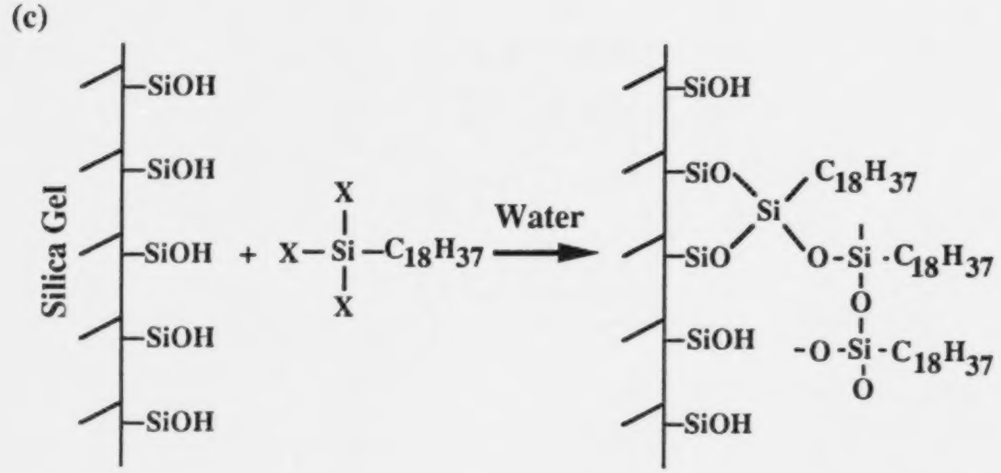
(c)
Silica Gel
SiOH
X
Si
C18H37
Water
SiO
C18H37
O-Si-C18H37
O
-O-Si-C18H37
O

Figure 2.1 Synthesis of octadecylsilyl (ODS) reversed phase bonded phases (RPBPs). (a) Synthesis of a monomeric phase from a monofunctional silane. (b) Synthesis of a monomeric phase from a trifunctional silane. (c) Synthesis of a polymeric phase. X = -Cl or -OR

51]. The carbon load is the weight percentage of carbon in the packing material as determined by elemental analysis. Surface coverage refers to the percentage of available silanols that have undergone reaction. As stated above, it is desirable to obtain 100% surface coverage for a well "end-capped" RPBP. Typical values, however, are much lower than this (≈ 60%).

Partisil-10 silica gel consists of irregularly shaped porous microparticles with an average diameter of 10 μm and a surface area of 400 m^2/g [56]. The pore size is about 8.5 nm. The ODS packing used in this work was prepared by bonding trichlorooctadecylsilane to Partisil-10 silica followed by end-capping with trimethylchlorosilane. The final product is a 10 μm chemically bonded C-18 polymeric phase with a carbon load of approximately 10.5% [56]. Its surface coverage as estimated by the manufacturer is at least 95% [56,57]. The specific surface area of the batch of Partisil-10 ODS-3 used in the column equilibration studies, as measured by the BET method, is 266 m^2/g.

2.3 Chemicals, Reagents and Solvents

Sodium naphthalene-2-sulfonate (NaNS) was prepared from 2-naphthalenesulfonic acid (Eastman Kodak) by converting the acid to the sodium salt by titrating with ≈ 1 mol/L NaOH past pH 7. The sodium salt was then recrystallized from water.

n-Butanol (A&C American Chemicals, Lot No. 830316), 1-pentanol, 99+% (Aldrich, Lot No. 06109BW) and hexyl alcohol, 98% (Aldrich, Lot No. 03505KP) were analytical grade and used as received.

n-Amyl amine, 97% (Aldrich, Lot No. HE 010897) was analytical grade and n-heptyl amine (Terochem Laboratories, Ltd.) was reagent grade. Both were used as received.

1-pentanesulfonic acid, sodium salt, 98% (Aldrich, Lot No. 03212JW), 1-hexanesulfonic acid, sodium salt, 98% (Aldrich, Lot No. 05523KW), 1-heptanesulfonic acid, sodium salt, 98% (Aldrich, Lot No. EX02727JW) and 1-octanesulfonic acid, sodium salt, 98% (Aldrich, Lot No. 03714TV) were analytical grade and used as received.

p-phenylazobenzenesulfonic acid (Pfaltz and Bauer, Lot No. P09080) was used as received.

4-nitrobenzyltrimethylammonium chloride, 98% ($NBTA^+Cl^-$) (Aldrich, Lot No. 03327 BP) and tetrabutylammonium chloride, 96% (TBA^+Cl^-) (Eastman Kodak, Lot No. A162070) were used as received. Both materials are hygroscopic, so stock solutions were standardized by titration with silver nitrate. Stock solutions of TBA^+Cl^- were filtered before use to remove traces of charcoal evidently left over from the purification process.

Sodium nitrate (BDH Chemicals) was analytical grade and used as received.

Phosphoric acid (McArthur Chemical Co., Fisher Scientific Co., BDH Chemicals) was analytical grade and used as received.

Sodium chloride (BDH Chemicals) was analytical grade and used as received.

Sodium hydroxide (BDH Chemicals) was analytical grade and used as received. Solutions were standardized by titrating solutions of potassium hydrogen phthalate with the prepared sodium hydroxide solution.

Glacial acetic acid (BDH Chemicals) was analytical grade and used as received. Diluted solutions of acetic acid were standardized by titration with sodium hydroxide.

Silver nitrate (Terochem Laboratories Ltd.), potassium hydrogen phthalate (Anachemia), phenolpthalein (Fisher Scientific Co.), potassium dichromate (Anachemia), potassium chloride (BDH Chemicals), calcium carbonate (BDH Chemicals) and sodium bicarbonate (Anachemia) were all used as received.

Picric acid (Matheson, Coleman and Bell) was reagent grade and used as received. Solutions were standardized by titration with sodium hydroxide.

Chloroform (Fisher Scientific Co.) was analytical grade and used as received.

Methanol (Fisher Scientific Co.) and ethanol (Commercial Alcohol Ltd.) were analytical grade and were distilled before use.

Water (Barnstead NANOpure, Boston, MA) was distilled and deionized.

2.4 Indirect UV Detection Elution and Frontal Chromatography

In these series of experiments, indirect UV detection elution chromatography is performed on an analytical column using NS^- as the probe. Various types of samples (neutral, anionic, cationic) are injected to observe the indirect detection response. Frontal chromatography is also performed for the case of a neutral sample.

2.4.1 Apparatus and Procedure

A schematic diagram of the apparatus used to perform indirect UV detection HPLC and frontal chromatography is shown in Figure 2.2. It is a typical HPLC setup. P is a Waters Model 590 HPLC pump (Waters Chromatography, Milford, MA), V1 is a six position selector valve (part no. 7060, Rheodyne, Inc., Berkeley, CA), F is a 2μm column inlet filter (part no. 7302, Rheodyne, Inc., Berkeley, CA), V2 is a sample injection valve fitted with a 20 μL injection loop (part no. 7120, Rheodyne, Inc., Berkeley, CA), C is a commercial analytical column (25 cm x 0.40 cm i.d.) of Whatman Partisil-10 ODS-3 (Catalog no. 4228-001, Whatman, Inc., Clifton, NJ), D is a Waters Model 481 Lambda Max UV-Vis spectrophotometer (Waters Chromatography, Milford, MA), and R is a Recordall Series 5000 recorder (Fisher Scientific Co.).

Valve V2 was thermostatted by circulating thermostatted water (25.00 ± 0.04 °C) from a water bath (Model R20, Haake, Berlin, Germany) through copper tubing (4 mm i.d., 6 mm o.d.) that was coiled around the body of the valve. The analytical column was thermostatted precisely to 25.00 ± 0.01 °C by circulating water from the same water bath through a specially designed column jacket. A double-walled column jacket constructed of concentric aluminum and stainless steel tubing shown in Figure 2.3 was used. Stagnant

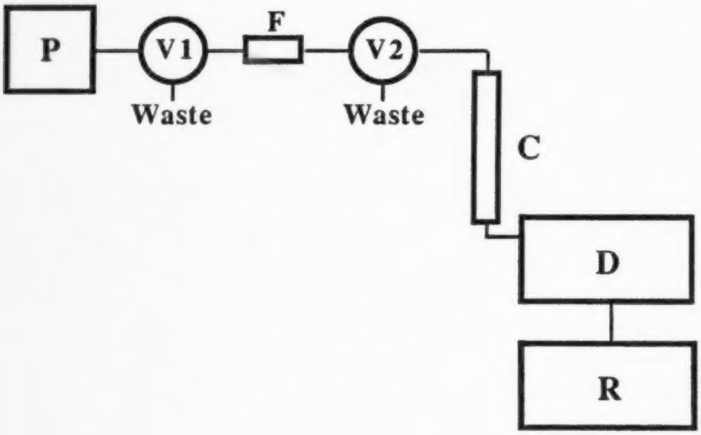

Figure 2.2 Indirect UV detection elution and frontal chromatography apparatus. P is a HPLC pump, V1 is a six position selector valve, F is a column inlet filter, V2 is a sample injection valve, C is an analytical column, D is a UV absorbance detector and R is a recorder.

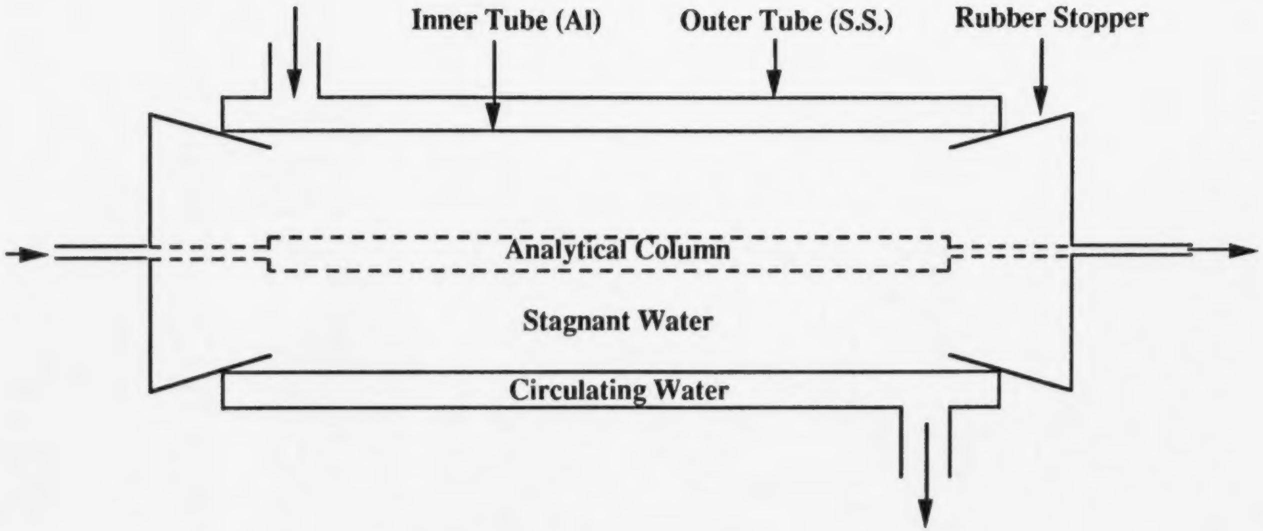
Inner Tube (Al)
Outer Tube (S.S.)
Rubber Stopper
Analytical Column
Stagnant Water
Circulating Water

Figure 2.3 Column jacket design for thermostatting the analytical column.

water filled the inner jacket and bathed the column contained therein, while thermostatted water (25.00 ± 0.04 °C) from the constant temperature bath circulated through the outer jacket. Mobile phases were also thermostatted by placing them in a constant temperature water bath (25.00 ± 0.04 °C).

The experimental parameters used to perform indirect UV detection are given in Table 2.1. In all experiments, the coarse zero on the detector was changed from 0 A.U. to -0.3 A.U. after probe breakthrough to offset the high absorbance to ≈ 0 A.U.

pH measurements were made with a Fisher Accumet Model 320 pH meter using a Fisher glass electrode (Catalog No. 13-639-3) and a Fisher saturated calomel reference electrode (Catalog No. 13-620-51). Any off-line absorbance measurements were made on a Model 8451A Hewlett Packard diode array spectrophotometer.

2.4.2 Mobile Phase and Sample Solutions

The mobile phase in indirect UV detection elution chromatography was 2.00×10^{-4} mol/L NS^- probe in 0.04 mol/L H_3PO_4 / 0.03 mol/L NaH_2PO_4 buffer at pH 2. It was prepared by dissolving ≈ 92 mg of NaNS in pH 2 buffer and diluting to 2.00 L with buffer. The buffer was prepared by dissolving 10.0 mL of phosphoric acid in ≈ 2 L of water. Approximately 1 mol/L NaOH was added to this solution until a pH of 2.0 was read by the pH meter.

Sample stock solutions were prepared by weighing a certain amount or pipetting a certain volume of chemical and diluting to volume with the mobile phase prepared above. Sample solutions to be injected into the indirect detection HPLC system were prepared by diluting known volumes of the appropriate stock solution with the mobile phase prepared above. In this manner, the sample solutions to be injected had the same mobile phase composition as that being pumped through the column.

Table 2.1 Experimental parameters for indirect UV detection elution and frontal chromatography.

Parameter	Value
Flow rate	1.0 mL/min
Detection wavelength	276 nm
Detector range (before probe breakthrough)	2.0 A.U.F.S. (a)
Detector range (after probe breakthrough) (b)	0.05 A.U.F.S. (a)
Recorder chart speed	0.25 cm/min
Column Temperature	25.0 ± 0.01 °C

(a) A.U.F.S. = absorbance units full scale

(b) For the frontal chromatography experiments, the detector range after probe breakthrough was 0.2 A.U.F.S. when 1.09×10^{-3} mol/L butanol was present in the mobile phase and was 1.0 A.U.F.S. when 1.09×10^{-2} mol/L butanol was present in the mobile phase.

To investigate the role of ionic strength on the elution chromatograms, sample solutions were prepared containing 2.00 x 10^{-4} mol/L NS^- in pH 2 buffer. The ionic strength was varied by changing the concentrations of H_3PO_4 and NaH_2PO_4 in the buffer while maintaining the pH at 2. In the high ionic strength sample, the concentrations were 0.084 mol/L H_3PO_4 and 0.063 mol/L NaH_2PO_4 while in the low ionic strength sample the concentrations were 0.021 mol/L H_3PO_4 and 0.015 mol/L NaH_2PO_4.

In the frontal chromatography experiments, the mobile phase was prepared as described above. In addition, mobile phases were prepared with the same composition as that above except that a certain concentration of butanol was also present. The concentration of butanol present was either 1.09 x 10^{-3} mol/L or 1.09 x 10^{-2} mol/L.

All mobile phases were filtered before use through a 0.45 µm pore size Nylon 66 filter (Alltech Associates Inc., Guelph, ON). They were degassed by sparging with helium (Linde), and then maintaining a blanket of helium over the solution.

2.5 Column Equilibration Technique

In these experiments the simultaneous sorption of a probe and a sample (either NS^-/ butanol or $NBTA^+$ / TBA^+) is studied by measuring the amount of each component sorbed on a small amount of the ODS packing at equilibrium. This simulates the situation in the sample zone during an indirect detection chromatogram and allows the effect of the sample on probe sorption to be investigated. Sorption isotherms for the sample and/or probe are also measured by this technique.

2.5.1 Precolumns

The precolumns were stainless steel guard columns (part no. 84550, Waters Chromatography) of varying dimensions. They were all dry-packed with Partisil-10 ODS-

3 bulk packing media (Batch no. 101409, Whatman, Inc., Clifton, NJ). Depending upon the experiment, different precolumns were used. They are identified by a number and described in Table 2.2. The holdup volume of each precolumn is determined by a separate procedure described in Section 2.5.5.

Precolumn #1 was used for the NS^- loading and elution experiments, the NS^- plus butanol loading and elution experiments and the butanol isotherm at low concentrations. Precolumn #2 was used for a NS^- loading and elution experiment with butanol present and for the NS^- isotherm without and with butanol present. Precolumn #3 was used for all other column equilibration experiments dealing with the NS^- and butanol case. Precolumn #4 was used in all the column equilibration experiments for the $NBTA^+$ and TBA^+ case.

2.5.2 Column Equilibration Apparatus and Procedure

The column equilibration apparatus is shown in Figure 2.4. It consists of a pump P1 (Model 501, Waters Chromatography) for the probe and/or sample solution, a pump P2 (Model 590, Waters Chromatography) for the eluent, and a precolumn C which contains the ODS packing. The precolumn is inserted in place of the injection loop of valve V. The precolumn and injection valve are placed in a water bath whose temperature is maintained at 25.00 ± 0.04 °C.

The basic procedure for the column equilibration experiment is as follows. With valve V in the "load" position (indicated by the dashed lines in Figure 2.4), a solution containing probe and/or sample is pumped through the precolumn to waste until equilibrium is achieved between the ODS packing and solution. This is the *loading* step. Valve V is then switched to the "inject" position (indicated by the solid lines in Figure 2.4) and eluent is pumped through the precolumn to elute whatever has sorbed on the packing. The eluate is collected for a certain period of time to ensure complete elution. It is collected in a volumetric flask up to the calibration mark or it is collected in a volumetric flask for a

Table 2.2 Description of precolumns used in column equilibration experiments.

Identification Number	Dimensions	Weight of Packing (g)
1	2.0- x 0.40-cm i.d.	0.1540
2	2.0- x 0.30-cm i.d.	0.0871
3	2.0- x 0.40-cm i.d.	0.1510
4	2.0- x 0.20-cm i.d.	0.0388

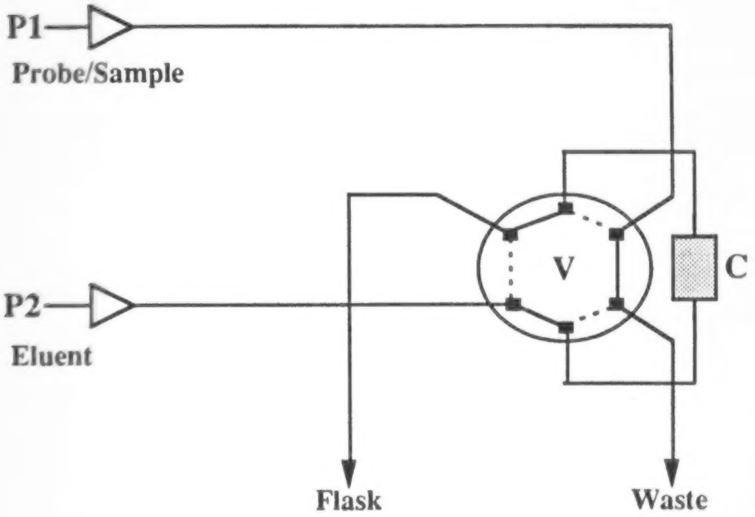
P1
Probe/Sample
P2
Eluent
V
C
Flask
Waste

Figure 2.4 Column equilibration apparatus. P1 and P2 are HPLC pumps, V is a sample injection valve and C is a small precolumn packed with the ODS packing.

certain period of time and then diluted to volume with eluent. This is the *elution* step. The total amounts of each species eluted from the precolumn, including that in the holdup volume, are then measured by determining the concentration of each of the species in the solution in the volumetric flask.

2.5.3 Procedure and Solution for Case I: Neutral Sample (Butanol) and Ionic Probe (NS^-)

For the measurement of the NS^- loading curve, a solution of NS^- was pumped through the precolumn for various times and at various flow rates (1, 2 or 3 mL/min). For the measurement of the NS^- and butanol loading curves, a solution containing NS^- and butanol was pumped through the precolumn for various times at a flow rate of 3 mL/min. In both cases, the eluent was pumped at a flow rate of 1 mL/min and collected in a 10 mL volumetric flask up to the calibration mark.

To determine the volume of eluent that is required to completely elute the sorbed NS^- from the precolumn, a solution of NS^- was pumped through the precolumn until equilibrium was achieved, as determined by the loading experiment. Eluent was then pumped through the precolumn at a flow rate of 1 mL/min and collected in 1 mL fractions. Each fraction was collected in a 10 mL volumetric flask, after which it was diluted to volume with eluent. Three fractions were collected for a total eluent volume of 3 mL. To determine the volume of eluent required to completely elute both sorbed NS^- and butanol from the precolumn, a solution containing NS^- and butanol was loaded onto the precolumn for 2 hours at 3 mL/min. Eluent was then pumped through the precolumn at a flow rate of 1 mL/min and collected in 2 mL fractions. Each fraction was collected in a 10 mL volumetric flask, after which it was diluted to volume with eluent. Five fractions were collected for a total eluent volume of 10 mL.

In the butanol isotherm experiment, solutions of butanol were loaded onto the precolumn for 2 hours at 3 mL/min. Eluent was then pumped through the precolumn at a flow rate of 1 mL/min and collected in a 10 mL volumetric flask to which pentanol (GC internal standard) dissolved in $\approx$ 1 mL of eluent was added. Eluent was collected up to the calibration mark of the volumetric flask.

In the NS^- isotherm without and with butanol present and in the experiments determining the effect of NS^- on butanol sorption and *vice versa*, solutions containing NS^- alone or NS^- plus butanol were loaded onto the precolumn at a flow rate of 3 mL/min for 20 min (*i.e.* 60 mL) and then at a flow rate of 1 mL/min for 100 min (*i.e.* 100 mL) for a total time of 2 hours and a total volume of 160 mL. In all of these experiments the eluent was pumped through the precolumn at a flow rate of 1 mL/min for 10 minutes. It was either collected in a 10 mL volumetric flask up to the calibration mark or it was collected in a larger volumetric flask and then diluted to volume with eluent. Pentanol dissolved in $\approx$ 1 mL of eluent was added to the volumetric flask in which the eluent was collected.

The concentration of NS^- in all the solutions collected from the various column equilibration experiments was determined spectrophotometrically at 276 nm on a Model 8451A Hewlett Packard diode array spectrophotometer. The concentration of butanol in the solutions was determined by gas chromatography using a procedure described in Section 2.6.

Depending upon the experiment being done, the sample solutions contained various concentrations of NS^- and/or butanol in 0.04 mol/L H_3PO_4 / 0.03 mol/L NaH_2PO_4 buffer at pH2. For the various experiments, the following concentrations were used: (a) For the NS^- loading and elution experiments, the NS^- concentration was 1.01×10^{-4} mol/L and 4.08×10^{-4} mol/L. (b) For the NS^- plus butanol loading and elution experiments, the NS^- concentration was 2.00×10^{-4} mol/L when precolumn #1 was used and it was 1.00×10^{-4} mol/L when precolumn #2 was used. The butanol concentration was 2.18×10^{-4} mol/L when precolumn #1 was used and it was 2.18×10^{-2} mol/L when precolumn #2 was used.

(c) For measurement of the butanol isotherm, the butanol concentration was varied from 0 to 0.654 mol/L. (d) In the study of the effect of NS^- on butanol sorption, the butanol concentration was kept constant at 1.09×10^{-3} mol/L and the NS^- concentration was varied from 0 to 0.157 mol/L. (e) For measurement of the probe isotherms in the absence and in the presence of butanol, the butanol concentration was kept constant at 0 and at 2.18×10^{-2} mol/L, respectively, and the NS^- concentration was varied from 0 to 3.62×10^{-3} mol/L. (f) In the study of the effect of butanol on NS^- sorption, the NS^- concentration was kept constant at 2.00×10^{-4} mol/L while the butanol concentration was varied from 0 to 4.36×10^{-2} mol/L.

The eluent used in these series of column equilibration experiments was methanol/water (1:1 v/v). Probe/sample and eluent solutions were filtered before use through a 0.45 μm pore size Nylon 66 filter (Alltech Associates Inc., Guelph, ON). Eluent and sample solutions were degassed by sparging with helium (Linde), after which a blanket of helium was maintained over the solution.

2.5.4 Procedure and Solutions for Case II: Cationic Sample (TBA^+) and Cationic Probe ($NBTA^+$)

Table 2.3 gives the experimental parameters and solution concentrations that were used to measure the loading curve for $NBTA^+$ and to determine the volume of eluent required to completely elute sorbed $NBTA^+$ from the precolumn. Also given in Table 2.3 are the experimental parameters and solution concentrations that were used to measure the $NBTA^+$ and TBA^+ loading curves when both were present in solution and to determine the volume of eluent required to completely elute both sorbed components from the precolumn. Each solution had a constant concentration of sodium chloride present as indicated in column 2 of Table 2.3 and each had its pH adjusted to 5.0 with 1×10^{-4} mol/L acetic acid/sodium acetate buffer.

Table 2.3 Experimental parameters for the determination of loading and elution volumes in column equilibration experiments for $NBTA^+$ and TBA^+.

Experiment	[NaCl] (mol/L)	$[NBTA^+] \times 10^4$ (mol/L)	$[TBA^+] \times 10^5$ (mol/L)	Loading Time (min) [a]	Eluent Time (min) [b]
$NBTA^+$ alone	0.050	1.97	-	varied	10
Loading	0.500	2.09			
$NBTA^+$ alone	0.050	1.97	-	30	10 [c]
Elution	0.500	2.09			
$NBTA^+$ plus	0.050	9.87	1.00	varied	10 [d]
TBA^+ Loading	0.500	9.31	1.00		
$NBTA^+$ plus	0.050	9.87	1.00	75	10 [e]
TBA^+ Elution	0.500	9.31	1.00		

(a) Loading flow rate was 2.0 mL/min.

(b) Eluent flow rate was 1.0 mL/min.

(c) Five, 2 mL fractions were collected and each fraction was diluted to a final volume of 10 mL. Total eluent volume was 10 mL.

(d) The collected eluate was diluted to a final volume of 25 mL.

(e) Five, 2 mL fractions were collected and each fraction was diluted to a final volume of 25 mL. Total eluent volume was 10 mL.

For the measurement of the NBTA$^+$ sorption isotherms, five series of five solutions each were prepared with water as the solvent. Each series contained a range of NBTA$^+$ concentrations from 2.00 x 10^{-3} mol/L to 2.00 x 10^{-2} mol/L and was characterized by the fact that it contained one of the following constant concentrations of sodium chloride: 0.050, 0.070, 0.100, 0.300 and 0.500 mol/L. Each of these twenty-five solutions had its pH adjusted to 5.0 with 1 x 10^{-4} mol/L acetic acid/sodium acetate buffer. Column equilibration experiments were performed in triplicate on each solution.

In the measurement of the NBTA$^+$ sorption isotherms, the solutions prepared above were pumped through the precolumn for 30 minutes at a flow rate of 2 mL/min (*i.e.* 60 mL). Eluent was then pumped through the precolumn at a flow rate of 1 mL/min for 10 minutes and collected in a 25 mL volumetric flask, after which it was diluted to volume with eluent.

For the studies of the simultaneous sorption of NBTA$^+$ and TBA$^+$ in the presence of one another, another five series of five solutions each were prepared in aqueous 1 x 10^{-4} mol/L acetic acid/sodium acetate buffer, pH = 5.0. All five solutions in any one series contained one of the five sodium chloride concentrations listed above. All twenty-five solutions contained the same concentration of NBTA$^+$, 1.86 x 10^{-3} mol/L, while within each series, the TBA$^+$ concentration was varied from 5.00 x 10^{-6} to 5.00 x 10^{-4} mol/L. Column equilibration experiments were performed in duplicate on these solutions.

In studying the effect of TBA$^+$ on NBTA$^+$ sorption, solutions containing both components were pumped through the precolumn at a flow rate of 2 mL/min for 75 minutes (*i.e.* 150 mL). Eluent was then pumped through the precolumn at a flow rate of 1 mL/min and collected in a 10 mL volumetric flask up to the calibration mark except for the lowest TBA$^+$ concentration used at each NaCl concentration. It was collected for 10 minutes at a flow rate of 1 mL/min in a 25 mL volumetric flask and then diluted to volume with eluent.

In all of the above experiments, the concentration of NBTA$^+$ in the solutions collected in the column equilibration experiments was determined spectrophotometrically at

260 nm on a Model 8451A Hewlett Packard diode array spectrophotometer. The concentration of TBA^+ in the solutions was determined by ion pair solvent extraction of TBA^+-picrate using solvent extraction/flow injection analysis. The procedure is described in Section 2.7.

The eluent used in this series of column equilibration experiments was methanol/water (1:1 v/v) containing 0.010 mol/L sodium chloride [34]. All probe and/or sample solutions and eluent solutions were filtered through a 0.45 µm pore size Nylon-66 filter (Alltech Associates Inc., Guelph,ON) before being pumped through the precolumn. All solutions were also degassed by sparging with helium (Linde), after which a blanket of helium was maintained over the solution.

2.5.5 Holdup Volume Measurement

The holdup volume includes the void volume of the packed bed and frits and the volume of the connecting tubing. In the holdup volume measurement, water is used as an unretained component and is determined by gas chromatography in ethanol solvent using methanol as an internal standard.

2.5.5.1 Apparatus and Procedure

The apparatus used to determine the holdup volume of the precolumns is the same as that shown in Figure 2.4 and described in Section 2.5.2. In this case, the solution pumped through the precolumn is water and the eluent is ethanol. With valve V in the "load" position (dashed lines), water is pumped through the precolumn at a flow rate of 1.0 mL/min for 15 min. Valve V is then switched to the "elute" position (solid lines) and ethanol is pumped through the precolumn at a flow rate of 1.0 mL/min into a 10 mL volumetric flask which contains a certain volume of methanol internal standard diluted in ≈

1 mL of ethanol. For precolumns #1 and #3, 0.50 mL of methanol was used, for precolumn #2, 0.40 mL of methanol was used and for precolumn #4, 0.20 mL of methanol was used. Eluate was collected up to the calibration mark of the volumetric flask. The concentration of water in the volumetric flask was determined by gas chromatography which is described below.

2.5.5.2 Gas Chromatography of Water for Holdup Volume Measurement

Gas chromatography was performed on a 2.9 m x 1.6 mm i.d. stainless steel column packed with 50/80 mesh Porapak Q-S (Waters Chromatography) using a Model 3700 gas chromatograph (Varian Associates) with a thermal conductivity detector (TCD). The parameters used for the holdup volume determination are given in Table 2.4.

Standards were prepared by diluting known volumes of water, along with methanol internal standard, with ethanol in 10 mL volumetric flasks. The range of concentrations used in the standards was 0 to 0.30 mL of water for precolumns #1, #2 and #3 and 0 to 0.10 mL of water for precolumn #4.

2.5.6 Calibration

In the column equilibration studies using NS^- probe, passage of sample solution through the precolumn for long periods of time was found to slowly deteriorate the ODS packing such that the effective number of sorption sites was reduced. Although no evidence was found for dissolution of the silica substrate itself and the volume of the packing in the column was not visibly reduced, this decrease in the number of sorption sites can formally be taken into account as a decrease in the weight of the stationary phase (W_S) in equation 1.2. To monitor the decrease in W_S, a solution which contained 2.00×10^{-4} mol/L NS^- in pH 2 buffer was used as a standard and was run between experiments.

Table 2.4 GC parameters for the determination of water in the measurement of precolumn holdup volumes.

Parameter	**Value**
Carrier gas	Helium
Carrier flow rate	40 mL/min
Column temperature	110 °C
Injector temperature	200 °C
TCD detector temperature	220 °C
TCD filament current	250 mA
Injection volume	1 μL

Using the amount of NS^- sorbed from this standard at any time, t, the correct weight of packing ($W_{S,t}$) to be used in place of W_S in equation 1.2 was calculated as

$$W_{S,t} = \frac{n_{NS,t}}{n_{NS,o}} W_{S,o} \tag{2.1}$$

where $n_{NS,t}$ is the amount of NS^- sorbed from the standard solution at time t, $n_{NS,o}$ is the amount of NS^- sorbed from the standard solution by the freshly packed precolumn, and $W_{S,o}$ is the actual weight of packing in the precolumn. The amount $W_{S,t}$ is equivalent to the effective weight of packing in the precolumn, W_{eff}.

No such calibration was necessary for the column equilibration experiments using $NBTA^+$ and TBA^+ since W_S did not change.

2.6 Gas Chromatography for Off-Line Determination of Butanol

In the column equilibration experiments described above, when butanol was eluted from the precolumn, a small amount of butanol was present in a large amount of methanol and water (*i.e.* eluent). Therefore, a method was required to determine small amounts of butanol under these conditions. Gas chromatography with flame ionization detection was found to be a suitable technique.

2.6.1 Apparatus and Procedure

The column used to determine butanol was a 3.0 m x 2.1 mm i.d. stainless steel column packed with 7% w/w Carbowax 20M (F&M Scientific Corp.) on Chromosorb WAW-DMCS mesh size 100/120 (Manville). The stationary phase was prepared using a procedure described in reference 58. Peak areas were measured with a Spectra–Physics

Autolab minigrator. The parameters used for the determination of butanol are given in Table 2.5.

2.6.2 Standard Solutions

Depending upon the concentration of butanol in the solution pumped through the precolumn, different concentration ranges of butanol were used in the standards and different concentrations of pentanol were used as an internal standard. All standards were prepared using methanol/water (1:1 v/v) as solvent. In the measurement of the butanol isotherm, when the butanol concentration in the solution pumped through the precolumn ranged from 0 to 2.18×10^{-2} mol/L, the standard solutions contained 0 to 4.90×10^{-3} mol/L butanol and 1.84×10^{-3} mol/L pentanol. When the butanol concentration ranged from 7.63×10^{-2} to 0.654 mol/L, the standard solutions contained 0 to 6.54×10^{-2} mol/L butanol and 0.0110 mol/L pentanol. For the effect of butanol on probe sorption and *vice versa*, when the butanol concentration in the solution pumped through the precolumn ranged from 0 to 1.09×10^{-3} mol/L, the standard solutions contained 0 to 3.27×10^{-4} mol/L butanol and 1.84×10^{-4} mol/L pentanol. When the butanol concentration in solution ranged from 5.45×10^{-3} to 4.36×10^{-2} mol/L, the standard solutions contained 0 to 7.63×10^{-3} mol/L butanol and 2.76×10^{-3} mol/L pentanol. Note that in the collected eluate solutions from the column equilibration experiments, the concentration of pentanol internal standard was the same as in the corresponding standard solutions.

Table 2.5 GC parameters for the determination of butanol.

Parameter	Value
Carrier gas	Helium
Carrier flow rate	30 mL/min
Air flow rate	300 mL/min
Hydrogen flow rate	30 mL/min
Injector temperature	200 °C
FID detector temperature	200 °C
Injection volume	5 µL
Temperature program	Hold 65 °C for 6 min Increase 4 °C/min for 2 min Increase 3 °C/min for remainder of chromatogram

2.7 Solvent Extraction/Flow Injection Analysis (SE/FIA) for Off-Line Determination of TBA$^+$

2.7.1 Principles of SE/FIA

Ion pair solvent extraction is a technique that is used for the analysis of ionic solutes in water [7,59]. It involves the formation of an ion pair between an ionic solute and an ion of opposite charge (*i.e.* pairing ion) which extracts into a water immiscible solvent (*i.e.* organic phase). By using an ion pairing reagent which absorbs UV or visible light, the amount of solute can be determined from an absorbance measurement of the organic phase. This technique has been used for the determination of amines and quaternary ammonium ions [60] where picrate is used as the pairing ion and dichloromethane is used as the organic phase. The concentration of ion pairs in the organic phase is determined by measuring its absorbance at 375 nm.

Liquid-liquid solvent extraction was automated into a flow injection analysis configuration by Karlberg and Thelander [61] and by Bergamin et al [62] in 1978. This technique is referred to as solvent extraction/flow injection analysis (SE/FIA) [63,64]. In a simple ion pair SE/FIA system, the ionic sample is introduced *via* an injection valve into a flowing aqueous phase which contains an excess of the ion pairing reagent. The aqueous phase is then merged with the flowing organic phase, typically at a "tee" junction, to produce alternating segments of aqueous phase and organic phase. These segments flow through a length of Teflon tubing (extraction coil) where the extraction occurs. The sample, which is initially in the aqueous segments, will extract into the adjoining organic segments as it flows along the extraction coil. After the extraction is complete, the two-phase flow enters a phase separator which allows only a portion of the organic phase to enter a detector where its absorbance is monitored. Porous membrane phase separators are the most popular type of phase separators [63,64]. They are based on selective permeability to the phase which wets the membrane material. For example, porous Teflon is wetted by organic solvents while porous paper is wetted by aqueous phases.

In the present study, SE/FIA based on TBA^+-picrate ion pair solvent extraction is used for the off-line determination of TBA^+ in the solutions collected in the column equilibration experiments. Although $NBTA^+$ is also present in the solutions, it has a very low extraction constant and does not appreciably extract to create an interference.

2.7.2 Apparatus and Procedure

A schematic diagram of the SE/FIA apparatus is shown is Figure 2.5. The reagent solution and solvents are contained in 2 L reagent bottles which are placed inside specially constructed sealed aluminum containers. Constant pressure (10 psig) from a nitrogen cylinder (Linde) is applied to the aluminum cylinders to produce solvent flow. Valves V1 (part no. CAV2031, Laboratory Data Control (LDC), Riviera Beach, FL) are 3-way valves which are used to stop or start the flow of a particular stream. Valve V2 (part no. CAV2031, LDC , Riviera Beach, FL) is a 3-way valve which allows either methanol or chloroform to be selected. Sample is introduced into a water stream first through a sample injection valve V3 equipped with a 50 µL loop (Cheminert R-6031 SWP, LDC). The aqueous reagent (*i.e.* picrate solution) joins the water stream at tee-fitting T1 (part no. CJ-3031, LDC). The combined aqueous stream then joins the chloroform stream at tee-fitting T2 and the resulting two-phase flow passes through a 190 cm long extraction coil constructed of 0.8 mm i.d. Teflon tubing where extraction of the ion pairs from the aqueous segments to the chloroform segments occurs. After passage through the extraction coil, part of the organic phase is separated from the aqueous/organic stream using two layers of Teflon membrane with pore size 10-20 µm (Zitex, part no. E249-122, Chemplast Inc., Wayne, NJ) inside the membrane phase separator M. Finally, the organic phase passes through a spectrophotometric detector D (Model 481, Waters Chromatography,

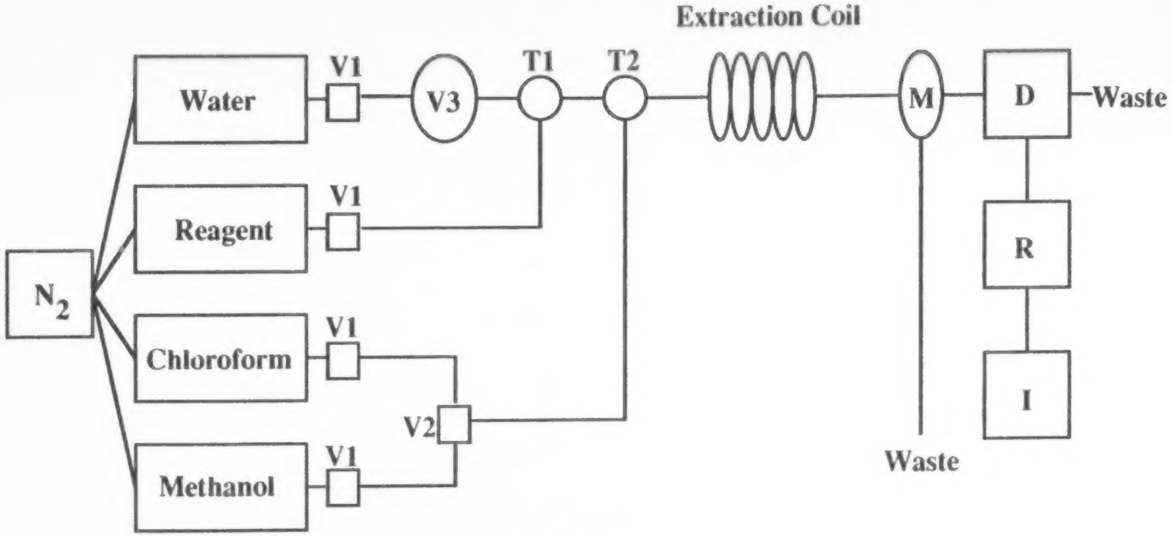
Extraction Coil
N_2
Water
Reagent
Chloroform
Methanol
V1
V1
V1
V1
V2
V3
T1
T2
M
D
R
I
Waste
Waste

Figure 2.5 Solvent extraction/flow injection analysis system for the determination of TBA^+. V1 and V2 are 3-way valves, V3 is an injection valve, T1 and T2 are tee-fittings, M is a membrane phase separator, D is a detector, R is a recorder and I is an integrator.

Milford, MA) whose wavelength is set at 368 nm. A Recordall Series 5000 recorder R (Fisher Scientific Co.) is used to record the peaks and a Hewlett Packard Model 3390A integrator I is used to measure the peak areas.

The flow rates used for the determination were as follows. Total chloroform flow rate: 1.4 mL/min; total aqueous flow rate: 1.0 mL/min; and chloroform flow rate through the membrane phase separator: 0.50 mL/min.

2.7.3 Reagent and Standard Solutions

Picric acid was converted to sodium picrate by adding an appropriate amount of sodium hydroxide to the picric acid solution. The reagent solution contained 0.005 mol/L sodium picrate. The pH was adjusted to 5 with 1×10^{-4} mol/L acetic acid/sodium acetate buffer and its ionic strength was adjusted to 0.10 mol/L with sodium chloride.

The solvent used to prepare the standards was methanol/water (1:1 v/v) containing 0.010 mol/L sodium chloride. The TBA^+ concentration in the standards ranged from 5.00×10^{-6} to 1.00×10^{-4} mol/L.

To test if $NBTA^+$ interfered in the determination of TBA^+ by SE/FIA, four solutions were prepared and injected into the SE/FIA system, each containing a constant concentration of 9.86×10^{-5} mol/L TBA^+, and one of the following concentrations of $NBTA^+$: 0, 9.85×10^{-6}, 9.85×10^{-5} and 9.85×10^{-4} mol/L.

Chapter 3

Indirect UV Detection Chromatography

3.1 Introduction

There are several examples in the literature in which indirect UV detection HPLC has been used to detect non-UV absorbing sample species. A variety of compounds have been used as probes and samples. Schill and co-workers primarily used naphthalene-2-sulfonate and 1-phenethyl-2-picolinium as an anionic and cationic probe, respectively [4,5,26,27,65]. Various straight chain amines, sulfates, sulfonates and alcohols were used as sample species.

Naphthalene-2-sulfonate has been used to indirectly detect amino acids [4] and more complex species such as metheneamine [66]. Amino acids have been indirectly detected using copper ions as a probe in which the formation of amino acid-copper complexes brings about the indirect detection [67]. Cationic probes have been used to indirectly detect carboxylic acids [4] and bile acids [68].

The technique has been applied to inorganic sample species. Inorganic anions have been detected using both organic cations [69-71] and iron (II) complexes as probes [72] while lanthanide ions have been detected using various sulfonic acids as probes [73].

Although indirect UV detection has mainly been used with ionic probe and sample species, it has also been applied to nonionic systems. Several neutral probes such as salicylamide [25,74], benzamide [75,76], anthracene [77], *p*-nitrophenol [78], toluene [79], theophylline [80] and benzyl alcohol [81] have been used to detect neutral sample species such as alcohols, esters and amides.

In addition to its use in quantitative analysis, the technique of indirect detection has been used in the study of system peaks [82-91]. System peaks are generally regarded as a nuisance in quantitative analysis since they can overlap with sample peaks in the chromatogram as well as influence the magnitude of the indirect detection response. However, several workers are interested in the information that can be obtained from them [87,88] as well as how they interact with the sample zone to bring about variations in response and peak shape [82,83,91].

As has been stated previously, the main requirement necessary to carry out indirect detection is the addition of a detectable component to the mobile phase. Although this thesis is primarily concerned with indirect UV detection, the technique has been applied to other modes of detection and to other forms of chromatography.

The principles for indirect fluorescence detection are the same as those for indirect UV detection except that fluorescence rather than UV absorbance is measured [92-96]. Indirect fluorescence detection has primarily found use in micro-column HPLC and in capillary zone electrophoresis.

One of the earliest applications of indirect detection was in ion exchange chromatography where a UV absorbing coion is added to the eluent [97-99]. As the probe exchanges for sample ions sorbed on the resin, negative peaks appear in the chromatogram at the sample retention time. Indirect conductivity detection has been used in ion exclusion chromatography where the sample species alter the conductivity of the the eluent [100]. Neutral sample species reduce the conductivity and give rise to negative peaks in the chromatogram.

Several different types of RPBPs have been used as the stationary phase in indirect detection systems [25,65,73,74,101,102]. In some cases it was found that residual silanol groups play a role in the separation [26]. By using a RPBP with a high surface coverage, effects from residual silanol groups can be minimized. Since Whatman Partisil-10 ODS-3 is reported to have at least 95% surface coverage, it was chosen as the stationary phase in all studies.

The primary purpose of the research described in this chapter was to observe indirect detection in chromatograms obtained using this particular RPBP and to achieve familiarity with the technique, in the process. The goal was to confirm the response patterns and other observations that have been described in the literature and that were presented in Chapter 1. Naphthalene-2-sulfonate was chosen as the probe in these studies since it has been widely used [4,5,26,27,65,66] and studied [103] as a probe for indirect UV detection. Both elution chromatography and frontal chromatography were done using indirect UV detection.

3.2 Theory

3.2.1 Sorption Isotherms

The sorption of a solute *i* onto a RPBP from a solution is usually presented in the form of a sorption isotherm [104-107]. A sorption isotherm is a plot of the solute concentration in the stationary phase, $C_{s,i}$ (mol/kg), *versus* the solute concentration in the mobile phase, $C_{m,i}$ (mol/L). A typical sorption isotherm is shown in Figure 3.1.

The distribution coefficient of a solute, $K_{D,i}$, is defined as follows.

$$K_{D,i} = \frac{C_{s,i}}{C_{m,i}} \tag{3.1}$$

Its value can be determined from the sorption isotherm, for any solute concentration in the mobile phase, by calculating the slope of the straight line drawn through the origin and the

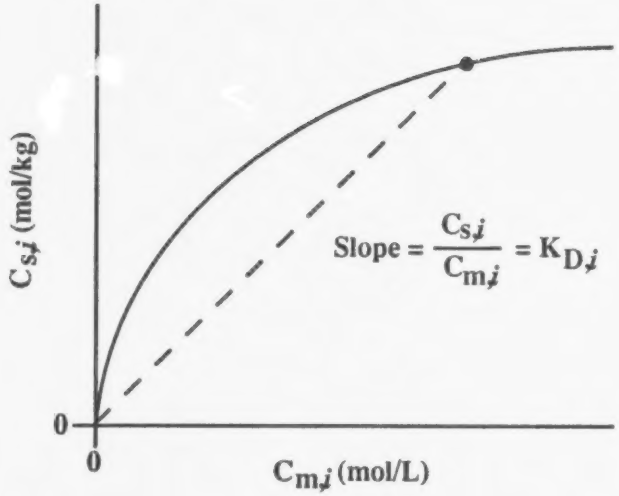

Figure 3.1 Hypothetical sorption isotherm (solid line) for a solute *i*. The distribution coefficient at any point is the ratio $C_{s,i}/C_{m,i}$.

point on the isotherm corresponding to the particular mobile phase concentration. This is illustrated in Figure 3.1.

There are generally three types of simple isotherm shapes that are observed experimentally [104-107]. They are shown in Figure 3.2 and are categorized by how the distribution coefficient varies with solute concentration in the mobile phase. For a linear isotherm, $K_{D,i}$ is constant at all $C_{m,i}$ (Figure 3.2a). In a convex isotherm, $K_{D,i}$ decreases as $C_{m,i}$ increases (Figure 3.2b) while in a concave isotherm, $K_{D,i}$ increases as $C_{m,i}$ increases (Figure 3.2c). It should be noted that both convex and concave isotherms become linear at very low $C_{m,i}$. Chromatography done in the linear region of the isotherm is referred to as linear chromatography while chromatography done outside the linear region of the isotherm is referred to as nonlinear chromatography.

A convex isotherm is the most common isotherm shape observed in chromatography. It is called a Langmuir isotherm when it reaches a plateau and can be described by the Langmuir equation [104,105,107]:

$$C_{s,i} = \frac{K\, C_{s,i,\max}\, C_{m,i}}{1 + K\, C_{m,i}} \tag{3.2}$$

In the equation K is a constant and $C_{s,i,\max}$ is the maximum concentration of solute in the stationary phase. Equation 3.2 can also be written in the following linear form.

$$\frac{1}{C_{s,i}} = \frac{1}{K\, C_{s,i,\max}\, C_{m,i}} + \frac{1}{C_{s,i,\max}} \tag{3.3}$$

According to this equation, a plot of $1/C_{s,i}$ *versus* $1/C_{m,i}$ is a straight line if the isotherm is Langmuirian. The basis for the Langmuir equation is that there is only a limited number of sorption sites for the solute molecules. When these sites are all occupied, solute can no longer sorb and the isotherm therefore approaches a constant value.

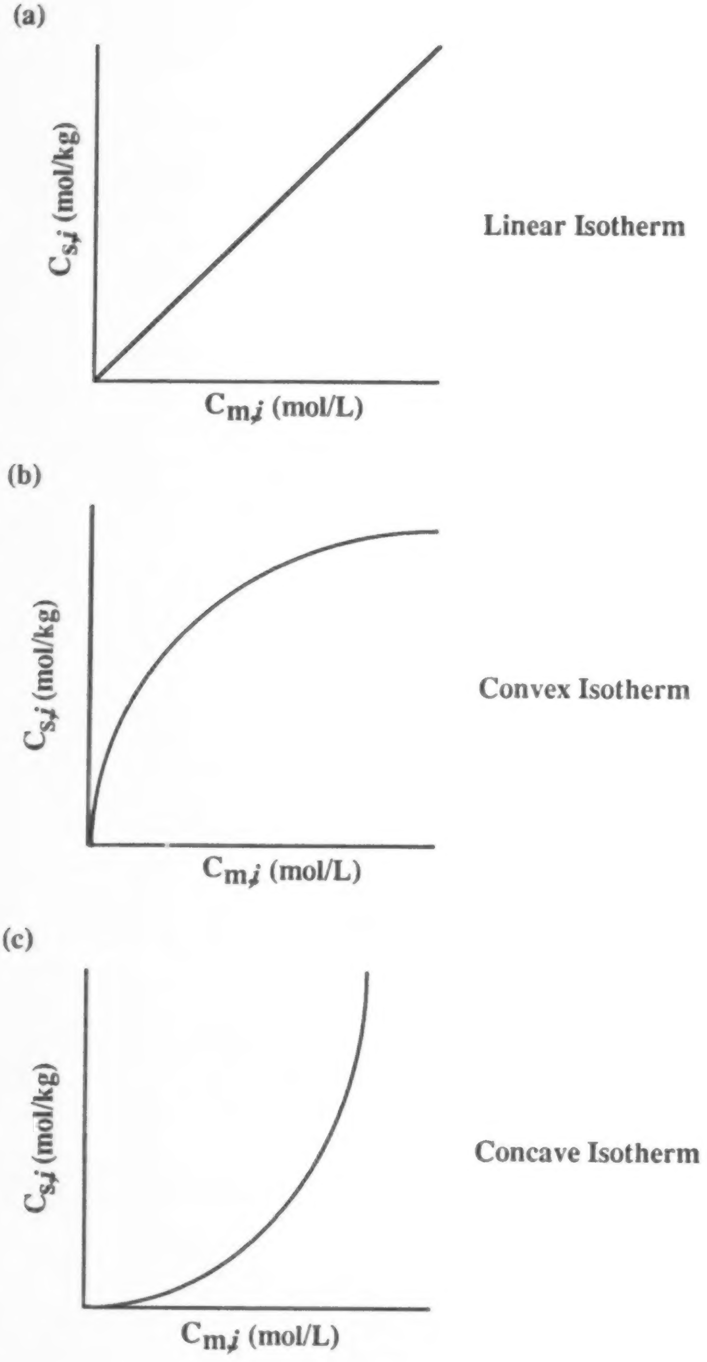

Figure 3.2 Common isotherm shapes in chromatography.

Convex isotherms can sometimes be described by the Freundlich equation [104,107]:

$$C_{s,i} = a\,(C_{m,i})^{b} \qquad (3.4)$$

where a and b (<1) are constants. Equation 3.4 can be written in the following linear form.

$$\ln C_{s,i} = \ln a + b \ln C_{m,i} \qquad (3.5)$$

A plot of $\ln C_{s,i}$ *versus* $\ln C_{m,i}$ is therefore a straight line if the isotherm follows the Freundlich equation. A Freundlich isotherm does not approach a limiting value. The Freundlich equation simply serves as an empirical fitting function.

3.2.2 Rate of Travel of Sample Molecules and of Probe Concentration Pulses

In indirect detection, a sample is injected onto a column and produces a disturbance in the probe equilibrium which gives rise to a probe pulse in which the probe concentration is either lower or higher than its concentration in the absence of sample. Figure 3.3 illustrates the various cases. In Figure 3.3a, a sample is injected onto a column in which there is no probe present. In Figure 3.3b and Figure 3.3c, a positive probe concentration pulse (*i.e.* higher probe concentration) and a negative probe concentration pulse (*i.e.* lower probe concentration), respectively, are injected onto a column which has come to equilibrium with probe. The equilibrium amount of probe in the region outside the injected zone is designated as C_{eq}. Figure 3.3d illustrates the case of indirect detection where a sample is injected onto a column that is at equilibrium with probe. In this particular example, a positive probe concentration pulse, whose retention time is longer than the

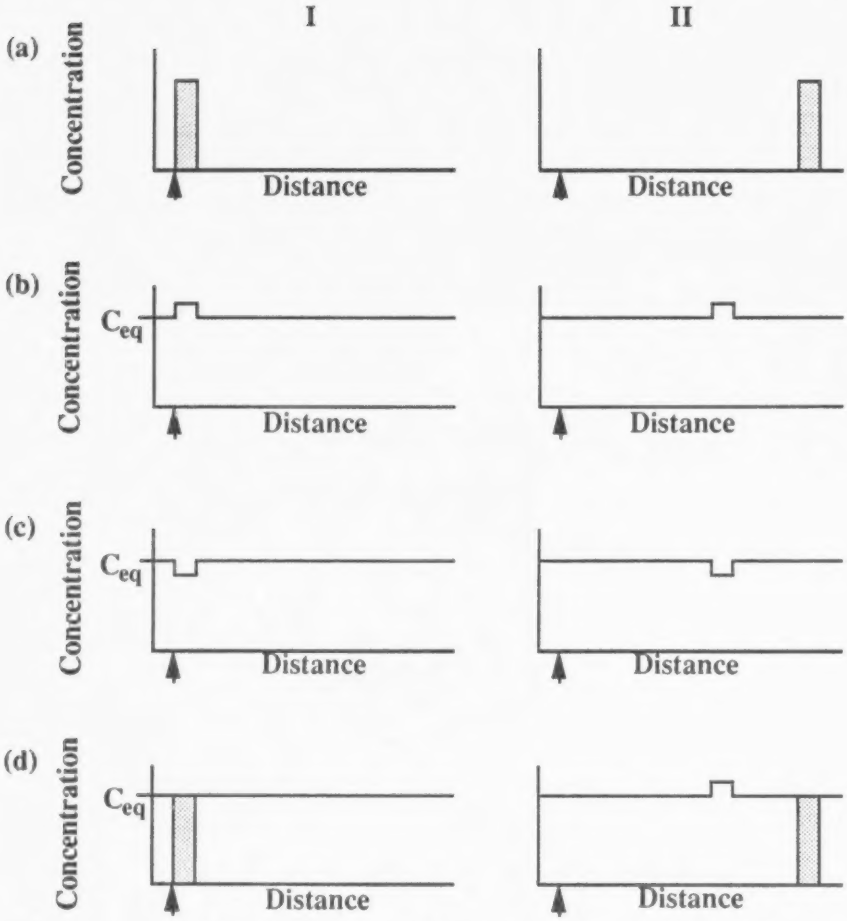

Figure 3.3 Rate of travel of sample molecules and of probe concentration pulses injected onto a column. The plots in column I are at the time of injection (indicated by arrow) while the plots in column II are some time after injection. Bandbroadening is neglected. (a) Injection of sample molecules onto a column which has not been equilibrated with probe. (b) Injection of a probe concentration pulse whose concentration is higher than the equilibrium probe concentration on the column, C_{eq}. (c) Injection of a probe concentration pulse whose concentration is lower than C_{eq}. (d) Injection of sample molecules onto a column which has come to equilibrium with probe.

sample retention time, is produced. Recall that both positive and negative probe concentration pulses can be produced by the injection of sample in indirect detection and that probe concentration pulses can have a shorter or longer retention time than the sample.

The rate of travel of sample molecules injected onto a column, v_m, is governed by the distribution coefficient (Figure 3.1) according to the following equation [108]:

$$v_m = \frac{1}{K_{D,i}\left(\frac{W_{SP}}{V_{MP}}\right) + 1} \times v_{MP} \tag{3.6}$$

where v_{MP} is the rate of travel of the mobile phase, W_{SP} is the weight of stationary phase in the column and V_{MP} is the volume of mobile phase in the column. The ratio W_{SP}/V_{MP} is the so-called phase ratio.

The propagation rate, v_p, of a probe concentration pulse which is either injected onto a column (Figures 3.3b and 3.3c) or which is produced by a sample injection (Figure 3.3d) is governed by the slope of the tangent to the isotherm, $\Delta C_{s,i}/\Delta C_{m,i}$, at $C_{m,i}$ according to the following equation [108]:

$$v_p = \frac{1}{\left(\frac{\Delta\ C_{s,i}}{\Delta\ C_{m,i}}\right)\left(\frac{W_{SP}}{V_{MP}}\right) + 1} \times v_{MP} \tag{3.7}$$

The calculation of $\Delta C_{s,i}/\Delta C_{m,i}$ is illustrated in Figure 3.4.

It is instructive to compare the migration rate of a zone of (sample) compound *i* upon its injection onto a column that initially contains no *i* with the migration rate of a pulse of the same compound *i* (now a probe) injected at a lower or higher concentration onto a column that initially was equilibrated with compound *i*. Comparing equations 3.6 and 3.7, the rate of travel of sample molecules and of a probe concentration pulse composed of the same compound will be identical only under the conditions of linear

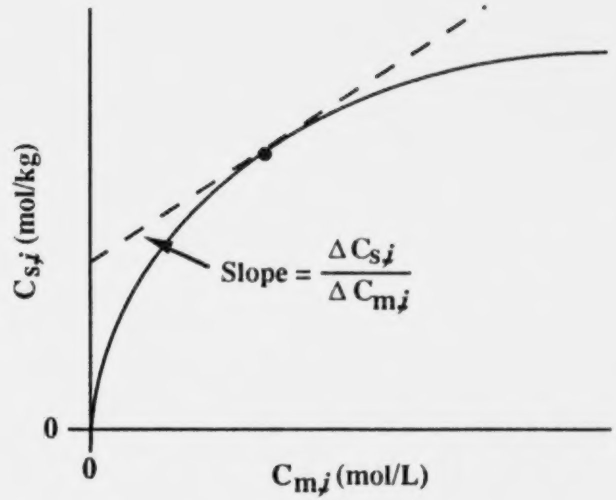

Figure 3.4 Calculation of the distribution coefficient for a probe concentration pulse.

chromatography (*i.e.* $K_{D,i}$ is constant). In the case of nonlinear chromatography, the two rates will not be the same. However, if the probe concentration in the injected pulse is only slightly different than the concentration of probe at equilibrium with the column, then the term $(\Delta C_{s,i}/\Delta C_{m,i})$ in equation 3.7 will be constant, but its value will be different from $K_{D,i}$ in equation 3.6.

3.3 Results and Discussion

3.3.1 Probe Breakthrough

The absorption spectrum of naphthalene-2-sulfonate (NS^-) is given in Figure 3.5. It has a wavelength of maximum absorption at 276 nm and the molar absorptivity at this wavelength is 4860 L/(mol·cm). Its molar absorptivity is sufficiently high to make it a good choice as a probe for indirect UV detection.

The breakthrough curve recorded for NS^- probe in pH 2 buffer on Partisil-10 ODS-3 is shown in Figure 3.6. The retention volume of the probe is 138 mL which corresponds to a capacity factor of 47.3 ± 0.2. A slightly larger volume than this is required in order to achieve complete probe breakthrough and baseline stability. Since the column is initially equilibrated with solvent only (*i.e.* no probe present), when the mobile phase containing probe is pumped through the column, the probe retention volume is related to its sorption isotherm in the manner shown in Figure 3.1. The probe capacity factor calculated above is the value that would be obtained if NS^- was injected as a sample into a mobile phase composed of pH 2 buffer only and if the NS^- concentration was in the linear region of its isotherm.

For the particular concentration of NS^- used in the mobile phase (2.00×10^{-4} mol/L), the baseline absorbance after breakthrough is approximately 1 A.U. Since the

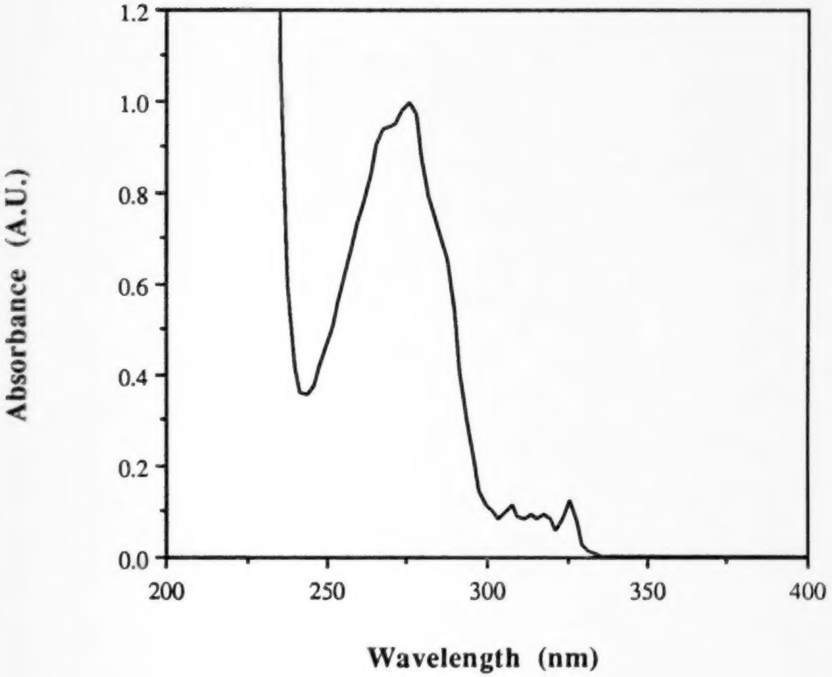

Figure 3.5 Absorption spectrum of 2.00 x 10^{-4} mol/L NS^- probe in 0.04 mol/L H_3PO_4/ 0.03 mol/L NaH_2PO_4 (pH=2) versus 0.04 mol/L H_3PO_4/0.03 mol/L NaH_2PO_4. Path length is 1 cm.

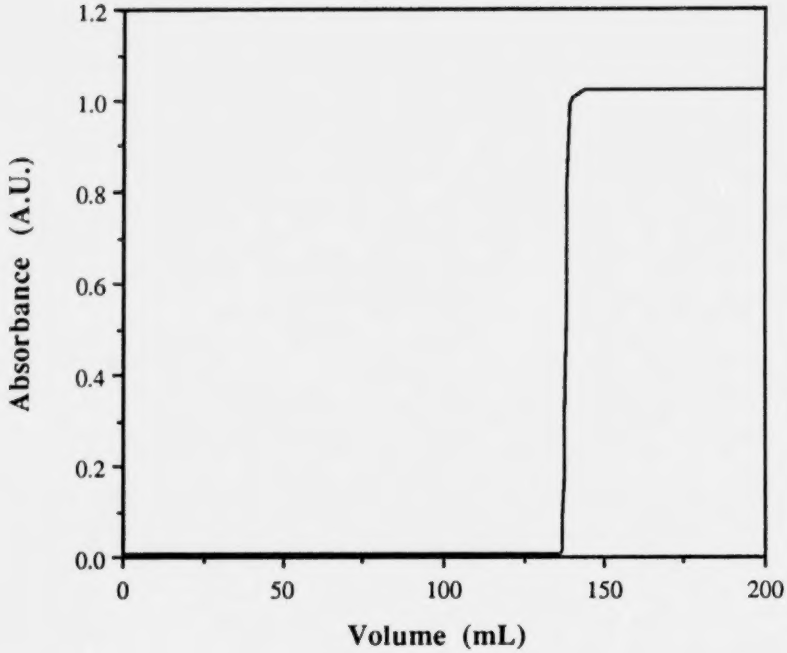

Figure 3.6 NS^- probe breakthrough curve on Partisil-10 ODS-3 analytical column. The composition of the mobile phase is 2.00×10^{-4} mol/L NS^- in 0.04 mol/L H_3PO_4/0.03 mol/L NaH_2PO_4 (pH=2). Experimental conditions are given in Table 2.1.

change in probe absorbance brought about by a sample injection will be small, the high absorbance is electronically offset to a value close to zero for subsequent sample injections.

3.3.2 Temperature Effect

Chromatographic systems used for indirect UV detection must be very stable in terms of temperature and (pulseless) flow rate in order to achieve good response and precision [4,6]. Due to the high background absorbance, baseline drifting and noise are inherent problems of indirect UV detection systems [109].

When indirect UV detection is performed by liquid chromatography, the absolute value of the mobile phase optical absorbance is what constitutes the baseline signal of the chromatogram. This baseline absorbance is relatively high, while the change in absorbance which is observed when a sample or system peak elutes is relatively small. This is because analytical chromatography is performed under conditions where the sample isotherm is linear, which requires a low sample concentration. Consequently, the additional number of moles of probe transferred from the stationary phase to the mobile phase, or *vice versa*, in the sample zone usually represents only a small fraction of the moles of probe present in the mobile phase in the absence of sample.

Another variable, in addition to the presence of sample, which can produce changes in the amount of probe sorbed from a given mobile phase, is temperature. Since changes in probe sorption induced by the presence of the sample are small, it is possible that small changes in temperature, such as the normal fluctuations in a constant temperature bath, can produce baseline absorbance shifts that are comparable in magnitude to sample and system peaks.

Previous reports of studies which have used NS^- as a probe have mentioned the need for thermostatting [4,6,77,109], but none have quantified the effect of temperature or demonstrated how critical the temperature control can be. Under the conditions employed in the present study, these temperature effects were profound. Shown in Figure 3.7 are the baseline changes that are brought about by small temperature changes. The baseline (dashed line) in Figure 3.7 represents the absorbance of the mobile phase at 25.1 °C, after the probe has achieved complete breakthrough on the column. At point "a", the column temperature is lowered by 1.7 °C and held at the new temperature (23.4 °C). This increases the distribution coefficient of NS^- along the whole column and causes the absorbance to decrease temporarily. The difference in volume between the descending front, at 130 mL, and the ascending rear, at 190 mL, of the broad negative plateau following point "a" is equal to the retention volume of the probe. In this case the retention volume is shorter than that found from the breakthrough curve in Figure 3.6 since probe is already present in the mobile phase. The retention volume is determined from the slope of the tangent to the probe isotherm at $C_{m,NS} = 2.00 \times 10^{-4}$ mol/L. After the plateau, the column has been completely re-equilibrated at 23.4 °C. This is indicated by a return of the signal to the original baseline since this represents the absorbance of the constant composition mobile phase entering the column. At point "b", the temperature is raised by 0.4 °C to 23.8 °C which decreases the probe distribution coefficient from its previous value at 23.4 °C and causes probe to desorb into the mobile phase. After the resulting positive plateau, the signal again returns to its original baseline value.

To show how sensitive the system is to changes in temperature, a plot of the plateau absorbance at various temperatures is shown in Figure 3.8 and the data are given in Table 3.1. The plot is linear over this small temperature range, with a slope of 0.0220 ± 0.0002 A.U./°C. This means that the baseline absorbance will shift by 0.022 A.U. for a 1 °C temperature change. This is seen to be a significant temperature dependence when it is realized that sample and systems peaks typically produce absorbance changes of approximately 0.02 A.U. and that the detector sensitivity is often set at 0.05 A.U.F.S. At this detector sensitivity, short term temperature fluctuations of ± 0.04 °C will produce baseline excursions of 2% of the full scale deflection which appears as baseline noise in the

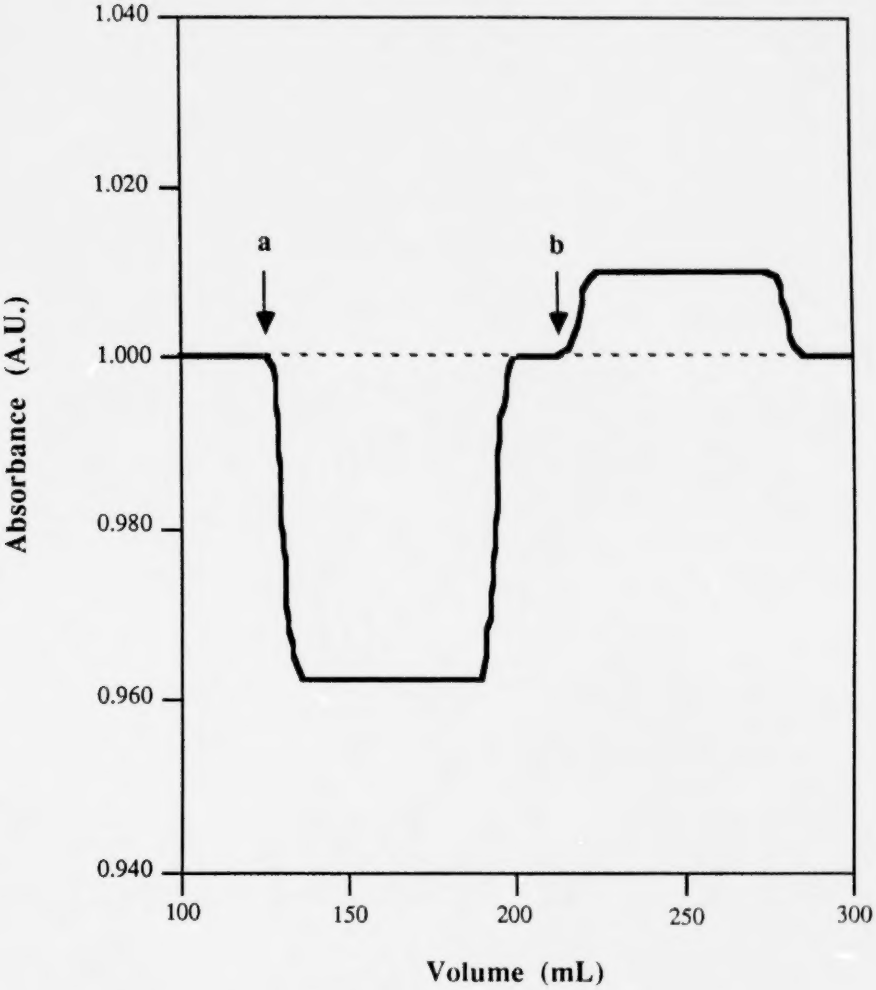

Figure 3.7 Absorbance versus volume of solution passed through column with changing temperature. The dashed line is the baseline absorbance for the mobile phase composition given in Figure 3.6, after the probe has achieved complete breakthrough on the column. The initial temperature was 25.1 °C. At point a, the temperature of the column was decreased to 23.4 °C. At point b, the temperature was increased to 23.8 °C. Experimental conditions are given in Table 2.1.

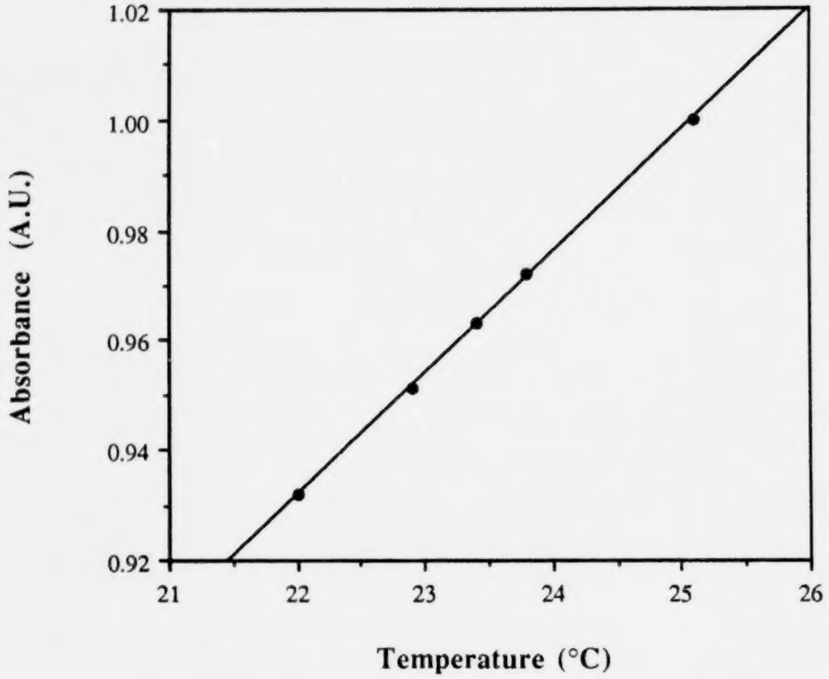

Figure 3.8 Plateau absorbance versus column temperature. See Figure 3.7 for details. Experimental conditions are given in Table 2.1.

Table 3.1 Plateau absorbance *versus* column temperature data. Mobile phase composition is 2.00 x 10^{-4} mol/L NS^- in 0.04 mol/L H_3PO_4/0.03 mol/L NaH_2PO_4 (pH = 2). Experimental conditions are given in Table 2.1.

Absorbance (A.U.)	**Temperature (°C)**
0.932 ± 0.002	22.0
0.951 ± 0.002	22.9
0.963 ± 0.002	23.4
0.972 ± 0.002	23.8
1.000 ± 0.002	25.1

chromatogram. Thus, it is desirable to thermostat the system with a precision closer to ± 0.01 °C. To achieve the necessary high precision temperature control while using a water bath that is rated at ± 0.04 °C precision, a special double-walled water jacket shown in Figure 2.3 was used.

3.3.3 Sample Injections

The rate of travel of the injected sample will be determined by Equation 3.6. When the sample is injected into an indirect detection chromatographic system, the change in the amount of probe sorbed is very small. As a result, the probe concentration pulse that is created can be treated as a linear perturbation such that the probe distribution coefficient is constant (*i.e.* $\Delta C_{s,i}/\Delta C_{m,i}$ in equation 3.7).

In the following sections, the chromatographic results for various samples that are injected and detected in an indirect UV detection mode using NS^- as probe are discussed. The results are summarized in Tables 3.2 - 3.4.

3.3.3.1 Injection of Mobile Phase without Probe as a Sample

With a mobile phase composition of 2.00×10^{-4} mol/L NS^- in 0.04 mol/L H_3PO_4/0.03 mol/L NaH_2PO_4 buffer (pH = 2), a solution of 0.04 mol/L H_3PO_4/0.03 mol/L NaH_2PO_4 buffer (*i.e.* mobile phase without probe) is injected as a sample into the chromatographic system. In the resulting chromatogram (not shown) a single peak in a negative direction appears at a retention volume of 61.6 mL ($k' = 19.5 \pm 0.1$).

In this case, there is only one peak. The additional peak of opposite direction usually observed in indirect detection chromatograms is absent. When a sample of buffer-only is injected onto the column, some probe desorbs from the stationary phase until equilibrium is established in the sample zone. The sample zone can simply be viewed as a zone migrating through the column which is deficient in probe compared to the equilibrium baseline probe concentration when no sample is present. As this zone passes through the detector it produces a negative peak. Considering the previous discussion in Section 3.2.2, injection of buffer-only is the same as injecting a negative probe concentration pulse onto the column (see Figure 3.3c). The retention volume of the negative peak produced in this case is related to the probe sorption isotherm in the manner shown in Figure 3.4 and its rate of travel is calculated from equation 3.7.

3.3.3.2 Injection of Probe as Sample

The results for the injection of two solutions, one containing 6.17 x 10^{-4} mol/L NS^- and the other containing 1.04 x 10^{-4} mol/L NS^-, both prepared with the same pH 2 buffer as that used to prepare the mobile phase, are given in Table 3.2. The NS^- concentration in the mobile phase is 2.00 x 10^{-4} mol/L in pH 2 buffer. In each chromatogram a single peak, one in the positive direction and the other in the negative direction, respectively, appears in the chromatogram at the k' of the probe. The k' is the same as that determined above by the injection of buffer only. These cases are similar to the injection of buffer-only and can simply be treated as probe concentration pulses migrating through the column which contain an excess and deficiency of probe respectively.

When a sample containing several components is injected into an indirect detection chromatograph, several peaks will appear in the chromatogram, one of which is the probe system peak. In the concentration range where $\Delta C_{s,i}/\Delta C_{m,i}$ has a constant value, the system peak has a constant retention volume, regardless of the sample injected. Therefore, injecting a sample of probe, whose concentration is lower or higher than the probe concentration in the mobile phase being pumped through the column, provides a means of identifying the probe system peak.

Table 3.2 Results for the injection of buffer and NS^- probe concentration pulses on Partisil-10 ODS-3. Experimental conditions are the same as in Table 2.1.

Sample [(a)]	k'_{smp}	k'_{sys}	Sample Peak	System Peak
Buffer	-	19.5	-	Negative
6.17×10^{-4} mol/L NS^-	-	19.7	-	Positive
1.04×10^{-4} mol/L NS^-	-	19.3	-	Negative

[(a)] Prepared in 0.04 mol/L H_3PO_4/0.03 mol/L NaH_2PO_4 buffer (pH = 2).

3.3.3.3 Injection of Inert Electrolyte Samples

To investigate the effect of ionic strength, samples were prepared which contained the same probe concentration as that in the mobile phase (*i.e.* 2.00×10^{-4} mol/L) using pH 2 buffer as solvent. However, the concentrations of H_3PO_4 and NaH_2PO_4 used to prepare the buffer were different than those used in the preparation of the mobile phase (*i.e.* 0.04 mol/L H_3PO_4/0.03 mol/L NaH_2PO_4) in order to vary the ionic strength. The samples were subsequently injected into the chromatographic system and the results are given in Table 3.3. A sample of 0.0710 mol/L sodium nitrate prepared with mobile phase (containing probe) as solvent was also injected.

Two peaks were observed in the cases of different buffer concentrations. The first peak was a sample peak due to the unretained buffer components and eluted at the void volume of the column. The second peak was the system peak due to the probe and eluted at k'_{sys}.

It is generally observed that when ionic strength is increased, sorption of an ionic species is increased [110,111]. Injection of a sample whose ionic strength is lower than that of the flowing mobile phase is therefore the same as the case of a sample which decreases probe sorption (see Figures 1.5 and 1.6). Similarly, injection of a sample whose ionic strength is higher than that of the flowing mobile phase is the same as the case of a sample which increases probe sorption (see Figures 1.7 and 1.8). In both cases, the pattern of peaks is consistent with the response pattern of a sample which elutes before the probe and decreases or increases probe sorption respectively.

Injection of a sample of sodium nitrate is the same as the case of a higher ionic strength sample which increases probe sorption. However, the chromatogram in this case had both sample ($NaNO_3$) and system peaks positive. The positive probe system peak was consistent with a sample that increases probe sorption. The positive sample peak, on the

Table 3.3 Results for the injection of inert electrolyte and water samples on Partisil-10 ODS-3. Experimental conditions are the same as in Table 2.1.

Sample	k'_{smp}	k'_{sys}	Sample Peak	System Peak
Low Ionic Strength (0.021 mol/L H_3PO_4 / 0.015 mol/L NaH_2PO_4)	0	17.8	Positive	Negative
High Ionic Strength (0.084 mol/L H_3PO_4 / 0.063 mol/L NaH_2PO_4)	0	18.1	Negative	Positive
0.0710 mol/L $NaNO_3$	0	18.0	Positive	Positive
Water	0	19.7	Positive	Positive/Negative*

* Split peak

other hand, was due to the inherent absorbance contribution of nitrate at 276 nm which dominates the (negative) indirect detection contribution of the probe and thus gave rise to a positive peak with $k' = 0$ since sodium nitrate is unretained [4].

3.3.3.4 Injection of Water as a Sample

Injection of water as a sample would be expected to give a result which is a combination of the buffer-only injection in Section 3.3.3.1 and the injection of a lower concentration of inert electrolyte in Section 3.3.3.3. The chromatogram obtained is shown in Figure 3.9. The results are summarized in Table 3.3.

The first peak is a sample peak due to the unretained buffer components which elute at the void volume of the column ($k'_{smp} = 0$). The second peak is the probe system peak since it elutes at k'_{sys} as determined from the probe concentration pulses injected in Section 3.3.3.2 (see Tables 3.2 and 3.3).

Since the sample is deficient in both probe and buffer components, the ionic strength of the sample zone is lower than that in the surrounding mobile phase. From the discussion in the previous section, the sample decreases probe sorption and produces a positive peak at the retention volume of the unretained buffer components.

In the case of the probe system peak, a negative peak should be observed at the probe retention volume since injection of water as a sample can be viewed as injection of a negative probe concentration pulse. Instead, a split peak is obtained which is centered at k'_{sys} (see Table 3.3 and Figure 3.9).

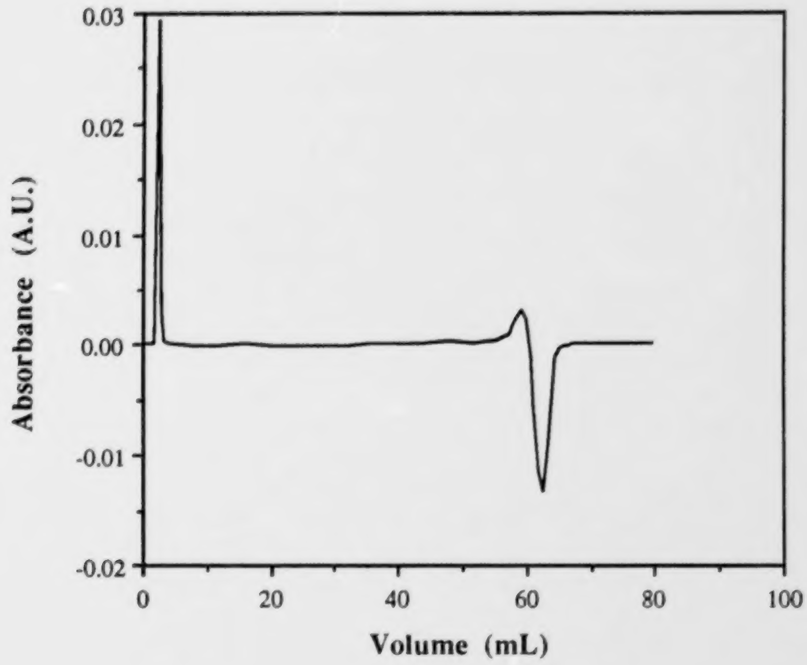

Figure 3.9 Indirect UV detection chromatogram on Partisil-10 ODS-3 for the injection of water as a sample using the experimental conditions given in Table 2.1.

3.3.3.5 Injection of Cationic, Anionic and Neutral Sample Species

Organic ammonium ions, sulfonates and alcohols are injected into the chromatographic system as cationic, anionic and neutral sample species respectively. The direction of the sample and system peaks and their capacity ratios are given in Table 3.4.

In all cases, the response pattern discussed in Chapter 1 and given in Table 1.1 is obeyed. The only exception is *p*-phenylazobenzenesulfonate (PBS^-) in which case both the sample and system peak are positive. In this particular case, where the sample elutes after the probe and has the same sign of charge as the probe, a positive system peak followed by a negative sample peak is expected to appear in the chromatogram. The positive sample peak that appears is easily accounted for by the fact that PBS^- has an inherent UV absorbance at the detection wavelength of 276 nm. The overall peak is the sum of the (negative) contribution from indirect detection and the (positive) contribution from the inherent absorbance, with the latter contribution dominating [4].

It should be noted that the variation in k'_{sys} in Tables 3.2 to 3.4 is due to the deterioration of the column over time as mobile phase is pumped through it, as was discussed in Section 2.5.6. The samples were not injected at the same time, but they were run over a period of time and in between several other experiments. Since previous experiments were run on the column before samples were injected, both the k'_{smp} and k'_{sys} experimental values are expected to be lower than they would have been on a new column. Experiments performed on a brand new column gave a value for $k'_{sys} = 26.4 \pm 0.1$. Therefore, the results in Tables 3.2 to 3.4 are 25 - 35 % lower than the original values.

3.3.3.6 Magnitude of Indirect Detection Response

In the case of the hexanesulfonate sample, a quantitative study was done in which various concentrations of hexanesulfonate were injected and the sample and system peak

Table 3.4 Results for the injection of cationic, anionic and neutral samples on Partisil-10 ODS-3. Experimental conditions are the same as in Table 2.1.

Sample	k'_{smp}	k'_{sys}	Sample Peak	System Peak
5.15×10^{-4} mol/L Pentanesulfonate	4.33 ± 0.02	19.8	Positive	Negative
6.05×10^{-4} mol/L Hexanesulfonate	13.6	18.2	Positive	Negative
1.32×10^{-3} mol/L Heptanesulfonate	44.5 ± 0.2	17.5	Negative	Positive
1.01×10^{-3} mol/L p-phenylazobenzene-sulfonate	35.5	17.1	Positive	Positive
4.18×10^{-4} mol/L Pentyl amine	6.28 ± 0.02	19.6	Negative	Positive
5.05×10^{-4} mol/L Heptyl amine	61.4 ± 0.2	20.8	Positive	Negative
1.09×10^{-2} mol/L Butanol	6.23 ± 0.02	17.9	Negative	Positive
1.82×10^{-3} mol/L Pentanol	20.8	17.7	Negative	Positive
1.17×10^{-2} mol/L Hexanol	66.7 ±0.2	17.7	Negative	Positive

heights were measured. The results are plotted in Figure 3.10 and are given in Table 3.5. Both the sample and system peaks gave a linear response with hexanesulfonate concentration which shows that the technique is suitable for quantitative analysis.

An in depth study into the magnitude of the response and how it varies with k'_{smp} *versus* k'_{sys} (see Figure 1.3) and sample type was not undertaken as it was not of primary concern in this thesis. As well, peak areas were not measured in the experiments. However, from simple observation it was found that much higher concentrations of neutral samples had to be injected compared to ionic samples in order to achieve the same indirect detection response. For example, pentyl amine and butanol have similar capacity ratios and give similar responses in terms of peak area (from visual observation), but the injected concentration of butanol was 25 times larger than that of pentyl amine (see Table 3.4). This behaviour is consistent with that generally observed in the literature for neutral samples.

3.3.4 Frontal Chromatography

Frontal chromatography is performed using indirect UV detection for the specific case of the butanol sample. Two cases are investigated using a low and a high concentration of butanol in the mobile phase. Based on the response pattern for the injection of a butanol sample, obtained by doing elution chromatography above, butanol decreases NS^- probe sorption. On a brand new column, when a 0.109 mol/L butanol sample is injected into the chromatographic system, the retention volume of the butanol sample peak was 27.3 mL ($k'_{smp} = 8.51 \pm 0.03$) and the retention volume of the probe system peak was 78.5 mL ($k'_{sys} = 26.4 \pm 0.1$). Frontal chromatography was done on the same new analytical column.

The frontal chromatograms obtained in the presence of a low butanol concentration (1.09×10^{-3} mol/L) and a high butanol concentration (1.09×10^{-2} mol/L) are shown in

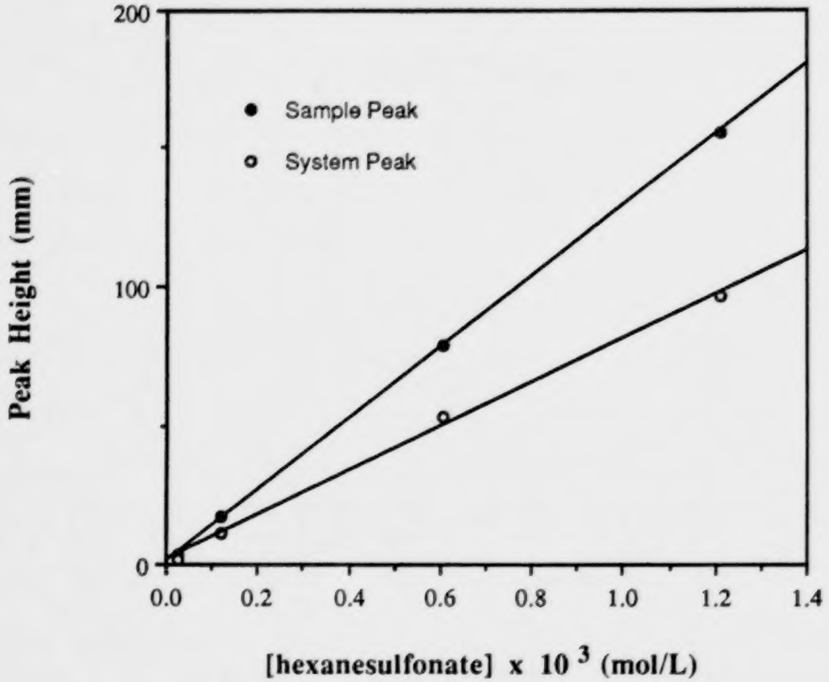

Figure 3.10 Magnitude of the indirect UV detection response for hexanesulfonate sample. Experimental conditions are given in Table 2.1.

Table 3.5 Response magnitude for hexanesulfonate sample on Partisil-10 ODS-3. Experimental conditions are the same as in Table 2.1.

[Hexanesulfonate] x 10^5 (mol/L)	Sample Peak Height (mm)	System Peak Height (mm)
2.42	3.3	2.0
12.1	17.1	11.3
60.5	78.6	52.6
121	155.6	96.2

Figures 3.11 and 3.12 respectively. The retention volumes of the various ascending and descending portions observed in both chromatograms are given in Table 3.6.

At point A in both figures, the mobile phase is changed from one containing 2.00 x 10^{-4} mol/L NS^- in pH 2 buffer to one containing the same NS^- and buffer concentrations and 1.09 x 10^{-3} mol/L or 1.09 x 10^{-2} mol/L butanol. Chromatograms #1 (Figure 3.11) and #3 (Figure 3.12) are subsequently obtained. At point B in both figures, the mobile phase is switched back to the original mobile phase containing probe only and chromatograms #2 (Figure 3.11) and #4 (Figure 3.12) are obtained. Since butanol decreases probe sorption, there is a positive plateau absorbance when butanol is introduced in the mobile phase and a corresponding negative plateau absorbance when butanol is removed from the mobile phase. Comparison of the retention volumes for the ascending and descending portions of the frontal chromatograms with those for the sample and system peaks in the elution chromatogram (given in the footnote of Table 3.6) shows that the initial absorbance increase or decrease in all chromatograms occurs at a volume close to the retention volume for butanol and the return to the original baseline in all chromatograms occurs at a volume close to the retention volume for the probe.

The general appearance of the frontal chromatograms at both low and high butanol concentrations can be explained as follows. Consider first only chromatograms #1 (Figure 3.11) and #3 (Figure 3.12). Mobile phase containing only probe in pH 2 buffer is pumped through the column until complete probe breakthrough has been achieved. Then, mobile phase containing both probe and butanol in pH 2 buffer is introduced into the column. The introduction of butanol can be viewed as a series of very small increments. When the first increment containing butanol enters the column, some probe desorbs from the stationary phase. As this initial increment migrates down the column, probe continues to desorb from the stationary phase. At some point probe no longer desorbs in this increment because equilibrium has been achieved between the mobile phase and the stationary phase. This process occurs for each successive increment containing butanol except that it has to travel

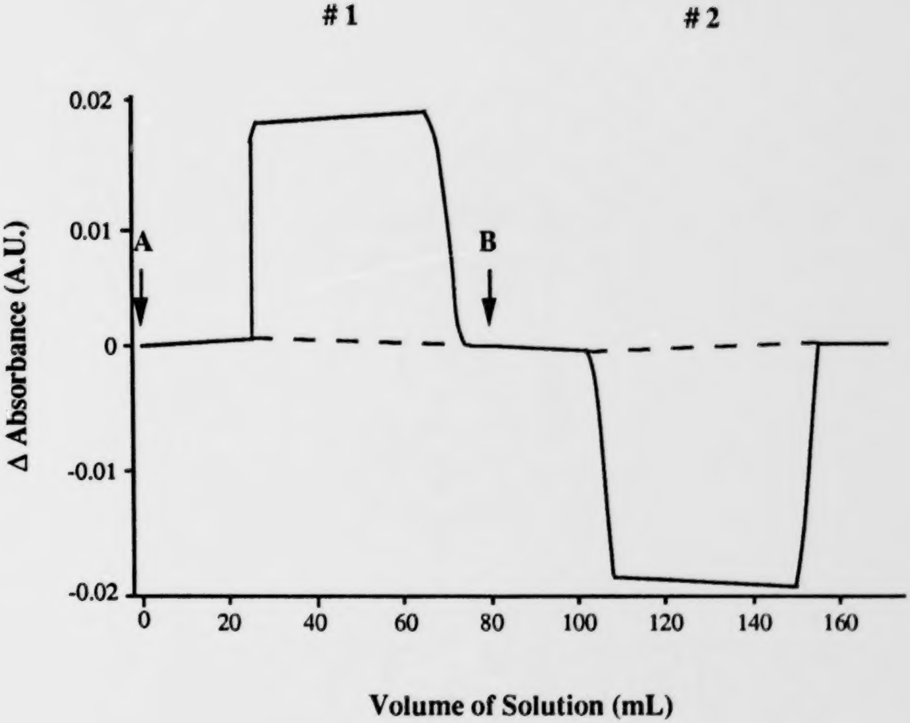

Figure 3.11 Frontal chromatograms for the low butanol concentration case. At point A, the mobile phase is changed from 2.00 x 10^{-4} mol/L NS^- in 0.04 mol/L H_3PO_4/0.03 mol/L NaH_2PO_4 (pH=2) to 2.00 x 10^{-4} mol/L NS^- and 1.09 x 10^{-3} mol/L butanol in pH 2 buffer and chromatogram #1 is obtained. At point B, the mobile phase is changed from 2.00 x 10^{-4} mol/L NS^- and 1.09 x 10^{-3} mol/L butanol in pH 2 buffer to 2.00 x 10^{-4} mol/L NS^- in pH 2 buffer and chromatogram #2 is obtained.

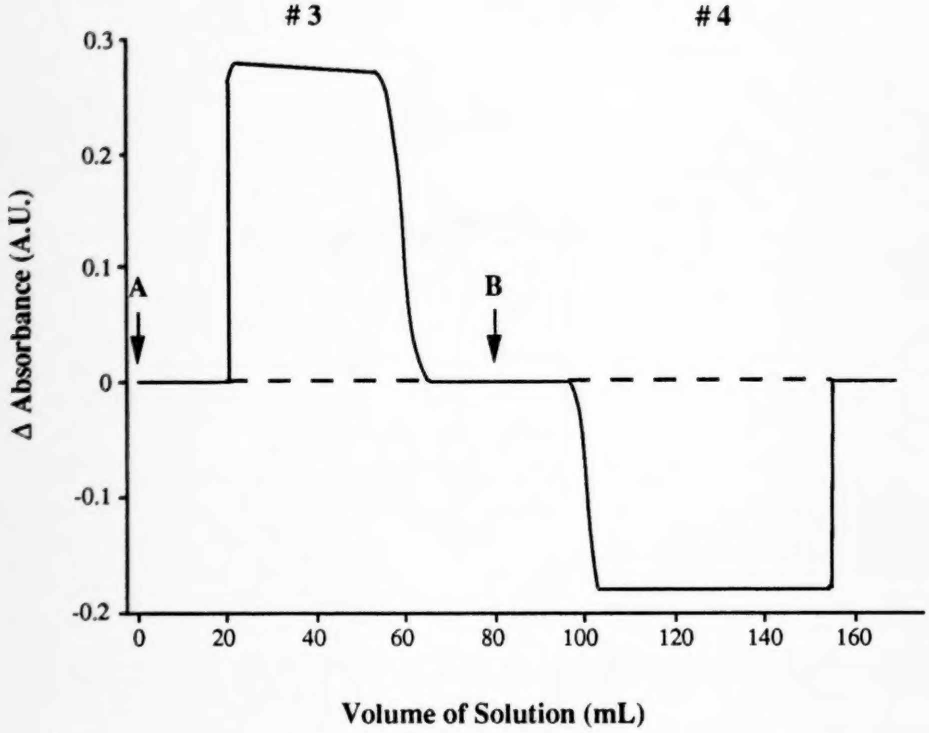

Figure 3.12 Frontal chromatograms for the high butanol concentration case. At point A, the mobile phase is changed from 2.00 x 10^{-4} mol/L NS^- in 0.04 mol/L H_3PO_4/0.03 mol/L NaH_2PO_4 (pH = 2) to 2.00 x 10^{-4} mol/L NS^- and 1.09 x 10^{-2} mol/L butanol in pH 2 buffer and chromatogram #3 is obtained. At point B, the mobile phase is changed from 2.00 x 10^{-4} mol/L NS^- and 1.09 x 10^{-2} mol/L butanol in pH 2 buffer to 2.00 x 10^{-4} mol/L NS^- in pH 2 buffer and chromatogram #4 is obtained.

Table 3.6 Frontal chromatography on Partisil-10 ODS-3 for two different butanol concentrations. The composition of the mobile phase was 2.00×10^{-4} mol/L NS^- in 0.04 mol/L H_3PO_4/0.03 mol/L NaH_2PO_4 (pH = 2) either without or with butanol present. The experimental conditions are given in Table 2.1.

1.09×10^{-3} mol/L butanol

	Mobile Phase Composition(a)	Ascending V_R (mL)(b)	Descending V_R (mL)(b)	Area (A.U.)(b)
#1	$NS^- \rightarrow NS^-$ + butanol	25.6 ± 0.2	69.1 ± 0.1	1110 ± 10
#2	NS^- + butanol $\rightarrow NS^-$	72.2 ± 0.3	26.0 ± 0.1	1120 ± 10

1.09×10^{-2} mol/L butanol

	Mobile Phase Composition(a)	Ascending V_R (mL)(b)	Descending V_R (mL)(b)	Area (A.U.)(b)
#3	$NS^- \rightarrow NS^-$ + butanol	21.6 ± 0.3	59.5 ± 0.1	1510 ± 10
#4	NS^- + butanol $\rightarrow NS^-$	74.3 ± 0.1	21.8 ± 0.1	1640 ± 10

(a) Indicates how the mobile phase composition was changed in obtaining the frontal chromatogram.

(b) Average of duplicate runs.

NOTE: From elution chromatography, $V_{R,butanol} = 27.3$ mL and $V_{R,NS} = 78.5$ mL.

a further distance down the column before it comes to equilibrium. When the first increment exits the column, the absorbance increases and an ascending front is observed in the chromatogram at the butanol retention volume. Since each successive increment has the same probe concentration in the mobile phase, the absorbance remains temporarily constant to give the plateau in the chromatogram. Eventually, the entire column comes to the new equilibrium concentrations such that additional increments entering the column are already at equilibrium and probe no longer is desorbed from the stationary phase. As a result, the increments have the same probe concentration as the initial mobile phase containing probe only, so the absorbance returns to the original value which produces the descending portion at the rear of the chromatogram. This descending portion occurs at the retention volume of the probe.

Relating these results to the indirect UV detection elution chromatogram that is obtained with butanol sample using NS^- probe, the positive butanol sample peak is the same as the ascending butanol front in the frontal chromatogram. Similarly, the negative probe system peak is a result of the column returning to the original equilibrium before sample was injected (*i.e.* descending portion at probe retention volume in frontal chromatogram).

When the mobile phase is switched back to mobile phase containing probe only in pH 2 buffer (chromatograms #2 in Figure 3.11 and #4 in Figure 3.12), the reverse process occurs with probe sorbing back into the stationary phase. A descending front is observed at the retention volume of butanol and there is an increase in absorbance at the retention volume of the probe, as seen at the rear of the frontal chromatograms.

In either case (*i.e.* low or high butanol concentration), the area above or below the frontal chromatograms, relative to the baseline (dashed line), should be the same since the amount of probe that is desorbed by butanol should be resorbed when butanol is removed. The areas below or above the broad plateaus, relative to the baseline, are given in Table 3.6. At low butanol concentration, the areas are essentially identical while at high butanol concentration there is a bit of discrepancy. This could perhaps be due to the nonlinearity of the detector as a result of the high absorbance due to desorption of probe in addition to the concentration of probe that is already present in the mobile phase. The smaller area obtained for chromatogram #3 compared to chromatogram #4 is consistent with the absorbance being out of the linear range of the detector.

Although the general behaviour is the same regardless of the butanol concentration present, the shapes and the locations of the ascending and descending portions depend upon the butanol concentration and are related to the butanol sorption isotherm. When a high concentration of butanol is present in the mobile phase, the ascending front in chromatogram #3 and the descending front in chromatogram #4 of Figure 3.12 occur at an earlier retention volume compared to when butanol is injected as a sample in elution chromatography and when a low concentration of butanol is present in the mobile phase (*i.e.* ascending front in chromatogram #1 and descending front in chromatogram #2 of Figure 3.11). This can be explained in terms of the butanol sorption isotherm. The higher concentration of 1.09 x 10^{-2} mol/L lies on the convex portion of the butanol isotherm (see Chapter 4), so its distribution coefficient and retention volume are smaller than at the lower concentration of 1.09 x 10^{-3} mol/L. The fronts are also sharper, which is evidence of the "self-sharpening" that is expected to result from a convex isotherm. In the case of the descending portion at the rear of chromatogram #3 in Figure 3.12, the presence of a high concentration of butanol displaces more probe such that the probe distribution coefficient is reduced. Since the NS^- probe isotherm is also convex and starting to become nonlinear at 2.00 x 10^{-4} mol/L (see Chapter 4) the descending portion should occur at a smaller probe retention volume which is indeed observed. On the other hand when the high concentration of butanol is removed, the probe distribution coefficient is increased and it migrates at a slower rate which is why the ascending portion at the rear of chromatogram #4 in Figure 3.12 occurs at a later time than the descending portion in chromatogram #3. In contrast, when the lower concentration of butanol (1.09 x 10^{-3} mol/L) is present in the mobile phase, the amount of probe which desorbs is small such that the probe distribution coefficient remains essentially constant. As a result, the retention volume of the descending portion at the rear of chromatogram #1 and the ascending portion at the rear of chromatogram #2 in Figure 3.11 are almost the same.

3.4 Conclusions

The results of the indirect detection studies done in this chapter confirm that certain sample species alter the sorption of the probe and thus give rise to the indirect detection phenomenon. How the sample affects probe sorption depends upon the sign of charge of the sample compared to that of the probe. The processes which are responsible for the change in probe sorption due to the presence of sample are now investigated in the next two chapters for the case of an anionic probe and a neutral sample and a cationic probe and a cationic sample.

Chapter 4

Origin of Indirect UV Detection of the Neutral Sample Butanol Using the Anionic Probe Naphthalene-2-Sulfonate

4.1 Introduction

From the elution chromatography results presented in Chapter 3, it can be seen that the neutral sample butanol decreases sorption of the anionic probe naphthalene-2-sulfonate (NS^-). Several studies have previously been reported in the literature dealing with indirect UV detection where the sample is neutral and the probe is either neutral or ionic [5,21,25,74-76,79,81,109,112,113]. The various explanations that have been given for the change in probe sorption due to the presence of the sample fall into one or more of the three categories given in Chapter 1. These are described in more detail below for the present case.

(1) The sample alters the solvent strength of the mobile phase. The presence of a neutral sample in the mobile phase has been suggested to alter its strength, including the possibility of complex formation, when either an ionic probe [109,113] or a neutral probe is used [25,79,112,115].

(2) The sample competes with the probe for space in the stationary phase. Sorption of a neutral sample may displace sorbed probe from the stationary phase [115,116] or it may reduce the effective surface area available for probe sorption [74,117,118]. Mixed Langmuir isotherms [25,26] and interfacial tension effects [81,114,119] have been suggested to describe this competition. In a contrary sense, the results of one study were interpreted as demonstrating that no competition occurs when a neutral sample is sorbed [120].

(3) The sample alters the sorbent strength of the stationary phase. It is possible that the chemical properties of the stationary phase may be modified by the presence of a sample [115,117]. Alcohols, in particular, can solvate the stationary phase and alter its polarity and structure when they are present at significant concentrations in the mobile phase [121-123]. When an ionic probe is used, the surface potential created by the probe sorbing onto the stationary phase may also be altered by the presence of sorbed sample [46,124].

The purpose of the work described in the present chapter is to determine the processes which cause less NS^- probe to be sorbed in the presence of the butanol sample, than in its absence. NS^- was chosen as the probe because it has previously been used in the literature in 0.05 mol/L phosphoric acid to perform indirect UV detection [4,20,21,26]. It was also used as the probe in the elution chromatography experiments described in Chapter 3. Similarly, alcohols, including *n*-butanol, have been used as neutral samples in indirect detection studies using both ionic and nonionic probes [26,75,76,81,109,113]. They were also used as samples in the elution chromatography experiments described in Chapter 3.

In the present chapter, the mutual effects of the sample on probe sorption and of the probe on sample sorption were studied by the column equilibration technique. This technique allows the measurement of the amounts of both probe and sample that are simultaneously sorbed at equilibrium. This simulates the situation in the butanol sample zone during an elution chromatogram. The simultaneous sorption data for NS^- and butanol are then evaluated to determine the reason why butanol sample causes decreased sorption of the probe. The evaluation is made in terms of the three categories described above. From the results of these studies, it was possible to identify the reason why the sorption of the NS^- probe is decreased when the sample is present, during indirect UV detection LC. The results of the work described in this chapter have recently been published [125].

4.2 Theory

In Section 4.2.1 equations are developed for the situation in which competition for space (*i.e.* category 2) is the only one of the three categories listed in Section 4.1, above, that is operative. In Section 4.2.2 some background concepts on solubility parameter theory are presented. These concepts are relevant to the situation in which the sample alters the solvent strength of the mobile phase (*i.e.* category 1, above).

4.2.1 Competition for Space

If a competition for space in the stationary phase occurs between NS^- probe and butanol sample, then there should be a mutual effect of the sample on probe sorption and of the probe on sample sorption. Consider the effect of the probe on sample sorption first. The distribution coefficient for butanol, $K_{D,BuOH}$ (*i.e.* Equation 3.1), can be expressed in the following form:

$$K_{D,BuOH} = \frac{C_{s,BuOH}}{C_{m,BuOH}} = \frac{n_{BuOH}}{A_s C_{m,BuOH}} \tag{4.1}$$

where n_{BuOH} is the moles of butanol sorbed in the stationary phase and A_s is the space available in the stationary phase for butanol sorption. If NS^- and butanol compete for available space in the stationary phase, then when NS^- is also present in the mobile phase, the available space for butanol sorption is decreased as a result of "blockage" of some of the surface by sorbed NS^-. This is expressed as

$$A_s = A_T - A_{s,NS} \tag{4.2}$$

Here, A_T is the total space available and $A_{s,NS}$ is the space occupied by NS^- which can be expressed as:

$$A_{s,NS} = \overline{A}_{NS}\, n_{NS} \tag{4.3}$$

where $\overline{A}_{NS}$ is the space occupied *per mole* of NS^- and n_{NS} is the moles of NS^- sorbed in the stationary phase. Combining equations 4.1 to 4.3, the amount of butanol sorbed in the stationary phase in the presence of NS^- is:

$$n_{BuOH} = (K_{D,BuOH}\, C_{m,BuOH}\, A_T) - (K_{D,BuOH}\, C_{m,BuOH}\, \overline{A}_{NS})\, n_{NS} \tag{4.4}$$

Assuming that the space occupied per NS^- molecule is independent of the fractional coverage of the stationary phase by NS^-, and considering a constant value of $C_{m,BuOH}$ and $K_{D,BuOH}$, then a plot of n_{BuOH} *versus* n_{NS} should be a straight line if a competition for space is occurring. Note that in the presence of NS^-, the distribution coefficient for butanol remains constant because as the space available for butanol sorption decreases, there is a corresponding decrease in the amount of butanol sorbed. This constancy of $K_{D,BuOH}$ will be true provided that the only effect of NS^- on butanol sorption is competition for space. That is, provided that NS^- does not significantly alter the solvent strength of the mobile phase or the sorbent strength of the stationary phase.

The space occupied per mole of NS^-, $\overline{A}_{NS}$, can be calculated from the slope and intercept of a plot of n_{BuOH} *versus* n_{NS} according to the following equation:

$$\overline{A}_{NS} = \frac{\text{slope}}{\text{intercept}}\, W_S\, S \tag{4.5}$$

where S is the total space available per unit weight of packing. The quantity $W_S \cdot S$ is equal to A_T.

If a competition for space is occurring, then the effect of butanol on probe sorption can be derived in a similar manner as the reverse case. A similar equation to equation 4.4 is derived to describe the amount of NS^- sorbed in the stationary phase in the presence of butanol.

$$n_{NS} = (K_{D,NS}\, C_{m,NS}\, A_T) - (K_{D,NS}\, C_{m,NS}\, \overline{A}_{BuOH})\, n_{BuOH} \qquad (4.6)$$

Assuming that the space occupied per butanol molecule is independent of the fractional coverage of the stationary phase by butanol, and considering a constant value of $C_{m,NS}$ and $K_{D,NS}$, then a plot of n_{NS} *versus* n_{BuOH} should be a straight line if a competition for space is occurring.

The space occupied per mole of butanol, $\overline{A}_{BuOH}$, can be calculated from the slope and intercept of a plot of n_{NS} *versus* n_{BuOH} according to an equation analogous to equation 4.5.

4.2.2 Extended Solubility Parameter Theory

There are several schemes that have been suggested as measures of solvent strength in liquid chromatography [123,126,127]. One of the more classical ones is solubility parameter theory. It is based on regular solution theory, in which the unequal intermolecular forces between molecules in solution are considered and the heat of mixing is not necessarily zero, as it is for ideal solutions [128].

The solubility parameter of a solute i, δ_i, is defined as the square root of the cohesive energy density [126]:

$$\delta_i = \sqrt{\frac{-E_i}{\overline{V}_i}} \qquad (4.7)$$

where E_i is the cohesive energy required to transfer one mole of *i* from the ideal gas phase to its liquid state and $\overline{V}_i$ is the molar volume. The solubility parameter is a measure of the intermolecular interactions of the liquid and its value increases with solvent polarity.

In chromatography, the distribution coefficient is a useful measure of retention. An expression for the distribution coefficient can be derived from solubility parameter theory as follows [128]. According to regular solution theory, the activity coefficient for solute *i*, γ_i, dissolved in *j*, using pure solute standard state, is given by

$$\ln\gamma_i = \frac{\overline{V}_i}{RT}(\delta_i - \delta_j)^2 \qquad (4.8)$$

In chromatography, the distribution coefficient for nonideal solution systems can be expressed as the ratio of the activity coefficient in the mobile phase, $\gamma_{i,MP}$, to that in the stationary phase, $\gamma_{i,SP}$:

$$K_{D,i} = \frac{\gamma_{i,MP}}{\gamma_{i,SP}} \qquad (4.9)$$

Combining equations 4.8 and 4.9, the distribution coefficient expressed in terms of solubility parameter theory is

$$\ln K_{D,i} = \frac{\overline{V}_i}{RT}\left[(\delta_i - \delta_{MP})^2 - (\delta_i - \delta_{SP})^2\right] \qquad (4.10)$$

The solubility parameter of a two component mixture (*i.e.* water and butanol in the present study), δ_m, is equal to the arithmetic sum of the individual solubility parameters weighted according to their volume fractions, ϕ, in the mixture as follows:

$$\delta_m = \phi_{H_2O}\,\delta_{H_2O} + \phi_{BuOH}\,\delta_{BuOH} \qquad (4.11)$$

Substituting the following equation into equation 4.11

$$\phi_{H_2O} = 1 - \phi_{BuOH} \tag{4.12}$$

and then substituting δ_m from the resulting equation for δ_{MP} in equation 4.10 allows equation 4.10 to be expanded into the following quadratic form by treating δ_{SP} as a constant.

$$\ln K_{D,i} = A\,\phi^2_{BuOH} + B\,\phi_{BuOH} + C \tag{4.13}$$

Here

$$A = \frac{\overline{V}_i}{RT}(\delta_{H_2O} - \delta_{BuOH})^2$$

$$B = \frac{2\overline{V}_i}{RT}(\delta_{H_2O}\,\delta_{BuOH} - \delta^2_{H_2O} - \delta_i\,\delta_{BuOH} + \delta_i\,\delta_{H_2O})$$

$$C = \frac{\overline{V}_i}{RT}[\delta_i^2 - (\delta_i - \delta_{SP})^2 - 2\delta_i\,\delta_{H_2O} + \delta^2_{H_2O}]$$

In the present chapter, the sorption of NS^- is studied as a function of butanol concentration in the mobile phase. The sorption of NS^- in the presence of butanol can be evaluated in terms of solubility parameter theory according to equation 4.13 in order to test the applicability of the extended solubility parameter theory to this system.

4.3 Results and Discussion

NOTE: Due to the large amount of data presented in this chapter, some of the tables which repeat data shown in the figures, are given in Appendix A. In addition, calibration curves used in the various determinations are also given in Appendix A.

4.3.1 Determination of Column Equilibration Conditions

4.3.1.1 Precolumn Holdup Volumes

In order to calculate the amount of NS^- or butanol sorbed on the ODS packing *via* equation 1.1, the holdup volume of the precolumn, V_m, must be known. Its value is determined according to the procedure described in Section 2.5.5 using the conditions in Table 2.4. In the measurement of V_m, water is pumped through the precolumn until it has established equilibrium with the stationary phase. According to a similar procedure described by Liu using the same ODS stationary phase, equilibrium is achieved when less than 4 mL of water is pumped through the precolumn [129]. To ensure complete equilibrium, 15 mL was used in all determinations of V_m.

The holdup volume of precolumns #1, #2 and #3 which were used in the experiments described in this chapter are given in Table 4.1 with their 95% confidence limits. Data for a typical GC calibration curve are given in Table A.1 and are plotted in Figure A.1.

4.3.1.2 Loading and Elution Volumes for NS^-

Since a concentration of 2.00×10^{-4} mol/L NS^- was used in the elution chromatography experiments described in Chapter 3, this was the concentration chosen to

Table 4.1 Precolumn holdup volumes for column equilibration studies dealing with NS$^-$ and butanol.

Precolumn	Weight of Packing (g)	Holdup Volume (mL)(a)
#1	0.1540	0.219 ± 0.003
#2	0.0871	0.127 ± 0.007
#3	0.1510	0.218 ± 0.006

(a) Standard deviation is expressed as the 95% confidence limit.

be used in the column equilibration experiments. To determine the volume of NS^- solution that must be pumped through the precolumn to establish equilibrium between the solution and the ODS packing, increasing volumes of a solution of 1.01×10^{-4} mol/L NS^- and of a solution of 4.08×10^{-4} mol/L NS^- both in pH 2 buffer were pumped through precolumn #1 and then eluted. The number of moles of NS^- sorbed on the packing was calculated for each loading volume using equation 1.1. Typical NS^- calibration curve data used in the NS^- determination are given in Table A.2 and are plotted in Figure A.2.

The probe distribution coefficient depends upon the linearity of the probe isotherm around 2.00×10^{-4} mol/L NS^-. The isotherm is convex and approaches linearity at low concentration as will be shown in Section 4.3.3. The probe distribution coefficient will therefore be larger at lower concentration. By using a NS^- solution concentration below the desired concentration (*i.e.* 2.00×10^{-4} mol/L), a more conservative measure is obtained for the minimum loading volume required to achieve equilibrium.

The NS^- loading curve obtained using 1.01×10^{-4} mol/L NS^- in pH 2 buffer is shown in Figure 4.1 and the data are given in Table A.3. In this case, flow rates of 1, 2 and 3 mL/min were used to obtain the loading curve and data were collected both before and after equilibrium was established. Regardless of the flow rate used, equilibrium was achieved after 30 mL of solution had been pumped through the precolumn. This suggests that, kinetically, the sorption process is rapid and that establishment of equilibrium depends only upon the volume of solution pumped through the column. In contrast, the NS^- loading curve obtained using 4.08×10^{-4} mol/L NS^- in pH 2 buffer and a flow rate of 2 mL/min, shown in Figure 4.2, achieves equilibrium in ≤ 15 mL. The data are given in Table A.4. No data were collected for volumes < 15 mL. In this case the loading volume was less that that found at lower concentration which is consistent with the probe isotherm being convex and having a smaller distribution coefficient as the concentration is increased.

The completeness of elution of NS^- was verified as follows. First, precolumn #1 was loaded with NS^- by pumping 30 mL of a 1.02×10^{-4} mol/L NS^- in pH 2 buffer

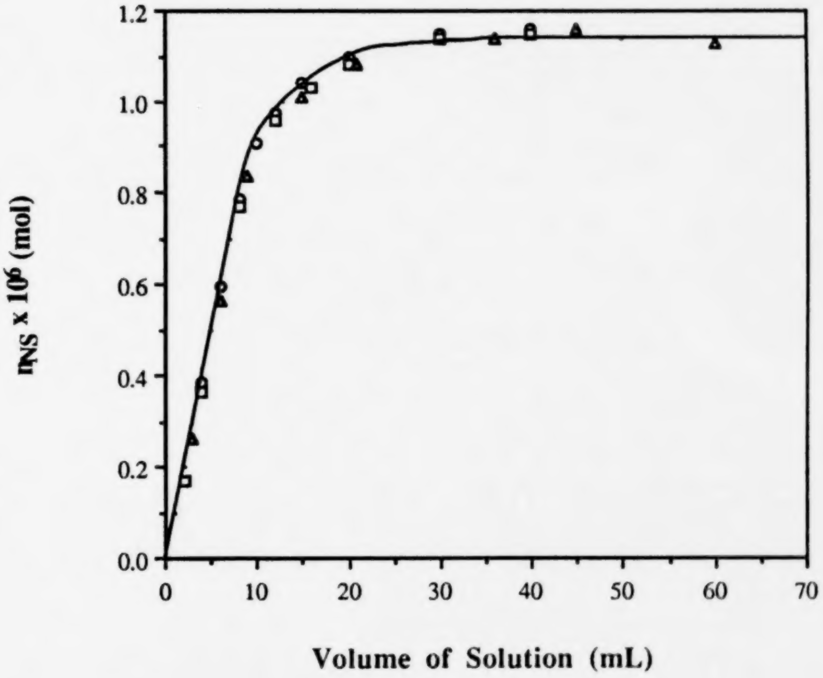

Figure 4.1 NS^- loading curve for 1.01×10^{-4} mol/L NS^- in pH 2 buffer on precolumn #1 ($W_S = 0.1540$ g) at various flow rates. The flow rates are designated by the following symbols: circles, 1 mL/min; squares, 2 mL/min; and triangles, 3 mL/min. The data are given in Table A.3.

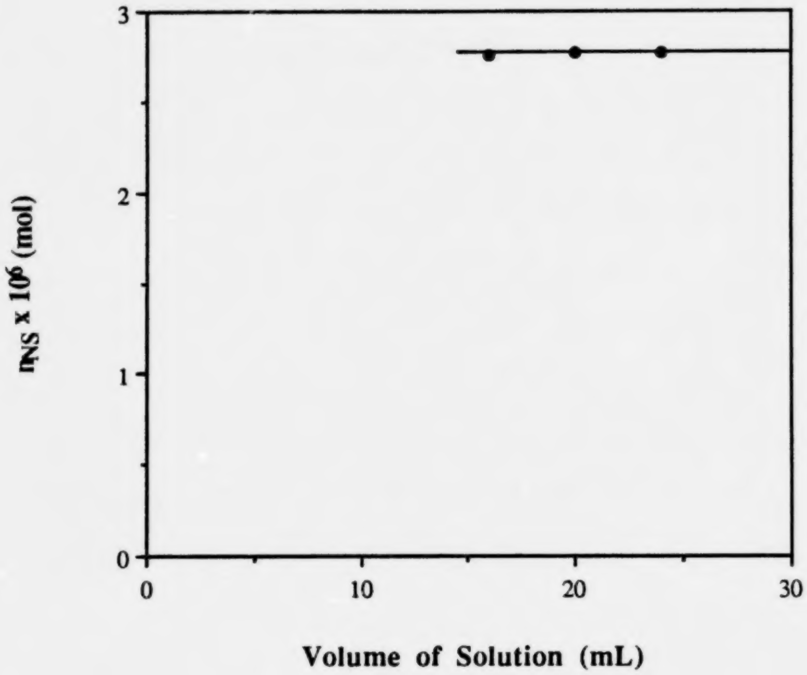

Figure 4.2 NS^- loading curve for 4.08×10^{-4} mol/L NS^- in pH 2 buffer on precolumn #1 (W_S = 0.1540 g). The flow rate was 2.0 mL/min. The data are given in Table A.4.

through it. Then the sorbed NS^- was eluted in three, 1 mL fractions. The NS^- absorbance at 276 nm was measured for each fraction. The results are shown in Figure 4.3 and are given in Table A.5. Essentially all of the NS^- is eluted in the first 1 mL.

4.3.1.3 Loading and Elution Volumes for NS^- and Butanol Together

In determining the effect of butanol on NS^- sorption or *vice versa*, solutions containing both NS^- and butanol are pumped through the precolumn. It is therefore necessary to determine the volume of solution that must be pumped through the precolumn in order that both NS^- and butanol achieve equilibrium between the ODS packing and solution.

Using precolumn #1, a solution of 2.01×10^{-4} mol/L NS^- and 2.18×10^{-4} mol/L butanol in pH 2 buffer was pumped through precolumn #1 for various times at a flow rate of 3 mL/min and was then eluted. Based on the experiments for NS^- alone discussed above, a flow rate of 3 mL/min was used in order to achieve equilibrium in a reasonable time. The number of moles of NS^- sorbed was determined at each loading volume using equation 1.1 and the calibration curve in Figure A.2. Data for the loading curve are shown in Figure 4.4a and are given in Table A.6. It can be seen that when 360 mL of solution is pumped through the precolumn, NS^- equilibrium has been established.

For butanol in the presence of NS^-, the establishment of sorption equilibrium was performed in an analogous manner. The amounts of butanol sorbed after various loading volumes were determined by gas chromatography, employing pentanol as an internal standard, using the conditions in Table 2.5 and measuring peak height ratios (*i.e.* P.H. BuOH/P.H. PeOH). Since it is not necessary to know the actual number of moles of butanol sorbed, but only to know that the number of moles sorbed is no longer increasing with loading volume, no standards were injected. A constant peak height ratio is evidence that equilibrium has been established. Because it was already known that NS^- equilibrium

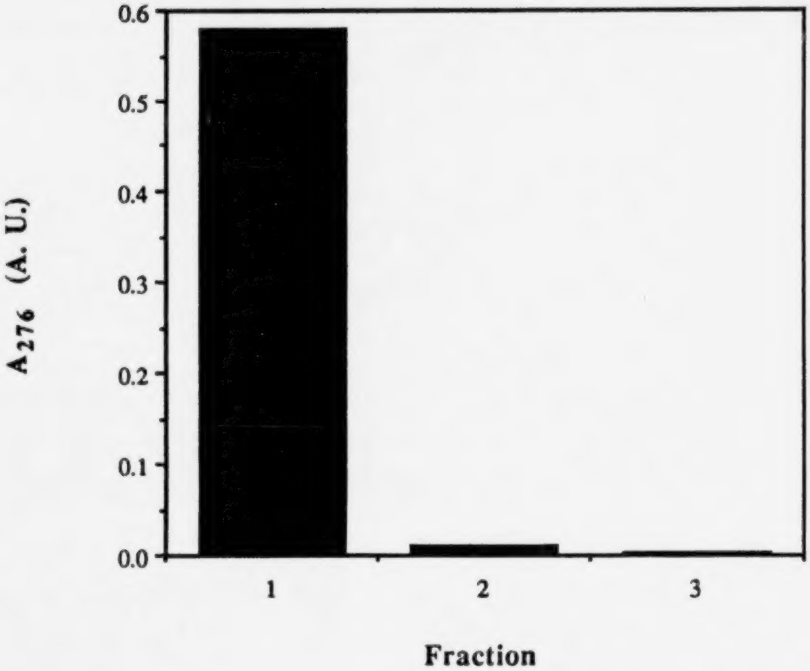

Figure 4.3 NS$^-$ elution curve for a solution of 1.02 x 10^{-4} mol/L NS$^-$ in pH 2 buffer which was loaded onto precolumn #1 (W_S = 0.1540 g) for 10 minutes at a flow rate of 3.0 mL/min (*i.e.* 30 mL). The eluent was methanol:water (1:1 v/v) pumped at a flow rate of 1.0 mL/min. Each fraction represents 1 mL of eluent which was collected in a 10 mL volumetric flask and then diluted to volume with eluent. The data are given in Table A.5.

(a)

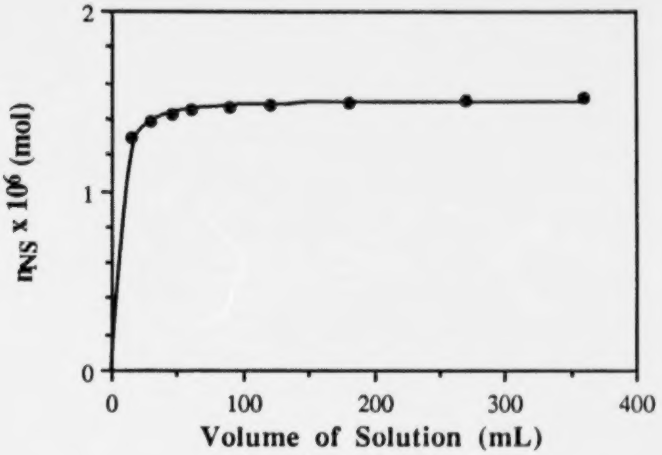

(b)

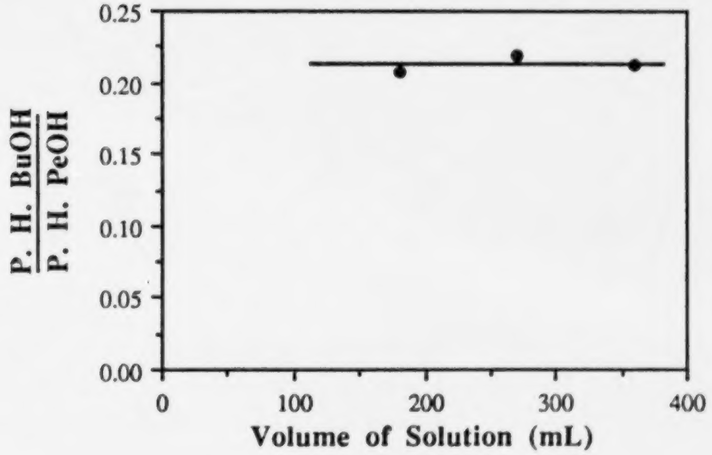

Figure 4.4 NS^- and butanol loading curves for a solution of 2.00×10^{-4} mol/L NS^- plus 2.18×10^{-4} mol/L butanol in pH 2 buffer pumped through precolumn #1 ($W_S = 0.1540$ g) for various volumes. The flow rate was 3.0 mL/min. (a) NS^- loading curve. (b) Butanol loading curve. The data are given in Table A.6.

was not achieved in less than 120 mL, only the higher loading volumes (120, 270 and 360 mL) were injected into the gas chromatograph. The results for the butanol loading curve are given in Figure 4.4b and Table A.6. In contrast to NS^-, butanol establishes equilibrium $\leq$ 120 mL. In order to insure that both NS^- and butanol establish equilibrium, a loading volume of 360 mL (*i.e.* loading time of 2 hours at 3 mL/min) was used in all subsequent probe isotherm experiments, without and with butanol, and also in the butanol isotherm experiments, without and with NS^-. Although NS^- alone establishes equilibrium in 30 mL and butanol alone also probably establishes equilibrium in a small volume, a 360 mL loading volume was used in experiments where either NS^- or butanol was present alone in solution.

The completeness of elution of NS^- and butanol was determined by pumping the solution containing NS^- and butanol in pH 2 buffer, described above, through precolumn #1 for 2 hours at 3 mL/min and then eluting the sorbed NS^- and butanol in five, 2 mL fractions. The NS^- absorbance at 276 nm and the butanol peak height ratio for each fraction were determined. The results are given in Figure 4.5 and Table A.7. Both NS^- and butanol are almost completely eluted in 2 mL of eluent. A total of 10 mL was used for all subsequent experiments.

Since the equilibration time was rather long (*i.e.* 2 hours), it was thought that equilibrium could be achieved sooner by using a smaller weight of packing. Precolumn #2 was used for this purpose. The loading and elution experiments for NS^- and butanol were repeated using this precolumn. However, measurements were done only for NS^- since butanol was found above to establish equilibrium faster.

The loading experiment was done in this case using a solution of 1.00×10^{-4} mol/L NS^- and 2.19×10^{-2} mol/L butanol in pH 2 buffer. These conditions were chosen so that $K_{D,NS}$ would be large. The NS^- loading curve is shown in Figure 4.6 and the data are given in Table A.8. The loading curve is similar to that obtained on the larger precolumn

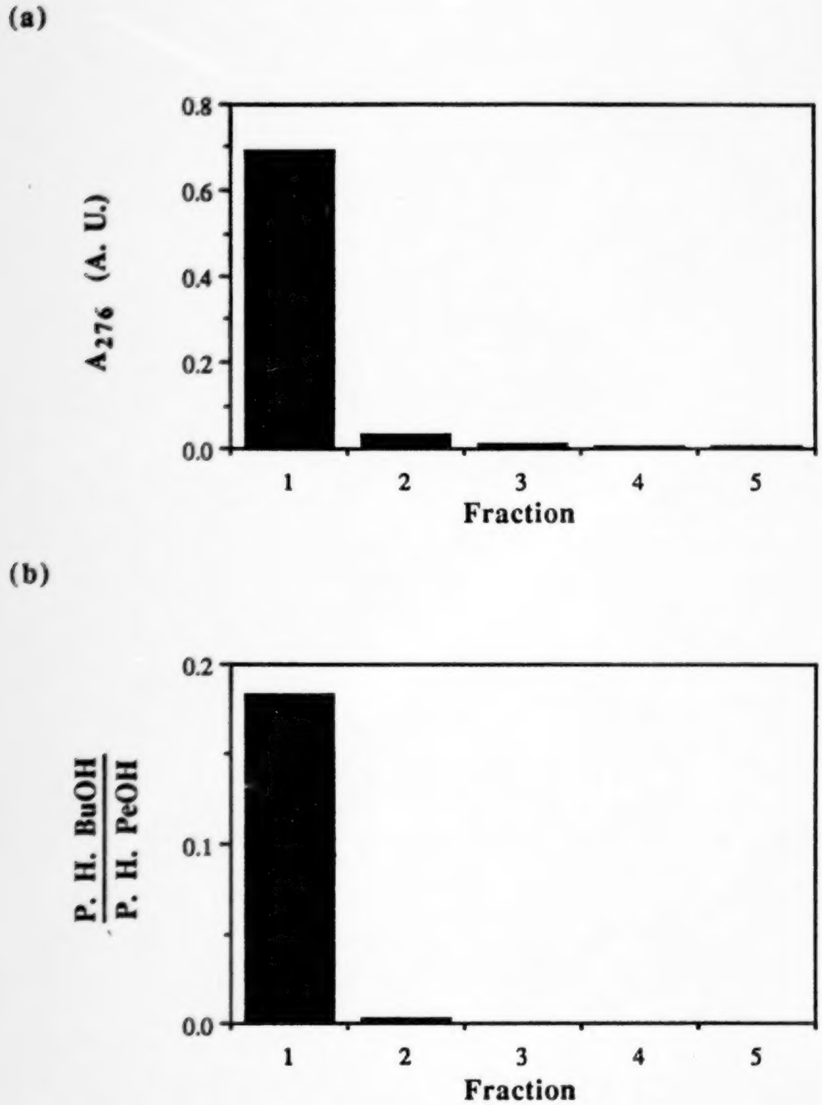

Figure 4.5 NS$^-$ and butanol elution curves for the solution in Figure 4.4 loaded onto precolumn #1 (W_S = 0.1540 g) for 2 hours at 3.0 mL/min. The eluent and eluent flow rate are the same as in Figure 4.3. Each fraction represents 2 mL of eluent collected in a 10 mL volumetric flask and then diluted to volume with eluent. (a) NS$^-$ elution curve. (b) Butanol elution curve. The data are given in Table A.7.

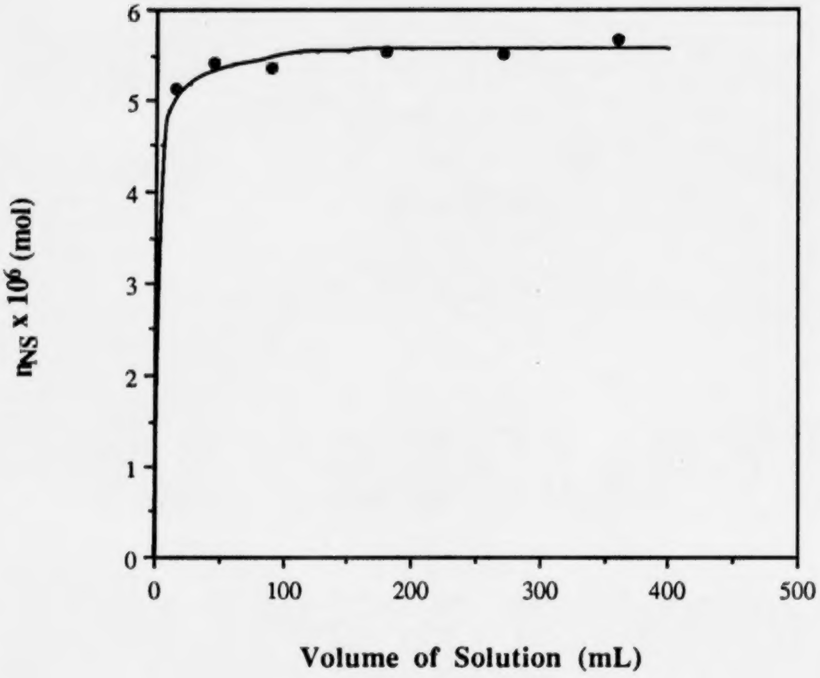

Figure 4.6 NS^- loading curve with butanol present for a solution of 1.00×10^{-4} mol/L NS^- and 2.18×10^{-2} mol/L butanol in pH 2 buffer pumped through precolumn #2 ($W_S = 0.0871$ g) for various volumes. The flow rate was 3.0 mL/min. The data are given in Table A.8.

(*i.e.* precolumn #1) in Figure 4.4a. Two hours was still found to be required to ensure complete equilibrium.

Examination of the NS^- loading curves with butanol present that were obtained using precolumns #1 and #2 (Figures 4.4a and 4.6), reveals that the initial rise to equilibrium in the early stages of the loading curve is rapid and depends only upon the volume of solution passed through the precolumn. The final approach to equilibrium in the later stage of the loading curve, however, is slower and depends upon the length of time that the solution flows through the column. In 20 minutes, or 60 mL, the amount of NS^- sorbed has started to plateau. Therefore, in order to reduce the volume of solution pumped through the precolumn, a flow rate of 3.0 mL/min was used for the first 20 minutes (*i.e.* 60 mL), followed by a flow rate of 1.0 mL/min for 100 minutes (*i.e.* 100 mL) for a total time of 2 hours and a total volume of 160 mL. These conditions were used for the column equilibration experiments in which the effect of the probe on butanol sorption and *vice versa* was studied.

An elution curve for NS^- was also obtained using precolumn #2 which had been loaded with the above solution. The solution was pumped through the precolumn for 20 minutes at 3 mL/min and then for 100 minutes at 1 mL/min. The NS^- and butanol sorbed on the precolumn were then eluted in five, 2 mL fractions. The NS^- absorbance at 276 nm for each fraction was determined. The results are shown in Figure 4.7 and the data are given in Table A.9. As before, most of the NS^- is eluted in 2 mL. Hence, 10 mL was used in all experiments.

4.3.2 Effect of NS^- Probe on Butanol Sample Sorption

The butanol sorption isotherm, measured on Partisil-10 ODS-3 in the present study, is shown as curve a in Figure 4.8, and the data are given in Table A.10 (Curve b and the vertical arrow in Figure 4.8 will be discussed later). The amounts of butanol sorbed on the

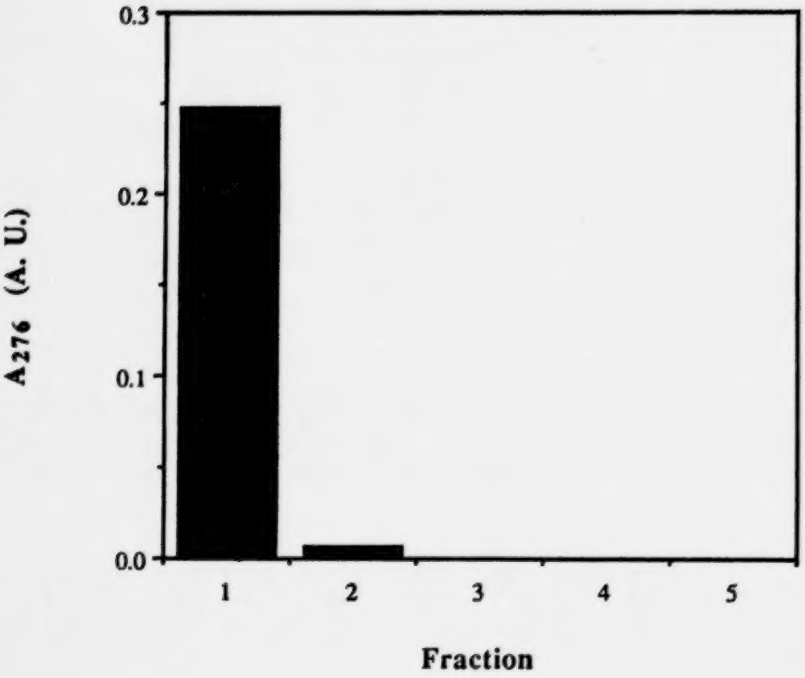

Figure 4.7 NS$^-$ elution curve with butanol present for the solution in Figure 4.6 loaded onto precolumn #2 ($W_S = 0.0871$ g) for 20 minutes at 3.0 mL/min and then 100 minutes at 1.0 mL/min (*i.e.* 160 mL). The eluent and eluent flow rate are the same as in Figure 4.3. Each fraction represents 2 mL of eluent collected in a 10 mL volumetric flask and then diluted to volume with eluent. The data are given in Table A.9.

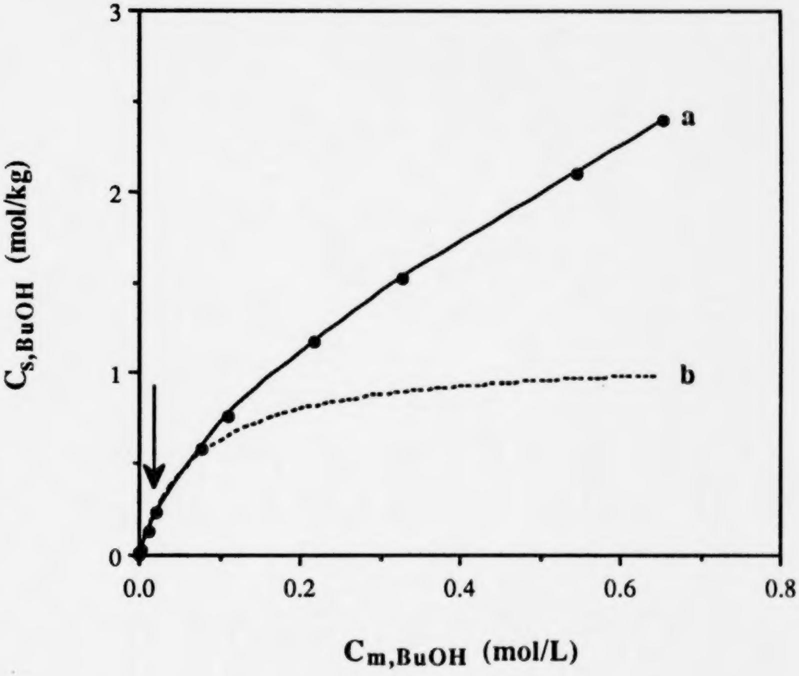

Figure 4.8 Butanol sorption isotherm on Partisil-10 ODS-3 from pH 2 aqueous solutions. Curve a is the experimental isotherm obtained by Stineman interpolation [147] through the experimental points (circles) using Cricket Graph 1.3. Curve b is the Langmuir isotherm generated from the Langmuir constants obtained from the straight line in Figures 4.14 and 4.15. The data and precolumns used are given in Table A.10.

packing were determined by the gas chromatography procedure described in Section 2.6 and using the conditions given in Table 2.5. Two calibration curves were done to cover the range of concentrations used to measure the isotherm. The data are given in Tables A.11 and A.12 and they are plotted in Figures A.3 and A.4.

At the highest butanol concentration employed (0.654 mol/L), the butanol isotherm in Figure 4.8 has not achieved the plateau that would indicate complete surface coverage. Since high butanol concentrations were of no special interest in the present chapter, the isotherm was not measured above 0.654 mol/L. Sorption of organic modifiers, including butanol, onto RPBPs has previously been studied [130,131].

To determine how the probe affected butanol sorption, column equilibration experiments were performed in which the butanol concentration was kept constant at 1.09×10^{-3} mol/L while the NS^- concentration was varied from 0 - 0.157 mol/L. Higher concentrations of NS^- could not be used because the solution was nearly saturated at 0.157 mol/L. The amount of NS^- sorbed was determined using the calibration curve in Figure A.2 and the amount of butanol sorbed was determined by gas chromatographing a known standard whose butanol concentration was similar to that in the collected eluate. The amounts sorbed are given in Table 4.2. Column 1 lists the various NS^- concentrations that were used.

The amounts of NS^- and butanol sorbed given in Table 4.2 were corrected for the change in the weight of packing due to deterioration of the packing caused by pumping solutions in pH 2 buffer through the precolumn. An effective weight of packing, W_{eff}, was determined using the procedure described in Section 2.5.6. A standard containing 2.00×10^{-4} mol/L NS^- in pH 2 buffer was run in between experiments to calculate a W_{eff} value using equation 2.1. The W_{eff} values calculated from the standard runs are given in Table 4.3. The experiments that were run are identified by a number in column 1. Column 2 describes the experiments that were run as being either a standard run or by the concentration of NS^- that was present in pH 2 buffer along with the constant butanol

Table 4.2 Sorption data for the effect of NS^- probe on butanol sample sorption on Partisil-10 ODS-3 using precolumn #3. The concentration of butanol in solution was kept constant at 1.09×10^{-3} mol/L. The solvent was pH 2 buffer.

$C_{m,NS}$ (mol/L)	$n_{NS} \times 10^5$ (mol) [(a)]	$n_{BuOH} \times 10^6$ (mol) [(a)]	W_{eff} (g)
0	0	2.32	0.1208
5.00×10^{-5}	0.0753	2.24	0.1203
1.00×10^{-4}	0.128	2.18	0.1181
2.00×10^{-4}	0.207	2.23	0.1159
5.00×10^{-4}	0.362	2.18	0.1197
1.00×10^{-3}	0.537	2.07	0.1175
2.00×10^{-3}	0.812	2.17	0.1154
5.04×10^{-3}	1.28	1.99	0.1130
7.58×10^{-3}	1.58	2.00	0.1122
1.01×10^{-2}	1.83	1.92	0.1138
5.02×10^{-2}	4.19	1.42	0.1075
9.99×10^{-2}	5.96	1.39	0.1063
0.157	7.15	1.25	0.1025

(a) These amounts were corrected to the original weight of packing in precolumn #3, $W_s = 0.1510$ g, using the W_{eff} values in column 4.

Table 4.3 Change in weight of packing in precolumn #3 for the study of the effect of NS^- probe on butanol sample sorption. The standard used to determine the effective weight of packing, W_{eff}, was 2.00×10^{-4} mol/L NS^- in pH 2 buffer.

Experiment Number	$C_{m,NS}$ (mol/L) [(a)]	W_{eff} (g)
1	Standard	0.1214
2	0	
3	5.00×10^{-5}	
4	5.00×10^{-4}	
5	Standard	0.1191
6	0	
7	1.00×10^{-4}	
8	1.00×10^{-3}	
9	Standard	0.1170
10	0	
11	2.00×10^{-4}	
12	2.00×10^{-3}	
13	Standard	0.1149
14	0	
15	1.01×10^{-2}	
16	5.04×10^{-3}	
17	7.58×10^{-3}	
18	Standard	0.1100
19	0	
20	5.02×10^{-2}	
21	9.99×10^{-2}	
22	Standard	0.1050
23	0	
24	0.157	

[(a)] This column identifies the experiment as either a standard run (*i.e.* Standard) or by the concentration of NS^- present in solution in studying the effect of NS^- probe on butanol sample sorption.

concentration of 1.09×10^{-3} mol/L. From Table 4.3, a total of 6 standards were run. Using the standard data, a plot of W_{eff} versus experiment number was made and is shown in Figure 4.9. The W_{eff} values given in column 4 of Table 4.2 were determined by obtaining the experiment number from Table 4.3 for the particular NS^- concentration used, and then reading the W_{eff} value off the plot in Figure 4.9.

The amount of butanol sorbed is plotted *versus* the amount of NS^- sorbed in Figure 4.10 from the data in Table 4.2. The amount of butanol sorbed decreases linearly with the amount of NS^- sorbed. The slope is -0.0148 ± 0.0010 moles butanol desorbed/moles NS^- sorbed and the x-intercept is $(1.50 \pm 0.12) \times 10^{-4}$ moles NS^- sorbed.

Assuming that the space occupied per NS^- molecule is independent of the fractional coverage of the stationary phase by NS^-, and considering a constant value of $C_{m,BuOH}$, the linearity of the plot of n_{BuOH} *versus* n_{NS} in Figure 4.10 suggests, *via* equation 4.4, that a competition for space is occurring. The linearity of the plot also shows that $K_{D,BuOH}$ is constant and is therefore independent of the concentration of NS^- in both the mobile and stationary phases. This means that neither the solvent strength of the mobile phase nor the sorbent strength of the stationary phase changes significantly in the presence of NS^-.

The space occupied per mole of NS^-, $\overline{A}_{NS}$, can be calculated from the slope and intercept of the plot in Figure 4.10 using equation 4.5. In equation 4.5, if "space" is considered in terms of surface area, then S is 266 m^2/g for this particular batch of Partisil-10 ODS-3 packing. The calculated value of $\overline{A}_{NS}$ is $(27 \pm 2) \times 10^4$ m^2/mol. This corresponds to a molecular area of $(45 \pm 3) \times 10^{-20}$ m^2/molecule, which is close to the value of 65×10^{-20} m^2/molecule measured on a space-filling model (CPK Models) of NS^-, by taking the average of two possible areas that NS^- could present to the surface (flat or side-on). The standard deviations given for $\overline{A}_{NS}$ and for the molecular area reflect the scatter in the data in Figure 4.10.

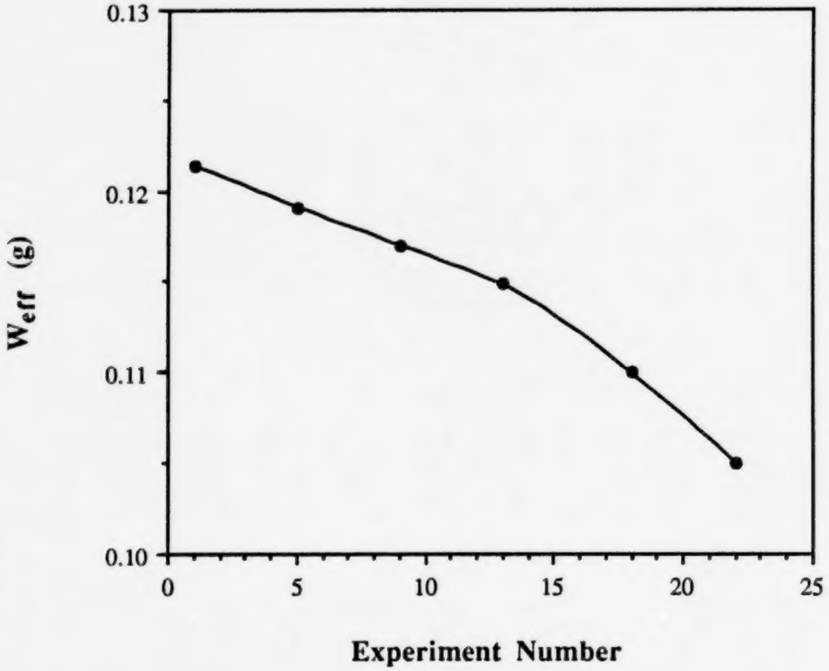

Figure 4.9 Change in the effective weight of packing in precolumn #3 for column equilibration experiments dealing with the effect of NS^- probe on butanol sample sorption. See Table 4.3 for the various experiments performed.

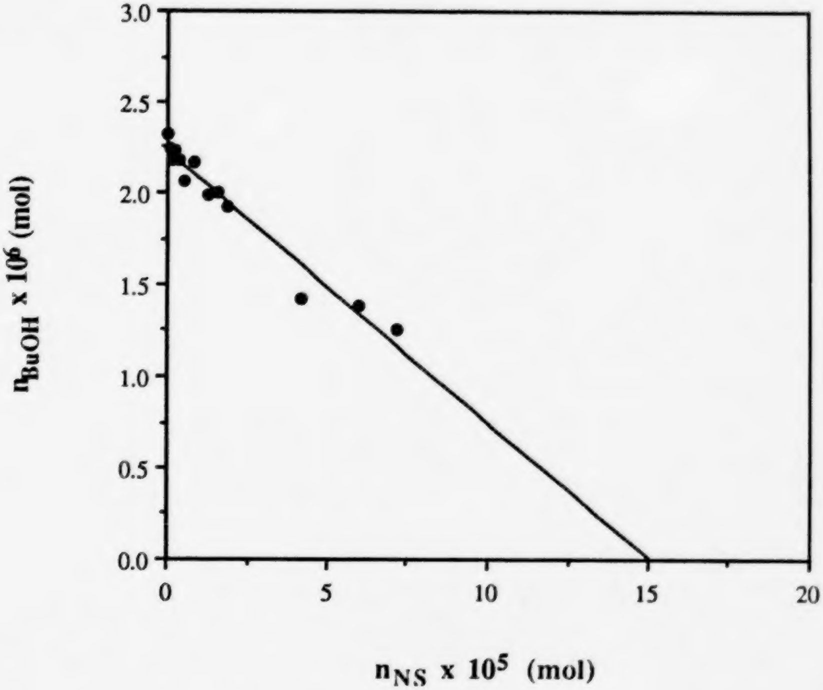

Figure 4.10 Effect of NS$^-$ probe on butanol sample sorption on Partisil-10 ODS-3 using precolumn #3 ($W_S = 0.1510$ g). In the column equilibration experiments the concentration of butanol was kept constant at 1.09×10^{-3} mol/L and the NS$^-$ concentration was varied from 0 to 0.157 mol/L. The solvent was pH 2 buffer.

4.3.3 Effect of Butanol Sample on NS^- Probe Sorption

Using the column equilibration technique, NS^- isotherms were measured without and with butanol present to demonstrate the effect of butanol on NS^- sorption. The isotherms are shown in Figure 4.11 and the data are given in Table 4.4. Table 4.5 shows the data for the standards that were used to determine the effective weights of packing for the probe isotherm experiments, which are given in column 5 of Table 4.4. The W_{eff} value used depended upon the date that the particular experiment was done. In both curves a and b in Figure 4.11, the NS^- concentration was varied from 0 to 3.62×10^{-3} mol/L. In curve a, no butanol was present and in curve b, the butanol concentration was kept constant at 2.18×10^{-2} mol/L. The amounts of NS^- sorbed without and with butanol present in solution were determined using a similar calibration curve to the one shown in Figure A.2.

From visual examination of the isotherms, it is obvious that the presence of butanol reduces the amount of NS^- sorbed. This is expected on the basis of the peak pattern observed in the elution chromatogram given in Chapter 3. However, the reason for this effect (*i.e.* categories 1-3 in Section 4.1) is not clear from the data in Figure 4.11 alone. If the decrease in NS^- sorption in the presence of butanol results from a decrease in the distribution coefficient ($K_{D,NS}$) alone, then it would imply that the presence of butanol strengthens the mobile phase as a solvent for NS^- and/or it weakens the stationary phase as a sorbent for NS^-. On the other hand, if the decrease in NS^- sorption in the presence of butanol results from only a decrease in available space in the stationary phase, then it implies that butanol is exerting its effect by competing for space.

From the results discussed above in connection with Figure 4.10, it is certain that at least part of the reduction in the amount of NS^- sorbed must be due to a competition between butanol and NS^- for space because a competition for space must be mutually reciprocal. In order to determine how much of the reduction in NS^- sorption is due to the competitive effect, a column equilibration experiment analogous to the one represented in

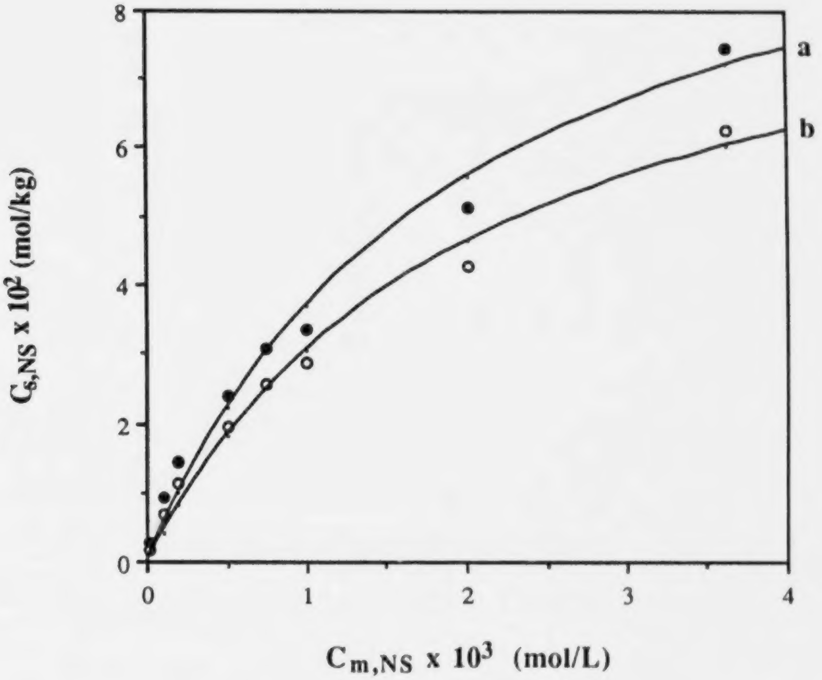

Figure 4.11 NS^- sorption isotherms on Partisil-10 ODS-3 from pH 2 aqueous solutions without and with butanol present using precolumn #2 ($W_S = 0.0871$ g). In curve a, 0 mol/L butanol is present and in curve b, 2.18×10^{-2} mol/L butanol is present. Solid lines are empirical while circles are experimental points.

Table 4.4 NS$^-$ sorption isotherm data on Partisil-10 ODS-3 without and with butanol present in solution from pH 2 aqueous solutions using precolumn #2.

Experiment Date	$C_{m,NS}$ x 10^3 (mol/L)	$C_{s,NS}$ x 10^2 (mol/kg) no BuOH [(a)]	$C_{s,NS}$ x 10^2 (mol/kg) with BuOH [(a)(b)]	W_{eff} (g)
December 8	0.0212	0.274	0.173	0.06504
December 5	0.100	0.923	0.685	0.07996
December 4	0.200	1.45	1.14	0.08182
December 6	0.501	2.41	1.96	0.07809
December 6	0.750	3.08	2.55	0.07809
December 7	1.00	3.36	2.88	0.07156
December 7	2.01	5.14	4.28	0.07156
December 8	3.62	7.45	6.26	0.06504

(a) The amounts of NS$^-$ sorbed were corrected to the original weight of packing in precolumn #2, $W_s = 0.08174$ g.

(b) Concentration of butanol was 2.18 x 10^{-2} mol/L.

Table 4.5 Standard data used to determine the effective weight of packing in precolumn #2 for the NS^- sorption isotherms without and with butanol present in solution. The standard was 2.00×10^{-4} mol/L NS^- in pH 2 buffer.

Standard Experiment Date	W_{eff} (g)
December 4	0.08182
December 6	0.07809
December 8	0.06504
December 9	0.06359

Figure 4.10 was performed in which the NS^- concentration in the mobile phase was kept constant at 2.00×10^{-4} mol/L in pH 2 buffer while the butanol concentration was varied from 0 to 4.36×10^{-2} mol/L.

The amounts of NS^- sorbed were determined using a similar calibration curve to the one shown in Figure A.2. The amounts of butanol sorbed were determined by constructing two calibration curves to cover the entire range of butanol concentrations that were used. Table A.13 and Figure A.5 present the data for the calibration curve for low butanol solution concentrations while Table A.14 and Figure A.6 present the data for the calibration curve for high butanol solution concentrations.

The amounts of NS^- and butanol sorbed are given in Table 4.6. These amounts were corrected for the change in the weight of packing using the procedure described in Section 2.5.6 and discussed in the previous section. A standard containing 2.00×10^{-4} mol/L NS^- in pH 2 buffer was run in between experiments to calculate a W_{eff} value using equation 2.1. The W_{eff} values calculated from the standard runs are given in Table 4.7. The experiments that were run are identified by a number in column 1. Column 2 describes the experiments that were run as being either a standard run or by the concentration of butanol that was present in pH 2 buffer along with the constant NS^- concentration of 2.00×10^{-4} mol/L. From Table 4.7, a total of 4 standards were run. Using the standard data, a plot of W_{eff} versus experiment number was made and is shown in Figure 4.12. The W_{eff} values given in column 4 of Table 4.6 were determined by obtaining the experiment number from Table 4.7 for the particular butanol concentration used, and then reading the W_{eff} value off the plot in Figure 4.12.

The amount of NS^- sorbed is plotted *versus* the amount of butanol sorbed in Figure 4.13 from the data in Table 4.6. A linear relationship is observed. The slope is -0.0135 ± 0.0005 moles NS^- desorbed/moles BuOH sorbed and the x-intercept is $(1.57 \pm 0.06) \times 10^{-4}$ moles BuOH sorbed.

Table 4.6 Sorption data for the effect of butanol sample on NS^- probe sorption on Partisil-10 ODS-3 using precolumn #3. The concentration of NS^- in solution was kept constant at 2.00×10^{-4} mol/L. The solvent was pH 2 buffer.

$C_{m,BuOH}$ (mol/L)	$n_{NS} \times 10^6$ (mol) [(a)]	$n_{BuOH} \times 10^5$ (mol) [(a)]	W_{eff} (g)
0	2.15	0	0.1510
2.18×10^{-4}	2.07	0.0558	0.1498
3.27×10^{-4}	2.13	0.0881	0.1323
4.36×10^{-4}	2.12	0.117	0.1285
5.45×10^{-4}	2.12	0.137	0.1423
7.63×10^{-4}	2.11	0.174	0.1262
1.09×10^{-3}	2.11	0.298	0.1388
5.45×10^{-3}	1.96	1.10	0.1341
1.09×10^{-2}	1.78	2.10	0.1294
2.18×10^{-2}	1.59	3.65	0.1256
3.27×10^{-2}	1.44	5.52	0.1274
4.36×10^{-2}	1.32	5.90	0.1315

[(a)] These amounts were corrected to the original weight of packing in precolumn #3, W_s = 0.1510 g, using the W_{eff} values in column 4.

Table 4.7 Change in weight of packing in precolumn #3 for the study of the effect of butanol sample on NS^- probe sorption. The standard used to determine the effective weight of packing, W_{eff}, was 2.00×10^{-4} mol/L NS^- in pH 2 buffer.

Experiment Number	$C_{m,BuOH}$ (mol/L) [(a)]	W_{eff} (g)
1	Standard	0.1510
2	2.18×10^{-4}	
3	5.45×10^{-4}	
4	1.09×10^{-3}	
5	Standard	0.1360
6	5.45×10^{-3}	
7	3.27×10^{-4}	
8	4.36×10^{-2}	
9	Standard	0.1301
10	4.36×10^{-4}	
11	1.09×10^{-2}	
12	3.27×10^{-2}	
13	Standard	0.1262
14	7.63×10^{-4}	
15	2.18×10^{-2}	

[(a)] This column identifies the experiment as either a standard run (*i.e.* Standard) or by the concentration of butanol present in solution in studying the effect of butanol sample on NS^- probe sorption.

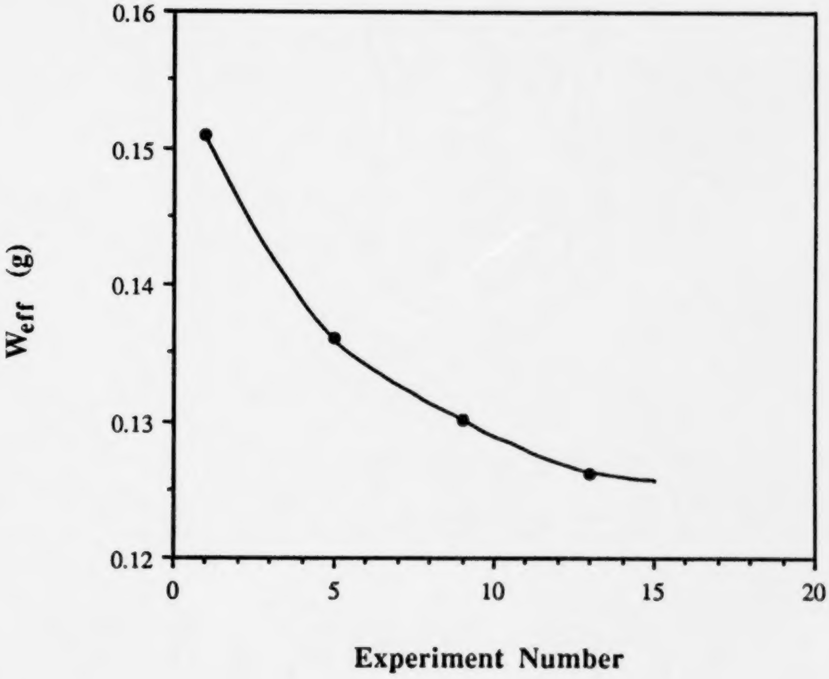

Figure 4.12 Change in the effective weight of packing in precolumn #3 for column equilibration experiments dealing with the effect of butanol sample on NS$^-$ probe sorption. See Table 4.7 for various experiments performed.

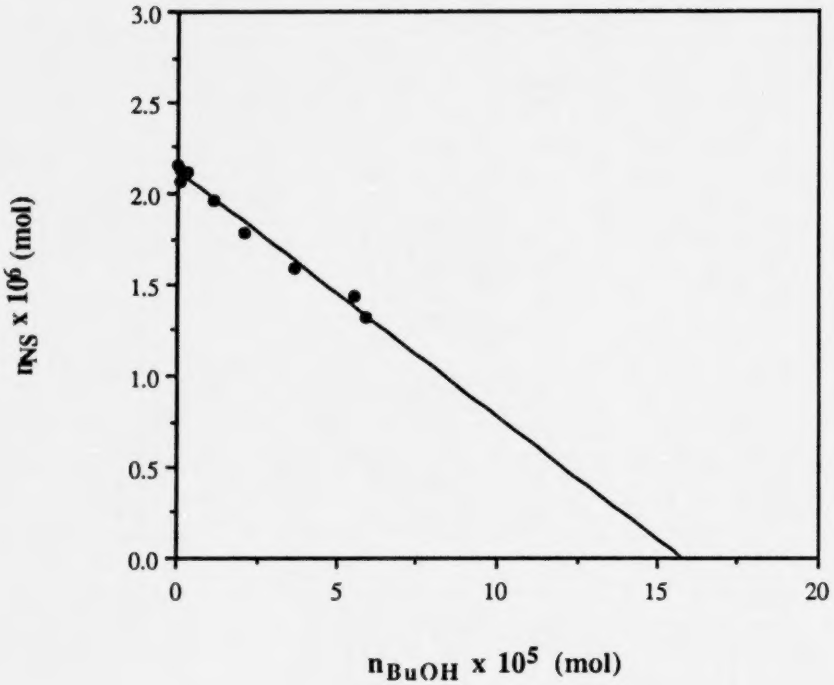

Figure 4.13 Effect of butanol sample on NS^- probe sorption on Partisil-10 ODS-3 using precolumn #3 ($W_S = 0.1510$ g). In the column equilibration experiments the concentration of NS^- was kept constant at 2.00×10^{-4} mol/L and the butanol concentration was varied from 0 to 4.36×10^{-2} mol/L. The solvent was pH 2 buffer.

According to equation 4.6, a competition for space is occurring if a plot of n_{NS} *versus* n_{BuOH} is linear. The linearity of the plot in Figure 4.13 indicates that $K_{D,NS}$ is constant and, consequently, that neither the mobile phase strength nor the stationary phase sorbent strength is altered to a detectable extent by the presence of these small amounts of butanol. That is to say, while the presence of even these low concentrations of butanol undoubtedly produces some changes in the mobile phase eluent strength (and perhaps also in the stationary phase sorbent strength), the magnitude of these changes are too small to be detected in the presence of the large competitive effect. The linearity of the plot in Figure 4.13 also implies that the space occupied per mole of butanol is independent of the fractional coverage of the stationary phase by butanol.

Also by analogy with the previous case, the area occupied per molecule of butanol can be calculated using equation 4.5. It was found to be $(43 \pm 2) \times 10^{-20}$ m^2/molecule which is close to the value of 35×10^{-20} m^2/molecule determined from a molecular model by taking the average of three possible areas that butanol could present to the surface.

4.3.4 Langmuir Isotherm Behaviour

It is noteworthy that the linearity implied by equations 4.4 and 4.6 and observed in Figures 4.10 and 4.13 does not require that either the NS^- or the butanol isotherms follow a particular equation (e.g. Langmuir equation). This is because the solution concentrations of $C_{m,BuOH}$, for equation 4.4 and $C_{m,NS}$ for equation 4.6, are held constant in the experiments. That is, the experiments represented in Figures 4.10 and 4.13 are conducted at a fixed point on the butanol or NS^- isotherm, respectively, at which $K_{D,BuOH}$ or $K_{D,NS}$ is expected to be a constant provided that the solvent strength and/or stationary phase sorbent strength are not changing. This simply means that n_{BuOH} in equation 4.1, for example, has decreased in proportion to A_S, the amount of space not "blocked" by NS^-, so that $C_{s,BuOH}$ remains constant. Thus, although the experiments represented in Figures

4.10 and 4.13 were carried out at concentrations falling in the linear regions of the butanol and NS^- isotherms, respectively (as can be seen from Figures 4.8 and 4.11), this was not a necessary condition to obtain constant values of $K_{D,BuOH}$ and $K_{D,NS}$.

Equations 4.4 and 4.6 reveal that the intercepts on the horizontal axes in Figures 4.10 and 4.13 correspond to the maximum stationary phase occupancy of NS^- ($n_{max,NS}$) and butanol ($n_{max,BuOH}$), respectively. If the butanol and/or NS^- isotherms could be described by an established theory, such as the Langmuir equation, then the interpretation of the experimental results could be carried further than is allowed by equations 4.4 and 4.6. In particular, the limiting values predicted by curve fitting the Langmuir equation to the experimental data could be compared with the values from the intercepts on the horizontal axes in Figures 4.10 and 4.13. This possibility is now examined.

A previous study showed that butanol sorption onto a polymeric bonded phase (Whatman Partisil-10 ODS-2) follows the Langmuir equation (equation 3.2) [117]. If the experimental data from curve a in Figure 4.8 conform to the Langmuir equation, then a double reciprocal plot of $1/C_{s,BuOH}$ *versus* $1/C_{m,BuOH}$ should be a straight line (equation 3.3). When such a plot is made using the data in Table A.10 (Figure 4.14), the points for which $1/C_{m,BuOH} \geq 12$ L/mol (*i.e.* $C_{m,BuOH} \leq 8 \times 10^{-2}$ mol/L) describe a straight line, from the slope and intercept of which may be calculated $K_{BuOH} = 13 \pm 7$ L/mol and $C_{s,max,BuOH} = 1.1 \pm 0.6$ mol/kg. However, as shown in Figure 4.15, the points for which $1/C_{m,BuOH} \leq 12$ L/mol deviate from this line, indicating an apparent deviation from Langmuir behaviour at high butanol concentrations. When the above values of K_{BuOH} and $C_{s,max,BuOH}$ are used in equation 3.2 to generate a plot of $C_{s,BuOH}$ *versus* $C_{m,BuOH}$, the dashed line curve that is shown as curve b in Figure 4.8 is obtained. Thus, the butanol isotherm follows the Langmuir equation in the concentration range of $(0\text{-}8) \times 10^{-2}$ mol/L but deviates from it at higher concentrations. In contrast, the experimental isotherm in curve a of Figure 4.8 (solid line) is not apparently approaching a limiting value of $C_{s,max,BuOH}$ at concentrations of $C_{m,BuOH}$ as high as 0.654 mol/L.

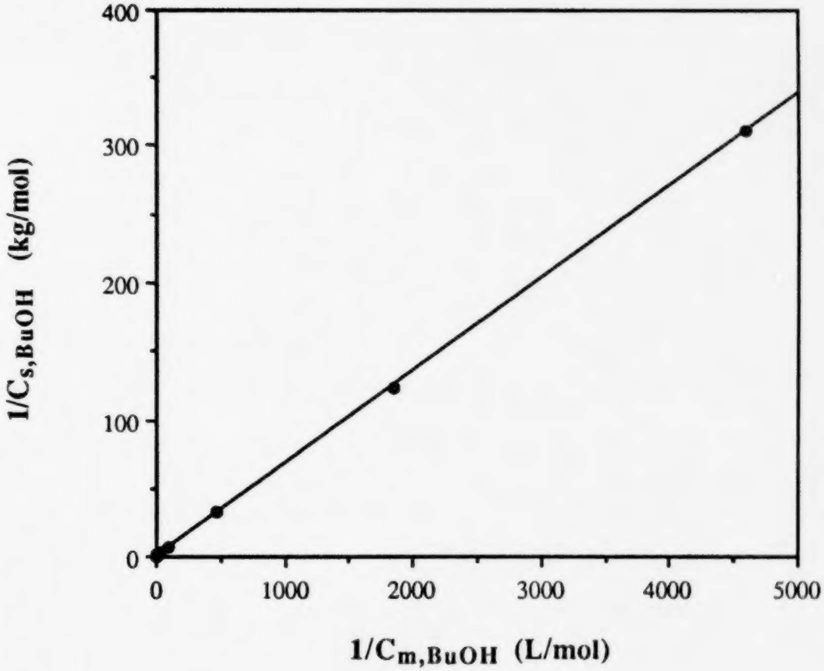

Figure 4.14 Double reciprocal plot of the butanol sorption isotherm shown as curve a in Figure 4.8 according to equation 3.3. The data are given in Table A.10.

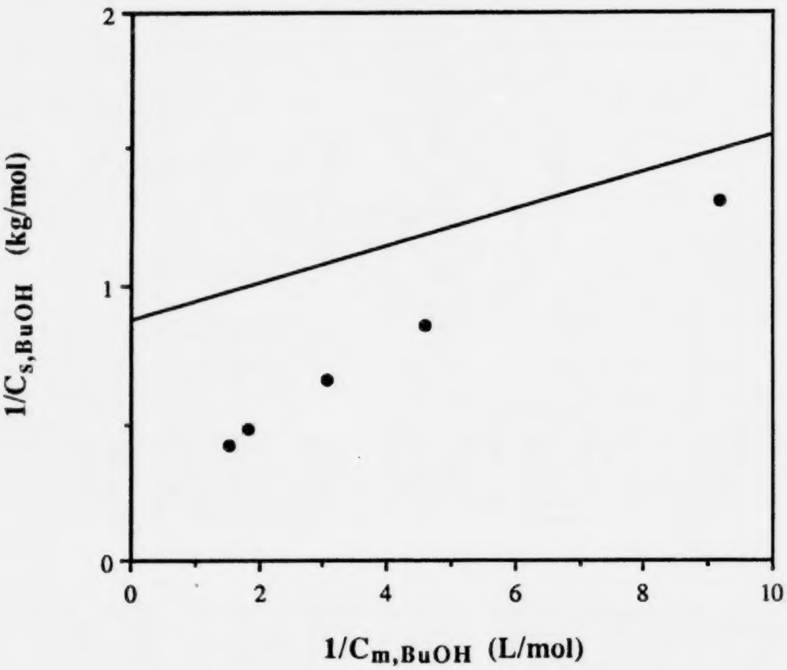

Figure 4.15 Expansion of the lower left hand corner of the plot in Figure 4.14.

From the Langmuir constant $C_{s,max,BuOH}$ obtained above, the value of $n_{max,BuOH}$ may be calculated. It is found to be (1.7 ± 0.9) x 10^{-4} mol, which agrees within experimental error with the value obtained from the horizontal axis intercept in Figure 4.13, *i.e.* (1.59 ± 0.07) x 10^{-4} mol. The vertical arrow shown in Figure 4.8 indicates the maximum butanol concentration that was used in studying the effect of butanol on probe sorption, the results of which study are given in Figure 4.13. Thus, the agreement of the horizontal axis intercept in Figure 4.13 with the limiting value of the dashed isotherm in curve b of Figure 4.8 is not surprising since the butanol concentration range studied in Figure 4.13 lies entirely within the Langmuirian region of the butanol isotherm. Though the evidence obtained from Figures 4.10 and 4.13 alone in support of a competition model is conclusive, it is pleasing to find the above agreement, based on the Langmuir equation, which represents further support for the view that the reduction in the amount of NS^- sorbed when butanol is present is strictly due to a competitive effect, *i.e.* category 2 in the Section 4.1.

Different behaviour is observed in the case of the NS^- isotherm shown in Figure 4.16 and given in Table A.15. The points in Figure 4.16 correspond to the points in Figure 4.10 which were measured at a constant butanol concentration of 1.09 x 10^{-3} mol/L. The presence of such a small concentration of butanol has very little effect on the sorption of NS^-, as seen from the very early points in Figure 4.13. Thus, a NS^- isotherm which would be measured in the absence of butanol would be virtually identical to the isotherm presented in Figure 4.16. A plot of $1/C_{s,NS}$ *versus* $1/C_{m,NS}$ is shown if Figure 4.17. It is nonlinear over the entire concentration range, demonstrating that the NS^- isotherm does not exhibit Langmuir behaviour. As a result, a value for $C_{s,max,NS}$ cannot be estimated from the data in Figure 4.16 for comparison to the horizontal axis intercept in Figure 4.10.

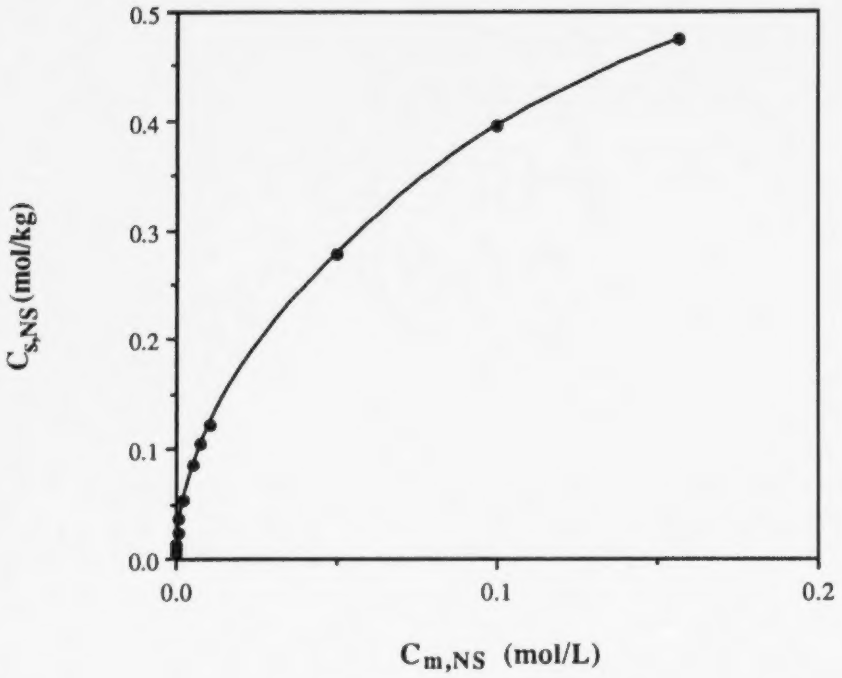

Figure 4.16 NS^- sorption isotherm on Partisil-10 ODS-3 from pH 2 aqueous solutions with 1.09×10^{-3} mol/L butanol present using precolumn #3 ($W_S = 0.1510$ g). The data were taken from Figure 4.10. The solid line was obtained by Stineman interpolation [147] through the experimental points (circles) using Cricket Graph 1.3. The data are given in Table A.15.

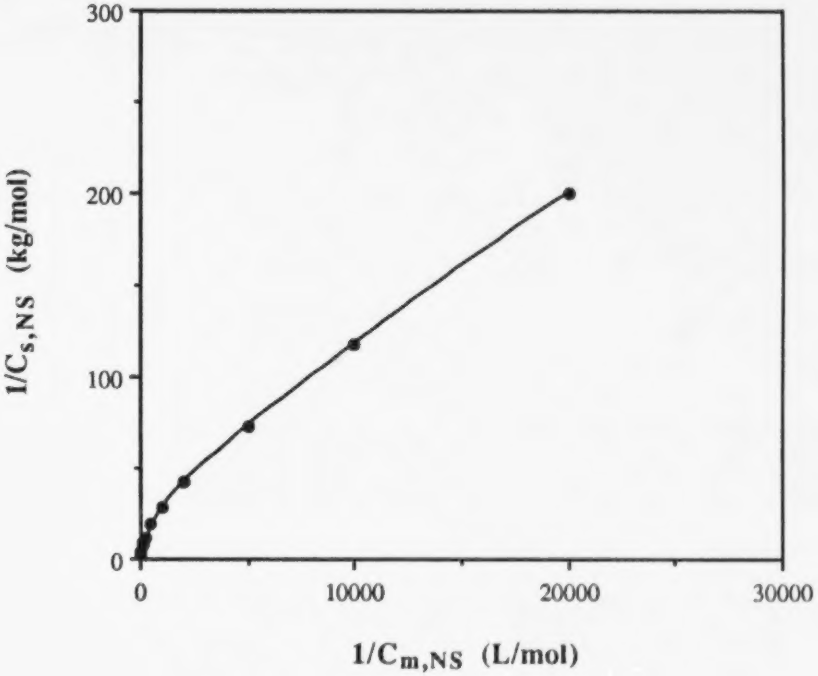

Figure 4.17 Double reciprocal plot of the NS^- sorption isotherm in Figure 4.16 according to equation 3.3.

4.3.5 Changing Eluent and Sorbent Strength

Figure 4.18 is a plot of the natural logarithm of the distribution coefficient for NS^- *versus* the volume fraction of butanol in the mobile phase, ϕ_{BuOH}. The data are given in Table A.16. The points in Figure 4.18 correspond to the points in Figure 4.13 which were measured at a constant NS^- concentration of 2.00×10^{-4} mol/L. The line in Figure 4.18 was obtained by nonlinear least squares curve fitting of the polynomial equation 4.13 to the experimental points. The least squares values obtained for the constants are $A = (1.48 \pm 0.27) \times 10^4$, $B = -180 \pm 10$, and $C = 4.256 \pm 0.004$, and the correlation coefficient is $r = 0.996$.

Current theories on the role of the mobile phase composition in RPLC, such as the extended solubility parameter theory [16,126,132,133], the E_T solvatochromic theory [123] and the linear solvation energy relationship (LSER) theory [127], when applied at low concentrations of "organic modifier" (*i.e.* butanol, in the present context), predict such a quadratic dependence of ln K_D on modifier concentration. Thus, the quadratic dependence of ln $K_{D,NS}$ on ϕ_{BuOH}, when considered in the absence of the correlations presented in Figures 4.10 and 4.13, might seem to suggest that the decrease in $K_{D,NS}$ with increasing concentration of butanol results from an increase in the mobile phase eluent strength accompanied, perhaps, by a consequent change in stationary phase sorbent strength (*i.e.* categories 1 and 3 in Section 4.1). However, comparison of the experimentally measured value of parameter A in equation 4.13 with the value predicted by theory does not support this view. Theory predicts that the value of A is given approximately as [16,126,132,133]:

$$A = \frac{\overline{V}_{NS}}{RT}(\delta_{H_2O} - \delta_{BuOH})^2 = 19$$

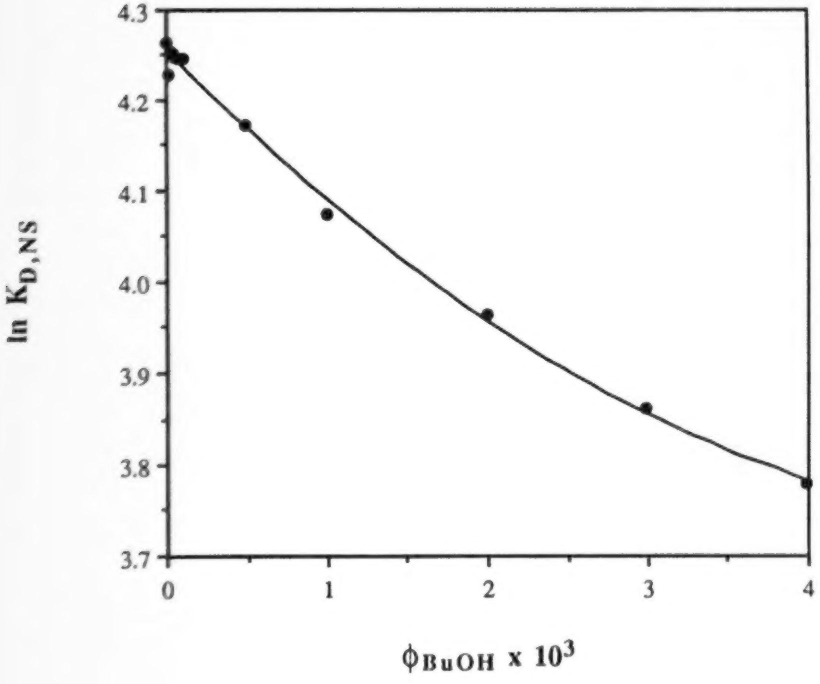

Figure 4.18 Solubility parameter plot of the data in Figure 4.13 based on equation 4.13 to test if a solvent effect is responsible for the decrease in NS^- sorption when butanol is present in solution. ϕ_{BuOH} is the volume fraction of butanol in solution. The solid line is from nonlinear curve fitting to a quadratic equation. The circles are experimental points. The data are given in Table A.16.

where $\overline{V}_{NS}$ is the molar volume of NS^- (approximately 78 cm^3/mol), δ_{H2O} and δ_{BuOH} are solubility parameters (23.4 and 11.4 $cal^{1/2}/cm^{3/2}$, respectively, from reference 134), R is the ideal gas constant (1.9865 cal/mol K) and T is 298 K. If one accepts the solubility parameter theory as a rough estimate of solution behaviour, then the fact that the experimentally measured value of A (1.55×10^4) is over three orders of magnitude larger than that predicted by theory indicates that the quadratic relationship observed between ln $K_{D,NS}$ and ϕ_{BuOH} does not arise from a change in eluent strength but, rather, arises fortuitously from a combination of the linear dependence of n_{NS} on n_{BuOH} (Figure 4.13) and the curved dependence of n_{BuOH} on $C_{m,BuOH}$ (Figure 4.8) and, therefore, on ϕ_{BuOH} at low $C_{m,BuOH}$. If the effect of butanol on NS^- sorption were due to the influence of butanol on solvent strength only, then the effect would have been very much smaller than the observed effect.

4.3.6 Adsorption versus Partitioning

Monomeric RPBPs have been studied more extensively than polymeric RPBPs and the dependence of their alkyl chain conformation upon eluent composition and temperature suggests that the structure of monomeric stationary phases is more variable than that of polymeric phases [11,16,135,136]. Only a polymeric bonded phase has been employed in the present thesis. However, it is to be expected that in a highly aqueous mobile phase the same kind of competitive sorption behaviour would be observed for butanol and NS^- on a monomeric bonded phase as is observed on the polymeric bonded phase. A persistent theme in the literature on RPBP sorbents [16], both monomeric and polymeric, is the dispute over whether the solute is sorbed by the stationary phase *via* interfacial adsorption onto its surface (*i.e.* onto the interface between the stationary and mobile phases) [19,130,137-144] or *via* partition into the stationary phase [13-15,139].

In the present study, it has been demonstrated that the two solutes, NS^- (probe) and butanol (sample), are in direct competition with one another for space in the stationary phase. However, this should not be interpreted as conclusive proof that these solutes are sorbed *via* interfacial adsorption rather than *via* partitioning, for the following reasons. The thickness of a bonded layer of C-18 on the silica gel surface, whether monomeric or polymeric, is not more than about 20 Å when methanol is the mobile phase [145]. With a highly aqueous mobile phase this thickness would be, if anything, even somewhat less because of more extensive collapsing of the chains [13]. Even for a solute as small as butanol [117] the bonded layer is only a few times thicker than the molecular diameter of the solute so that the fraction of the total stationary phase volume occupied by the solute molecule, if partitioned, would be highly correlated with the fraction of the total stationary phase area occupied by the solute molecule, if interfacially adsorbed. Even if the NS^- and butanol were completely "dissolved" in a "bulk liquid" bonded phase, there could be a competition between these sorbed species with one another for volume in such a thin layer of bonded phase. If only a limited part of the bonded phase interacts with the solute, as has been suggested [146], then this competition for "volume" would be even more pronounced. Thus, in this chapter we have chosen to use the more general terms "sorption" and "competition for space" rather than "interfacial adsorption" and "competition for area" and to adopt neither side in the adsorption-partition debate. In the next chapter where electrostatic effects are important, the additional retention process of exclusion occurs. The term "sorption" will therefore be used to include this additional effect and the term "adsorption" will be used to refer to adsorption/partitioning (*i.e.* sorption in the present chapter). This will be necessary to make the distinction between an "adsorption" process and an exclusion process.

4.4 Conclusions

From the results of the column equilibration experiments described in Figure 4.10 and 4.13, a competition for space between butanol sample and NS^- probe is responsible for the decrease in probe sorption in the butanol sample zone during an elution chromatogram. It is likely that the presence of butanol in the mobile phase and/or the presence of sorbed butanol in the stationary phase also plays a role in affecting the sorption of the probe. However, under the conditions in the present chapter these effects could not be detected since the competitive effect dominated. This competition for space in the RPBP is the origin of indirect UV detection of butanol using NS^- as probe.

Chapter 5

Origin of Indirect UV Detection of the Cationic Sample Tetrabutylammonium Ion Using the Cationic Probe 4-Nitrobenzyltrimethylammonium Ion

5.1 Introduction

When two different ions are simultaneously sorbed from the mobile phase onto a RPBP liquid chromatography packing, it is to be expected that each will exert an influence on the sorption of the other. For example, when a reagent ion is present in the mobile phase at a much higher concentration than a sample ion of *opposite charge* then the conditions of so-called "ion-pair reversed phase liquid chromatography" (IP-RPLC) are created and the retention time of the sample ion is markedly greater than it would be in the absence of the reagent ion [32,148-151]. It is also well known that if the sample ion has the *same sign* of charge as the reagent ion under IP-RPLC conditions then the retention of the sample ion is decreased compared to its value in the absence of the reagent ion [32,46,114,120,138,152].

It has been suggested that the name "ion-modified reversed phase liquid chromatography" (IM-RPLC) is more appropriate than the name "ion-pair reversed phase liquid chromatography", whether the sample ion has the same or opposite charge as the reagent ion, since the formation of ion-pairs has not unambiguously been demonstrated to occur in either case [32]. It has also been suggested that the reagent ion should be called a modifier ion. The newer nomenclature will be used in the remainder of this thesis.

It is now well established that a modifier ion is sorbed onto or into the RPBP and thereby establishes an electrical potential gradient and an electrical "double layer" in the vicinity of the interface between the bonded phase and the mobile phase. Several models based on electrical double layer theory have been proposed and tested experimentally on RPBP sorbents. These models have recently been reviewed and compared both among themselves and with non-double layer models [32]. Speaking generally, any ion which is sorbed from the mobile phase to the stationary phase in excess over oppositely charged ions will contribute to the establishment of an electrical potential difference between the two phases. Such an ion may be called a "potential producing ion" (PPI). The existence of this potential will, in turn, contribute to the overall free energy (*i.e.* electrochemical potential) for sorption of ions - favoring sorption of ions of opposite charge and disfavoring sorption of ions of like charge.

A version of the Stern-Gouy-Chapman (SGC) theory of the electrical double layer has previously been used to explain the processes responsible both for the sorption of ions [34] and for IM-RPLC on ODS bonded phases [37]. In this version of the SGC theory, modifier ions adsorb onto the RPBP with their charge centers all lying in the same plane, thereby creating a charge surface having a surface potential Ψ_0. The double layer region is thought to be divided into a compact part and a diffuse part. Heretofore, in the application of this SGC model, it was assumed that when more than one type of ion is adsorbed, the adsorption occurs in the same plane for all adsorbed ions. For example, in a study of ion-modified retention, an anionic sample ion was considered to adsorb at the very same charge surface which was created by the adsorption of a cationic modifier ion, and it was the potential at that plane which was used in calculating the electrochemical potential of the sample ion [37].

One of the purposes of the study in the present chapter is to test the applicability of the SGC model to the simultaneous sorption of two ions having the same charge. The ion tetra-*n*-butylammonium (TBA^+) might be considered the "sample" ion because in most experiments it is present at lower concentration. Its sorption on an ODS packing has previously been characterized [34]. The other cation is 4-nitrobenzyltrimethylammonium

(NBTA$^+$). Experimentally, the column equilibration technique [34,37] is used to measure simultaneously the amounts of TBA$^+$ and NBTA$^+$ sorbed at equilibrium. The solution concentration of NBTA$^+$ is held constant while both the concentration of TBA$^+$ and the ionic strength are varied. The experimental results are evaluated in terms of a modified version of the previously employed SGC model. The modification which has to be made to the SGC model is to allow the centers of charge of adsorbed TBA$^+$ and NBTA$^+$ to lie at different planes within the compact part of the double layer.

The second purpose of this chapter is to use the results obtained from employing the SGC model in order to determine the origin of indirect UV detection of the cationic sample TBA$^+$ using the cationic probe NBTA$^+$. The three general categories that were presented in Chapter 1 as to how a sample can affect probe sorption are applicable to this case. The pattern of eluted sample and system peaks that is observed when the probe and the sample have the same sign of charge reveals that there is a local decrease in the amount of probe sorbed in the sample zone [22,120]. A number of physicochemical retention models have been proposed in the literature to explain this decreased sorption of probe ion in the presence of sample ion, several of which invoke a competition for space in the stationary phase [26,46,65,101,102,114,120,138,142,152-154].

In some of these models the competition for space is between ion pairs that are said to be formed, both by the probe ion and the sample ion, with an oppositely charged ion from the mobile phase. These ion pairs are said to exist either only in the stationary phase or in both the stationary and mobile phases [26,65,101,102,142,153]. The competition for space is expressed in terms of mixed Langmuir isotherms for sorption onto either one or two types of surface sites.

Other models invoke an electrostatic repulsion effect, either with or without competition for space [46,110,120,124,138,152]. Most of these models are formulated in terms of either the "ion interaction" theory, which does not explicitly invoke an electrical potential at the interface between the reversed phase bonded phase (RPBP) and the mobile phase [110,114,120]; or in terms of electrical double layer theory, in which the electrical potential plays a major role [46,152]. The model proposed in the present chapter falls in the latter category.

Normally in indirect detection systems both the probe ion and the sample ion are PPIs, so that the sorption of each would be expected to exert an influence on the sorption of the other. If probe and sample ions have the same sign of charge, then sorption of the sample ion will alter the electrical potential at the interface in such a way as to cause desorption of some probe. When, as is usually the case, the probe ion is present in the mobile phase at much higher concentrations than the sample ion, the sorbed probe ion is largely responsible for development of the potential. However, this does not mean that sorption of the sample ion makes no contribution to the potential - only that it causes a small change in potential with consequent desorption of only a small fraction of the probe. Here it is important to note that, under the conditions typically used for indirect detection chromatography, sample- and system- elution peaks correspond to the desorption of only a small fraction of probe ion. Thus, in terms of electrical double layer models, there are two likely reasons for a sorbed sample ion to cause a decrease in the sorption of a similarly charged probe ion - competition for space and contribution to a less favorable electrical potential [46]. Any one of the several electrical double layer models would correctly account for the observed signs of sample and system peaks in indirect detection chromatography of a sample ion with a probe ion of like charge. It is only in their details that the various double layer models would differ in their explanation of the phenomenon.

The purpose of the research described in this chapter is to determine why the positively charged sample ion tetra-*n*-butylammonium (TBA^+) causes decreased sorption of the positively charged probe ion 4-nitrobenzyltrimethylammonium ($NBTA^+$) on the RPBP Partisil-10 ODS-3. The dependence of the moles of $NBTA^+$ probe sorbed is evaluated as a function of the moles of TBA^+ sorbed and the ionic strength. TBA^+ was chosen as the sample ion because it is non-UV absorbing and $NBTA^+$ was chosen as the probe ion because similar quaternary ammonium ions have previously been used as probes for indirect UV detection [155].

In this chapter the experimental results are evaluated with an equation which combines both the competition for space model, which was shown in Chapter 4 to explain the effect of the neutral sample butanol on the sorption of an ionic probe; and a *modified* version of the SGC double layer sorption model which takes into account the sorption of TBA^+ and $NBTA^+$ at different charge surfaces within the compact part of the double layer.

5.2 Theory

5.2.1 SGC Theory of the Electrical Double Layer

In this description of the electrical double layer, it is not critical whether the presence of ions in the ODS RPBP is due to "partitioning" or "adsorption". However, for the present purpose, a solute molecule that is in (or on) the ODS phase will be said to be "adsorbed" in order to distinguish this type of sorption from that associated with the solute in the diffuse layer (*i.e.* coion exclusion). In the case of a highly end capped ODS bonded phase, it is assumed that the amount of residual silanol groups on the ODS surface is negligible, so there is no coulombic (electrical) interaction between the ODS surface and adsorbed ions. The description of the electrical double layer presented in this section is based on references 33, 35 and 36.

For a solution which contains a single adsorbable cation (e.g. $NBTA^+$) present as its chloride salt in inert electrolyte (e.g. NaCl), the electrical double layer that develops at the interface between the bonded phase and solution, as a result of adsorption of $NBTA^+$ onto the surface, is shown in Figure 5.1. In this case, $NBTA^+$ is referred to as a potential producing ion (PPI) because its adsorption, in excess over other ions from solution, produces an electrical potential difference Ψ_0 between the surface and bulk solution. Since

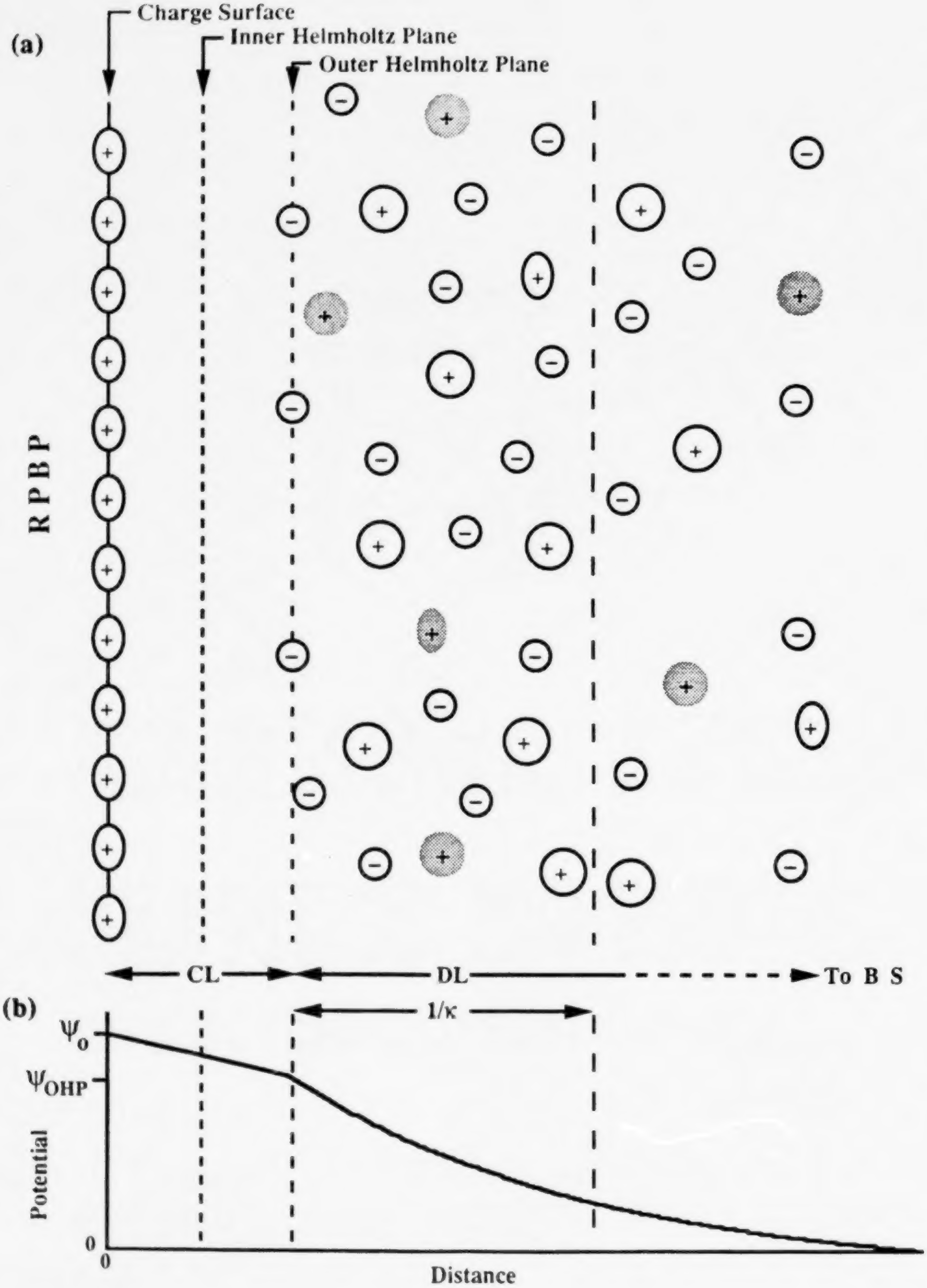
(a)
Charge Surface
Inner Helmholtz Plane
Outer Helmholtz Plane
R P B P
CL
DL
To B S
(b)
1/κ
ψ_o
ψ_{OHP}
Potential
0
0
Distance

Figure 5.1 (a) Diagrammatic representation of the electrical double layer region for a RPBP with adsorption of a cationic PPI (oval shaped ions) at the interface to create the charge surface, having potential Ψ_o. (b) Potential in the electrical double layer as a function of distance. Circular cations and anions are from the inert (non-adsorbed) electrolyte. Potential decreases linearly over the compact layer (CL) to a value Ψ_{OHP} at the Outer Helmholtz Plane, which is the plane of closest approach of nonadsorbed negative counterions. The thickness of the diffuse part (DL) of the double layer is $1/\kappa$ and depends on ionic strength of the bulk solution (BS). The potential decays approximately exponentially across the DL toward a value of 0 Volt in the BS. The surface excess of adsorbed PPIs (Γ_i^{AD}) is counterbalanced by an equal surface excess of negative ions in the DL, which is due partly to the attraction of negative counterions into the DL in numbers exceeding their concentration in bulk solution, and partly to expulsion of cationic coions from the DL which causes the cation concentrations in the DL to be lower than in bulk solution giving a negative surface excess of coions. These absent cations are shown as stipled "ghosts". PPI coions are expelled along with inert coions, which creates a negative surface excess of PPIs in the DL (Γ_i^{DL}) and causes the total surface excess of PPIs in the whole double layer region to be lower than the number that are adsorbed.

electroneutrality must be maintained, the surface charge created by adsorbed $NBTA^+$ is balanced by an equal amount of opposite charge on the solution side. Ions of opposite charge, *i.e.* counterions such as Cl^-, are attracted to the charge surface such that their concentration near the surface is greater than in bulk solution. At the same time, ions having the same charge as the charge surface, *i.e.* coions such as Na^+ and $NBTA^+$, one of which is the potential producing ion $NBTA^+$, are repelled from the surface so their concentration in solution near the surface is lower than in bulk solution. Due to random thermal motion, the counterions are not confined to a single plane, but rather, they are spread out diffusely in solution.

The concentration of an ion i in the interfacial region is expressed as its surface excess, Γ_i, which is the number of moles of i per square centimeter of surface, and in its adjoining double layer in solution, which are in excess of the moles of the same species contained in an equivalent volume of bulk solution. An equivalent volume of bulk solution is defined as that volume of bulk solution containing the same total moles of charge of all species as there are in one square centimeter of the surface under consideration. The equation for calculation of the surface excess (mol/cm^2) is as follows:

$$\Gamma_i = \frac{n_i}{W_S\,S} = \frac{n_i}{A_T} \tag{5.1}$$

where n_i is the moles of i sorbed, W_S is the weight of packing (g), S is the specific surface area of the packing (cm^2/g) and A_T is the total surface area/space available for sorption (cm^2).

In the version of the SGC theory [156,157] that is used in this thesis, the adsorbed PPIs are considered to be part of the surface and to be true "potential determining ions" (PDI) in the sense that when the activities of these ions in bulk solution, e.g. a_{NBTA}, are held constant, then the surface potential Ψ_0 is constant even if the ionic strength of the solution is altered [32,34,37]. Sometimes the relation between Ψ_0 and solution activity of

PDI obeys the well-known Nernst equation:

$$\Psi_o = k + \left(\frac{RT}{ZF}\right) \ln a_{NBTA} \tag{5.2}$$

where k is a constant, R is the ideal gas constant (8.314 J/(mol·K), T is the temperature (298 K), Z (equivalents/mole) is the charge on the ion and F is the Faraday constant (96487 Coulomb/mole). In the present treatment however, it is not necessary that the Nernst equation be valid, but only that Ψ_o is constant at a constant a_{NBTA}.

Since the hydrated counterions have a finite size, they can only approach the bonded phase to within a certain distance which is usually taken as the radius of a hydrated counterion. This plane of closest approach is referred to as the Outer Helmholtz Plane (OHP). It is possible for counterions or coions with most or all of the hydrated water molecules being absent to be "specifically adsorbed" to the surface in an Inner Helmholtz Plane (IHP) which lies between the charge surface and the OHP. According to SGC theory, there may or may not be ions in the IHP depending upon the nature of the ions and the nature of the bonded phase and solution phase.

The electrical double layer can be divided into two parts. The *compact part* of the electrical double layer extends from the charge surface up to, but not including the OHP. In this region the potential decays linearly. It can be treated as an electrical capacitor of constant thickness δ (cm) and capacitance C_1 (Farad/cm^2) where one plate is the charge surface and the other plate is the OHP.

$$C_1 = \frac{\sigma_o}{\Psi_o - \Psi_{OHP}} \tag{5.3}$$

In the equation σ_o (Coulomb/cm^2) is the surface charge density of the PDI and Ψ_{OHP} (Volt) is the potential at the OHP. The compact layer thickness is given by

$$\delta = \frac{\varepsilon}{4\pi C_1} \tag{5.4}$$

where ε is the permittivity of solution which is equal to the product of the unitless dielectric constant and the constant 1.12×10^{-12} Coulomb/(Volt·cm) [156].

The *diffuse part* of the electrical double layer extends from the OHP to bulk solution. Since the ions are randomly spread out in this region, there is an exponential decrease in potential to a value of zero in bulk solution. This region can also be treated as an electrical capacitor with the OHP as one plate and a hypothetical plate located in the diffuse layer at a distance $1/\kappa$ from the OHP as the other plate. $1/\kappa$ is the distance at which the potential has decayed to a value of Ψ_{OHP}/e ($e = 2.718$) and it is taken as the thickness of the diffuse layer. The value of $1/\kappa$ varies with the ionic strength of the bulk solution, decreasing as the ionic strength of the bulk solution is increased.

For the electrical double layer shown in Figure 5.1, electroneutrality requires that

$$\sigma_o = - \sigma_{DL} \tag{5.5}$$

where σ_{DL} is the charge density in and beyond the OHP due to a positive surface excess of counterions and a negative surface excess of coions. From SGC theory for a univalent electrolyte,

$$- \sigma_{DL} = 2c^{1/2}\left(\frac{\varepsilon RT}{2000\pi}\right)^{1/2}\sinh\left(\frac{ZF\Psi_{OHP}}{2RT}\right) \tag{5.6}$$

where c (mol/L) is the ionic strength. It can be shown that

$$2\left(\frac{\varepsilon RTc}{2000\pi}\right)^{1/2} = \left(\frac{\varepsilon\kappa}{4\pi}\right)\left(\frac{2RT}{ZF}\right) \tag{5.7}$$

where κ has the value

$$\kappa = \left(\frac{8\pi Z^2F^2c}{1000\varepsilon RT}\right)^{1/2} \tag{5.8}$$

Substituting equations 5.5 and 5.7 into equation 5.6 gives

$$\sigma_o = \left(\frac{\varepsilon\kappa}{4\pi}\right)\left(\frac{2RT}{ZF}\right)\sinh\left(\frac{ZF\Psi_{OHP}}{2RT}\right) \tag{5.9}$$

The capacitance of the diffuse part of the double layer, C_2, is defined as

$$C_2 = \frac{-\sigma_{DL}}{\Psi_{OHP}} = \frac{\sigma_o}{\Psi_{OHP}} \tag{5.10}$$

Substituting equation 5.9 into equation 5.10,

$$C_2 = \sinh\left(\frac{ZF\Psi_{OHP}}{2RT}\right)\left(\frac{\varepsilon\kappa}{4\pi}\right)\left(\frac{ZF\Psi_{OHP}}{2RT}\right)^{-1} \tag{5.11}$$

Solving for Ψ_{OHP} in equation 5.3, substituting into equation 5.10 and combining with equation 5.11 yields the following important equation.

$$\frac{1}{\sigma_o} = \frac{1}{C_1\Psi_o} + \frac{1}{2.28 \times 10^{-4}\,\Psi_o\,c^{1/2}\left[\left(\frac{ZF\Psi_{OHP}}{2RT}\right)^{-1}\sinh\left(\frac{ZF\Psi_{OHP}}{2RT}\right)\right]} \tag{5.12}$$

According to this equation, under conditions where Ψ_o is constant, the following straight line plot is predicted

$$\frac{1}{\sigma_o} \; versus \; \frac{1}{c^{1/2}\left[\left(\frac{ZF\Psi_{OHP}}{2RT}\right)^{-1}\sinh\left(\frac{ZF\Psi_{OHP}}{2RT}\right)\right]}$$

From this plot it is possible to obtain Ψ_o and C_1 from the slope and intercept.

$$\text{slope} = \frac{1}{2.28 \times 10^{-4}\,\Psi_o} \tag{5.13}$$

$$\text{intercept} = \frac{1}{C_1\,\Psi_o} \tag{5.14}$$

In the present study the sorption isotherm of $NBTA^+$ is measured as a function of ionic strength. In order to apply equation 5.12 to the experimental data, the surface charge density must be determined from the experimentally measured surface excess. Surface charge arises from only those $NBTA^+$ ions that are adsorbed on the bonded phase while the experimentally measured surface excess, Γ_{NBTA}, includes all the $NBTA^+$ in the entire double layer region. That is, Γ_{NBTA} includes the $NBTA^+$ adsorbed on the bonded phase, Γ^{AD}_{NBTA}, and in a negative sense (*i.e.* its value is negative), that which is expelled from the diffuse layer, Γ^{DL}_{NBTA}.

$$\Gamma_{NBTA} = \Gamma^{AD}_{NBTA} + \Gamma^{DL}_{NBTA} \tag{5.15}$$

The charge density is directly proportional to Γ^{AD}_{NBTA} by the following equation

$$\sigma_o = Z_+ F\,\Gamma^{AD}_{NBTA} \tag{5.16}$$

The following iterative process is used to calculate σ_o.

(1) As a first approximation assume

$$\Gamma^{AD}_{NBTA} = \Gamma_{NBTA} \tag{5.17}$$

(2) Calculate the charge density by the equation

$$\sigma_o = Z_+F\,\Gamma_{NBTA} \tag{5.18}$$

(3) For symmetrical Z:Z type electrolytes (e.g. NBTA$^+$Cl$^-$ or Na$^+$Cl$^-$), the value of Ψ_{OHP} can be evaluated from the equation

$$\sinh\left(\frac{ZF\Psi_{OHP}}{2RT}\right) = 8.53 \times 10^4\sigma_o c^{-1/2} \tag{5.19}$$

where Z is the absolute value of the charge number.

(4) The ratio of the surface excess of positive ions in the diffuse layer (Na$^+$ and NBTA$^+$), Γ^{DL}_{+}, to the surface excess of negative ions in the diffuse layer (Cl$^-$), Γ^{DL}_{-} (at 25 °C) is calculated from the following equation [33]:

$$\frac{\Gamma^{DL}_{+}}{\Gamma^{DL}_{-}} = \frac{\exp(-19.47\Psi_{OHP}) - 1}{\exp(19.47\Psi_{OHP}) - 1} \tag{5.20}$$

(5) Next, a better estimate of the charge density is obtained from the equation

$$\sigma_o = Z_+F\Gamma_{NBTA}\left[\frac{\alpha - R}{\alpha - R(1 - \alpha)}\right] \tag{5.21}$$

where

$$\alpha = \frac{[\mathrm{NBTA^+}]}{c} \tag{5.22}$$

$$R = \alpha \frac{\Gamma_+^{DL}}{\Gamma_-^{DL}} \tag{5.23}$$

The new estimate of σ_0 from equation 5.21 is used iteratively in steps 3 to 5 until a constant value of σ_0 is obtained. Ψ_{OHP} can then be calculated from equation 5.19.

5.2.2 Modified SGC Theory for Simultaneous Sorption of Different Ions of the Same Charge

For the simultaneous sorption of two ions of the same charge (*i.e.* $NBTA^+$ and TBA^+ in the present chapter), a diagrammatic representation of the electrical double layer which is consistent with the evidence is shown in Figure 5.2. The inert electrolyte is sodium chloride. The adsorption of $NBTA^+$ and TBA^+ produces two separate charge surfaces. That is, the charge centers of the two ions do not lie in the same plane. Adsorbed TBA^+ produces a charge surface with charge density σ_{TBA} and a potential that is denoted Ψ_0. Adsorbed $NBTA^+$ produces a charge surface with charge density σ_{NBTA} and a potential denoted Ψ_I. These designations are consistent with the nomenclature that is usually used in discussing electrical double layer theory.

In Figure 5.2 TBA^+ ions are adsorbed in such a way that their charge centers lie somewhat farther into the bonded phase than those of $NBTA^+$. The OHP is still the plane of closest approach of hydrated, nonadsorbed counterions (Cl^-). The locations of the TBA^+, $NBTA^+$ and OHP planes are considered to be fixed, independent of solution composition.

The definition of the *diffuse part* of the double layer is the same as that defined in the previous section. The *compact part* of the double layer, however, now extends from

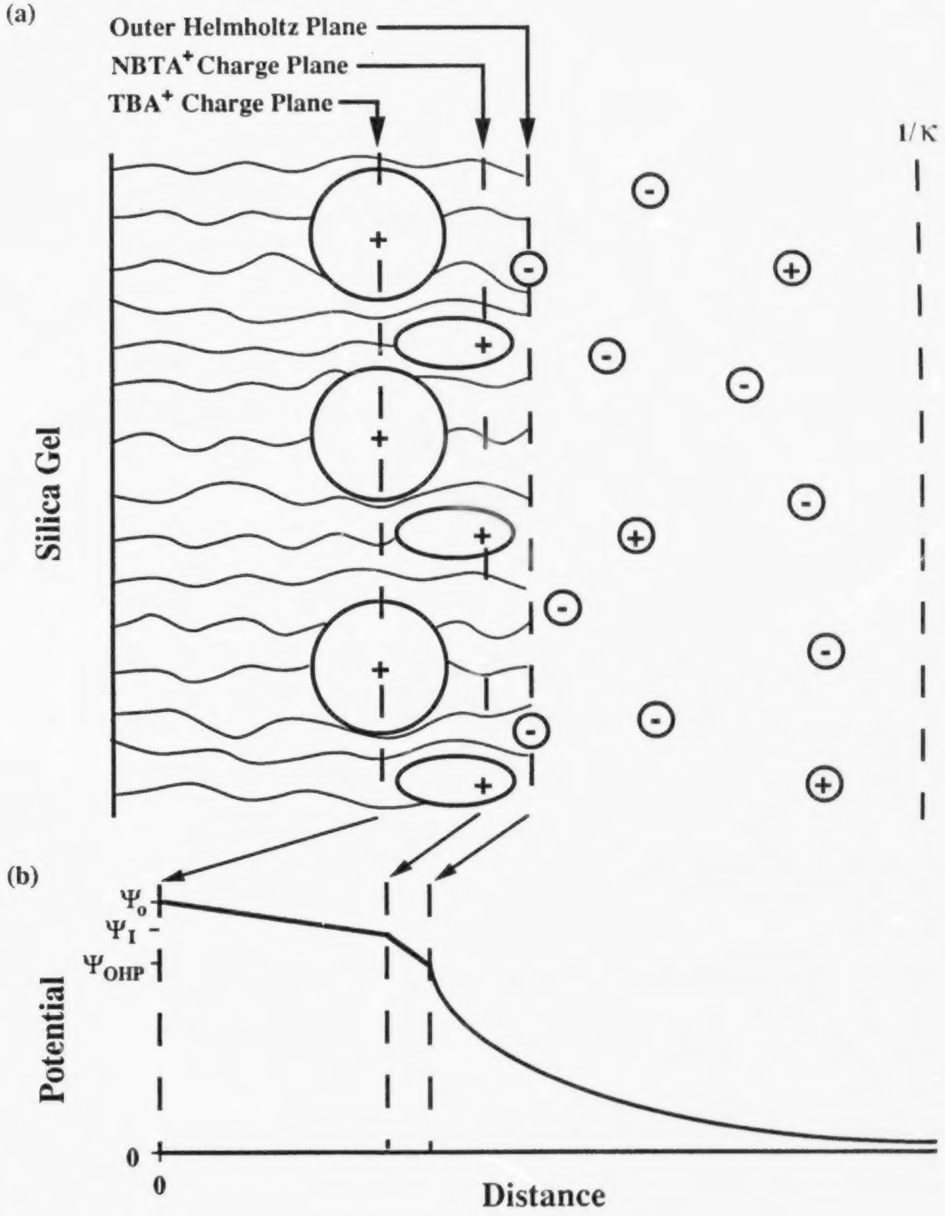
(a)
Outer Helmholtz Plane
NBTA$^+$ Charge Plane
TBA$^+$ Charge Plane
1/κ
Silica Gel
+
-
(b)
Ψ_o
Ψ_I
Ψ_{OHP}
Potential
0
0
Distance

Figure 5.2 (a) Diagrammatic representation of the electrical double layer region due to the adsorption of $NBTA^+$ and TBA^+ on an ODS RPBP. Wavy lines drawn from the silica gel surface are the C-18 chains of the bonded phase. Large circular cations and oval shaped cations are TBA^+ and $NBTA^+$ ions, respectively, while small circular cations and anions are from the inert electrolyte (*i.e.* NaCl). Not illustrated in the figure are the $NBTA^+$ and TBA^+ ions present in solution and the coions (Na^+, $NBTA^+$, TBA^+) that are expelled from the diffuse part of the double layer. (b) Potential in the electrical double layer region as a function of distance. The inner region of the compact layer has an integral capacitance K_{inner} which produces a linear decrease in potential across this region. The outer region of the compact layer has an integral capacitance K_{outer} which produces a different linear decrease in potential across this region.

the TBA$^+$ charge surface up to, but not including the OHP and includes the NBTA$^+$ charge surface. The compact layer is further divided into two regions. The region extending from the TBA$^+$ charge surface to the NBTA$^+$ charge surface is referred to as the *inner region* of the compact layer and that extending from the NBTA$^+$ charge surface to the OHP is referred to as the *outer region* of the compact layer.

In the present case, electroneutrality requires that

$$\sigma_T = - \sigma_{DL} = \sigma_{NBTA} + \sigma_{TBA} \tag{5.24}$$

where σ_T is the total charge density due to both adsorbed NBTA$^+$ and TBA$^+$ and σ_{DL} is the charge density in the diffuse layer which arises from a combination of positive surface excess of counterions (e.g. Cl$^-$) and a negative surface excess of coions (Na$^+$, NBTA$^+$, TBA$^+$) in the diffuse layer.

Following the derivation in the previous section for the sorption of a single ion (equations 5.5 to 5.11), the following equation is derived from SGC theory.

$$\frac{1}{\sigma_T} = \frac{1}{C_1 \Psi_o} + \frac{1}{2.28 \times 10^{-4}\, \Psi_o\, c^{1/2} \left[\left(\frac{ZF\Psi_{OHP}}{2RT} \right)^{-1} \sinh\left(\frac{ZF\Psi_{OHP}}{2RT} \right) \right]} \tag{5.25}$$

This equation is similar to equation 5.12 except that C_1, which is still the capacitance of the whole compact part of the double layer, is now composed of two parts. It is assumed that when the ionic activities of NBTA$^+$ and of TBA$^+$ are both constant, then Ψ_o will have a constant value even if ionic strength is varied. The following straight line plot is then predicted

$$\frac{1}{\sigma_T} \textit{ versus } \frac{1}{c^{1/2} \left[\left(\frac{ZF\Psi_{OHP}}{2RT} \right)^{-1} \sinh\left(\frac{ZF\Psi_{OHP}}{2RT} \right) \right]}$$

From the slope and intercept Ψ_o and C_1 are obtained as given in equations 5.13 and 5.14.

The total charge density can be calculated from the following expression which is equivalent to equation 5.24

$$\sigma_T = Z_+F\Gamma_+^{AD} = Z_+F\left(\Gamma_{NBTA}^{AD} + \Gamma_{TBA}^{AD}\right) \tag{5.26}$$

where Γ_+^{AD} represents the positive surface excess due to the sum of both types of adsorbed cations, while Γ_{NBTA}^{AD} and Γ_{TBA}^{AD} represent the individual contributions of the two types of cations, each adsorbed at its respective charge surface.

Experimentally, it is not the adsorbed surface excesses that are measured, but rather the overall surface excesses Γ_{NBTA} and Γ_{TBA} (and their sum Γ_+), which have smaller values than the corresponding adsorbed surface excesses. For the sum of the two PDIs, the overall excess is

$$\Gamma_+ = \Gamma_+^{AD} + \Gamma_+^{DL} \tag{5.27}$$

where Γ_+^{AD} is a positive surface excess which is equal to the moles/cm^2 of adsorbed ions and Γ_+^{DL} is a negative surface excess (*i.e.* its value is negative) which is associated with the moles/cm^2 of both NBTA$^+$ and TBA$^+$ that have been expelled, as coions, from the diffuse layer. The values of Γ_+^{AD} and Γ_+^{DL} are calculated from the experimentally measured value of Γ_+ by an iterative process which follows the same steps as described in the previous section for a single PDI (equations 5.17 to 5.23). The modifications needed to adapt the iterative process to the case of two PDIs are as follows: Replace σ_o with σ_T; replace Γ_{NBTA} with Γ_+; replace Γ_{NBTA}^{AD} with Γ_+^{AD}; redefine α in equation 5.22 as:

$$\alpha = \frac{[TBA^+] + [NBTA^+]}{c} \tag{5.28}$$

and define the relationship:

$$\frac{\Gamma^{DL}_{NBTA}}{\Gamma^{DL}_{TBA}} = \frac{[NBTA^+]}{[TBA^+]} \tag{5.29}$$

From the iterative process, values are obtained for the following parameters: Γ^{AD}_{+}, Γ^{DL}_{+}, σ_T and Ψ_{OHP}. The latter two can be used in equation 5.25 to calculate C_1 and Ψ_o.

In the derivations of equations 5.12 and 5.25, an expression for the capacitance of the diffuse layer is combined with an expression for C_1. Equations 5.12 and 5.25 have the same form whether there is only one PDI (e.g. NBTA$^+$ or TBA$^+$); whether there are two PDIs which are adsorbed at the same charge surface; or whether there are two PDIs each of which is adsorbed at a different charge surface as in the present case. What is different among these three cases is the significance of the capacitance C_1. When ions are adsorbed at only one charge surface in the compact layer, then the compact layer itself is accurately represented as one capacitor with charge $\sigma_T = \sigma_o$ and there is no difference between the integral capacitance and the differential capacitance [156-158].

However, when, as in the present case, PDIs can be adsorbed at two charge surfaces, then there is a difference between the differential- and integral-capacitance across the whole compact layer. The compact layer itself can now be thought of as two capacitors. The *individual integral capacitances* of the inner and outer capacitors in the compact layer are defined as follows [157]:

$$K_{inner} = \frac{\sigma_{TBA}}{\Psi_o - \Psi_I} \tag{5.30}$$

and

$$K_{outer} = \frac{\sigma_T}{\Psi_I - \Psi_{OHP}} \tag{5.31}$$

(In this and subsequent discussions integral capacitances will be represented as "K" and the differential capacitance will be represented as "C").

The potential difference across the whole compact layer is:

$$\left(\Psi_o - \Psi_{OHP}\right) = \left(\Psi_o - \Psi_I\right) + \left(\Psi_I - \Psi_{OHP}\right) \tag{5.32}$$

Substituting equations 5.30 and 5.31 into equation 5.32 gives:

$$\left(\Psi_o - \Psi_{OHP}\right) = \frac{\sigma_{TBA}}{K_{inner}} + \frac{\sigma_T}{K_{outer}} \tag{5.33}$$

The reciprocal of the *differential capacitance* C_1 across the whole compact layer is obtained by differentiating equation 5.33:

$$\frac{1}{C_1} = \frac{d\left(\Psi_o - \Psi_{OHP}\right)}{d\sigma_T} = \frac{1}{K_{inner}}\left(\frac{d\sigma_{TBA}}{d\sigma_T}\right) + \frac{1}{K_{outer}} \tag{5.34}$$

The differentiation is performed with respect to σ_T because it is the experimental value of σ_T that is used in equation 5.25 to obtain the value of C_1. *A key point here is that the capacitance C_1 which is obtained experimentally from equation 5.25 is a differential capacitance.* Furthermore, taking equation 5.34 together with equation 5.24 shows that the value of C_1 will vary as the ratio of the adsorbed charges in the two charge surfaces varies.

The values of the integral capacitances K_{inner} and K_{outer} can be obtained *via* equation 5.34 as follows. First, for each combination of constant values of both a_{TBA} and a_{NBTA}, σ_{TBA} is plotted *versus* σ_T. The slopes of these straight line plots provide the values of $(d\sigma_{TBA}/d\sigma_T)$ that are needed in equation 5.34. Values of C_1 at the same combinations of constant a_{NBTA} and a_{TBA} are available from plots based on equation 5.25, as described above. Then, as equation 5.34 shows, K_{inner} and K_{outer} can be obtained from the single straight line plot of $1/C_1$ *versus* $(d\sigma_{TBA}/d\sigma_T)$.

These integral capacitances, in turn, can be used to calculate the thickness of the two capacitors:

$$\delta_{inner} = \frac{\varepsilon}{4\pi K_{inner}} \tag{5.35}$$

and

$$\delta_{outer} = \frac{\varepsilon}{4\pi K_{outer}} \tag{5.36}$$

where δ_{inner} is the distance between the TBA$^+$ charge surface and the NBTA$^+$ charge surface, δ_{outer} is the distance between the NBTA$^+$ charge surface and the OHP, and ε is the permittivity of the medium between the charge surfaces in each capacitor. The integral capacitances K_{inner} and K_{outer} are constant properties of the system whose values are set by the physical constants on the right hand sides of equations 5.30 and 5.31.

The remaining parameter to be evaluated is Ψ_I, the potential at the NBTA$^+$ charge surface. To evaluate Ψ_I, the compact layer must be treated as though the inner and outer capacitors were connected in series, for which the following equation can be written:

$$\frac{1}{K_C} = \frac{1}{K_{inner}} + \frac{1}{K_{outer}} \tag{5.37}$$

where K_C is the *integral capacitance* across the whole compact layer. (Equations 5.30 and 5.31 cannot be used to evaluate Ψ_I because they are valid for two isolated capacitors. They will generally not both yield the same value for Ψ_I.) If the compact layer is to be treated as two capacitors in series, then it is necessary to employ a formalism, which can be understood as follows. For real capacitors in series in an electrical circuit the magnitude of charge on *every plate* would be equal. (Signs would be opposite across each capacitor.) It is this condition of equal charge that leads to the familiar sum of reciprocals equation such as that in equation 5.37. Thus, the formalism which allows the compact layer to be treated as capacitors in series is to employ an "effective charge", σ'_T, in place of both σ_{TBA} and σ_T in equations 5.30 and 5.31. The magnitude of the effective charge can be calculated from the expression:

$$K_C = \frac{\sigma'_T}{\Psi_o - \Psi_{OHP}} \tag{5.38}$$

Substitution of σ'_T in equations 5.30 and 5.31 and rearranging gives:

$$\Psi_I = \Psi_o - \frac{\sigma'_T}{K_{inner}} = \Psi_{OHP} + \frac{\sigma'_T}{K_{outer}} \tag{5.39}$$

5.2.3 Sorption of NBTA$^+$ Probe Ion

In determining the origin of indirect UV detection, the interest is in explaining how the sorption of the sample ion TBA$^+$ reduces the sorption of the probe ion NBTA$^+$. In order to do this, the distribution coefficient of the probe must be considered. Equations based on electrical double layer theory have been developed which describe the retention of an ionic species on a charge surface [36]. Here, the relevant equations are adapted to the present case and are given below.

There are two processes which control the retention of NBTA$^+$: coion exclusion and adsorption. The concept of coion exclusion is important when converting the experimentally measured amounts of NBTA$^+$ and of TBA$^+$ *sorbed* in the entire electrical double layer into the amounts of NBTA$^+$ and of TBA$^+$ *adsorbed* on the ODS bonded phase. The amounts adsorbed are required in order to develop a model for the effect of TBA$^+$ on NBTA$^+$ sorption which includes both a competition for space and an electrostatic potential effect. Each process will now be considered separately below.

5.2.3.1 Coion Exclusion of NBTA$^+$

Adsorption of NBTA$^+$ and TBA$^+$ gives rise to a positive electrical potential at the OHP which causes some NBTA$^+$ and TBA$^+$ to be excluded from the diffuse part of the electrical double layer. The moles of NBTA$^+$ excluded from the diffuse layer, $n_{NBTA,DL}$, can be calculated from the expression [36]:

$$n_{NBTA,DL} = K_{NBTA,IEX} c^{-1/2} (Z_+F)^{-1} \left(\frac{\varepsilon RT}{2000\pi}\right)^{1/2} \left[\exp\left(-\frac{Z_+F\Psi_{OHP}}{2RT}\right) - 1\right] (C_{m,NBTA} A_T) \qquad (5.40)$$

where $C_{m,NBTA}$ is the molar concentration of NBTA$^+$ in the mobile phase and $K_{NBTA,IEX}$ is a selectivity constant for "coion exchange" of NBTA$^+$ over Na$^+$ in the diffuse layer. Sodium ion is the coion of the swamping electrolyte (NaCl). In equation 5.40, $K_{NBTA,IEX}$ is assumed to be approximately equal to 1 which assumes that there is no selectivity in the diffuse layer. Also, there is no competition for space between NBTA$^+$ and TBA$^+$ in the solution of the diffuse layer. Adsorbed TBA$^+$ affects the amount of NBTA$^+$ excluded from the diffuse layer only by its effect on Ψ_{OHP} and *vice versa.*

Since the exponential term in equation 5.40 has a value less than 1, it follows that $n_{NBTA,DL}$ will be negative. This is consistent with the fact that it arises from a negative surface excess of excluded ions.

To develop an equation which includes both a competition for space and an electrostatic potential effect, only the NBTA$^+$ *adsorption* distribution coefficient, $K_{NBTA,ADS}$, is used (see next section). To calculate only $K_{NBTA,ADS}$, it is necessary to know the amount of NBTA$^+$ adsorbed. Experimentally, the amount of NBTA$^+$ sorbed in the entire double layer is measured, Γ_{NBTA}. This includes the amount of NBTA$^+$ which is adsorbed at the interface, Γ^{AD}_{NBTA}, and in a negative sense, the amount which is excluded from the diffuse layer, Γ_{NBTA}^{DL}. This can be expressed as

$$\Gamma_{NBTA} = \Gamma_{NBTA}^{AD} + \Gamma_{NBTA}^{DL} \tag{5.41}$$

or in terms of moles, it is expressed as

$$n_{NBTA} = n_{NBTA,ADS} + n_{NBTA,DL} \tag{5.42}$$

where n_{NBTA} is the amount sorbed in the entire electrical double layer and $n_{NBTA,ADS}$ is the amount adsorbed. The amount $n_{NBTA,DL}$ calculated from equation 5.40 can be subtracted from the experimentally measured n_{NBTA} to obtain $n_{NBTA,ADS}$. Since $n_{NBTA,DL}$ has a negative value, the experimentally measured n_{NBTA} is *smaller* than $n_{NBTA,ADS}$. That is, the experimentally measured value reflects the loss of $NBTA^+$ from the diffuse layer.

5.2.3.2 Adsorption Distribution Coefficient of NBTA+

A *dimensionless* equilibrium constant for the adsorption of $NBTA^+$ in the bonded phase can be written as follows:

$$K'_{NBTA,ADS} = \frac{10^3\, \Gamma_{NBTA}^{AD}\, \gamma_{NBTA,ADS}}{C_{m,NBTA}\, \gamma_{NBTA}\, d} \tag{5.43}$$

where 10^3 is a factor which converts cm^3 to L, $\gamma_{NBTA,ADS}$ is the activity coefficient of $NBTA^+$ on the surface, γ_{NBTA} is the bulk solution activity coefficient and d is a thickness (cm) in the bonded phase. The value of d is somewhat arbitrarily chosen [32]. For example, d may, but need not necessarily, be taken as equal to the thickness of the bonded phase, the thickness of the compact layer, or the thickness of the outer capacitor in the compact layer. In general, if a larger value is chosen for d, then a smaller value of $K'_{NBTA,ADS}$ will be obtained and the value of the product $d \cdot K'_{NBTA,ADS}$ will be unchanged.

The thermodynamic expression for the dimensionless $K'_{NBTA,ADS}$ is [32]:

$$K'_{NBTA,ADS} = \exp\left(-\frac{Z_+ F \Psi_I + \mu^\circ_{NBTA,ADS}}{R T}\right) \tag{5.44}$$

where $\mu^\circ_{NBTA,ADS}$ is the standard chemical potential in J/mol for the transfer of $NBTA^+$ from bulk solution to the bonded phase when $\Psi_I = 0$ V. The extrapolated infinite dilution standard state is used for both the solution phase and the bonded phase. The standard state is extrapolated from infinite dilution to a concentration of 1 mol/L. The reference state for the solution phase, in which $\gamma_{NBTA} \equiv 1$, is pure water with no ions present, *i.e.* infinite dilution. The reference state for the bonded phase, in which $\gamma_{NBTA,ADS} \equiv 1$, is the bonded phase that is free of all ions (*i.e.* $NBTA^+$ and TBA^+), that is, "infinite dilution" on the surface. Note that it is the potential at the $NBTA^+$ charge plane, Ψ_I, which appears in equation 5.44 since it is Ψ_I which influences the adsorption of $NBTA^+$.

An adsorption distribution coefficient for $NBTA^+$ with units of L/cm^2 is defined as follows:

$$K_{NBTA,ADS} = \frac{\Gamma^{AD}_{NBTA}}{C_{m,NBTA}} \tag{5.45}$$

or

$$K_{NBTA,ADS} = \frac{n_{NBTA,ADS}}{A_S \, C_{m,NBTA}} \tag{5.46}$$

Combination of equations 5.43 to 5.45 yields the following equation for the $NBTA^+$

adsorption distribution coefficient :

$$K_{NBTA,ADS} = \left(\frac{10^{-3}\,\gamma_{NBTA}\,d}{\gamma_{NBTA,ADS}}\right)\exp\left(-\frac{\overset{\circ}{\mu}_{NBTA,ADS} + Z_{+}\,F\,\Psi_{I}}{R\,T}\right) \qquad (5.47)$$

The term ($\mu^{\circ}_{NBTA,ADS} + Z_{+}F\Psi_{I}$) in equation 5.47 is the "electrochemical potential" for adsorption of NBTA^{+}. It is *via* this term that Ψ_I influences the adsorption distribution coefficient of NBTA^{+}. Adsorption of NBTA^{+} is discussed in the next section.

5.2.3.3 Adsorption of NBTA^{+}

An expression for the amount of NBTA^{+} adsorbed can be obtained by substituting into equation 5.46 for $K_{NBTA,ADS}$ from equation 5.47 and rearranging to give:

$$n_{NBTA,ADS} = C_{m,NBTA}\,A_{S}\left(\frac{10^{-3}\,\gamma_{NBTA}\,d}{\gamma_{NBTA,ADS}}\right)\exp\left(-\frac{\overset{\circ}{\mu}_{NBTA,ADS} + Z_{+}\,F\,\Psi_{I}}{R\,T}\right) \qquad (5.48)$$

The two parenthetic terms on the right hand side of equation 5.48 are equal to $K_{NBTA,ADS}$ so that equation 5.48 reveals how a change in Ψ_I due to adsorption of TBA^{+} will affect $n_{NBTA,ADS}$ *via* $K_{NBTA,ADS}$. The second way in which adsorption of TBA^{+} might produce desorption of NBTA^{+} is *via* a competition for space. This effect is not mediated *via* a change in $K_{NBTA,ADS}$, but rather through a decrease in the space available for adsorption.

In this section the concept of a competition for space is similar to that discussed in Chapter 4 for the neutral sample butanol and the ionic probe NS^{-}. When no TBA^{+} sample is adsorbed then the area available for NBTA^{+} adsorption, A_S, is equal to the total area available for adsorption, A_T. On the other hand, when TBA^{+} is adsorbed the value of A_S depends on the amount of TBA^{+} adsorbed. This can be expressed as follows:

$$A_S = A_T - \overline{A}'_{TBA}\, n_{TBA,ADS} \tag{5.49}$$

where $\overline{A}'_{TBA}$ is the area per mole of TBA$^+$ (cm^2/mol) that is effectively "occupied" by TBA$^+$ *in the NBTA$^+$ charge plane*. Since the center of charge of TBA$^+$ lies in the TBA$^+$ charge plane and not in the NBTA$^+$ charge plane, it would be expected that $\overline{A}'_{TBA}$ would be smaller than $\overline{A}_{TBA}$, the area per mole occupied by TBA$^+$ in its own charge plane.

Substituting A_S from equation 5.49 into equation 5.48 gives the final equation which describes NBTA$^+$ adsorption when both a competition for space and an electrostatic potential effect are occurring due to the presence of TBA$^+$.

$$n_{NBTA,ADS} = C_{m,NBTA}\left(A_T - \overline{A}'_{TBA}\, n_{TBA,ADS}\right)\left(\frac{10^{-3}\,\gamma_{NBTA}\, d}{\gamma_{NBTA,ADS}}\right)\exp\left(-\frac{\overset{\circ}{\mu}_{NBTA,ADS} + Z_+ F\, \Psi_I}{R\,T}\right) \tag{5.50}$$

At a fixed ionic strength and a fixed NBTA$^+$ concentration, $C_{m,NBTA}$, A_T, γ_{NBTA}, Z, F, R, and T have known and constant values. The parameters $\mu^{\circ}_{NBTA,ADS}$, $\overline{A}'_{TBA}$ and d have constant but unknown values. The parameter $\gamma_{NBTA,ADS}$ has an unknown but presumably constant value [36,37]. Therefore, the variables in the above equation are $n_{NBTA,ADS}$, $n_{TBA,\,ADS}$ and Ψ_I. The manner in which $n_{TBA,ADS}$ is obtained for use in equations 5.49 and 5.50 is similar to the manner in which $n_{NBTA,ADS}$ was calculated above and is described in Section 5.2.4, below. The way in which Ψ_I is obtained was described in Section 5.2.2, above. To test if equation 5.50 is valid, nonlinear least squares curve fitting of the equation to the experimental data is done.

5.2.4 Adsorption of TBA$^+$

In equation 5.50 it is necessary to know the value of $n_{TBA,ADS}$. This value can be calculated in a similar manner to that described above to calculate $n_{NBTA,ADS}$. Since TBA$^+$ also experiences coion exclusion when it sorbs, a similar equation to equation 5.40 can be written for TBA$^+$ as shown.

$$n_{TBA,DL} = K_{TBA,IEX}\, c^{-1/2} (Z_+ F)^{-1} \left(\frac{\varepsilon R T}{2000\, \pi}\right)^{1/2} \left[\exp\left(- \frac{Z_+ F \Psi_{OHP}}{2 R T}\right) - 1\right] (C_{m,TBA} A_T) \tag{5.51}$$

As for NBTA$^+$, the experimentally measured amount of TBA$^+$ is that which is sorbed in the entire electrical double layer, Γ_{TBA}. This includes the amount of TBA$^+$ which is adsorbed at the interface, Γ^{AD}_{TBA}, and in a negative sense, the amount which is excluded from the diffuse layer, Γ^{DL}_{TBA}. Equations similar to equations 5.41 and 5.42 can be written for TBA$^+$ as shown:

$$\Gamma_{TBA} = \Gamma^{AD}_{TBA} + \Gamma^{DL}_{TBA} \tag{5.52}$$

$$n_{TBA} = n_{TBA,ADS} + n_{TBA,DL} \tag{5.53}$$

The value of $n_{TBA,DL}$ calculated from equation 5.51 is subtracted from n_{TBA} in order to obtain the value of $n_{TBA,ADS}$.

5.3 Results and Discussion

NOTE: Due to the large amount of data presented in this chapter, some of the tables, which repeat data in figures, are given in Appendix B , rather than being interleaved with the text. Calibration curves are also given in Appendix B.

5.3.1 Determination of Column Equilibration Conditions

5.3.1.1 Precolumn Holdup Volume

The holdup volume of precolumn #4, which was used in all column equilibration experiments discussed in this chapter, was determined according to the procedure described in Section 2.5.5 and discussed in Section 4.3.1.1. The holdup volume and its 95% confidence limits are 70.7 ± 4.0 μL. The GC calibration curve data used in this determination are given in Table B.1 and are plotted in Figure B.1. The plot is linear ($r = 0.999$) with the slope equal to 12.3 ± 0.3 $(\mathrm{mL})^{-1}$ and the intercept equal to 0.09 ± 0.02 $(\mathrm{mL})^{-1}$. The curve does not pass through zero due to the presence of some water in the ethanol solvent.

5.3.1.2 Loading and Elution Volumes for $NBTA^+$

In order to measure the sorption isotherms of $NBTA^+$, the volume of solution that must be pumped through the precolumn to establish equilibrium between the solution and the ODS packing has to be determined. Since the sorption isotherms are measured at different concentrations of NaCl in solution (*i.e.* ionic strength), the loading and elution experiments were conducted at the lowest and highest NaCl concentrations that were going to be used.

At low ionic strength, various volumes of a solution of 1.97 x 10^{-4} mol/L $NBTA^+$ in 0.050 mol/L NaCl and 1 x 10^{-4} mol/L HOAc/NaOAc buffer (pH = 5) were pumped through the precolumn and then eluted. The number of moles of $NBTA^+$ eluted for each volume was determined using equation 1.1. Typical $NBTA^+$ calibration curve data are given in Table B.2 and are plotted in Figure B.2. A similar procedure was done at high ionic strength using a solution of 2.09 x 10^{-4} mol/L $NBTA^+$ in 0.500 mol/L NaCl and 1 x 10^{-4} mol/L HOAc/NaOAc buffer (pH = 5).

The $NBTA^+$ loading curves at low and high ionic strength are shown in Figure 5.3 and Figure 5.4, respectively. The corresponding data are given in Tables B.3 and B.4. At low ionic strength, equilibrium is achieved in ≤ 30 mL while at high ionic strength equilibrium appears to be achieved rapidly (≤ 2 mL). No data were collected before equilibrium in the high ionic strength case. To ensure that equilibrium would be established in all cases a volume of 60 mL was used in all $NBTA^+$ isotherm experiments.

To verify that $NBTA^+$ was completely eluted, the solutions described above at low and high ionic strength were pumped through precolumn #4 for 30 minutes at 2 mL/min (*i.e.* 60 mL) and then eluted in five, 2 mL fractions. The $NBTA^+$ absorbance at 260 nm for each fraction was measured. The elution results for loadings done at low and high ionic strength are shown in Figure 5.5 and Figure 5.6, respectively. The corresponding data are given in Tables B.5 and B.6. In both cases, $NBTA^+$ is completely eluted in 2 mL. Therefore, 10 mL was used in all subsequent experiments.

5.3.1.3 Loading and Elution Volumes for $NBTA^+$ and TBA^+ Together

In determining the effect of TBA^+ on $NBTA^+$ sorption, solutions containing both $NBTA^+$ and TBA^+ are pumped through the precolumn. It is therefore necessary to determine the volume of solution that must be pumped through the precolumn in order that both $NBTA^+$ and TBA^+ achieve equilibrium between the ODS packing and solution. Since

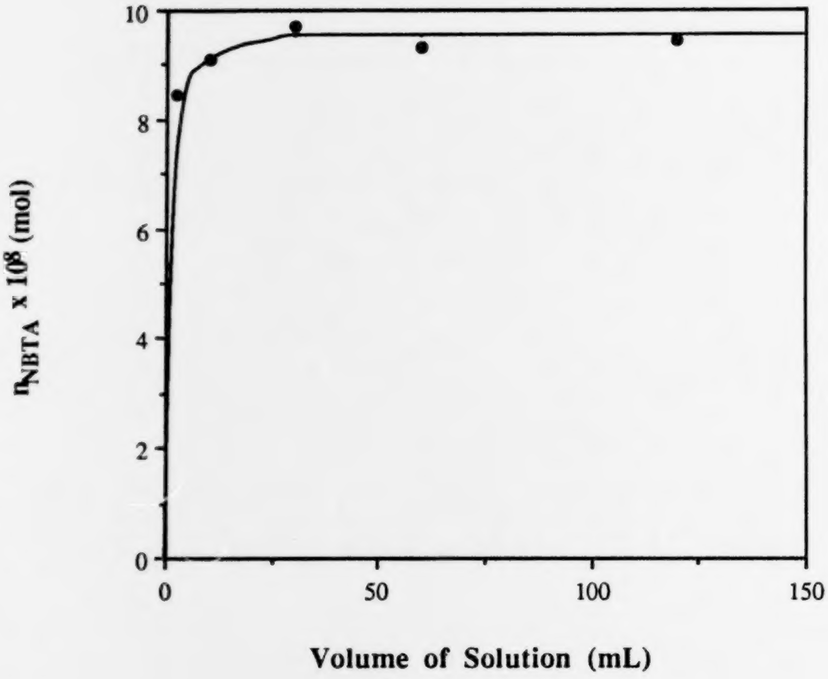

Figure 5.3 NBTA$^+$ loading curve for 1.97×10^{-4} mol/L NBTA$^+$ in 0.050 mol/L NaCl and pH 5 buffer. The flow rate was 2.0 mL/min. Data are given in Table B.3.

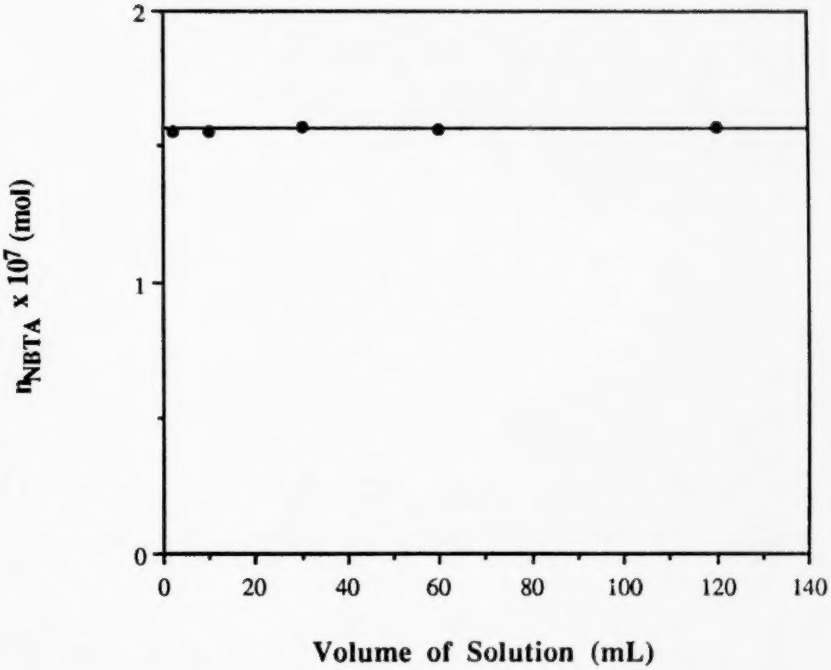

Figure 5.4 NBTA$^+$ loading curve for 2.09 x 10^{-4} mol/L NBTA$^+$ in 0.500 mol/L NaCl and pH 5 buffer. The flow rate was 2.0 mL/min. Data are given in Table B.4.

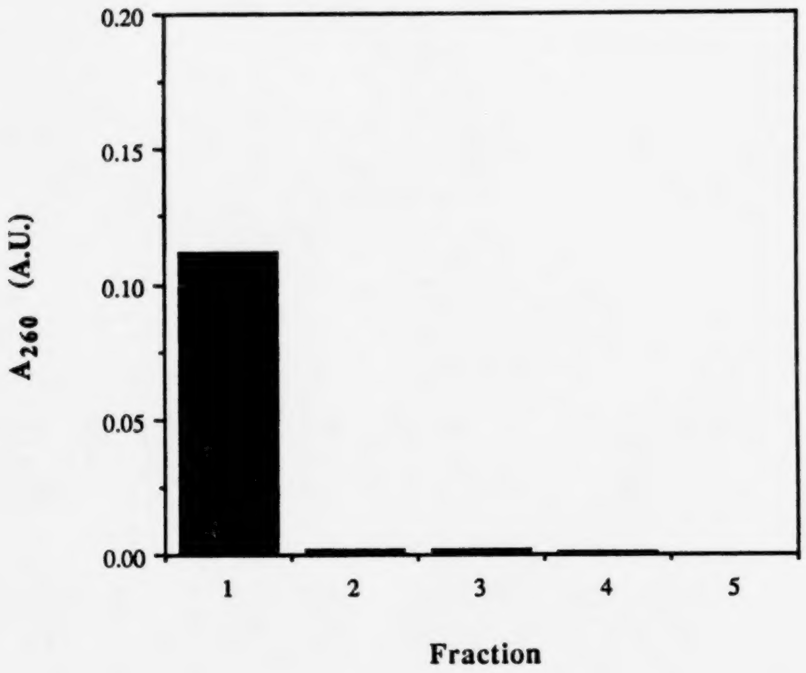

Figure 5.5 NBTA$^+$ elution curve for the solution in Figure 5.3 loaded onto precolumn #4 for 30 minutes at a flow rate of 2.0 mL/min (*i.e.* 60 mL). The eluent was methanol:water (1:1 v/v) containing 0.010 mol/L NaCl pumped at a flow rate of 1.0 mL/min. Each fraction represents 2 mL of eluent collected in a 10 mL volumetric flask and then diluted to volume with eluent. Data are given in Table B.5.

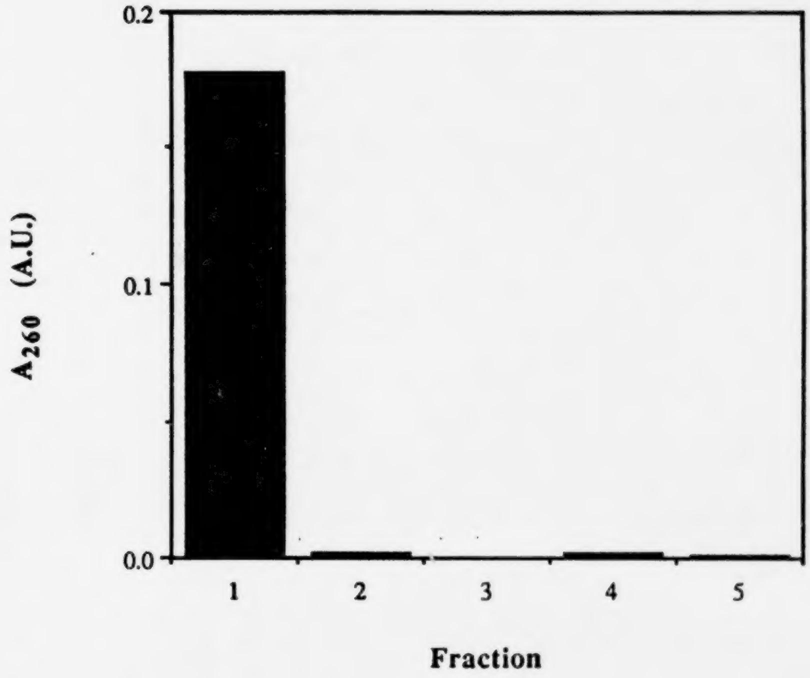

Figure 5.6 NBTA$^+$ elution curve for the solution in Figure 5.4 loaded onto precolumn #4 for 30 minutes at a flow rate of 2.0 mL/min (*i.e.* 60 mL). The eluent and experimental conditions are the same as in Figure 5.5. Data are given in Table B.6.

the effect of TBA^+ on $NBTA^+$ sorption was studied as a function of NaCl concentration (*i.e.* ionic strength), the loading and elution volumes were determined at the lowest and highest ionic strengths that were going to be used, as in the case above for $NBTA^+$ alone.

At low ionic strength, a solution of 9.87×10^{-4} mol/L $NBTA^+$ and 1.00×10^{-5} mol/L TBA^+ in 0.050 mol/L NaCl and 1×10^{-4} mol /L HOAc/NaOAc buffer (pH = 5) was pumped through precolumn #4 for various volumes and then eluted. The amount of $NBTA^+$ eluted was analytically determined as described in Section 5.3.1.2 and the amount of TBA^+ eluted was determined by SE/FIA as described in Section. 2.7. A similar procedure was done at high ionic strength using a solution of 9.31×10^{-4} mol/L $NBTA^+$ and 1.00×10^{-5} mol/L TBA^+ in 0.500 mol/L NaCl and 1×10^{-4} mol/L HOAc/NaOAc buffer (pH = 5).

To test if $NBTA^+$ would produce an interference in the SE/FIA system, a series of solutions in which the TBA^+ concentration was kept constant and the $NBTA^+$ concentration was varied over three orders of magnitude was injected into the SE/FIA system. The results are given in Table 5.1. For all solutions the peak areas had the same value within experimental error and the value was the same as that for the blank (*i.e.* only TBA^+ present). Only the solution having the lowest concentration of $NBTA^+$ showed a slight deviation. From the results of these experiments, it was concluded that under the conditions used in the SE/FIA apparatus $NBTA^+$ does not appreciably extract as an ion pair and therefore it does not interfere in the determination of TBA^+. Typical calibration curve data used in the SE/FIA determination of TBA^+ are given in Table B.7 and are plotted in Figure B.3.

The $NBTA^+$ and TBA^+ loading curves at low and high ionic strength are shown in Figure 5.7 and Figure 5.8, respectively. The corresponding data are given in Tables B.8 and B.9. The shape of the $NBTA^+$ loading curve in both figures is interesting in that it illustrates the fact that TBA^+ does reduce $NBTA^+$ sorption. The $NBTA^+$ loading curve initially rises and then slowly decreases and plateaus as more TBA^+ sorbs, as indicated

Table 5.1 Interference of $NBTA^+$-picrate on the determination of TBA^+-picrate by SE/FIA. The experimental parameters were: chloroform flow rate, 1.4 mL/min; aqueous flow rate, 1.0 mL/min; chloroform flow rate through the membrane phase separator, 0.50 mL/min; and detection wavelength, 368 nm.

[$NBTA^+$] (mol/L) (a)	**Peak Area x 10^{-7} (A.U.)** (b)
0	2.64 ± 0.22
9.85×10^{-6}	3.66 ± 0.53
9.85×10^{-5}	2.68 ± 0.32
9.85×10^{-4}	2.63 ± 0.15

(a) 9.86×10^{-5} mol/L TBA^+ was present in each solution.

(b) Average and standard deviation of five replicate injections.

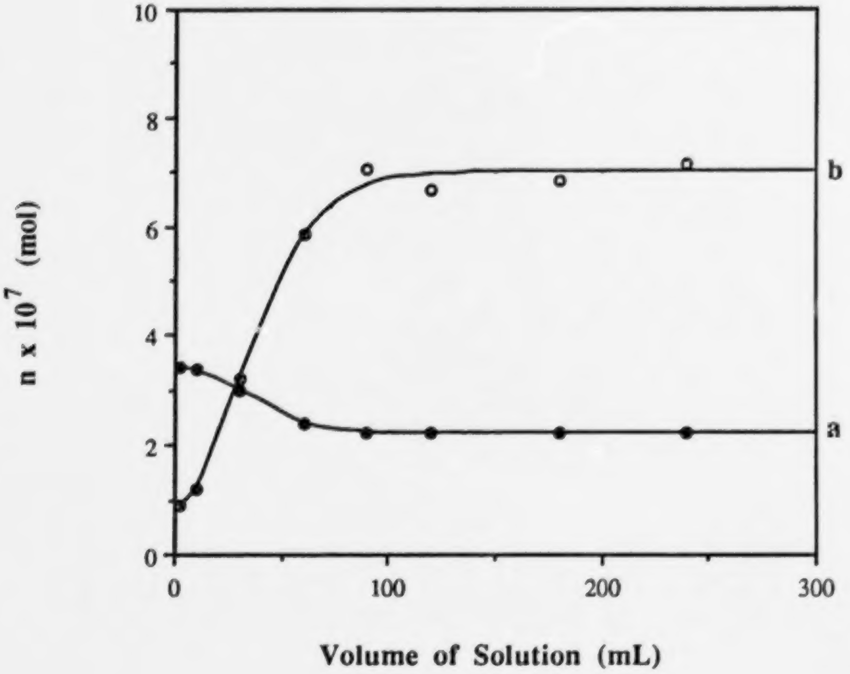

Figure 5.7 NBTA⁺ and TBA⁺ loading curves for a solution of 9.87 x 10^{-4} mol/L NBTA⁺ and 1.00 x 10^{-5} mol/L TBA⁺ in 0.050 mol/L NaCl and pH 5 buffer. The flow rate was 2.0 mL/min. Data are given in Table B.8. (a) NBTA⁺ loading curve. (b) TBA⁺ loading curve.

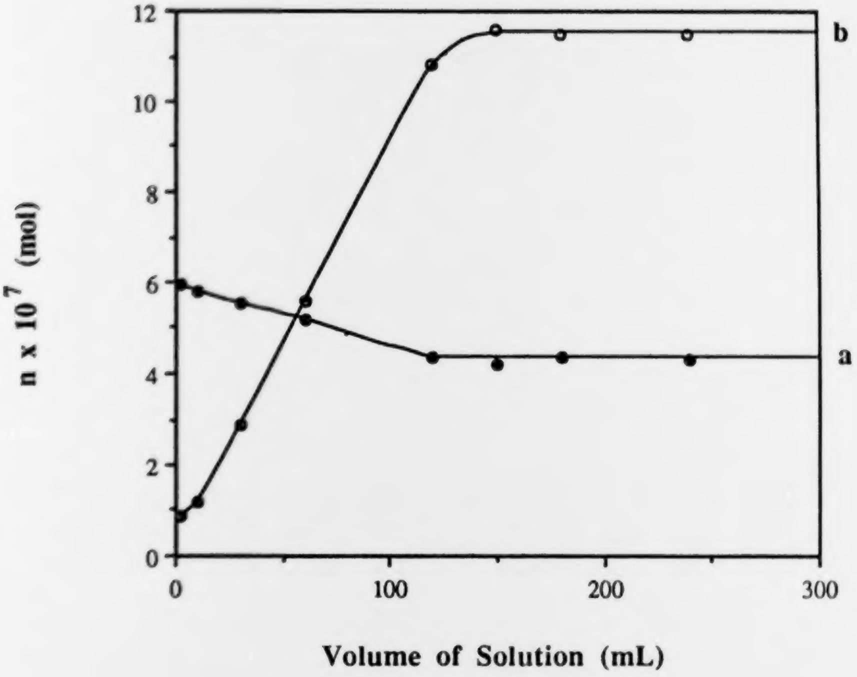

Figure 5.8 NBTA$^+$ and TBA$^+$ loading curves for a solution of 9.31 x 10^{-4} mol/L NBTA$^+$ and 1.00 x 10^{-5} mol/L TBA$^+$ in 0.500 mol/L NaCl and pH 5 buffer. The flow rate was 2.0 mL/min. Data are given in Table B.9. (a) NBTA$^+$ loading curve. (b) TBA$^+$ loading curve.

from the TBA^+ loading curve. In contrast, the $NBTA^+$ loading curve, when it is the only sorbable ion present in solution, has the typical loading curve shape as shown in Figure 1.12 (see Figures 5.3 and 5.4). The TBA^+ loading curve with $NBTA^+$ present, on the other hand, does not show an increase and then a decrease. Instead, it has the shape that would be expected for a single sorbable ion (*i.e.* Figure 1.12). This is due to the fact that TBA^+ is much more strongly sorbed than $NBTA^+$, as will be shown in Section 5.3.2. At low ionic strength, both $NBTA^+$ and TBA^+ achieve equilibrium in 120 mL. At high ionic strength, both achieve equilibrium in 150 mL. A loading volume of 150 mL was therefore used in all subsequent experiments when both $NBTA^+$ and TBA^+ were present in solution.

To verify that both $NBTA^+$ and TBA^+ are completely eluted, the above solutions at low and high ionic strength were pumped through precolumn #4 for 75 minutes at a flow rate of 2 mL/min (*i.e.* 150 mL) and then eluted in five, 2 mL fractions. The $NBTA^+$ absorbance at 260 nm and the TBA^+-picrate peak area of each fraction were measured as in the loading experiment. The results at low and high ionic strength are shown in Figure 5.9 and Figure 5.10, respectively. The corresponding data are given in Tables B.10 and B.11. In the case of the TBA^+ elution curves at both ionic strengths, the peak areas determined for fractions 2 to 5 were the same as the blank value within error. Therefore, it may be concluded that both $NBTA^+$ and TBA^+ are completely eluted in 2 mL at low and high ionic strength. A volume of 10 mL was used in all subsequent experiments.

5.3.2 Sorption of $NBTA^+$ Alone

It has previously been shown that the sorption of TBA^+ on Partisil-10 ODS-3 could be quantitatively described by the SGC model [34]. In the present work, the sorption behavior of $NBTA^+$ on Partisil-10 ODS-3 is studied and is interpreted in terms of the SGC model. Shown in Figure 5.11 are five sorption isotherms for $NBTA^+$, each measured at a different constant concentration of the inert electrolyte NaCl. The isotherm data at each

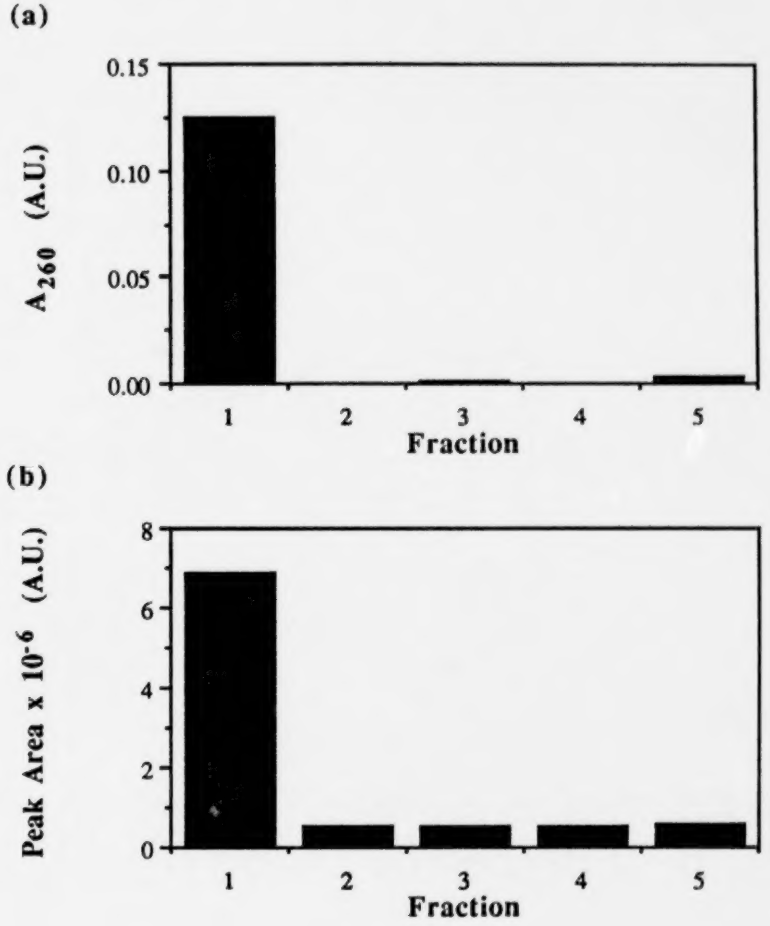

Figure 5.9 NBTA$^+$ and TBA$^+$ elution curves for the solution in Figure 5.7 loaded onto precolumn #4 for 75 minutes at 2.0 mL/min (*i.e.* 150 mL). The eluent and eluent flow rate are the same as in Figure 5.5. Each fraction represents 2 mL of eluent collected in a 25 mL volumetric flask and then diluted to volume with eluent. Data are given in Table B.10. (a) NBTA$^+$ elution curve. (b) TBA$^+$ elution curve. The peak area for the blank was $(0.623 \pm 0.046) \times 10^6$ A.U.

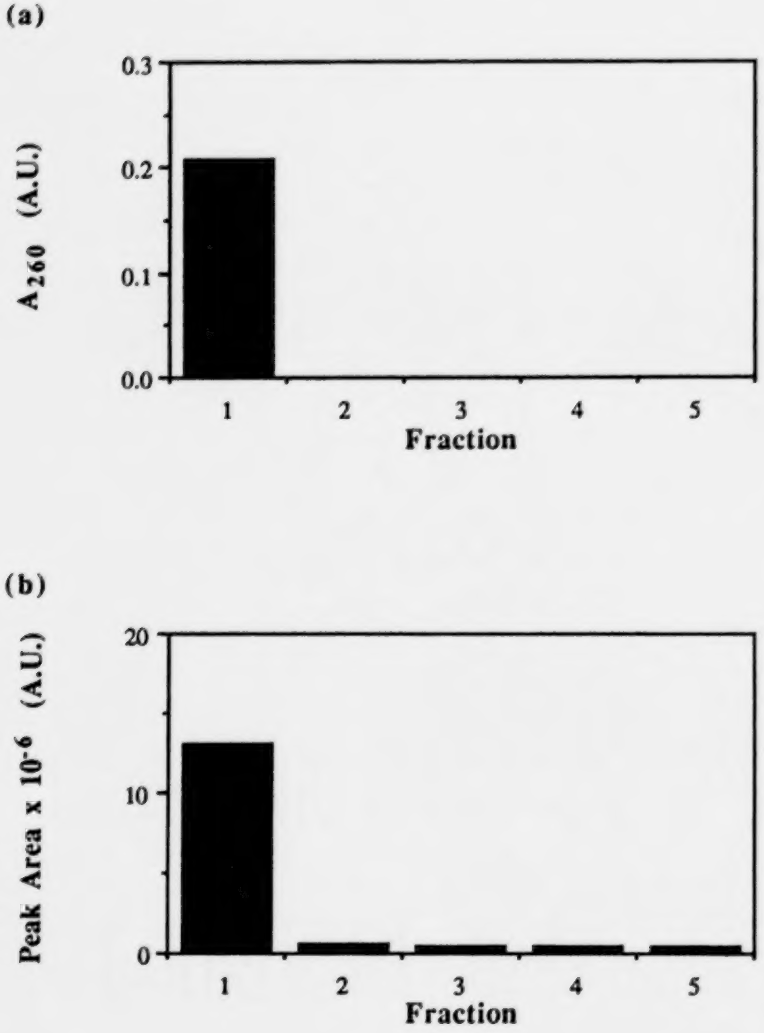

Figure 5.10 NBTA$^+$ and TBA$^+$ elution curves for the solution in Figure 5.8 loaded onto precolumn #4 for 75 minutes at 2.0 mL/min (*i.e.* 150 mL). Experimental conditions were the same as in Figure 5.9. Data are given in Table B.11. (a) NBTA$^+$ elution curve. (b) TBA$^+$ elution curve. The peak area for the blank was (0.505 ± 0.057) x 10^6 A.U.

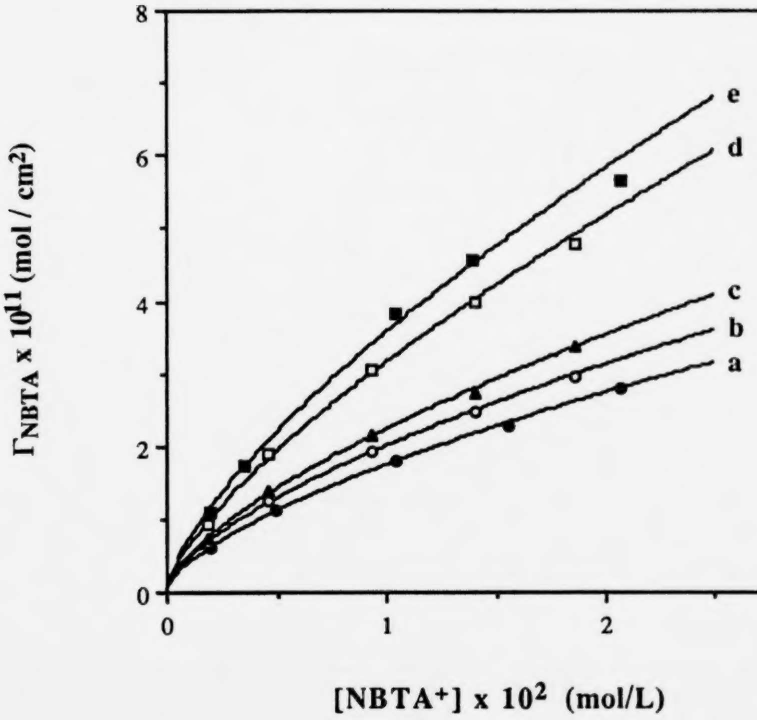

Figure 5.11 $NBTA^+$ sorption isotherms on Partisil-10 ODS-3 from pH 5 aqueous solutions at five concentrations of NaCl in solution. The concentrations of NaCl in solution were (a) 0.050 mol/L, (b) 0.070 mol/L, (c) 0.100 mol/L, (d) 0.300 mol/L and (e) 0.500 mol/L. Data are given in Table B.12.

NaCl concentration are given in Table B.12. The amount of $NBTA^+$ sorbed increases with increasing ionic strength. The solid lines in Figure 5.11 represent empirical fits, having been obtained by fitting the Freundlich equation (equation 3.4) to the data in each isotherm. Comparison of these $NBTA^+$ isotherms to the TBA^+ isotherms obtained at the same ionic strengths [34] reveals that $NBTA^+$ is less strongly sorbed than TBA^+.

When there is only one type of PDI then there is only one charge surface, whose charge density is represented as σ_0, rather than σ_T, and whose surface potential is represented as Ψ_0. It is to be noted that when TBA^+ and $NBTA^+$ are both adsorbed, then the potential at the TBA^+ charge surface will be designated as Ψ_0 and that at the $NBTA^+$ charge surface will be designated as Ψ_I, for consistency with the nomenclature usually employed with equations 5.12 and 5.25.

According to the SGC theory, if $NBTA^+$ is the only adsorbed ion then the surface potential Ψ_0 is a constant for a constant activity of $NBTA^+$, a_{NBTA}, in bulk solution. As discussed in Section 5.2.1, the criterion of conformity to the SGC model is linearity of the plots based on equation 5.12. The following steps are used to construct these plots. (i) The ionic activity coefficients of $NBTA^+$ in the aqueous phase were used to convert molar concentrations, $[NBTA^+]$, into activities, a_{NBTA}. Ionic activity coefficients of $NBTA^+$, γ_{NBTA}, needed for these calculations were obtained as follows: For ionic strengths greater and equal to 0.1 mol/L, γ_{NBTA} was assumed to be equal to the activity coefficient of benzyltrimethylammonium, which can be found in reference 159; for ionic strengths less than 0.1 mol/L, γ_{NBTA} was estimated from the extended Debye-Huckel equation, using an ionic size parameter of 3.0×10^{-8} cm for $NBTA^+$ [160]. (ii) At a fixed activity of $NBTA^+$, a value of Γ_{NBTA} was read from each of the five isotherms in Figure 5.11, corresponding to five different ionic strengths. This was repeated for five different a_{NBTA} values. (iii) A value of σ_0 was calculated *via* the iterative process described in Section 5.2.1 for each of the twenty-five values of Γ_{NBTA}. (iv) For each of the five a_{NBTA} values a plot was made of $1/\sigma_0$ *versus* $c^{-1/2}\ [(ZF\Psi_{OHP}/2RT)^{-1} \sinh (ZF\Psi_{OHP}/2RT)]^{-1}$ according to equation 5.12.

These plots are shown in Figure 5.12. The data used to construct the plot at each a_{NBTA} are given in Table B.13. (v) For each straight line, the values of Ψ_o, C_1 and r were calculated. They are presented in Table 5.2.

Using the average value of C_1, $(1.1 \pm 0.4) \times 10^{-3}$ Farad/cm^2, the thickness of the compact layer, δ, is calculated *via* equation 5.4 to be 0.6 ± 0.2 Å when NBTA$^+$ is the only PDI. This may be contrasted with the thickness of 12 Å (there is an error in reference 34) which was found when TBA$^+$ was the only PDI on Partisil-10 ODS-3 [34]. This is an interesting observation. When SGC theory is applied to traditional electrode surfaces, such as that of mercury, it is usually found that the thickness of the compact layer is approximately equal to the radius of the hydrated counterion [156,157]. For NBTA$^+$ and TBA$^+$ on Partisil-10 ODS-3 the counterion was Cl$^-$ in both cases (hydrated radius *ca.* 3 Å) but there was an *ca.* ten-fold difference in δ. This suggests that perhaps the plane of hydrated Cl$^-$ counterions (*i.e.* the OHP) is at approximately the same location for both NBTA$^+$ and TBA$^+$ on Partisil-10 ODS-3 in an aqueous medium, but that the plane of adsorbed PDI (*i.e.* the charge surface) is at different locations for NBTA$^+$ and TBA$^+$. That is, whereas a metal electrode surface is essentially two dimensional so that the electronic charges at the electrode surface are at a fixed location, the ODS bonded phase is three dimensional so that some types of PDI can penetrate more deeply than others into the bonded phase. Thus the location of the charge surface on the ODS bonded phase depends on the nature of the adsorbed PDI. The TBA$^+$ ion is a symmetrical tetraalkylammonium ion whereas the NBTA$^+$ ion has a longer nitrobenzyl substituent group in one position on the nitrogen, with the less hydrophobic methyl groups in the other three positions. Thus, an adsorbed TBA$^+$ can readily be envisioned with its charge center, and thus its charge surface located more deeply in the bonded phase than those of an adsorbed NBTA$^+$.

When NBTA$^+$ and TBA$^+$ are sorbed simultaneously, the situation shown diagrammatically in Figure 5.2 might be expected. Based on the observed 12 Å and 0.6 Å values of δ for TBA$^+$ and NBTA$^+$ alone, the values of δ_{inner} and δ_{outer} might be expected

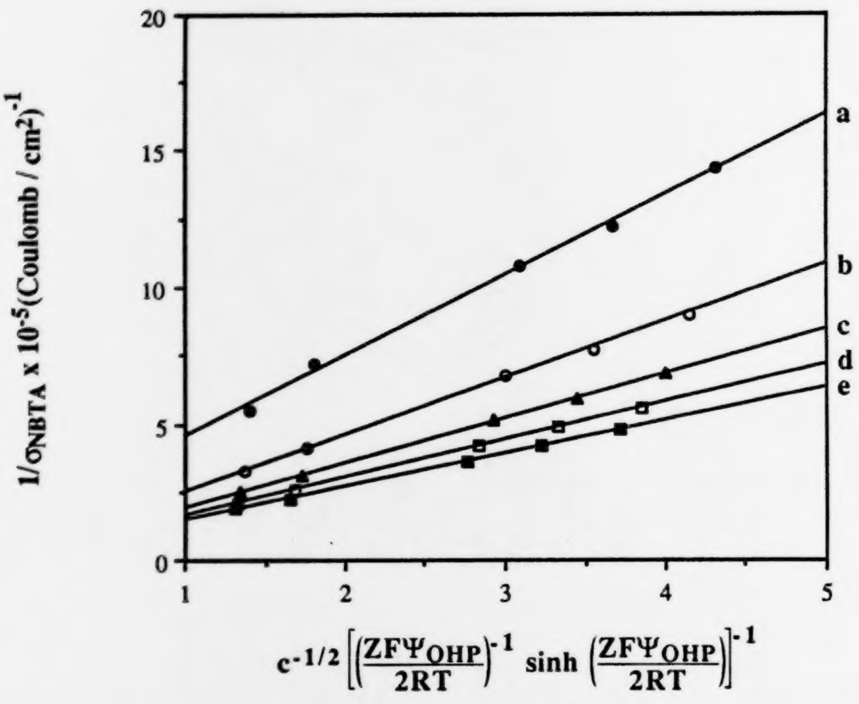

Figure 5.12 Plots of data from Figure 5.11 for $NBTA^+$ at five activities of $NBTA^+$ according to equation 5.12 to show SGC behavior. The activities of $NBTA^+$ are (a) 2.00×10^{-3} mol/L, (b) 4.00×10^{-3} mol/L, (c) 6.00×10^{-3} mol/L, (d) 8.00×10^{-3} mol/L and (e) 1.00×10^{-2} mol/L. Data are given in Table B.13.

Table 5.2 SGC behavior of $NBTA^+$ on Partisil-10 ODS-3 from linear plots of σ_o^{-1} *versus* $c^{-1/2}[(ZF\Psi_{OHP}/2RT)^{-1} \sinh (ZF\Psi_{OHP}/2RT)]^{-1}$ at five activities of $NBTA^+$ in solution (see Figure 5.12).

$a_{NBTA} \times 10^3$ (mol/L)	r (a)	$\Psi_o \times 10^3$ (V)	$C_1 \times 10^6$ (Farad/cm^2) (b)
2.00	0.998	14.8 ± 0.5	426 ± 82
4.00	0.999	21.1 ± 0.4	1130 ± 278
6.00	1.000	26.7 ± 0.3	1530 ± 310
8.00	1.000	31.6 ± 0.2	1400 ± 154
10.0	1.000	36.2 ± 0.3	1130 ± 144

Mean =1100 ± 400 (b)

(a) r = correlation coefficients of linear regression of plots in Figure 5.12.

(b) Uncertainties of Ψ_o and C_l values are standard deviations.

to be about 11.4 Å and 0.6 Å, respectively. Simultaneous sorption of both $NBTA^+$ and TBA^+ are discussed in the next section.

5.3.3 Sorption of Both $NBTA^+$ and TBA^+

Presented in Figure 5.13 are plots of the total surface excess of $NBTA^+$ plus TBA^+, Γ_+, *versus* the concentration of TBA^+ in bulk solution, $[TBA^+]$, measured at five different concentrations of NaCl in solution. The sorption data are given in Table B.14. Among all of these twenty-five solutions the concentration of $NBTA^+$ was held constant at 1.86×10^{-3} mol/L. The solid lines in Figure 5.13 represent empirical fits of the Freundlich equation to the data. These data were evaluated in terms of the SGC model, as discussed above in Section 5.2.2. According to the model, Ψ_0 is a constant at a constant a_{NBTA} and a_{TBA}. The criterion of conformity to the SGC model is linearity of the plots based on equation 5.25. The following steps are used to construct these plots. (i) The ionic activity coefficients of $NBTA^+$ and of TBA^+ in the aqueous phase were used to convert molar concentrations, $[NBTA^+]$ and $[TBA^+]$, into activities, a_{NBTA} and a_{TBA}. Activity coefficients used for $NBTA^+$ were as described in Section 5.3.2 and those used for TBA^+ were as follows. For ionic strengths ≥ 0.100 mol/L the values are available in the literature [161] while at ionic strengths < 0.100 mol/L, the values were calculated using the extended Debye-Huckel equation and an ionic size parameter of 3.0×10^{-8} cm [160]. (ii) Γ_+ was calculated for five combinations of constant a_{NBTA} and a_{TBA}. The steps used in this calculation are given in Appendix C. Twenty-five values were obtained. (iii) A value of σ_T was calculated *via* the iterative process described in Section 5.2.2 for each of the twenty-five values of Γ_+. (iv) For each combination of constant a_{NBTA} and a_{TBA}, a plot was made of $1/\sigma_T$ *versus* $c^{-1/2}[(ZF\Psi_{OHP}/2RT)^{-1} \sinh(ZF\Psi_{OHP}/2RT)]^{-1}$ according to equation 5.25. These plots are shown in Figure 5.14. The data used to construct the plots are given in Tables B.15 to B.19. The corresponding amounts of $n_{NBTA,ADS}$, $n_{TBA,ADS}$,

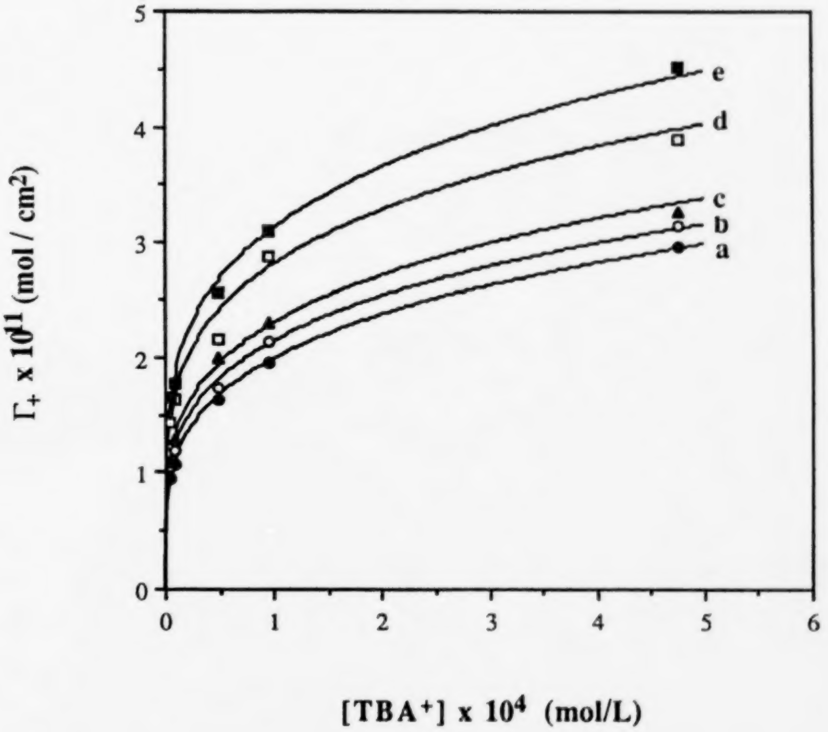

Figure 5.13 Surface excess of NBTA$^+$ and TBA$^+$, Γ_+, on Partisil-10 ODS-3 from pH 5 aqueous solution at five concentrations of NaCl in solution. The concentration of NBTA$^+$ in solution was kept constant at 1.86 x 10^{-3} mol/L while the concentration of TBA$^+$ in solution was varied from 5.00 x 10^{-6} to 5.00 x 10^{-4} mol/L. The NaCl concentrations were the same as in Figure 5.11. Data are given in Table B.14.

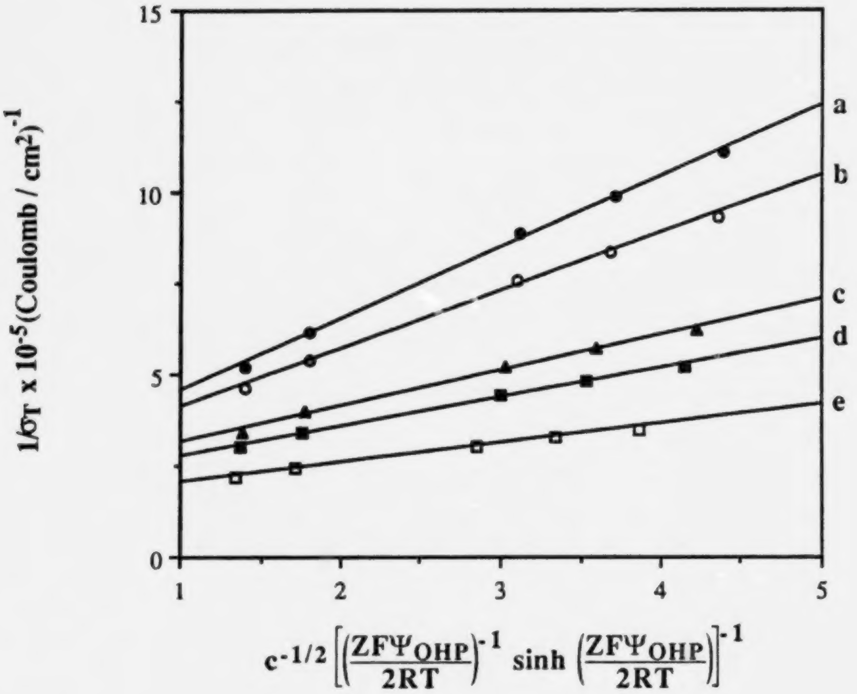

Figure 5.14 Plots of data from Figure 5.13 for the sum of $NBTA^+$ plus TBA^+ at a constant activity of $NBTA^+$ (1.50×10^{-3} mol/L) and five activities of TBA^+ according to equation 5.25, to show SGC behavior. The activities of TBA^+ are (a) 3.84×10^{-6} mol/L, (b) 7.86×10^{-6} mol/L, (c) 3.84×10^{-5} mol/L, (d) 7.86×10^{-5} mol/L and (e) 3.84×10^{-4} mol/L. Data are given in Tables B.15 to B.19.

$n_{NBTA,DL}$ and $n_{TBA,DL}$ are given in Table 5.3. (v) For each straight line, the values of Ψ_o, C_1 and r were calculated. They are presented in Table 5.4.

It is notable that C_1 is not a constant, but decreases monotonically as a_{TBA} is increased. This behavior is consistent with the view that $NBTA^+$ and TBA^+ are adsorbed at different locations and that C_1 is a differential capacitance.

The idea of ions sorbing in individual planes has recently been applied to ion exchange resins [162-164]. Unlike the present case, the surface charge in an ion exchanger is due to the fixed charge sites on the resin, which are located in a single plane. This surface charge is neutralized by counterions, each type of which, according to the model, is located in a different plane within the compact layer rather than being spread out in a diffuse layer. The sequence of the planes reflects the selectivity of the resin toward the different types of counterions. The entire compact layer in this case is treated as a series of capacitors. By contrast, in the present model the surface charges arise from adsorption of ions in planes within the compact layer while the counterions (anions) occupy the diffuse layer.

Evaluation of the integral capacitances K_{inner} and K_{outer} *via* equation 5.34 requires a knowledge of the differential quantity $(d\sigma_{TBA}/d\sigma_T)$ for each pair of a_{TBA} and a_{NBTA}. Plots of σ_{TBA} *versus* σ_T at constant a_{NBTA}, in combination with five different constant values of a_{TBA}, are shown in Figure 5.15. The charge densities used to construct the plots are given in columns 9 and 10 of Table 5.3. The plots are all linear as seen from the correlation coefficients in Table 5.5. Values of $(d\sigma_{TBA}/d\sigma_T)$, obtained as the slopes of these plots, are presented in Table 5.5 where it can be seen that as a_{TBA} increases, $(d\sigma_{TBA}/d\sigma_T)$ increases. This is because more TBA^+ gets adsorbed as a_{TBA} is increased, making a greater contribution to σ_T. Also presented in Table 5.5 are the reciprocals of the value of C_1 taken from Table 5.4. Equation 5.34 predicts that a plot of $1/C_1$ *versus* $(d\sigma_{TBA}/d\sigma_T)$ should be linear with a slope equal to $1/K_{inner}$ and intercept equal to $1/K_{outer}$. Such a plot is indeed linear, as shown in Figure 5.16. Its correlation coefficient, slope and

Table 5.3 Amounts of NBTA$^+$ and of TBA$^+$ sorbed in the electrical double layer (n_{NBTA}, n_{TBA}), excluded from the diffuse part of the electrical double layer ($n_{NBTA,DL}$, $n_{TBA,DL}$) and adsorbed in the compact part of the electrical double layer ($n_{NBTA,ADS}$, $n_{TBA,ADS}$) at a constant activity of NBTA$^+$ = 1.50 x 10^{-3} mol/L and five different activities of TBA$^+$.

a_{TBA} x 10^4 (mol/L)	c (mol/L)	n_{NBTA} x 10^6 (mol)	n_{TBA} x 10^6 (mol)	$n_{NBTA,DL}$ x 10^8 (mol)	$n_{TBA,DL}$ x 10^9 (mol)	$n_{NBTA,ADS}$ x 10^6 (mol)	$n_{TBA,ADS}$ x 10^6 (mol)	σ_{NBTA} x 10^6 (Coulomb/cm^2)	σ_{TBA} x 10^6 (Coulomb/cm^2)
0.0384	0.050	0.519	0.432	-1.50	-0.0385	0.534	0.432	0.498	0.403
	0.070	0.586	0.489	-1.25	-0.0321	0.598	0.489	0.559	0.457
	0.100	0.625	0.571	-1.06	-0.0264	0.636	0.571	0.594	0.534
	0.300	0.980	0.752	-0.650	-0.0146	0.986	0.752	0.921	0.702
	0.500	1.21	0.836	-0.533	-0.0110	1.22	0.836	1.14	0.781
0.0768	0.050	0.476	0.656	-1.73	-0.0885	0.494	0.656	0.461	0.613
	0.070	0.541	0.726	-1.43	-0.0734	0.555	0.726	0.519	0.678
	0.100	0.587	0.817	-1.20	-0.0601	0.599	0.817	0.559	0.763
	0.300	0.927	1.05	-0.728	-0.0328	0.934	1.05	0.873	0.981
	0.500	1.13	1.18	-0.594	-0.0246	1.14	1.18	1.06	1.10
0.384	0.050	0.346	1.35	-2.31	-0.593	0.369	1.36	0.345	1.27
	0.070	0.397	1.47	-1.90	-0.487	0.416	1.47	0.389	1.37
	0.100	0.431	1.61	-1.60	-0.400	0.447	1.61	0.418	1.51
	0.300	0.713	1.99	-0.939	-0.211	0.722	1.99	0.674	1.86
	0.500	0.878	2.24	-0.760	-0.157	0.886	2.24	0.827	2.09
0.768	0.050	0.289	1.74	-2.58	-1.32	0.315	1.74	0.294	1.62
	0.070	0.338	1.86	-2.12	-1.09	0.359	1.86	0.335	1.74
	0.100	0.373	2.03	-1.79	-0.892	0.390	2.03	0.365	1.90
	0.300	0.632	2.49	-1.05	-0.472	0.642	2.49	0.600	2.32
	0.500	0.790	2.79	-0.848	-0.351	0.798	2.79	0.745	2.61
3.84	0.050	0.193	2.85	-3.22	-8.24	0.289	2.86	0.210	2.67
	0.070	0.222	3.02	-2.65	-6.79	0.249	3.03	0.232	2.83
	0.100	0.251	3.27	-2.25	-5.63	0.273	3.28	0.255	3.06
	0.300	0.437	3.93	-1.33	-2.98	0.450	3.93	0.421	3.67
	0.500	0.544	4.43	-1.08	-2.23	0.554	4.43	0.518	4.13

Table 5.4 SGC behavior of $NBTA^+$ and TBA^+ on Partisil-10 ODS-3 from linear plots of σ_T^{-1} *versus* $c^{-1/2}$ $[(ZF\Psi_{OHP}/2RT)^{-1} \sinh (ZF\Psi_{OHP}/2RT)]^{-1}$ at a constant $NBTA^+$ activity and five activities of TBA^+ in solution (Figure 5.14).

$a_{NBTA} \times 10^3$ (mol/L)	$a_{TBA} \times 10^4$ (mol/L)	r (a)	Ψ_o (mV) (b)	$C_1 \times 10^6$ (Farad/cm^2)
1.50	0.0384	0.999	22.3 ± 0.6	174 ± 11
1.50	0.0768	0.999	27.6 ± 0.8	145 ± 8
1.50	0.384	0.998	45.0 ± 1.6	103 ± 5
1.50	0.768	0.997	54.7 ± 2.2	93.5 ± 4.5
1.50	3.84	0.996	84.0 ± 4.0	79.4 ± 3.7

(a) r = correlation coefficients of linear regression of linear plots in Figure 5.14.

(b) Uncertainties of Ψ_o and C_1 values are standard deviations.

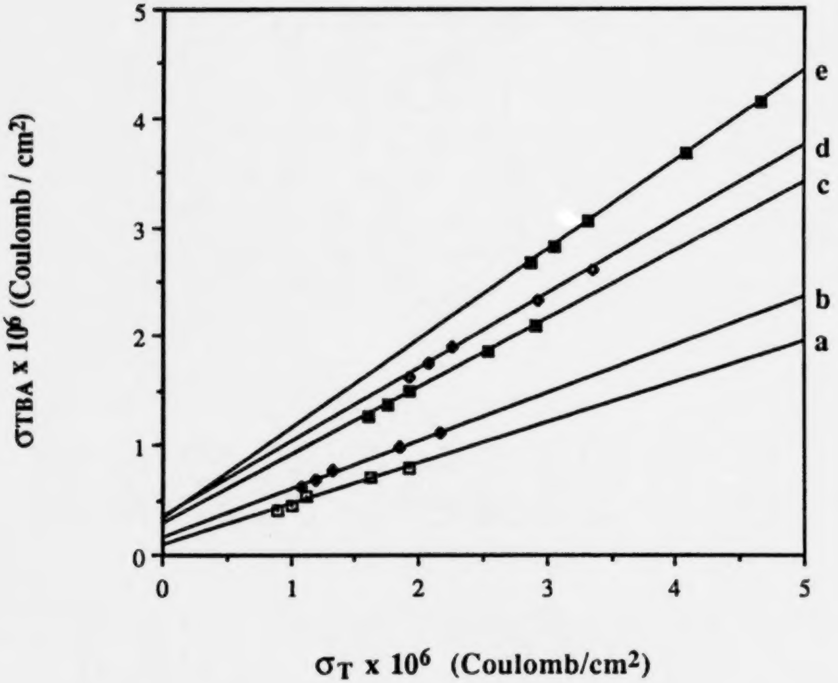

Figure 5.15 TBA$^+$ charge density *versus* total charge density at a constant activity of NBTA$^+$ (1.50×10^{-3} mol/L) and five activities of TBA$^+$. The activities of TBA$^+$ were the same as in Figure 5.14.

Table 5.5 Values for ($d\sigma_{TBA}/d\sigma_T$) at a constant $a_{NBTA} = 1.50 \times 10^{-3}$ mol/L and five activities of TBA^+ from Figure 5.15.

$a_{TBA} \times 10^4$ (mol/L)	r [(a)]	$(d\sigma_{TBA}/d\sigma_T)$[(b)]	Intercept x 10^8[(b)]	$1/C_1$ $(Farad/cm^2)^{-1}$
0.0384	0.992	0.368 ± 0.027	9.08 ± 3.71	5750 ± 360
0.0768	0.997	0.443 ± 0.020	15.2 ± 3.1	6900 ± 380
0.384	0.999	0.623 ± 0.017	27.9 ± 3.8	9710 ± 470
0.768	0.999	0.679 ± 0.014	33.6 ± 3.7	10700 ± 510
3.84	1.000	0.821 ± 0.010	31.8 ± 3.6	12600 ± 590

[(a)] r = correlation coefficients of linear regression of plots in Figure 5.15.

[(b)] Values for slopes and intercepts and their respective standard deviations were obtained from the straight line plots in Figure 5.15.

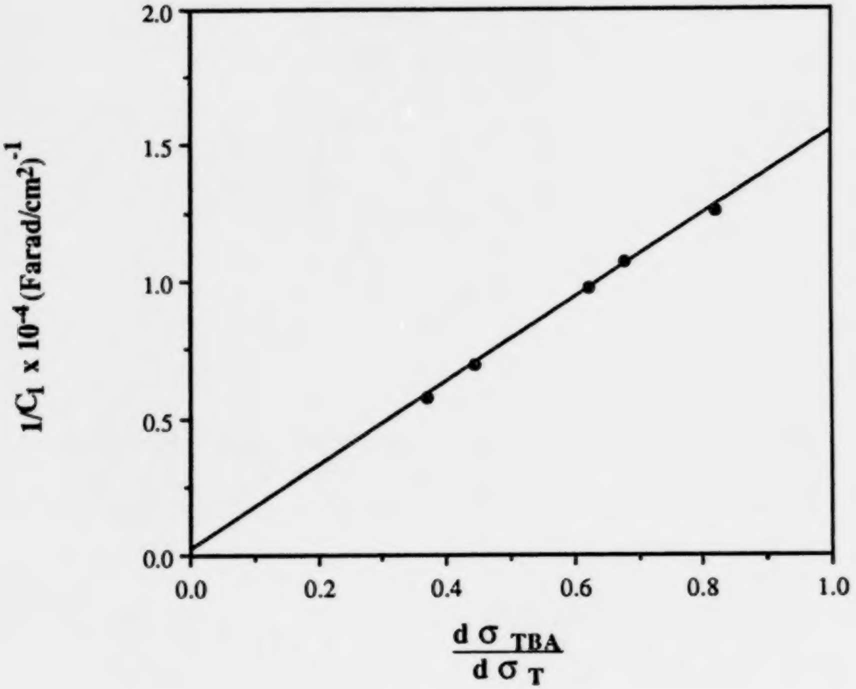

Figure 5.16 Reciprocal compact layer differential capacitance from the intercept of the straight line plots in Figure 5.14 *versus* the slopes of the straight line plots in Figure 5.15.

intercept are 0.999, $(1.53 \pm 0.01) \times 10^4$ $(\text{Farad/cm}^2)^{-1}$ and 150 ± 196 $(\text{Farad/cm}^2)^{-1}$, respectively. The integral capacitances are therefore $K_{\text{inner}} = (6.5 \pm 0.1) \times 10^{-5}$ Farad/cm^2 and $K_{\text{outer}} = (7 \pm 9) \times 10^{-3}$ Farad/cm^2.

From equation 5.35 the thickness of the inner capacitor between the TBA$^+$ and NBTA$^+$ charge surface is 11 ± 1 Å. This is in good agreement with the value of $11._4$ Å predicted as the difference between the value of δ obtained from the sorption of TBA$^+$ alone (12 Å) and the value of δ obtained from the sorption of NBTA$^+$ alone (0.6 Å). From equation 5.36 the thickness of the outer capacitor that is obtained when TBA$^+$ and NBTA$^+$ are simultaneously sorbed is 0.1 ± 1.3 Å. This, likewise, is in agreement with the value of 0.6 ± 0.2 Å obtained from the sorption of NBTA$^+$ alone. Evidently, both in the presence and absence of co-adsorbed TBA$^+$, the ion NBTA$^+$ is adsorbed with its charge center quite close to, or at, the OHP. The asymmetric shape of this ion gives it a hydrophobic "tail" and a charged polar head, thus making is likely that this ion is surface active and, therefore, sorbed closer to the OHP than is the symmetrical TBA$^+$ ion.

The permittivity, ε, employed in equations 5.35 and 5.36, and implicitly in equation 5.25, is 8.79×10^{-11} Coulomb/(Volt·cm), which is the value for bulk water at 25 °C. It may reasonably be argued that the permittivity of water near the C-18 groups would be lower than that of bulk water [165,166]. However, since there are no accurate values for it, the bulk water value has been chosen, as usual [33,34,36]. While this choice may lead to somewhat inaccurate values of δ_{inner} and δ_{outer}, it will likewise lead to the same inaccuracies in the values of δ measured in the TBA$^+$- alone and NBTA$^+$- alone systems, with which δ_{inner} and δ_{outer} are compared. Thus the comparisons remain valid and such inaccuracies do not invalidate the main conclusions. These conclusions are that TBA$^+$ and NBTA$^+$ are adsorbed in different charge planes and that the compact layer on the ODS bonded phase exhibits the classical behavior of capacitors in series.

The integral capacitance, K_C, is calculated from equation 5.37 to be $(6 \pm 8) \times 10^{-5}$ Farad/cm^2. The large uncertainty in K_C, of course, arises because K_{outer} is much smaller than K_{inner} and it has a large uncertainty. The total effective charge, σ'_T, is calculated using the tabulated values of Ψ_o and Ψ_{OHP}, given in columns 3 and 4 of Table 5.6, in equation 5.38. The resulting σ'_T values are given in column 5 of Table 5.6. They are used in equation 5.39 to calculate the value of Ψ_I at the NBTA$^+$ charge surface. Values of Ψ_I are tabulated in column 6 of Table 5.6. Comparison of the calculated values of Ψ_I with the corresponding values of Ψ_{OHP} in Table 5.6 shows that the two are nearly identical which, of course, is a direct consequence of the fact that the position of the NBTA$^+$ charge surface is within experimental error of the position of the OHP.

The fact that NBTA$^+$ happens to be located very close to the OHP is an accidental consequence of the properties of this particular ion. Presumably, other adsorbed ions would lie at various other positions within the compact layer than those occupied by either NBTA$^+$ or TBA$^+$ and, when co-adsorbed with, for example, TBA$^+$, would exhibit behavior consistent with the capacitors in series model of the compact layer. What is important to note here is that if, in contrast to the present model, different types of sorbed ions are all assumed to lie in the same plane, then the consequences would be the following: (i) $\sigma_{TBA} + \sigma_{NBTA} = \sigma_T \equiv \sigma_o$; (ii) the compact layer would be considered as a single capacitor whose measured value C_1 would be treated as an integral capacitance; (iii) the decrease in the measured value of C_1 with increasing sorption of TBA$^+$ (Table 5.4) would then be inconsistent with the SGC model.

5.3.4 Effect of TBA$^+$ on NBTA$^+$ Sorption

In the previous section, the sorption of NBTA$^+$ and of TBA$^+$ was treated in terms of electrical double layer theory. The results from that section, in particular the potentials calculated at the NBTA$^+$ charge plane, the TBA$^+$ charge plane and the Outer Helmholtz Plane, are now used to determine how TBA$^+$ influences the sorption of NBTA$^+$.

Figure 5.17 shows plots of Γ_{NBTA} versus TBA$^+$ concentration at five different

Table 5.6 Calculation of potentials at NBTA$^+$ charge plane at five ionic strengths and a constant $a_{NBTA} = 1.50 \times 10^{-3}$ mol/L.

c (mol/L)	$a_{TBA} \times 10^4$ (mol/L)	Ψ_o (mV)	Ψ_{OHP} (mV)	$\sigma'_T \times 10^6$ (Coulomb/cm^2)	Ψ_I (mV)
0.050	0.0384	22.3	17.3	0.324	17.4 ± 0.6
	0.0768	27.6	20.5	0.462	20.6 ± 0.8
	0.384	45.0	29.8	0.981	30.0 ± 1.6
	0.768	54.7	34.8	1.29	35.0 ± 2.2
	3.84	84.0	48.8	2.28	49.1 ± 4.0
0.070	0.0384	22.3	16.5	0.376	16.6 ± 0.6
	0.0768	27.6	19.4	0.536	19.4 ± 0.8
	0.384	45.0	27.8	1.12	27.9 ± 1.6
	0.768	54.7	32.2	1.46	32.4 ± 2.2
	3.84	84.0	44.8	2.54	45.1 ± 4.1
0.100	0.0384	22.3	15.4	0.450	15.4 ± 0.6
	0.0768	27.6	18.0	0.624	18.1 ± 0.8
	0.384	45.0	25.6	1.26	25.8 ± 1.6
	0.768	54.7	29.7	1.62	29.9 ± 2.2
	3.84	84.0	41.3	2.76	41.8 ± 4.1
0.300	0.0384	22.3	12.8	0.614	12.9 ± 0.6
	0.0768	27.6	14.6	0.842	14.8 ± 0.8
	0.384	45.0	19.8	1.63	20.0 ± 1.6
	0.768	54.7	22.6	2.08	23.0 ± 2.2
	3.84	84.0	30.8	3.44	31.4 ± 4.1
0.500	0.0384	22.3	11.8	0.684	11.9 ± 0.6
	0.0768	27.6	13.3	0.928	13.4 ± 0.8
	0.384	45.0	17.7	1.77	18.0 ± 1.6
	0.768	54.7	20.2	2.23	20.6 ± 2.2
	3.84	84.0	27.5	3.66	28.0 ± 4.1

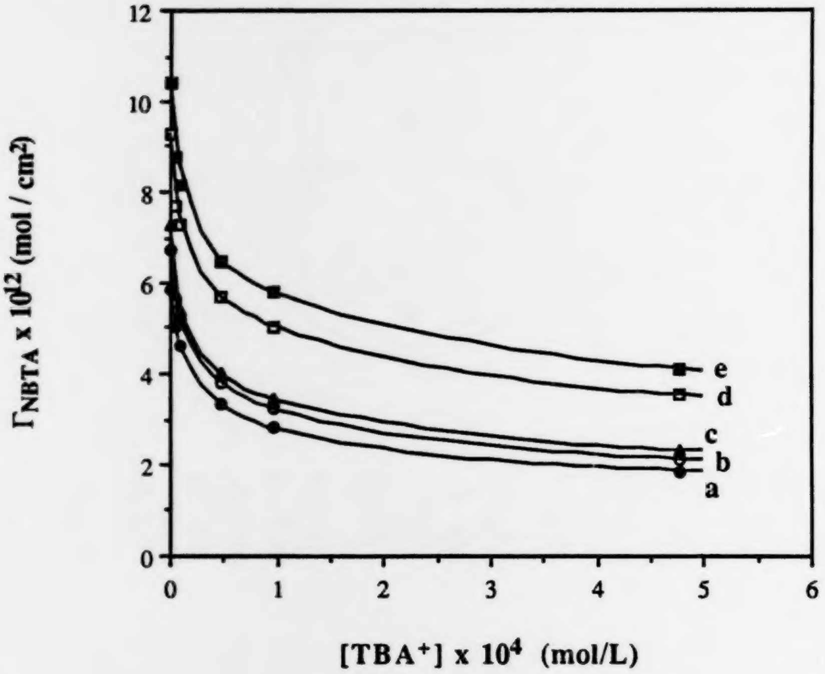

Figure 5.17 Surface excess of NBTA$^+$ as a function of TBA$^+$ concentration and NaCl concentration (*i.e.* ionic strength) in solution. The concentrations of NBTA$^+$, TBA$^+$ and NaCl were the same as in Figure 5.13. Data are given in Table B.14.

concentrations of NaCl in solution (*i.e.* ionic strength). Here, the surface excess of $NBTA^+$ is due to the experimentally measured amount of $NBTA^+$ sorbed in the entire electrical double layer (*i.e.* the amounts have not been adjusted for coion exclusion). The data are taken from Table B.14. The solid line curves were fit to the experimental points with the aid of French curves. The data for each curve were obtained by performing the column equilibration experiment with solutions containing a constant concentration of $NBTA^+$ and increasing concentrations of TBA^+. Since the concentrations of $NBTA^+$ and TBA^+ were small in comparison to the NaCl concentrations, the [NaCl] was taken to be the ionic strength. In the remainder of this chapter [NaCl] is equivalent to the ionic strength. For a constant bulk solution concentration of $NBTA^+$ and a constant ionic strength, it is obvious from these curves that the amount of sorbed $NBTA^+$ decreases with increasing solution concentration of TBA^+. In addition, as the ionic strength is increased, more $NBTA^+$ is sorbed, so each curve is shifted upward.

The behavior shown in Figure 5.17 is expected based on previous results observed for indirect detection of an ionic sample with the same charge as an ionic probe [20-22,26,65,101,102,114,120,124138,142,153,154]. In fact, plots similar to those in Figure 5.17 have been reported in the literature when the sample ion has the same sign of charge as the ion adsorbed on the bonded phase [22,65,114,118120,124,138,142]. Plots such as these constitute a demonstration of the phenomenon in which probe sorption is decreased in the presence of a sample which has the same sign of charge. The main purpose of the work described in this chapter is to provide an explanation for the cause of this phenomenon.

5.3.4.1 Coion Exclusion of $NBTA^+$ and of TBA^+

The potentials at the Outer Helmholtz Plane, Ψ_{OHP}, were calculated in Section 5.3.3 at a constant activity of $NBTA^+$ and various constant activities of TBA^+. They are given in column 4 of Table 5.6. These values were used in equations 5.40 and 5.51 to calculate the amounts of $NBTA^+$ and of TBA^+, respectively, that are excluded from the diffuse layer. These amounts, $n_{NBTA,DL}$ and $n_{TBA,DL}$, are given in columns 5 and 6 of Table 5.3. Note that the values in Table 5.3 are grouped according to a constant a_{TBA} with ionic strength being the variable. The values are negative as expected. At a constant ionic strength, Ψ_{OHP} increases as a_{TBA} increases, such that more $NBTA^+$ and TBA^+ ions are excluded. On the other hand, at a constant a_{TBA}, fewer ions are excluded as the ionic strength is increased. There are two reasons for the latter behavior. First, an increase in ionic strength causes a compression of the diffuse part of the electrical double layer with a consequent decrease in Ψ_{OHP} [33,167]. Second, the fraction of coions represented by $NBTA^+$ (and TBA^+) decreases as the concentration of Na^+ is increased. This appears as a decrease in α in equation 5.28 and it brings about a decrease in the moles of $NBTA^+$ (and TBA^+) excluded.

Shown in columns 3 and 4 of Table 5.3 are the experimentally measured amounts of $NBTA^+$ and TBA^+ sorbed in the entire electrical double layer. In columns 7 and 8 are presented the corresponding amounts of adsorbed $NBTA^+$ and TBA^+. These were calculated *via* equation 5.42 and 5.53, respectively, by subtracting the amounts excluded (determined above) from the corresponding experimentally determined amounts in the entire double layer.

5.3.4.2 Testing of the Competition for Space and Electrical Potential Effect Model

Knowing the amounts of $NBTA^+$ and of TBA^+ adsorbed, it is now possible to test if both a competition for space and an electrical potential effect are responsible for the decrease in $NBTA^+$ sorption when TBA^+ is present. The physicochemical model which is proposed to explain the effect of the adsorption of TBA^+ on the adsorption of $NBTA^+$ is embodied in equation 5.50. A test of the validity of the proposed model is performed by fitting equation 5.50 to the variables $n_{NBTA,ADS}$, $n_{TBA,ADS}$ and Ψ_I. The previously calculated values of Ψ_I are given in column 6 of Table 5.6. For the purposes of curve fitting, equation 5.50 can be expressed in the following form:

$$n_{NBTA,ADS} = C_{m,NBTA}\, \gamma_{NBTA} \left(A_T - \bar{A}'_{TBA} n_{TBA,ADS}\right) m \, \exp\left(- \frac{Z_+ F \Psi_I}{RT}\right) \qquad (5.54)$$

where

$$m = \left(\frac{10^{-3}\, d}{\gamma_{NBTA,ADS}}\right) \exp\left(- \frac{\overset{\circ}{\mu}_{NBTA,ADS}}{R\,T}\right)$$

Before attempting to curve fit equation 5.54, the assumption was made that no competition for space was occurring. That is, the change in Ψ_I (*i.e.* potential effect) due to adsorbed TBA^+ was solely responsible for the decrease in adsorbed $NBTA^+$. Equation 5.48 with $A_S = A_T$ applies in this case. To test if only a potential effect was occurring, a plot of $n_{NBTA,ADS}$ *versus* $\exp(-Z_+F\Psi_I/RT)$ was made. The plot is shown in Figure 5.18 and the values of the correlation coefficients, slopes and intercepts for each straight line are given in Table 5.7. The data used to construct the plots are given in Table B.20. According to equation 5.48, if no competition for space is occurring then the plots should be linear with a zero intercept. The plots are linear, but the intercepts do not go through zero. At low ionic strength the intercepts are positive and they become smaller as ionic strength is increased until they have negative values at high ionic strength. Since the results do not agree with theory it was concluded that an additional effect must be occurring (*i.e.* competition for space).

To test if both effects were occurring, curve fitting of equation 5.54 was performed with a nonlinear least squares program which uses a Newton-Raphson procedure described

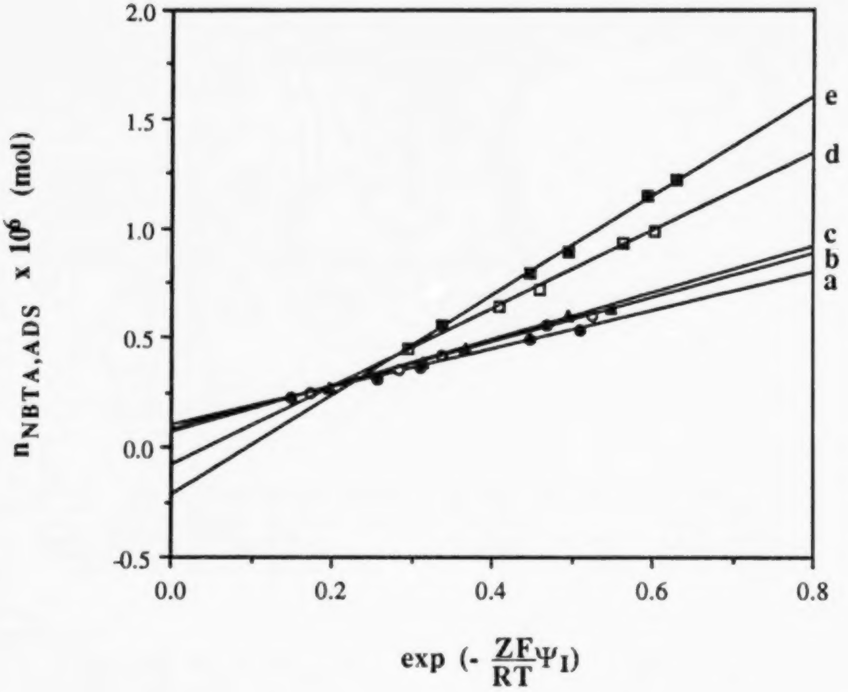

Figure 5.18 Plots according to equation 5.48 for a potential effect only at five concentrations of NaCl in solution. The NaCl concentrations were the same as in Figure 5.11. Data are given in Table B.20. Slopes, intercepts and correlation coefficients of the straight lines are given in Table 5.7.

Table 5.7 Results of the linear plots in Figure 5.18 for a potential effect only at five ionic strengths.

c (mol/L)	**r** [(a)]	**slope x 10^6 (mol)** [(b)]	**intercept x 10^7 (mol)** [(b)]
0.050	0.999	0.872 ± 0.020	0.955 ± 0.070
0.070	0.999	1.00 ± 0.02	0.755 ± 0.068
0.100	0.998	1.06 ± 0.03	0.617 ± 0.124
0.300	0.998	1.77 ± 0.05	-0.800 ± 0.247
0.500	0.998	2.29 ± 0.07	-2.25 + 0.35

(a) Correlation coefficient

(b) The error is given as the standard deviation.

in reference 168. Only $\overline{A}'_{TBA}$ and *m* were allowed to vary in the curve fitting process. Values obtained for the floating constants $\overline{A}'_{TBA}$ and *m* are presented in Table 5.8 for each of the five ionic strengths employed. These results are discussed below.

The goodness of fit of the data to equation 5.54 is illustrated graphically by the linearity of the plots shown in Figure 5.19. To make these plots, equation 5.54 is rearranged as follows:

$$\frac{n_{NBTA,ADS}}{C_{m,NBTA}\,\gamma_{NBTA}\left(A_T - \overline{A}'_{TBA}n_{TBA,ADS}\right)} = m\ \exp\left(-\frac{Z_+F\Psi_I}{RT}\right) \qquad (5.55)$$

The values of $\overline{A}'_{TBA}$ from Table 5.8 are employed in evaluating the left hand term in equation 5.55. This left hand term is equal to $K_{NBTA,ADS}\cdot(\gamma_{NBTA})^{-1}$ as can be seen by comparison with equations 5.46 and 5.47. In Figure 5.19 the left hand side of equation 5.55 is plotted *versus* the exponential term on the right hand side. The data used to construct the plots are given in Table B.20. The slopes, intercepts and correlation coefficients from linear least squares regression analysis of these plots are given in Table 5.9. Near unity values of the correlation coefficients along with zero intercepts for these linear plots demonstrate the goodness of fit of equation 5.54 (*i.e.* of equation 5.50) to the data.

The values of $\overline{A}'_{TBA}$ reveal how much of the change in $NBTA^+$ sorption is due to an alteration of available space. Looking at the values obtained in Table 5.8, the negative values at low ionic strength are initially quite surprising. Since the values are not zero within error, the effect is real and agrees with the result obtained from Figure 5.18. Negative values for $\overline{A}'_{TBA}$ suggest that the area available for $NBTA^+$ sorption, A_S, is *increased* in the presence of TBA^+. To understand how this is possible it is important to remember that $NBTA^+$ and TBA^+ do not adsorb in the same charge plane, but that the TBA^+ charge plane lies further within the bonded phase. In addition, when TBA^+ adsorbs

Table 5.8 Nonlinear curve fitting of equation 5.54 to fit the constants $\overline{A}'_{TBA}$ and *m* at five ionic strengths. In equation 5.54 $C_{m,NBTA} = 1.86 \times 10^{-3}$ mol/L and $A_T = 1.03 \times 10^5$ cm^2.

c (mol/L)	**$\overline{A}'_{TBA} \times 10^{-9}$ (cm^2) (a)**	**$m \times 10^9$ (L/cm^2) (a)**
0.050	-17.3 ± 2.4	6.35 ± 0.11
0.070	-9.74 ± 1.23	7.29 ± 0.07
0.100	-6.11 ± 1.57	8.05 ± 0.11
0.300	2.56 ± 0.67	14.9 ± 0.1
0.500	4.29 ± 0.45	20.5 ± 0.1

(a) The error is given as the standard deviation.

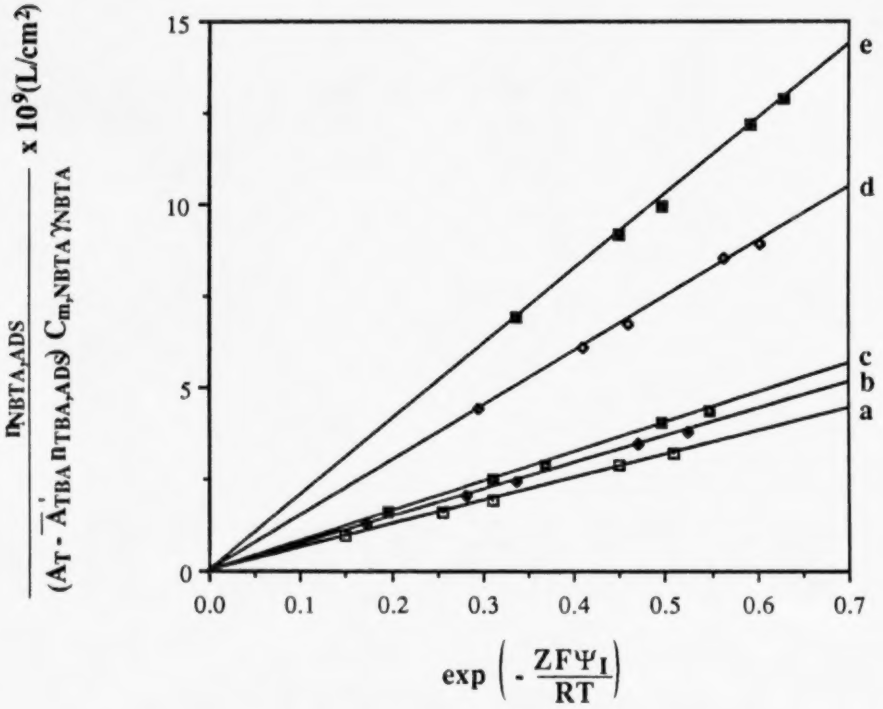

Figure 5.19 Plots according to equation 5.55 for a competition for space and an electrostatic potential effect at five ionic strengths. The ionic strengths (*i.e.* [NaCl]) are the same as in Figure 5.11. The data are given in Table B.20. The slopes, intercepts and correlation coefficients are given in Table 5.9.

Table 5.9 Results of the linear plots in Figure 5.19 for a competition for space and an electrostatic potential effect at five ionic strengths.

c (mol/L)	r [(a)]	slope x 10^9 (mol/cm^2) [(b)]	intercept x 10^{10} (mol/cm^2) [(b)]
0.050	0.999	6.34 ± 0.16	0.0586 ± 0.573
0.070	0.999	7.27 ± 0.13	0.0421 ± 0.481
0.100	0.998	7.58 ± 0.39	2.18 ± 1.57
0.300	0.999	14.9 ± 0.4	-0.144 ± 2.05
0.500	0.999	20.5 ± 0.5	-0.216 ± 2.67

(a) Correlation coefficient.

(b) The error is given as the standard deviation.

it affects Ψ_I which causes some NBTA$^+$ to desorb. This loss of some NBTA$^+$ (due to a change in Ψ_I) will produce an increase in the available space for NBTA$^+$ adsorption. However, this effect is not great enough to produce the large negative $\overline{A}'_{TBA}$ values in Table 5.8. What is more likely to be happening is that adsorption of TBA$^+$ changes the nature of the bonded phase (*i.e.* the arrangement of the alkyl chains) such that the area available for NBTA$^+$ sorption is in fact increased. That is, the value of A_S in the NBTA$^+$ adsorption plane is increased in the presence of large ions in the TBA$^+$ adsorption plane.

The trend in the values of $\overline{A}'_{TBA}$ in Table 5.8 is such that as the ionic strength is increased, $\overline{A}'_{TBA}$ becomes larger until it is positive at the higher ionic strengths. Positive values mean that the space available for NBTA$^+$ sorption is decreased, which is generally the type of behavior expected when a competition for space occurs. At high ionic strength a decrease in available space for NBTA$^+$ adsorption is expected to occur since more TBA$^+$ ions are adsorbed. The trend in Table 5.8 is consistent with this.

In light of these results, TBA$^+$ adsorption affects NBTA$^+$ adsorption in three ways: (i) it changes the value of Ψ_I; (ii) it competes for space by decreasing A_S; and (iii) it changes the nature of the bonded phase in the NBTA$^+$ charge plane such that A_S increases. In the case of the latter two effects (*i.e.* alteration of available space), at low ionic strengths the third effect is greater than the second while at high ionic strengths the second effect is greater than the third.

It is possible to estimate whether alteration of available space or change in electrostatic potential is the overall dominating effect. To do this it is necessary to look at how $n_{NBTA,ADS}$ changes with the competition for space term, A_S $(=A_T-A_{TBA}{\cdot}n_{TBA,ADS})$, and with the electrostatic potential term, $\exp(-Z_+F\Psi_I/RT)$. These two terms are given in Table 5.10 along with $n_{NBTA,ADS}$ and $n_{TBA,ADS}$. The value of $n_{NBTA,ADS}$ is relatively insensitive to $\overline{A}'_{TBA}$. The term $\overline{A}'_{TBA}{\cdot}n_{TBA,ADS}$ is small, never being higher than about 20% of the quantity from which it is subtracted, *i.e.* A_T, and also the relative change in the value of the whole multiplier term $(A_T - \overline{A}'_{TBA}{\cdot}n_{TBA,ADS})$ with a change in $n_{TBA,ADS}$ is

Table 5.10 Values of the competition for space term, A_S, and the electrostatic potential effect term, $\exp(-Z_+F\Psi_I/RT)$, in equation 5.54 at five ionic strengths.

c (mol/L)	$n_{NBTA,ADS} \times 10^6$ (mol)	$n_{TBA,ADS} \times 10^6$ (mol)	$A_S \times 10^{-5}$ (cm^2) (a)	$\exp\left(-\frac{ZF\Psi_I}{RT}\right)$
0.050	0.534	0.432	1.10	0.509
	0.494	0.656	1.14	0.449
	0.369	1.36	1.27	0.311
	0.315	1.74	1.33	0.256
	0.225	2.86	1.52	0.148
0.070	0.598	0.489	1.08	0.525
	0.555	0.726	1.10	0.470
	0.416	1.47	1.17	0.338
	0.359	1.86	1.21	0.283
	0.249	3.03	1.33	0.173
0.100	0.636	0.571	1.06	0.548
	0.599	0.817	1.08	0.495
	0.447	1.61	1.13	0.367
	0.390	2.03	1.15	0.312
	0.273	3.28	1.23	0.173
0.300	0.986	0.752	1.01	0.604
	0.934	1.05	1.00	0.563
	0.722	1.99	0.979	0.459
	0.642	2.49	0.966	0.410
	0.450	3.93	0.929	0.295
0.500	1.22	0.836	0.994	0.630
	1.14	1.18	0.979	0.593
	0.886	2.24	0.934	0.496
	0.798	2.79	0.910	0.449
	0.554	4.43	0.840	0.336

(a) $A_S = A_T - \overline{A}'_{TBA} \cdot n_{TBA,ADS}$

smaller than the relative change in the multiplier term exp ($-Z_+F\Psi_I/RT$). Comparison of the last two columns in Table 5.10 suggests that the change in Ψ_I makes a larger contribution to the decrease in $n_{NBTA,ADS}$ than does A_S. Therefore, the conclusion is that an electrostatic potential effect is primarily responsible for the reduction in $n_{NBTA,ADS}$ when TBA^+ adsorbs.

The value of 4.29×10^9 cm^2/mol that is obtained for the effective area contribution of TBA^+ to the $NBTA^+$ charge surface at the highest ionic strength is only about one-fourth as large as the value of 2×10^{10} cm^2/mol which was obtained for $\overline{A}_{TBA}$, the area contribution of TBA^+ *to its own charge plane* in an earlier study [34]. The relationship $\overline{A}'_{TBA} < \overline{A}_{TBA}$ is consistent with the qualitative picture of the compact part of the electrical double layer shown in Figure 5.2.

The other term that is obtained from curve fitting is *m*. Its value is expected to be constant and independent of ionic strength. Looking at the values in Table 5.8, they are not constant. Instead, they increase with ionic strength. Considering the constants that make up *m*, the chemical potential is constant since it is defined for standard state conditions. The value of *d* is defined to be a thickness in the bonded phase. While the choice of *d* is arbitrary, once the value is chosen it is fixed. The arbitrariness of *d* is reflected in the product $d \cdot \exp(-\mu^o_{NBTA,ADS}/RT)$. If *d* is chosen to be smaller of larger, then $\mu^o_{NBTA,ADS}$ will change accordingly in order that the product $d \cdot \exp(-\mu^o_{NBTA,ADS}/RT)$ stays the same. Therefore, it is not likely that the change in *m* with ionic strength is due to a change in *d*.

The remaining constant that makes up *m* is $\gamma_{NBTA,ADS}$. The possibility of this value changing with ionic strength will now be addressed. The surface activity coefficient, $\gamma_{NBTA,ADS}$, is a nonionic activity coefficient. That is, it is not related to the ionic strength or the electrical potential [35]. In equation 5.47, it can be combined with the electrochemical potential to give the following expression:

$$K_{NBTA,ADS} = 10^{-3}\, \gamma_{NBTA}\, d \exp\left(- \frac{\mu_{NBTA,ADS} + Z_{+} F \Psi_{I}}{R\,T}\right) \qquad (5.56)$$

where

$$\mu_{NBTA,ADS} = \mu^{o}_{NBTA,ADS} + RT \ln \gamma_{NBTA,ADS} \qquad (5.57)$$

In equation 5.57, $\gamma_{NBTA,ADS}$ accounts for the fact that the value of the chemical potential may change due to a change in the nature of the bonded phase. In the present case, as more large TBA^{+} ions adsorb at high ionic strength, there will be more rearrangement of the alkyl chains. It was already shown above how this rearrangement leads to an increase in the space available for NBTA^{+} adsorption. Therefore, it is quite likely that the change observed in the value of *m* with ionic strength is due to a change in $\gamma_{NBTA,ADS}$.

5.3.4.3 Indirect Detection Chromatography

The preceding section has revealed the origin of the change in the amount of NBTA^{+} probe (*i.e.* the decrease in $n_{NBTA,ADS}$) with increasing amounts of adsorbed TBA^{+} sample. This change in the moles of adsorbed NBTA^{+}, $\Delta n_{NBTA,ADS}$, and therefore in its contribution to the magnitude of the sample (and system) peak, can be calculated from the equation:

$$\Delta n_{NBTA,ADS} = n_{NBTA,ADS}(\mathrm{TBA}^{+}\text{ present}) - n_{NBTA,ADS}(\mathrm{TBA}^{+}\text{ absent}) \qquad (5.58)$$

in which $n_{NBTA,ADS}$(TBA^{+} present) and $n_{NBTA,ADS}$(TBA^{+} absent) are calculated from equation 5.50 for concentrations that prevail at the top of the column just after and just before the moment of injection of a TBA^{+} sample dissolved in the mobile phase containing

$NBTA^+$ probe. Since the former is smaller than the latter, the quantity $\Delta n_{NBTA,ADS}$ has a negative value. However, the magnitude of the sample (and system) peak depends also on any change that the presence of TBA^+ sample causes in the amount of $NBTA^+$ excluded from the diffuse part of the double layer (*i.e.* a change in $n_{NBTA,DL}$). This change, $\Delta n_{NBTA,DL}$, can be calculated from the equation:

$$\Delta n_{NBTA,DL} = n_{NBTA,DL}(TBA^+ \text{ present}) - n_{NBTA,DL}(TBA^+ \text{ absent}) \qquad (5.59)$$

In the presence of TBA^+, Ψ_{OHP} will have a larger positive value (see Table 5.6) so that $n_{NBTA,DL}(TBA^+ \text{ present})$ has a larger negative value than does $n_{NBTA,DL}(TBA^+ \text{ absent})$ and consequently $\Delta n_{NBTA,DL}$ has a negative value.

The overall change in sorbed $NBTA^+$ is given by the expression:

$$\Delta n_{NBTA} = \Delta n_{NBTA,ADS} + \Delta n_{NBTA,DL} \qquad (5.60)$$

The two terms on the right are negative (as, of course, is the term on the left) meaning that in the presence of TBA^+ the amount of adsorbed $NBTA^+$ decreases and the amount of $NBTA^+$ in the diffuse layer also decreases. Both terms contribute to decreased sorption of $NBTA^+$ in the presence of TBA^+. For the conditions employed in this study the absolute magnitude of $\Delta n_{NBTA,ADS}$ is much larger than the absolute magnitude of $\Delta n_{NBTA,DL}$ such that $\Delta n_{NBTA,ADS}$ is largely responsible for the indirect detection response. This can be seen in Table 5.3 by inspection of the way in which $n_{NBTA,ADS}$ and $n_{NBTA,DL}$ change with increasing amounts of added TBA^+ at a constant ionic strength.

Another feature of an elution chromatogram is the sample capacity factor, e.g. k'_{TBA}, which is related to the total amount of sorbed TBA^+ as follows:

$$k'_{TBA} = \frac{n_{TBA}}{C_{m,TBA}V'_m} = \frac{n_{TBA,ADS} + n_{TBA,DL}}{C_{m,TBA}V'_m} \tag{5.61}$$

Here, V'_m is the void volume of the column containing the zone of n_{TBA} moles of sample. The quantities $n_{TBA,DL}$ and $n_{TBA,ADS}$ come from equations 5.51 and 5.53, respectively.

The conditions used in this study were chosen to produce a relatively large change in n_{NBTA}, n_{TBA} and the electrical potentials, for the purpose of testing the proposed model. If elution chromatography for analytical purposes was performed under these conditions, unacceptable behavior would be observed. In the conditions of this study Ψ_I and Ψ_{OHP} depend significantly on $n_{TBA,ADS}$. As a TBA$^+$ sample zone migrates along a column its concentration decreases and its concentration profile tends to become non-constant (e.g. perhaps Gaussian). The decreased and spatially varying $C_{m,TBA}$ leads, in turn, to decreased and spatially varying $n_{TBA,ADS}$, Ψ_I, Ψ_{OHP}, n_{TBA} and k'_{TBA}. At high TBA$^+$ concentration, its sorption isotherm would be nonlinear and the sample peak would be highly asymmetric. The indirect detection response, Δn_{NBTA}, would not be linearly related to the amount of TBA$^+$ sample injected.

To avoid these undesirable effects in analytical indirect detection chromatography of a sample ion in the presence of a probe ion, conditions are employed for which $n_{probe,ADS} >> n_{sample,ADS}$ so that adsorption of the sample ion produces only very small relative changes in Ψ_I and Ψ_{OHP}. In this case Ψ_o, Ψ_I and Ψ_{OHP} remain essentially constant (small change) for a given amount of sample injected, and k'_{smp} becomes essentially constant, independent of the amount of sample injected. The magnitude of the indirect detection response, Δn_{probe}, is considerably reduced under these conditions but it becomes linearly proportional to the amount of sample injected.

5.4 Conclusions

The results obtained in Sections 5.3.2 and 5.3.3 dealing with the SGC theory for two potential determining ions are significant to the interpretation of the sorption of ionic species onto RPBPs. The electrical double layer treatment as it applies to the sorption of ions onto RPBPs is different than the treatment for an electrode surface since the RPBP is a three-dimensional surface as opposed to a two-dimensional surface. The sorption of two different ions of the same charge onto a RPBP cannot be treated as though both ions lie in the same charge surface. The location of the charge surface depends on both the size of the ion and the nature of the ion. Charge centers of symmetrical ions having more non-polar groups present are expected to penetrate more deeply within the bonded phase while charge centers of asymmetrical ions having more polar groups are expected to lie closer to the ends of the alkyl chains.

When indirect detection is done with ionic species, the change in electrical potential that is created by the sorption of sample ions is largely responsible for the change in probe sorption. Sorption of a positively charged sample ion with the same sign of charge as the probe increases the potential and changes the electrochemical potential of the probe such that it disfavors further probe sorption (equation 5.47). On the other hand, a negatively charged sample ion with opposite sign of charge to the probe decreases the electrical potential and changes the electrochemical potential such that it favors further probe sorption. The contribution of the sample to the potential, although relatively small, is significant enough to alter the sorption of the probe by a small amount, such as is observed in indirect UV detection elution chromatograms.

An alteration of the space available for adsorption was found to play a minor role in the present study since the electrostatic potential effect dominates. The alteration of available space was such that at low ionic strength, TBA^+ adsorption increased the available space for $NBTA^+$ adsorption by changing the structure of the bonded phase while at high ionic strength it decreased the space available for $NBTA^+$ adsorption by occupying more space. Another model has recently been proposed in the literature for indirect detection in which equations have been derived that include both a competition for space and an electrostatic potential effect [46]. It has been tested using previous literature data and agreement was found only when the effect of competition for space was neglected. This suggests that competition for space has only a minor effect and that the electrostatic potential effect dominates, which is in agreement with the results obtained in this chapter.

Chapter 6

Conclusions

6.1 Summary of Results

The experiments in this thesis have demonstrated how a sample can affect the sorption of a probe. It is this effect which is responsible for the indirect detection phenomenon. There are three general ways in which a sample can affect probe sorption. These were presented in Chapter 1. The way in which a sample affects probe sorption depends upon the charge of the sample relative to that of the probe. In the case of a neutral sample and an ionic probe, a competition for space between the two is primarily responsible. It is possible to reason that when both the sample and the probe are neutral, a competition for space would also occur.

These results are significant since the presence of organic modifiers, in particular alcohols, in the mobile phase and/or stationary phase is usually treated in terms of a solvent effect or a change in the nature of the stationary phase. The results of Chapter 4 quantitatively show that a competition for space can also occur. As a result, a competition for space should also be considered in addition to solvent and sorbent effects when dealing with systems in which there are several components in the mobile phase.

Chapter 5 dealt with an ionic sample and an ionic probe having the same charge. The electrostatic potential has previously been found to play a large role in IM-RPLC. The significance of the results in Chapter 5 to indirect detection is in the effect that the sample has on the electrostatic potential. In the electrostatic theories of IM-RPLC the small contribution of the sample to the electrostatic potential is often neglected. This was not the case in the present thesis. In Chapter 5 the contribution of the sample to the electrostatic potential was considered and it was found that when two different ions sorb, they each produce their own charge surface and give rise to the potentials at each charge surface. These results are very important to the understanding of how ionic species sorb on RPBPs. Sorption cannot be treated as occurring in the same charge plane, as has previously been thought. This is a significant advancement in the interpretation of the electrical double layer that develops when ionic species sorb on RPBPs.

The significance of this result to indirect detection is that when the sample sorbs on the stationary phase it can produce a small change in the potential which will affect the sorption of the probe. Electrical double layer theory has been suggested previously in a model for indirect detection in which the sample alters the electrical potential [46]. The results in this thesis clearly show that the sample can affect the potential and bring about the small changes in probe sorption that are observed in indirect detection.

Another interesting result from Chapter 5 is that when two species sorb on a RPBP, the alteration in the space available for sorption is such that there may be either an increase or a decrease in the space available. The behavior that is observed depends upon ionic strength and on how the structure of the bonded phase is changed by sorption and/or desorption of the species competing for space.

A conclusion which can be made from the column equilibration studies and which is related to indirect detection is the dependence of the magnitude of the indirect detection response on sample type (*i.e.* neutral or ionic). Ionic sample species produce a larger response compared to a similar concentration of a neutral sample species. The results of the column equilibration studies verify this observation. Rather than dealing with concentrations though, the column equilibration technique measured the actual amount of a particular component sorbed on the stationary phase. Considering the results of the two studies presented in Tables 4.6 (neutral sample) and B.14 (ionic sample), it can be seen that to produce approximately the same change in the number of moles of probe sorbed, approximately ten times more neutral sample (*i.e.* butanol) had to be sorbed than ionic sample (*i.e.* TBA$^+$). The larger response is due to the stronger effect of the electrostatic potential. It can also be reasoned that when both the sample and the probe are ionic, the presence of two effects (*i.e.* competition for space and electrostatic potential) leads to a larger response compared to neutral systems where only a single effect (*i.e.* competition for space) is occurring.

6.2 Directions for Future Work

6.2.1 Sample and Probe with Opposite Charge

A logical continuation of the research done in this thesis is to do a column equilibration study for the case where the sample and the probe have opposite signs of charge. This case has previously been studied for IM-RPLC where the sample was present at "trace concentrations" and its contribution to the electrostatic potential was neglected [37]. The emphasis would be different now since the contribution of the sample to the potential would be the important variable. By using sample concentrations which are not at trace conditions, the contribution of the sample to the potential can be considered. In addition it would be possible to test if both a competition for space and an electrostatic potential effect occur when the sample and probe have opposite charges. It would be interesting to see if a competition for space occurs in this case since the electrostatic potential effect is expected to be large when the sample and probe have opposite signs of charge.

6.2.2 Role of the Compact Layer

A further study which could be done on the role of the compact layer is one in which TBA$^+$ is still the sample ion, but various types of cationic probe ions are used. This would make it possible to see how the compact layer changes as the size of the probe ion and/or the nature of the probe ion changes. In particular, if the two ions are similar, then the assumption that both ions sorb in the same charge plane could be tested. On the other hand, if the two ions are different, then it would be possible to see how the location of the charge planes changes with the size and/or nature of the ion. For example, if another quaternary ammonium ion such as tetraethylammonium (TEA^+) was used, it might be expected that the TEA^+ charge plane would lie further within the bonded phase compared to the $NBTA^+$ charge plane, but not as much as the TBA^+ charge plane.

Bibliography

1. Snyder, L. R.; Kirkland, J. J. *Introduction to Modern Liquid Chromatography* , 2nd ed.; Wiley: Toronto, 1979; Chapter 4.
2. Lawrence, J. F.; Brinkman, U. A. Th.; Frei, R. W. In *Reaction Detection in Liquid Chromatography* ; Krull, I. S., Ed.; Marcel Dekker: New York, 1986; Vol. 34, Chapter 6.
3. Krull, I. S.; Colgan, S. T.; Selavka, C. M. In *High Performance Liquid Chromatography* ; Brown, P. R.; Hartwick, R. A., Eds.; Wiley: Toronto, 1989; Vol. 98, Chapter 10.
4. Denkert, M.; Hackzell, L.; Schill, G.; Sjogren, E. *J. Chromatogr.* **1981**, *218*, 31-43.
5. Hackzell, L.; Schill, G. *Chromatographia* **1982**, *15*, 437-444.
6. Hackzell, L.; Rydberg, T.; Schill, G. *J. Chromatogr.* **1983**, *282*, 179-191.
7. Schill, G.; Ehrsson, H.; Vessman, J.; Westerlund, D. *Separation Methods for Drugs and Related Organic Compounds*, 2nd. ed.; Swedish Pharmaceutical Press: Stockholm, 1983; Chapter 1.
8. Hackzell, L.; Schill, G. *Acta. Pharm. Suecica* 1981, 18, 257-270.
9. Hackzell, L.; Denkert, M.; Schill, G. *Acta. Pharm. Suecica* 1981, 18, 271-282.
10. Melander, W. R.; Horvath, Cs. In *High Performance Liquid Chromatography: Advances and Perspectives* ; Horvath, Cs., Ed.; Academic Press: Toronto, 1980; Vol. 2, Chapter 3.
11. Sander, L. C.; Wise, S. A. *CRC Reviews in Anal. Chem.* **1987**, *18*, 299-415.
12. Snyder, L. R.; Kirkland, J. J. *Introduction to Modern Liquid Chromatography* , 2nd ed.; Wiley: Toronto, 1979; pp.281, 587-588.
13. Martire, D. E.; Boehm, R. E. *J. Phys. Chem.* **1983**, *87*, 1045-1062.

14. Lochmuller, C. H.; Wilder, D. R. *J. Chromatogr. Sci.* **1979**, *17*, 574-579.

15. Dill, K. A. *J. Phys. Chem.* **1987**, *91*, 1980-1988.

16. Dorsey, J. G.; Dill, K. A. *Chem. Rev.* **1989**, *89*, 331-346.

17. Bogar, R. G.; Thomas, J. C.; Callis, J. B. *Anal. Chem.* **1984**, *56*, 1080-1084.

18. Colin, H.; Guiochon, G. *J. Chromatogr.* **1977**, *141*, 289-312.

19. Colin, H.; Guiochon, G. *J. Chrom*atogr. **1978**, *158*, 183-205.

20. Schill, G.; Crommen, J. *Trends Anal. Chem.* **1987**, *6*, 111-116.

21. Schill, G.; Arvidsson, E. *J. Chromatogr.* **1989**, *492*, 299-318.

22. Levin, S.; Grushka, E. *Anal. Chem.* **1986**, *58*, 1602-1607.

23. Stranahan, J. J.; Deming, S. N. *Anal. Chem.* **1982**, *54*, 1540-1546.

24. Barber, W. E.; Carr, P. W. *J. Chromatogr.* **1984**, *316*, 211-225.

25. Crommen, J.; Schill, G.; Herne, P. *Chromatographia* **1988**, *25*, 397-403.

26. Crommen, J.; Schill, G.; Westerlund, D.; Hackzell, L. *Chromatographia* **1987**, *24*, 252-260.

27. Arvidsson, E.; Crommen, J.; Schill, G.; Westerlund, D. *J. Chromatogr.* **1989**, *461*, 429-441.

28. Conder, J. R.; Young, C. L. *Physicochemical Measurement by Gas Chromatography* ; Wiley: Toronto, 1979; Chapter 9.

29. Karger, B. L.; Snyder, L. R.; Horvath, Cs. *An Introduction to Separation Science* ; Wiley: Toronto, 1973; Chapter 5.

30. Hux, R. A. Ph.D Thesis, University of Alberta, 1983.

31. May, S.; Hux, R.; Cantwell, F. F. *Anal. Chem.* **1982**, *54*, 1279-1282.

32. Chen, J.; Weber, S. G.; Glavina, L. L.; Cantwell, F. F. in press, *Journal of Chromatography.*

33. Cantwell, F. F.; Puon, S. *Anal. Chem.* **1979**, *51* , 623-632.

34. Liu, H.; Cantwell, F. F. *Anal. Chem.* **1991**, *63* , 993-1000.

35. Cantwell, F. F. *J. Pharm. Biomed. Anal.* **1984**, *2* , 153-164.

36. Cantwell, F. F. In *Ion Exchange and Solvent Extraction* : A Series of Advances; Marinsky, J. A.; Marcus, Y., Eds.; Marcel Dekker: New York, 1985; Vol. 9, Chapter 6.

37. Liu, H.; Cantwell, F. F. *Anal. Chem.* **1991,** *63* , 2032-2037.

38. Stahlberg, J. *J. Chromatogr.* **1986,** *356* , 231-245.

39. Stahlberg, J. *Chromatographia* **1987,** *24* , 820-826.

40. Stahlberg, J.; Furangen, A. *Chromatographia* **1987,** *24* , 783-789.

41. Weber, S. G. *Talanta,* **1989,** *36* , 99-106.

42. Weber, S. G.; Orr, J. D. *J. Chromatogr.* **1985,** *322*, 433-441.

43. Deelder, R. S.; vanden Berg, J. H. M. *J. Chromatogr.* **1981,** *218*, 327-339.

44. Rudzinski, W. G.; Bennett, D.; Garcia, V. *J. Liq. Chromatogr.* **1982,** *5*, 1295-1312.

45. Zhou, D.; Pietrzyk, D. J. *Anal. Chem.* **1992,** *64*, 1003-1008.

46. Stahlberg, J.; Almgren, M. *Anal. Chem.* **1989,** *61*, 1109-1112.

47. Krstulovic, A. M.; Brown, P. R. *Reversed-Phase High Performance Liquid Chromatography* ; Wiley: New York, 1982; Chapter 1.

48. ibid. Chapter 4.

49. Snyder, L. R.; Kirkland, J. J. *Introduction to Modern Liquid Chromatography* , 2nd ed.; Wiley: Toronto, 1979; Chapter 7.

50. Grushka, E.; Kikta, Jr., E. J. *Anal. Chem.* **1977,** *49*, 1004A-1014A.

51. Unger, K. K.; Becker, N.; Roumeliotis, P. *J. Chromatogr.* **1976,** *125*, 115-127.

52. Unger, K. K.; Roumeliotis, P. *J. Chromatogr.* **1978,** *149*, 211-224.

53. Berendsen, K. A.; Pikaart, K. A.; de Galan, L. *J. Liq. Chromatogr.* **1980,** *3*, 1437-1464.

54. Sokolowski, A.; Wahlund, K. G. *J. Chromatogr.* **1980,** *189*, 299-316.

55. Englehardt, H.; Ahr, G. *Chromatographia* **1981,** *14*, 227-233.

56. *Chromatography Product Guide,* Whatman, Inc.: Clifton, NJ, 1991, p.18.

57. Technical Bulletin, LC-111-6183; Whatman, Inc.: Clifton, NJ, 1985.

58. McNair, H. M.; Bonelli, E. J. *Basic Gas Chromatography*; Varian: California, 1969; pp. 64-68.

59. Schill, G. In *Ion Exchange and Solvent Extraction*, Marinsky, J. A.; Marcus, Y., Eds.; Marcel Dekker: New York, 1974; Vol. 6, Chapter 1.

60. Gustavii, K.; Schill, G. *Acta. Pharm. Suecica* **1966**, *3* , 241-258.

61. Karlberg, B.; Thelander, S. *Anal. Chim. Acta* **1978**, *98*, 1-7.

62. Bergamin, F. H.; Medeiros, J. X.; Reis, B. F.; Zagatto, E. A. G. *Anal. Chim. Acta* **1978**, *101*, 9-16.

63. Fossey, L.; Cantwell, F. F. *Anal. Chem.* **1982**, *54* , 1693-1697.

64. Lucy, C. A.; Cantwell, F. F. *Anal. Chem.* **1986**, *58* , 2727-2731.

65. Arvidsson, E.; Hackzell, L.; Schill, G.; Westerlund, D. *Chromatographia* **1988**, *25* , 430-436.

66. Nair, J. B.; Delaney, M. F.; Combs, K. J. *Anal. Letters* **1983**, *16* , 711-721.

67. Levin, S.; Grushka, E. *Anal. Chem.* **1985**, *57* , 1830-1835.

68. Parris, N. *Anal. Biochem.* **1979**, *100* , 260-263.

69. Barber, W. E.; Carr, P. W. *J. Chromatogr.* **1983**, *260* , 89-96.

70. Dorland, P.; Tod, M.; Postaire, E.; Pradeau, D. *J. Chromaatogr.* **1989**, *478* , 131-140.

71. Bidlingmeyer, B. A.; Santasania, C. T.; Warren, Jr., F. V. *Anal. Chem.* **1987**, *59*, 1843-1846.

72. Rigas, P. G.; Pietrzyk, D. J. *Anal. Chem.* **1986**, *58* , 2226-2233.

73. Michaelis, R.; Cassidy, R. M. *Adv. Ion Chromatogr.* **1990**, *2* , 21-43.

74. Herne, P.; Renson, M.; Crommen, J. *Chromatographia* **1984**, *19*, 274-279.

75. Parkin, J. E.; Lau, H. T. *J. Chromatogr.* **1984**, *314*, 488-494.

76. Parkin, J. E. *J. Chromatogr.* **1984**, *287*, 457-461.

77. Takeuchi, T.; Ishii. D. *J. Chromatogr.* **1987**, *393* , 419-425.

78. Gosselet, M.; Sebille, B. *J. Chromatogr.* **1991**, *552*, 563-573.

79. Banerjee, S. *Anal. Chem.* **1985**, *57*, 2590-2592.

80. Takeuchi, T.; Murase, K.; Ishii, D. *J. Chromatogr.* **1988**, *445*, 139-144.

81. Vigh, G.; Leitold, A. *J. Chromatogr.* **1984**, *312*, 345-356.

82. Fornstedt, T.; Westerlund, D.; Sokolowski, A. *J. Liq. Chromatogr.* **1988**, *11*, 2645-2684.

83. Johansson, M.; Westerlund, D. *J. Chromatogr.* **1988**, *452*, 241-255.

84. Yamamoto, A.; Matsunaga, A.; Ohto, M.; Mizukami, E.; Hayakawa, K.; Miyazaki, M. *J. Chromatogr.* **1989**, *482*, 145-154.

85. Golshanshirazi, S.; Guiochon, G. *J. Chromatogr.* **1989**, *461*, 1-18.

86. Golshanshirazi, S.; Guiochon, G. *J. Chromatogr.* **1989**, *461*, 19-34.

87. Levin, S.; Grushka, E. *Anal. Chem.* **1987**, *59*, 1157-1164.

88. Golshanshirazi, S.; Guiochon, G. *Anal. Chem.* **1989**, *61*, 2373-2380.

89. Golshanshirazi, S.; Guiochon, G. *Anal. Chem.* **1989**, *61*, 2380-2388.

90. Golshanshirazi, S.; Guiochon, G. *Anal. Chem.* **1989**, *62*, 923-932.

91. Fornstedt, T.; Westerlund, D. submitted for publication to *Journal of Chromatography*.

92. Gross, L.; Yeung, E. S. *J. Chromatogr.* **1989**, *480*, 169-178.

93. Garner, T. W.; Yeung, E. S. *J. Chromatogr.* **1990**, *515*, 639-644.

94. Takeuchi, T.; Yeung, E. S. *J. Chromatogr.* **1986**, *366*, 145-152.

95. Gross, L.; Yeung, E. S. *Anal. Chem.* **1990**, *62*, 427-431.

96. Rigas, P. G.; Pietrzyk, D. J. *Anal. Chem.* **1988**, *60*, 1650-1654.

97. Small, H.; Miller, Jr., T. E. *Anal. Chem.* **1982**, *54*, 462-469.

98. Walker, T. A. *J. Liq. Chromatogr.* **1988**, *11*, 1513-1530.

99. Jardy, A.; Caude, M.; Diop, A.; Curvale, C.; Rosset, R. *J. Chromatogr.* **1988**, *439*, 137-149.

100. Tanake, K.; Fritz, J. S. *J. Chromatogr.* **1987**, *409*, 271-279.

101. Arvidsson, E.; Crommen, J.; Schill, G.; Westerlund, D. *Chromatographia* **1987**, *24* , 460-468.

102. Arvidsson, E.; Crommen, J.; Schill, G.; Westerlund, D. *Chromatographia* **1988**, *26* , 45-52.

103. Maki, S. A.; Danielson, N. D. *J. Chromatogr.* **1991**, *542*, 101-113.

104. Miller, J. M. *Separation Methods in Chemical Analysis*; Wiley: Toronto, 1975; Chapter 5.

105. Snyder, L. R. *Principles of Adsorption Chromatography*; Marcel Dekker: New York, 1968; Chapter 3.

106. Conder, J. R.; Young, C. L. *Physicochemical Measurement by Gas Chromatography* ; Wiley: Toronto, 1979; Chapters 2, 9.

107. Karger, B. L.; Snyder, L. R.; Horvath, Cs.*An Introduction to Separation Science* ; Wiley: Toronto, 1973; Chapters 2, 5.

108. Helfferich, F. *J. Chem. Ed.* **1964**, *41*, 410-413.

109. Berthod, A.; Glick, M.; Winefordner, J. D. *J. Chromatogr.* **1990**, *502*, 305-315.

110. Bidlingmeyer, B. A.; Warren, Jr., F. V. *Anal. Chem.* **1982**, *54*, 2351-2356.

111. Rigas, P. G.; Pietrzyk, D. J. *Anal. Chem.* **1988**, *60*, 454-459.

112. Takeuchi, T.; Watanabe, S.; Murase, K.; Ishii, D. *Chromatographia* **1988**, *25*, 107-110.

113. Freiser, H.; Gnanasambandan, T. *Anal. Chem.* **1982**, *54*, 1282-1285.

114. Stranahan, J. J.; Deming, S. N. *Anal. Chem.* **1982**, *54*, 2251-2256.

115. McCormick, R. M.; Karger, B. L. *J. Chromatogr.* **1980**, *199*, 259-273.

116. Geng, X.; Regnier, F. E. *J. Chromatogr.* **1985**, *332*, 147-168.

117. Scott, R. P. W.; Simpson, C. F. *Faraday Symp. Chem. Soc.* **1980**, *15*, 69-82.

118. Bartha, A.; Vigh, Gy.; Billiet, H.; De Galan, L. *Chromatographia* **1985**, *20*, 587-590.

119. Tang, M.; Deming, S. N. *Anal. Chem.* **1983**, *55*, 425-428.

120. Bidlingmeyer, B.; Deming, S.; Price, W.; Sachok, B.; Petrusek, M. *J. Chromatogr.* **1979,** *186*, 419-434.

121. Stahlberg, J.; Almgren, M. *Anal. Chem.* **1985,** *57*, 817-821.

122. Carr, J. W.; Harris, J. M. *Anal. Chem.* **1986,** *58*, 626-631.

123. Michels, J. J.; Dorsey, J. G. *J. Chromatogr.* **1988,** *457*, 85-98.

124. Knox, J. H.; Hartwick, R. A. *J. Chromatogr.* **1981,** *204*, 3-21.

125. Glavina, L. L. M.; Cantwell, F. F. *Anal. Chem.* **1993,** *65*, 268-276.

126. Schoenmakers, P. J.; Billiet, H. A. H.; De Galan, L. *Chromatographia* **1982,** *15*, 205-214.

127. Cheong, W. J.; Carr, P. W. *Anal. Chem.* **1989,** *61*, 1524-1529.

128. Karger, B. L.; Snyder, L. R.; Horvath, Cs. *An Introduction to Separation Science*; Wiley: Toronto, 1973; pp. 49-55, 268-271.

129. Liu, H. Ph. D. Thesis, University of Alberta, 1988.

130. Scott, R. P. W.; Kucera, P. *J. Chromatogr.* **1979,** *175*, 51-63.

131. McCormick, R. M.; Karger, B. L. *Anal. Chem.* **1980,** *52*, 2249-2257.

132. Schoenmakers, P. J.; Billiet, H. A. H.; Tijssen, R.; De Galan, L. *J. Chromatogr.* **1978,** *149*, 519-537.

133. Schoenmakers, P. J.; Billiet, H. A. H.; De Galan, L. *J. Chromatogr.* **1983,** *282*, 107-121.

134. Barton, A. F. M. *CRC Handbook of Solubility Parameters and Other Cohesion Parameters*; CRC Press: Boca Raton, Florida, 1983; pp. 142-149.

135. Scott, R. P. W.; Simpson, C. F. *J. Chromatogr.* **1980,** *197*, 11-20.

136. Gilpin, R. K.; Gangoda, M. E. *Anal. Chem.* **1984,** *56*, 1470-1473.

137. Locke, D. C. *J. Chromatogr. Sci.* **1974,** *12*, 433-437.

138. Bedard, P. R.; Purdy, W. C. *J. Liq. Chrom.* **1985,** *8*, 2417-2443.

139. Yonker, C. R.; Zwier, T. A.; Burke, M. F. *J. Chromatogr.* **1982,** *241*, 257-268.

140. Hammers, W. E.; Meurs, G. J.; Deligny, C. L. *J. Chromatogr.* **1982**, *246*, 169-189.

141. Hammers, W. E.; Verschoor, P. B. A. *J. Chromatogr.* **1983**, *282*, 41-58.

142. Tilly-Melin, A.; Askemark, Y.; Wahlund, K.-G.; Schill, G. *Anal. Chem.* **1979**, *51*, 976-983.

143. Scott, R. P. W.; Kucera, P. *J. Chromatogr.* **1977**, *142*, 213-232.

144. Katz, E. D.; Ogan, K.; Scott, R. P. W. *J. Chromatogr.* **1986**, *352*, 67-90.

145. Sander, L. C.; Glinka, C. J.; Wise, S. A. *Anal. Chem.* **1990**, *62*, 1099-1101.

146. Berendsen, G. E.; DeGalan, L. *J. Chromatogr.* **1980**, *196*, 21-37.

147. Stineman, R. W. *Creative Comput.* **1980**, *6*, 54-57.

148. Karger, B. L.; LePage, J. N.; Tanaka, N. In *HPLC: Advances and Perspectives*; Horvath, C., Ed.; Academic Press: Toronto, 1980; pp. 113-206.

149. Hearn, M. T. M., Ed.; *Ion Pair Chromatography: Theory and Biological and Pharmaceutical Applications*; Marcel Dekker: New York, 1985.

150. Sorel, R. H. A.; Hulshoff, A. In *Advances in Chromatography*; Giddings, J. C.; Grushka, E.; Brown, P. R., Eds.; Marcel Dekker: New York, 1983; Vol. 21; pp. 87-129.

151. Deming, S. N. In *Handbook of HPLC for the Separation of Amino Acids, Peptides and Proteins*; Hancock, W. S., Ed.; CRC Press: Boca Raton, FL, 1984; Vol. 1; pp. 141-152.

152. Stahlberg, J.; Bartha, A. *J. Chromatogr.* **1988**, *456*, 253-265.

153. Sokolowski, A. *Chromatographia* **1986**, *22*, 168-176.

154. Crommen, J.; Herne, P. *J. Pharm. Biomed. Anal.* **1984**, *2*, 241-253.

155. Barber, W. E.; Carr, P. W. *J. Chromatogr.* **1984**, *301*, 25-38.

156. Grahame, D. C. *Chem. Rev.* **1947**, *41* , 441-501.

157. Bockris, J. O'M.; Reddy, A. K. N. *Modern Electrochemistry* ; Plenum: New York, 1970; Vol. 2; Chapter 7.

158. Conway, B. E. *Theory and Principles of Electrode Processes* ; Ronald Press Company: New York, 1965; Chapters 3, 5.

159. Boyd, G. E.; Schwarz, A.; Lindenbaum, S. *J. Phys. Chem.* **1966,** *70* , 821-825.

160. Kielland, J. *J. Am. Chem. Soc.* **1937,** *59* , 1675-1678.

161. Lindenbaum, S.; Boyd, G. E. *J. Phys. Chem.* **1964,** *68*, 911-917.

162. Horst, J.; Holl, W. H.; Eberle, S. H. *Reactive Polymers* **1990,** *13* , 209-231.

163. Holl, W. H.; Horst, J.; Wernet, M. *Reactive Polymers* **1991,** *14*, 251-261.

164. Holl, W. H.; Horst, J.; Franzreb, M. *Reactive Polymers* **1993,** *19*, 123-136.

165. Dandliker, W. B.; de Saussure, V. A. In *The Chemistry of Biosurfaces*; Hair, M. L., Ed.; Marcel Dekker: New York, 1971; Vol. 1; Chapter1.

166. Shaw, D. J. *Introduction to Colloid and Surface Chemistry*, 3rd. ed.; Butterworths: Toronto, 1980; p. 158.

167. Knox, J. H.; Kaliszan, R.; Kennedy, G. J. *Far. Symp. Chem. Soc.* **1981,** *15*, 1-13.

168. Share No. SDA 3094, IBM 360-365.

Appendix A

Tables and Figures for Chapter Four

In this appendix data which was presented in some of the figures in Chapter Four are tabulated. The corresponding figure in which the data were plotted is indicated in the tables. In addition, calibration curves not shown in Chapter Four are presented in this appendix.

Table A.1 GC calibration curve data for the determination of the holdup volumes for precolumns #1, #2 and #3. Experimental parameters are given in Table 2.4. The data are plotted in Figure A.1.

Volume of Water (mL)	$\frac{\text{P. H. Water}}{\text{P. H. Methanol}}$ (a)
0	0.028 ± 0.007
0.15	0.743 ± 0.002
0.20	1.001 ± 0.010
0.25	1.270 ± 0.009
0.30	1.519 ± 0.004

(a) Average and standard deviation of 4 replicate injections.

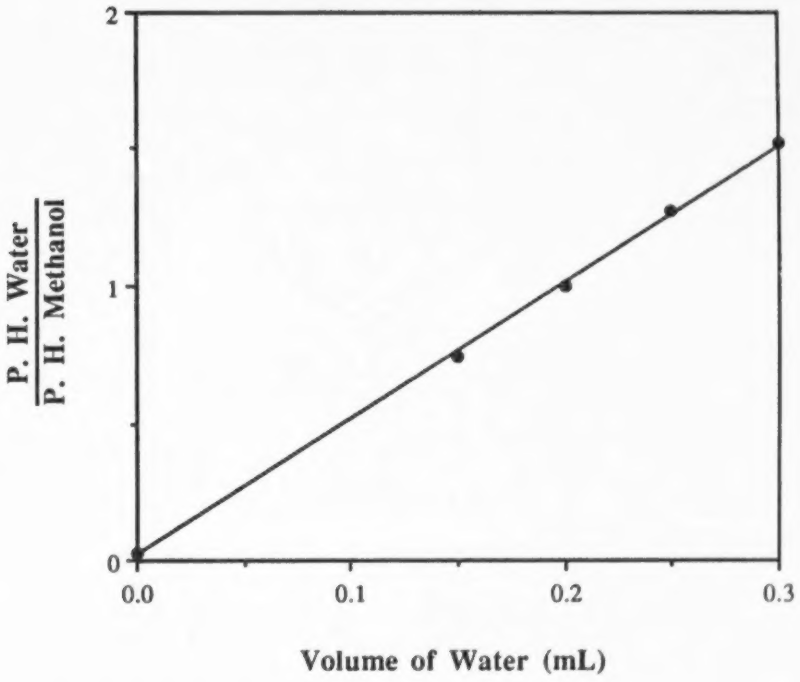

Figure A.1 GC calibration curve for the determination of the holdup volume for precolumns #1, #2 and #3. Methanol is an internal standard. The data are given in Table A.1. For the straight line the slope is 4.98 ± 0.07 $(\mathrm{mL})^{-1}$, the intercept is 0.0160 ± 0.0150 and the correlation coefficient is 0.999.

Table A.2 NS^- calibration curve data for the determination of the amount of NS^- sorbed on the precolumn. The NS^- absorbance at 276 nm was measured, A_{276}. The solvent was methanol:water (1:1 v/v). The data are plotted in Figure A.2.

$[NS^-] \times 10^4$ (mol/L)	A_{276} (A. U.)
0.0820	0.0390
0.164	0.0810
0.246	0.120
0.410	0.200
0.820	0.402
1.23	0.603
1.64	0.796
2.05	0.994

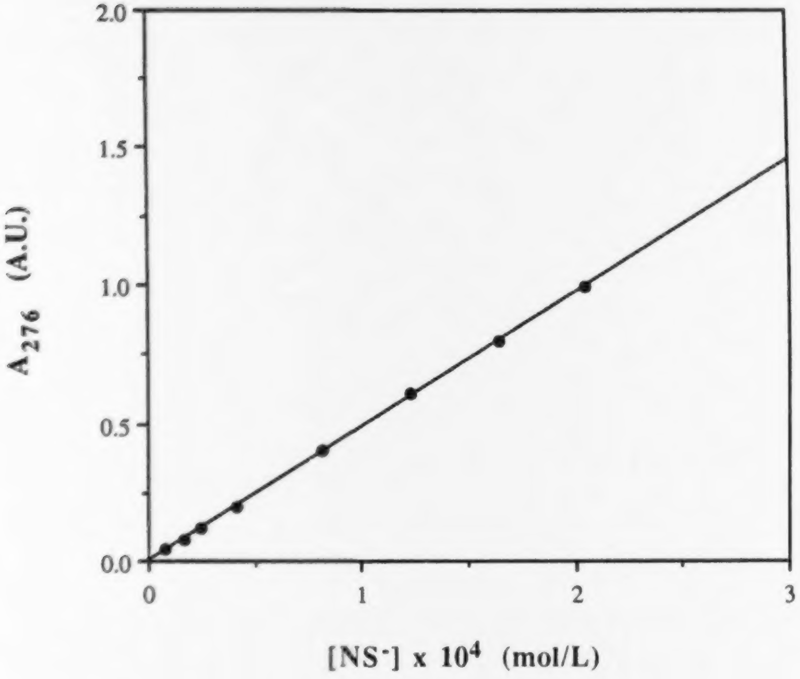

Figure A.2 NS⁻ calibration curve for the determination of the amount of NS⁻ sorbed on the precolumn. The NS⁻ absorbance was measured at 276 nm, A_{276}. The solvent was methanol:water (1:1 v/v). The data are given in Table A.2. For the straight line the slope is 4850 ± 10 A.U./(mol/L), the intercept is (1.39 ± 1.45) x 10^{-3} A.U and the correlation coefficient is 1.000.

Table A.3 NS$^-$ loading curve data for 1.01×10^{-4} mol/L NS$^-$ in pH 2 buffer pumped through precolumn #1 ($W_S = 0.1540$ g) for various volumes and at various flow rates. The data are plotted in Figure 4.1.

(a) 1.0 mL/min

Volume of Solution (mL)	$n_{NS} \times 10^6$ (mol)
4	0.383
6	0.593
8	0.785
10	0.910
12	0.974
15	1.04
20	1.10
30	1.15
40	1.16

(b) 2.0 mL/min

Volume of Solution (mL)	$n_{NS} \times 10^6$ (mol)
2	0.167
4	0.366
8	0.770
12	0.958
16	1.03
20	1.08
30	1.14
40	1.15

(c) 3.0 mL/min

Volume of Solution (mL)	$n_{NS} \times 10^6$ (mol)
3	0.263
6	0.562
9	0.838
15	1.01
21	1.08
30	1.12
36	1.14
45	1.16
60	1.13

Table A.4 NS^- loading curve data for 4.08×10^{-4} mol/L NS^- in pH 2 buffer pumped through precolumn #1 ($W_S = 0.1540$ g) for various volumes. The flow rate was 2.0 mL/min. The data are plotted in Figure 4.2.

Volume of Solution (mL)	$n_{NS} \times 10^6$ (mol)
16	2.75
20	2.77
24	2.77

Table A.5 NS^- elution data for a solution of 1.02×10^{-4} mol/L NS^- in pH 2 buffer loaded onto precolumn #1 ($W_S = 0.1540$ g) for a volume of 30 mL. The data are plotted in Figure 4.3. Experimental parameters are given in Figure 4.3.

Fraction	**A_{276} (A. U.)** (a)
1	0.580 ± 0.008
2	0.011 ± 0.001
3	0.002 ± 0.001

(a) Average and standard deviation of 3 runs.

Table A.6 NS^- and butanol loading curve data using precolumn #1 ($W_S = 0.1540$ g). The composition of the solution pumped through the precolumn for various volumes was 2.00×10^{-4} mol/L NS^- and 2.18×10^{-4} mol/L butanol in pH 2 buffer. The flow rate was 3.0 mL/min. The data are plotted in Figure 4.4.

Volume of Solution (mL)	$n_{NS} \times 10^6$ (mol)	$\frac{\text{P. H. BuOH}}{\text{P. H. PeOH}}$ (a)
15	1.29	
30	1.39	
45	1.43	
60	1.45	
90	1.47	
120	1.48	
180	1.49	0.208 ± 0.010
270	1.50	0.219 ± 0.008
360	1.51	0.212 ± 0.006

(a) Average and standard deviation of 4 replicate injections.

Table A.7 NS^- and butanol elution data using precolumn #1 ($W_S = 0.1540$ g). The solution composition is the same as in Table A.6. The solution was loaded onto precolumn #1 for a volume of 360 mL. The data are plotted in Figure 4.5.

Fraction	A_{276} (A. U.) (a)	$\frac{\text{P. H. BuOH}}{\text{P. H. PeOH}}$ (b)	
		Run 1	**Run 2**
1	0.694 ± 0.001	0.179 ± 0.009	0.188 ± 0.015
2	0.032 ± 0.001	0.006 ± 0.008	0.001 ± 0.008
3	0.010 ± 0.001	-0.004 ± 0.010	-0.003 ± 0.008
4	0.005 ± 0.001	-0.002 ± 0.009	-0.008 ± 0.008
5	0.003 ± 0.001	-0.006 ± 0.008	-0.009 ± 0.009

(a) Average and standard deviation of duplicate runs.

(b) Average and standard deviation of duplicate injections.

Table A.8 NS^- loading curve data with butanol present using precolumn #2 (W_S = 0.0871 g). The composition of the solution pumped through the precolumn for various volumes was 1.00×10^{-4} mol/L NS^- and 2.18×10^{-2} mol/L butanol in pH 2 buffer. The flow rate was 3.0 mL/min. The data are plotted in Figure 4.6.

Volume of Solution (mL)	$n_{NS} \times 10^7$ (mol)
15	5.12
45	5.41
90	5.45
180	5.63
270	5.54
360	5.79

Table A.9 NS^- elution data with butanol present using precolumn #2 ($W_S = 0.0871$ g). The solution composition is the same as in Table A.8. The solution was loaded onto precolumn #2 for 20 minutes at 3.0 mL/min and then 100 minutes at 1.0 mL/min (*i.e.* 360 mL). The data are plotted in Figure 4.7.

Fraction	**A_{276} (A. U.) [(a)]**
1	0.248 ± 0.003
2	0.006 ± 0.002
3	-0.002 ± 0.001
4	-0.002 ± 0.001
5	-0.002 ± 0.001

(a) Average and standard deviation of duplicate runs.

Table A.10 Butanol sorption isotherm data on Partisil-10 ODS-3 from pH 2 aqueous solutions. The data are plotted in Figure 4.8.

$C_{m,BuOH}$ (mol/L)	$n_{BuOH} \times 10^4$ (mol)	$C_{s,BuOH}$ (mol/kg)	$1/C_{m,BuOH}$ $(mol/L)^{-1}$	$1/C_{s,BuOH}$ $(mol/kg)^{-1}$
$2.18 \times 10^{-4(a)}$	0.00496	3.22×10^{-3}	4590	311
$5.45 \times 10^{-4(a)}$	0.0126	8.15×10^{-3}	1840	123
$2.18 \times 10^{-3(a)}$	0.0479	3.11×10^{-2}	459	32.2
$1.09 \times 10^{-2(a)}$	0.201	0.131	91.7	7.66
$2.18 \times 10^{-2(a)}$	0.366	0.237	45.9	4.21
$7.63 \times 10^{-2(b)}$	0.879	0.582	13.1	1.72
$0.109^{(b)}$	1.15	0.765	9.17	1.31
$0.218^{(b)}$	1.77	1.17	4.59	0.854
$0.327^{(b)}$	2.30	1.52	3.06	0.657
$0.545^{(b)}$	3.17	2.10	1.83	0.476
$0.654^{(b)}$	3.61	2.39	1.53	0.418

(a) Precolumn #1 was used. Amounts of butanol sorbed in column 2 were corrected to the original weight of packing in precolumn #1, Ws = 0.1540 g. The effective weight of packing used was 0.09849 g.

(b) Precolumn #3 was used. Amounts of butanol sorbed in column 2 were corrected to the original weight of packing in precolumn #3, Ws = 0.1510 g. The effective weight of packing used was 0.1025 g.

Table A.11 Butanol calibration curve data for the determination of the butanol sorption isotherm at low concentrations of butanol in the solution pumped through the precolumn (2.18×10^{-4} to 2.18×10^{-2} mol/L). The data are plotted in Figure A.3.

[BuOH] x 10^3 (mol/L)	**$\frac{\text{P. H. BuOH}}{\text{P. H. PeOH}}$ (a)**
0.765	0.374 ± 0.003
0.981	0.466 ± 0.006
2.94	1.485 ± 0.009
4.90	2.479 ± 0.003

(a) Average and standard deviation of four replicate injections.

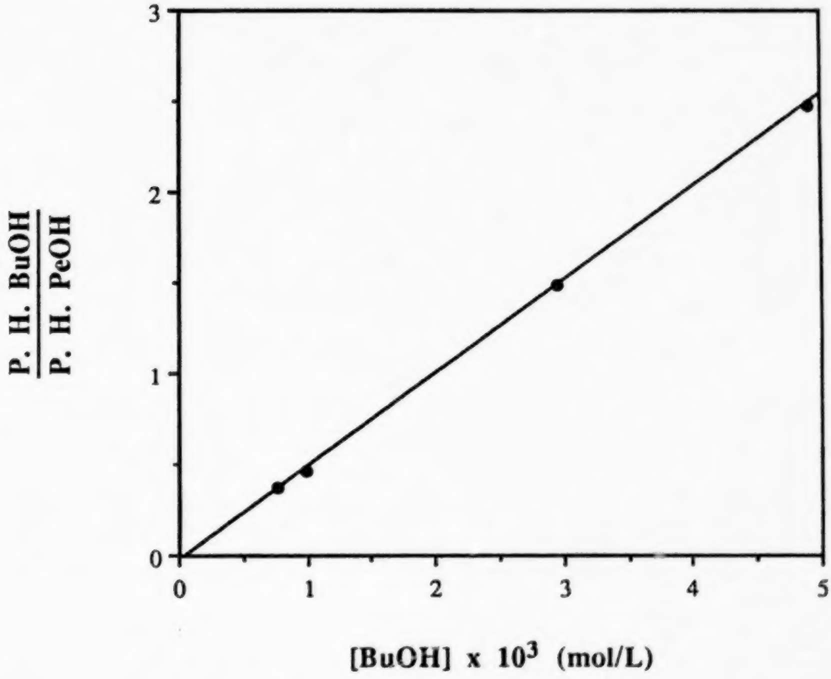

Figure A.3 Butanol calibration curve for the determination of the butanol sorption isotherm at low butanol concentrations in the solution pumped through the precolumn (2.18×10^{-4} to 2.18×10^{-2} mol/L). The data are given in Table A.11. For the straight line the slope is 511 ± 3 $(\text{mol/L})^{-1}$ and the intercept is -0.024 ± 0.009.

Table A.12 Butanol calibration curve data for the determination of the butanol sorption isotherm at high concentrations of butanol in the solution pumped through the precolumn (7.63×10^{-2} to 0.654 mol/L). The data are plotted in Figure A.4.

[BuOH] x 10^2 (mol/L)	$\frac{\text{P. H. BuOH}}{\text{P. H. PeOH}}$ [(a)]
0.763	0.639 ± 0.007
0.981	0.812 ± 0.001
1.09	0.912 ± 0.008
1.64	1.321 ± 0.001
2.18	1.738 ± 0.003
3.27	2.614 ± 0.030
6.54	5.064 ± 0.050

(a) Average and standard deviation of duplicate injections.

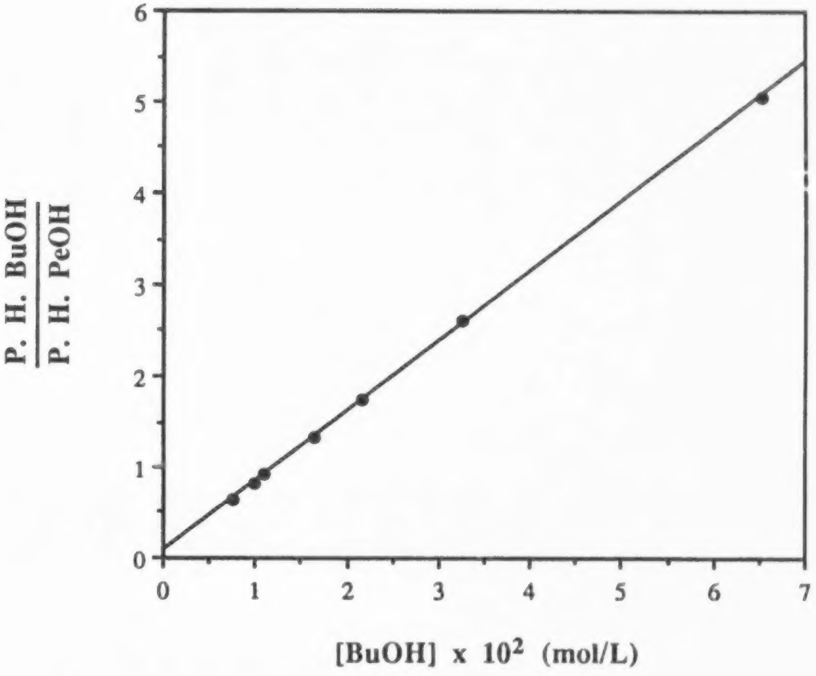

Figure A.4 Butanol calibration curve for the determination of the butanol sorption isotherm at high butanol concentrations in the solution pumped through the precolumn (7.63×10^{-2} to 0.654 mol/L). The data are given in Table A.12. For the straight line the slope is 76.6 ± 0.4 $(mol/L)^{-1}$ and the intercept is 0.070 ± 0.013.

Table A.13 Butanol calibration curve data for the determination of the amount of butanol sorbed on precolumn #3 in the study of the effect of butanol sample on NS$^-$ probe sorption at low concentrations of butanol in the solution pumped through the precolumn (2.18 x 10^{-4} to 1.09 x 10^{-3} mol/L). The data are plotted in Figure A.5.

[BuOH] x 10^4 (mol/L)	$\frac{\text{P. A. BuOH}}{\text{P. A. PeOH}}$
0	0
0.272	0.110
0.545	0.229
0.818	0.335
3.27	1.363

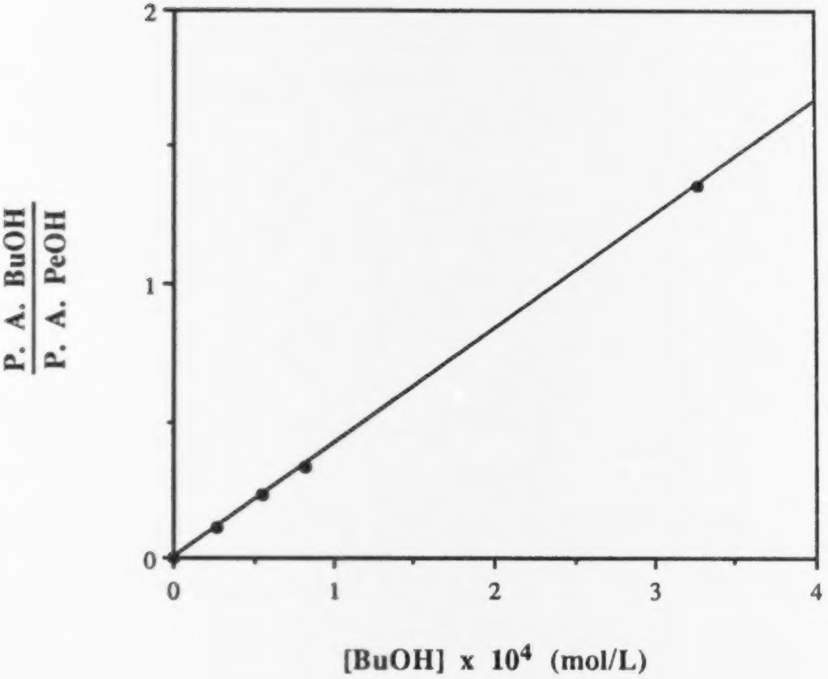

Figure A.5 Butanol calibration curve for the determination of the amount of butanol sorbed on precolumn #3 in the study of the effect of butanol sample on NS$^-$ probe sorption for the following range of butanol concentrations in solution: 2.18 x 10^{-4} to 1.09 x 10^{-3} mol/L. The data are given in Table A.13. For the straight line the slope is 4170 ± 10 (mol/L)$^{-1}$ and the intercept is -0.0019 ± 0.0021.

Table A.14 Butanol calibration curve data for the determination of the amount of butanol sorbed on precolumn #3 in the study of the effect of butanol sample on NS$^-$ probe sorption at high concentrations of butanol in the solution pumped through the precolumn (5.45×10^{-3} to 4.36×10^{-2} mol/L). The data are plotted in Figure A.6.

[BuOH] x 10^3 (mol/L)	$\frac{\text{P. A. BuOH}}{\text{P. A. PeOH}}$
0	0
0.981	0.287
2.83	0.853
5.45	1.526
7.63	2.122

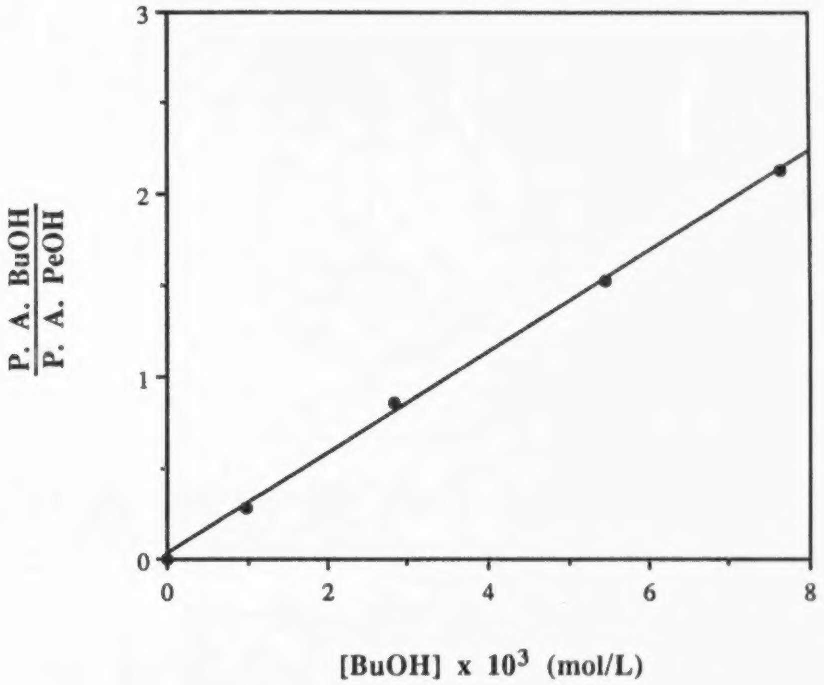

Figure A.6 Butanol calibration curve for the determination of the amount of butanol sorbed on precolumn #3 in the study of the effect of butanol sample on NS$^-$ probe sorption for the following range of butanol concentrations in solution: 5.45×10^{-3} to 4.36×10^{-2} mol/L. The data are given in Table A.14. For the straight line the slope is 277 ± 5 $(\mathrm{mol/L})^{-1}$ and the intercept is 0.022 ± 0.022.

Table A.15 NS^- sorption isotherm data on Partisil-10 ODS-3 from pH 2 aqueous solutions with 1.09×10^{-3} mol/L butanol present. The data are plotted in Figure 4.16.

$C_{m,NS}$ (mol/L)	$C_{s,NS}$ (mol/kg)	$1/C_{m,NS}$ (mol/L)$^{-1}$	$1/C_{s,NS}$ (mol/kg)$^{-1}$
5.00×10^{-5}	4.99×10^{-3}	20000	200
1.00×10^{-4}	8.46×10^{-3}	10000	118
2.00×10^{-4}	1.37×10^{-2}	5000	73.0
5.00×10^{-4}	2.40×10^{-2}	2000	41.7
1.00×10^{-3}	3.56×10^{-2}	1000	28.1
2.00×10^{-3}	5.38×10^{-2}	500	18.6
5.04×10^{-3}	8.46×10^{-2}	198	11.8
7.58×10^{-3}	0.104	132	9.57
1.01×10^{-2}	0.121	99.0	8.25
5.02×10^{-2}	0.278	19.9	3.60
9.99×10^{-2}	0.395	10.0	2.53
0.157	0.474	6.37	2.11

Table A.16 Solvent effect of butanol on NS$^-$ sorption using solubility parameter theory. Data are taken from Table 4.6. The data are plotted in Figure 4.18.

$C_{m,BuOH}$ (mol/L)	n_{NS} x 10^6 (mol)	ϕ_{BuOH} x 10^3	$K_{D,NS}$	ln $K_{D,NS}$
0	2.15	0	71.19	4.265
2.18 x 10^{-4}	2.07	0.0200	68.54	4.227
3.27 x 10^{-4}	2.13	0.0299	70.53	4.256
4.36 x 10^{-4}	2.12	0.0399	70.20	4.251
5.45 x 10^{-4}	2.12	0.0499	70.20	4.251
7.63 x 10^{-4}	2.11	0.0698	69.87	4.247
1.09 x 10^{-3}	2.11	0.0997	69.87	4.247
5.45 x 10^{-3}	1.96	0.499	64.90	4.173
1.09 x 10^{-2}	1.78	0.997	58.94	4.077
2.18 x 10^{-2}	1.59	2.00	52.65	3.964
3.27 x 10^{-2}	1.44	2.99	47.68	3.865
4.36 x 10^{-2}	1.32	3.99	43.71	3.778

Appendix B

Tables and Figures for Chapter Five

In this appendix data which was presented in some of the figures in Chapter Five are tabulated. The corresponding figure in which the data were plotted is indicated in the tables. In addition, calibration curves not shown in Chapter Five are presented in this appendix.

Table B.1 GC calibration curve data for the determination of the holdup volume of precolumn #4. Experimental parameters are given in Table 2.4. The data are plotted in Figure B.1.

Volume of Water (mL)	$\frac{\text{P. H. Water}}{\text{P. H. Methanol}}$ (a)
0	0.119 ± 0.015
0.020	0.308 ± 0.010
0.060	0.803 ± 0.012
0.080	1.087 ± 0.021
0.10	1.328 ± 0.007

(a) Average and standard deviation of 4 replicate injections.

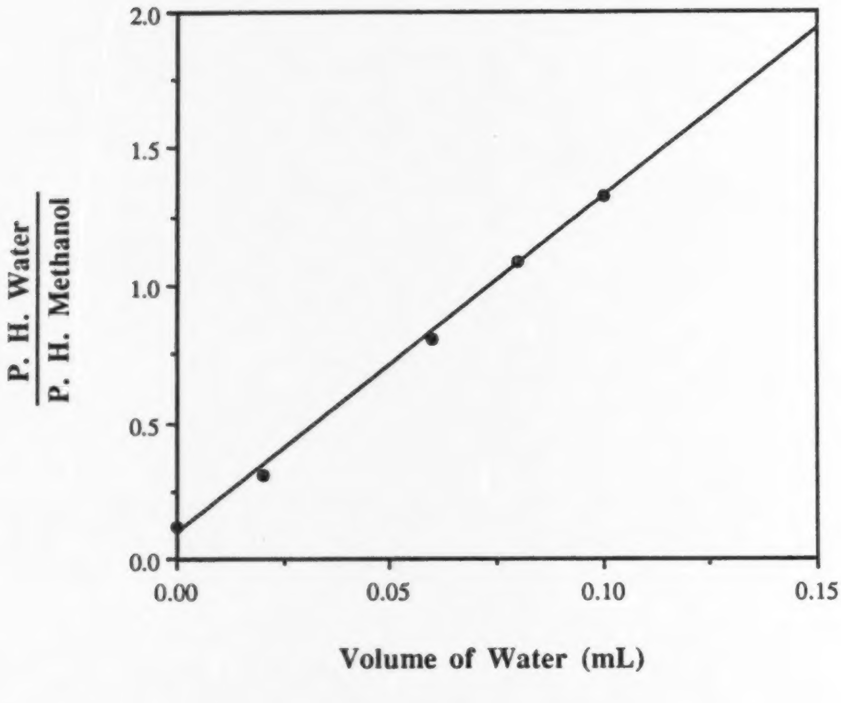

Figure B.1 GC calibration curve for the determination of the holdup volume of precolumn #4. Data are given in Table B.1.

Table B.2 NBTA$^+$ calibration curve data for the determination of the amount of NBTA$^+$ sorbed on precolumn #4. The NBTA$^+$ absorbance at 260 nm was measured, A_{260}. The solvent was methanol:water (1:1 v/v) containing 0.010 mol/L NaCl. The data are plotted in Figure B.2.

$[NBTA^+] \times 10^4$ (mol/L)	A_{260} (A.U.)
0.0419	0.0462
0.105	0.115
0.210	0.219
0.419	0.434
0.629	0.650
0.838	0.871
1.05	1.083

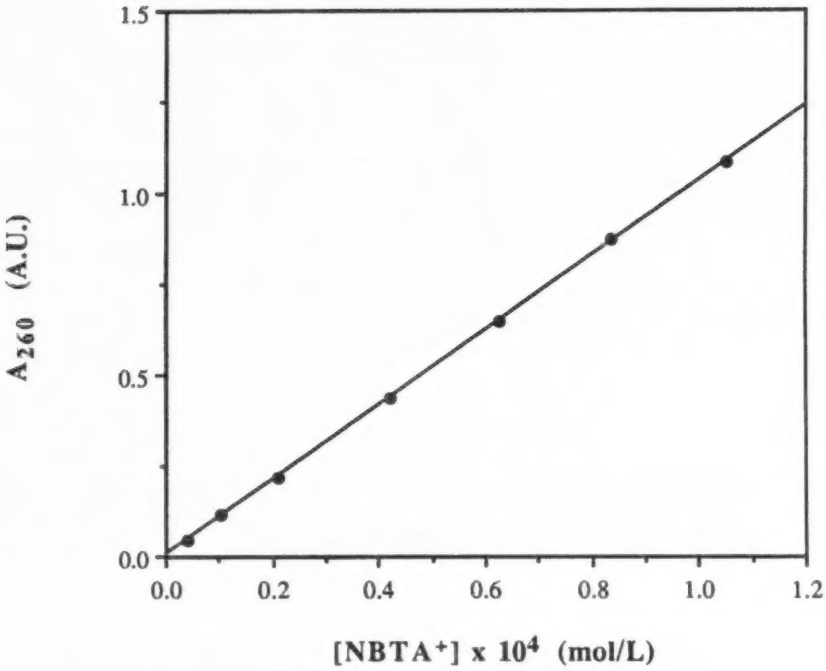

Figure B.2 NBTA$^+$ calibration curve for the determination of the amount of NBTA$^+$ sorbed on precolumn #4. The NBTA$^+$ absorbance was measured at 260 nm, A_{260}. The solvent was methanol:water (1:1 v/v) containing 0.010 mol/L NaCl. Data are given in Table B.2. For the straight line the correlation coefficient is 1.000, the slope is 10290 ± 30 A.U./(mol/L) and the intercept is $(4.07 \pm 1.71) \times 10^{-3}$ A.U.

Table B.3 NBTA$^+$ loading curve data for 1.97 x 10^{-4} mol/L NBTA$^+$ in 0.050 mol/L NaCl and pH 5 buffer pumped through precolumn #4 for various volumes. The flow rate was 2.0 mL/min. The data are plotted in Figure 5.3.

Volume of Solution (mL)	n_{NBTA} x 10^8 (mol)
2	8.46
10	9.09
30	9.72
60	9.32
120	9.44

Table B.4 $NBTA^+$ loading curve data for 2.09×10^{-4} mol/L $NBTA^+$ in 0.500 mol/L NaCl and pH 5 buffer pumped through precolumn #4 for various volumes. The flow rate was 2.0 mL/min. The data are plotted in Figure 5.4.

Volume of Solution (mL)	$n_{NBTA} \times 10^7$ (mol) [(a)]
2	1.55 ± 0.01
10	1.55 ± 0.01
30	1.57 ± 0.01
60	1.56 ± 0.01
120	1.57 ± 0.01

(a) Average and standard deviation of duplicate runs.

Table B.5 $NBTA^+$ elution data for the solution in Table B.3 loaded onto precolumn #4 for a volume of 60 mL. The eluent was methanol:water (1:1 v/v) containing 0.010 mol/L NaCl pumped at a flow rate of 1.0 mL/min. Each fraction represents 2 mL of eluent collected in a 10 mL volumetric flask and then diluted to volume with eluent. The data are plotted in Figure 5.5.

Fraction	A_{260} (A. U.) (a)
1	0.112 ± 0.001
2	0.002 ± 0.001
3	0.002 ± 0.001
4	0.001 ± 0.001
5	0.000 ± 0.001

(a) Average and standard deviation of duplicate runs.

Table B.6 NBTA$^+$ elution data for the solution in Table B.4 loaded onto precolumn #4 for a volume of 60 mL. The eluent and experimental parameters are the same as in Table B.5. The data are plotted in Figure 5.6.

Fraction	A_{260} (A. U.) (a)
1	0.178 ± 0.001
2	0.002 ± 0.001
3	0.000 ± 0.001
4	0.002 ± 0.001
5	0.001 ± 0.002

(a) Average and standard deviation of duplicate runs.

Table B.7 TBA^+ calibration curve data for the determination of the amount of TBA^+ sorbed on precolumn #4. The SE/FIA parameters were: chloroform flow rate, 1.4 mL/min; aqueous flow rate, 1.0 mL/min; chloroform flow rate through the membrane phase separator, 0.50 mL/min; and detection wavelength, 368 nm. The solvent was methanol:water (1:1 v/v) containing 0.010 mol/L NaCl. The data are plotted in Figure B.3.

$[TBA^+] \times 10^4$ (mol/L)	Peak Area $\times 10^{-7}$ (A.U.) $^{(a)}$
0.0473	0.119 ± 0.004
0.0946	0.242 ± 0.001
0.473	1.29 ± 0.01
0.946	2.66 ± 0.05
1.89	5.60 ± 0.12
2.84	8.16 ± 0.03

(a) Average and standard deviation of 5 replicate injections.

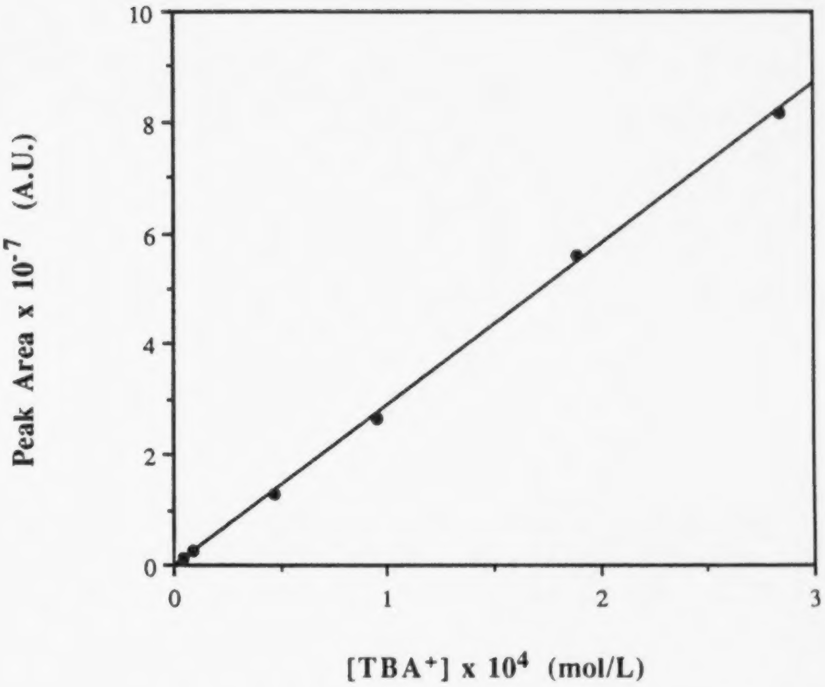

Figure B.3 TBA$^+$ calibration curve for the determination of the amount of TBA$^+$ sorbed on precolumn #4. Experimental parameters and data are given in Table B.7. For the straight line the correlation coefficient is 0.999, the slope is (2.91 ± 0.03) x 10^{11} A.U./(mol/L) and the intercept is (-3.96 ± 5.01) x 10^5 A.U.

Table B.8 NBTA$^+$ and TBA$^+$ loading curve data for a solution of 9.87 x 10^{-4} mol/L NBTA$^+$ and 1.00 x 10^{-5} mol/L TBA$^+$ in 0.050 mol/L NaCl and pH 5 buffer pumped through precolumn #4 for various volumes. The flow rate was 2.0 mL/min. The data are plotted in Figure 5.7.

Volume of Solution (mL)	n_{NBTA} x 10^7 (mol) [(a)]	n_{TBA} x 10^7 (mol) [(a)]
2	3.41 ± 0.03	0.880 ± 0.119
10	3.36 ± 0.01	1.18 ± 0.10
30	3.01 ± 0.08	3.22 ± 0.24
60	2.40 ± 0.03	5.85 ± 0.23
90	2.23 ± 0.01	6.66 ± 0.47
120	2.23	7.07
180	2.22	6.85
240	2.22	7.15

(a) Average and standard deviation for 3 runs. Where no standard deviation is reported, only a single run was done.

Table B.9 $NBTA^+$ and TBA^+ loading curve data for a solution of 9.31 x 10^{-4} mol/L $NBTA^+$ and 1.00 x 10^{-5} mol/L TBA^+ in 0.500 mol/L NaCl and pH 5 buffer pumped through precolumn #4 for various volumes. The flow rate was 2.0 mL/min. The data are plotted in Figure 5.8.

Volume of Solution (mL)	n_{NBTA} x 10^7 (mol)	n_{TBA} x 10^7 (mol)
2	5.96	0.872
10	5.79	1.19
30	5.54	2.86
60	5.18	5.57
90	4.34	10.8
120	4.22	11.6
180	4.36	11.5
240	4.33	11.5

Table B.10 NBTA$^+$ and TBA$^+$ elution data for the solution in Table B.8 loaded onto precolumn #4 for 150 mL. The eluent was methanol:water (1:1 v/v) containing 0.010 mol/L NaCl pumped at a flow rate of 1.0 mL/min. Each fraction represents 2 mL of eluent collected in a 25 mL volumetric flask and then diluted to volume with eluent. The data are plotted in Figure 5.9.

Fraction	**A_{260} (A. U.) (a)**	**Peak Area x 10^{-6} (A.U.) (a)**	**Peak Area x 10^{-6} (A.U.) (a) (b)**
1	0.125 ± 0.003	6.88 ± 0.04	6.26 ± 0.09
2	0.0001 ± 0.0004	0.512 ± 0.100	-0.111 ± 0.146
3	0.0006 ± 0.0001	0.558 ± 0.054	-0.065 ± 0.100
4	0.0001 ± 0.0001	0.528 ± 0.074	-0.095 ± 0.120
5	0.003 ± 0.004	0.567 ± 0.001	-0.056 ± 0.047

(a) Average and standard deviation of duplicate runs.

(b) Blank value was subtracted, (0.623 ± 0.046) x 10^6 A. U.

Table B.11 NBTA$^+$ and TBA$^+$ elution data for the solution in Table B.9 loaded onto precolumn #4 for 150 mL. The eluent and experimental parameters are the same as in Table B.10. The data are plotted in Figure 5.10.

Fraction	A_{260} (A. U.) (b)	Peak Area x 10^{-6} (A.U.) (a)	Peak Area x 10^{-6} (A.U.) (a) (b)
1	0.207	13.1 ± 1.2	12.6 ± 1.3
2	-0.001	0.523 ± 0.043	0.018 ± 0.100
3	0.001	0.502 ± 0.044	-0.003 ± 0.101
4	-0.002	0.510 ± 0.079	0.005 ± 0.136
5	0.001	0.471 ± 0.085	-0.034 ± 0.142

(a) Average and standard deviation of 4 replicate injections.

(b) Blank value was subtracted, (0.505 ± 0.057) x 10^6 A. U.

Table B.12 NBTA⁺ sorption isotherm data on Partisil-10 ODS-3 from pH 5 aqueous solutions at five different concentrations of NaCl in solution. The data are plotted in Figure 5.11.

[NaCl] (mol/L)	$C_{m,NBTA}$ x 10^2 (mol/L)	n_{NBTA} x 10^6 (mol) (a)	Γ_{NBTA} x 10^{11} (mol/cm^2) (a)
0.050	0.197	0.621 ± 0.008	0.601 ± 0.008
	0.494	1.15 ± 0.02	1.11 ± 0.02
	1.04	1.86 ± 0.01	1.80 ± 0.01
	1.55	2.36 ± 0.05	2.28 ± 0.05
	2.07	2.90 ± 0.04	2.81 ± 0.04
0.070	0.186	0.694 ± 0.006	0.672 ± 0.006
	0.465	1.28 ± 0.01	1.24 ± 0.01
	0.931	1.99 ± 0.01	1.93 ± 0.01
	1.40	2.54 ± 0.08	2.46 ± 0.08
	1.86	3.07 ± 0.07	2.97 ± 0.07
0.100	0.186	0.754 ± 0.004	0.730 ± 0.004
	0.465	1.41 ± 0.01	1.36 ± 0.01
	0.931	2.21 ± 0.01	2.14 ± 0.01
	1.40	2.83 ± 0.04	2.74 ± 0.04
	1.86	3.48 ± 0.08	3.37 ± 0.08
0.300	0.186	0.957 ± 0.007	0.926 ± 0.007
	0.465	1.94 ± 0.01	1.88 ± 0.01
	0.931	3.16 ± 0.01	3.06 ± 0.01
	1.40	4.12 ± 0.10	3.99 ± 0.10
	1.86	4.94 ± 0.11	4.78 ± 0.11
0.500	0.197	1.14 ± 0.01	1.10 ± 0.01
	0.352	1.81 ± 0.02	1.75 ± 0.02
	1.04	3.94 ± 0.03	3.81 ± 0.03
	1.39	4.72 ± 0.02	4.57 ± 0.02
	2.07	5.85 ± 0.05	5.66 ± 0.05

(a) Average and standard deviation of three column equilibration experiments.

Table B.13 Data for plot of σ_0^{-1} *versus* $c^{-1/2}[(ZF\Psi_{OHP}/2RT)^{-1}\sinh(ZF\Psi_{OHP}/2RT)]^{-1}$ for five constant activities of NBTA$^+$. The data are plotted in Figure 5.12.

$a_{NBTA} \times 10^3$ (mol/L)	c (mol/L)	γ_{NBTA}	$C_{m,NBTA} \times 10^2$ (mol/L)	$\Gamma_{NBTA} \times 10^{11}$ (mol/cm^2)	$\sigma_0 \times 10^6$ (Coulomb/cm^2)	$\Psi_{OHP} \times 10^3$ (V)	U* [(a)]
2.00	0.0526	0.804	0.249	0.706	0.696	13.1	0.989
	0.0727	0.780	0.256	0.834	0.817	13.1	0.989
	0.103	0.730	0.274	0.950	0.927	12.5	0.990
	0.304	0.585	0.342	1.44	1.39	11.0	0.992
	0.500	0.513	0.390	1.88	1.82	11.2	0.992
4.00	0.0551	0.801	0.499	1.11	1.11	20.2	0.975
	0.0752	0.778	0.514	1.30	1.29	20.1	0.975
	0.106	0.728	0.550	1.50	1.48	19.5	0.976
	0.307	0.583	0.686	2.51	2.44	18.9	0.978
	0.508	0.509	0.786	3.21	3.12	18.7	0.978
6.00	0.0576	0.798	0.752	1.45	1.47	25.8	0.959
	0.0778	0.775	0.774	1.70	1.70	25.6	0.960
	0.108	0.726	0.826	1.97	1.96	25.1	0.961
	0.310	0.583	1.03	3.34	3.26	24.7	0.963
	0.512	0.508	1.18	4.18	4.07	24.0	0.965
8.00	0.0602	0.794	1.01	1.75	1.80	30.3	0.944
	0.0805	0.772	1.04	2.04	2.07	30.2	0.945
	0.111	0.720	1.11	2.39	2.39	29.8	0.946
	0.314	0.581	1.38	4.00	3.92	29.1	0.949
	0.516	0.507	1.58	4.92	4.80	27.9	0.953
10.0	0.0627	0.791	1.26	2.03	2.10	34.2	0.930
	0.0831	0.770	1.30	2.36	2.41	34.1	0.930
	0.114	0.716	1.40	2.78	2.80	33.8	0.931
	0.317	0.579	1.73	4.55	4.47	32.6	0.936
	0.520	0.505	1.98	5.52	5.40	30.9	0.942

[(a)] $U^* = [(ZF\Psi_{OHP}/2RT)\sinh(ZF\Psi_{OHP}/2RT)]^{-1}$

Table B.14 Sorption data for $NBTA^+$ and TBA^+ on Partisil-10 ODS-3 from pH 5 aqueous solutions at five concentrations of NaCl in solution. The concentration of $NBTA^+$ was kept constant at 1.86 x 10^{-3} mol/L. The data are plotted in Figure 5.13.

[NaCl] (mol/L)	$C_{m,TBA}$ x 10^4 (mol/L)	n_{NBTA} x 10^7 (mol) (a)	n_{TBA} x 10^7 (mol) (a)	Γ_{NBTA} x 10^{12} (mol/cm^2)	Γ_{TBA} x 10^{12} (mol/cm^2)	Γ_+ x 10^{12} (mol/cm^2)
0.050	0.0477	5.18	4.58	5.02	4.43	9.45
	0.0954	4.76	6.27	4.61	6.07	10.7
	0.477	3.46	13.4	3.35	13.0	16.4
	0.954	2.89	17.3	2.80	16.8	19.6
	4.77	1.93	28.8	1.87	27.9	29.8
0.070	0.0477	5.77	5.07	5.59	4.90	10.5
	0.0954	5.33	6.95	5.16	6.73	11.9
	0.477	3.93	14.1	3.80	13.6	17.4
	0.954	3.33	18.6	3.22	18.0	21.2
	4.77	2.19	30.3	2.12	29.4	31.5
0.100	0.0477	5.94 ± 0.03	5.24 + 0.07	5.74 ± 0.03	5.07 ± 0.07	10.8 ± 0.1
	0.0954	5.56 ± 0.04	7.90 ± 0.13	5.38 ± 0.01	7.64 ± 0.13	13.0 ± 0.1
	0.477	4.12 ± 0.03	16.4 ± 0.1	3.99 ± 0.01	15.9 ± 0.1	19.9 ± 0.1
	0.954	3.55 ± 0.02	20.1 ± 0.1	3.43 ± 0.02	19.5 ± 0.1	22.9 ± 0.1
	4.77	2.38 ± 0.04	31.3 ± 0.1	2.31 ± 0.04	30.3 ± 0.1	32.6 ± 0.1
0.300	0.0477	7.97 ± 0.01	6.80 ± 0.04	7.71 ± 0.01	6.58 ± 0.04	14.3 ± 0.1
	0.0954	7.54 ± 0.02	9.30 ± 0.25	7.30 ± 0.02	9.00 ± 0.25	16.3 ± 0.3
	0.477	5.87 ± 0.02	16.3 ± 0.1	5.68 ± 0.02	15.8 ± 0.1	21.5 ± 0.1
	0.954	5.21 ± 0.07	24.6 ± 0.1	5.04 ± 0.07	23.8 ± 0.1	28.8 ± 0.2
	4.77	3.65 ± 0.05	36.5 ± 0.1	3.54 ± 0.05	35.4 ± 0.1	38.9 + 0.2
0.500	0.0477	9.05 ± 0.04	8.02 ± 0.15	8.76 ± 0.04	7.76 ± 0.15	16.5 ± 0.2
	0.0954	8.43 ± 0.11	9.89 ± 0.01	8.16 ± 0.11	9.57 ± 0.01	17.7 + 0.1
	0.477	6.68 ± 0.02	19.8 ± 0.1	6.47 ± 0.02	19.2 ± 0.1	25.7 ± 0.1
	0.954	5.98 ± 0.08	26.0 ± 0.1	5.79 ± 0.08	25.2 ± 0.1	31.0 ± 0.2
	4.77	4.24 ± 0.01	42.3 ± 0.1	4.10 ± 0.01	41.0 ± 0.1	45.1 ± 0.1

(a) Average and standard deviation of duplicate column equilibration experiments. Where no standard deviation is given, the duplicate run was discarded.

Table B.15 Data for plot of σ_T^{-1} *versus* $c^{-1/2}$ $[(ZF\Psi_{OHP}/2RT)^{-1} \sinh (ZF\Psi_{OHP}/2RT)]^{-1}$ for NBTA$^+$ and TBA$^+$ at a constant NBTA$^+$ activity = 1.50 x 10^{-3} mol/L and a constant TBA$^+$ activity = 3.84 x 10^{-6} mol/L. Data are plotted in Figure 5.14.

c (mol/L)	$C_{m,TBA}$ x 10^6 (mol/L)	Γ_+ x 10^{11} (mol/cm^2)$^{(a)}$	$C_{m,NBTA}$ x 10^3 (mol/L)	Γ_{NBTA} x 10^{12} (mol/cm^2)	Ratio	$\Delta\Gamma_{NBTA}$ x 10^{11} (mol/cm^2)	Γ_+ x 10^{11} (mol/cm^2)$^{(b)}$	σ_T x 10^6 (Coulomb /cm^2)	Ψ_{OHP} (mV)	U*(c)
0.05	4.77	0.920	1.86	5.02	-	0	0.920	0.902	17.3	0.981
0.07	4.90	1.03	1.91	5.57	1.02	0.01	1.04	1.02	16.5	0.983
0.10	5.11	1.12	2.04	5.69	1.06	0.04	1.16	1.13	15.4	0.985
0.30	5.73	1.48	2.55	7.57	1.25	0.19	1.67	1.62	12.8	0.990
0.50	6.03	1.66	2.92	8.54	1.37	0.32	1.98	1.92	11.8	0.991

(a) Constant a_{TBA} (see Appendix C)

(b) Constant a_{TBA} and a_{NBTA} (see Appendix C)

(c) $U^* = [(ZF\Psi_{OHP}/2RT) \sinh (ZF\Psi_{OHP}/2RT)]^{-1}$

Table B.16 Data for plot of σ_T^{-1} *versus* $c^{-1/2}$ $[(ZF\Psi_{OHP}/2RT)^{-1} \sinh (ZF\Psi_{OHP}/2RT)]^{-1}$ for $NBTA^+$ and TBA^+ at a constant $NBTA^+$ activity = 1.50 x 10^{-3} mol/L and a constant TBA^+ activity = 7.68 x 10^{-6} mol/L. Data are plotted in Figure 5.14.

c (mol/L)	$C_{m,TBA}$ x 10^5 (mol/L)	Γ_+ x 10^{11} (mol/cm^2)$^{(a)}$	$C_{m,NBTA}$ x 10^3 (mol/L)	Γ_{NBTA} x 10^{12} (mol/cm^2)	Ratio	$\Delta\Gamma_{NBTA}$ x 10^{11} (mol/cm^2)	Γ_+ x 10^{11} (mol/cm^2)$^{(b)}$	σ_T x 10^6 (Coulomb /cm^2)	Ψ_{OHP} (mV)	$U^{*(c)}$
0.05	0.954	1.10	1.86	4.61	-	0	1.10	1.07	20.5	0.974
0.07	0.981	1.22	1.91	5.14	1.02	0.01	1.23	1.20	19.4	0.977
0.10	1.02	1.32	2.04	5.34	1.06	0.03	1.35	1.33	18.0	0.980
0.30	1.15	1.73	2.55	7.16	1.25	0.18	1.91	1.85	14.6	0.986
0.50	1.21	1.94	2.92	7.99	1.37	0.30	2.24	2.17	13.3	0.989

(a) Constant a_{TBA} (see Appendix C)

(b) Constant a_{TBA} and a_{NBTA} (see Appendix C)

(c) $U^* = [(ZF\Psi_{OHP}/2RT) \sinh (ZF\Psi_{OHP}/2RT)]^{-1}$

Table B.17 Data for plot of σ_T^{-1} *versus* $c^{-1/2}$ $[(ZF\Psi_{OHP}/2RT)^{-1} \sinh (ZF\Psi_{OHP}/2RT)]^{-1}$ for $NBTA^+$ and TBA^+ at a constant $NBTA^+$ activity = 1.50×10^{-3} mol/L and a constant TBA^+ activity = 3.84×10^{-5} mol/L. Data are plotted in Figure 5.14.

c (mol/L)	$C_{m,TBA}$ x 10^5 (mol/L)	Γ_+ x 10^{11} (mol/cm^2)(a)	$C_{m,NBTA}$ x 10^3 (mol/L)	Γ_{NBTA} x 10^{12} (mol/cm^2)	Ratio	$\Delta\Gamma_{NBTA}$ x 10^{11} (mol/cm^2)	Γ_+ x 10^{11} (mol/cm^2)(b)	σ_T x 10^6 (Coulomb /cm^2)	Ψ_{OHP} (mV)	U*(c)
0.05	4.77	1.65	1.86	3.35	-	0	1.65	1.61	29.8	0.946
0.07	4.90	1.80	1.91	3.78	1.02	0.01	1.81	1.81	27.8	0.953
0.10	5.11	1.95	2.04	3.92	1.06	0.03	1.98	1.98	25.6	0.960
0.30	5.73	2.48	2.55	5.51	1.25	0.14	2.62	2.62	19.8	0.975
0.50	6.03	2.79	2.92	6.19	1.37	0.23	3.02	3.02	17.7	0.981

(a) Constant a_{TBA} (see Appendix C)

(b) Constant a_{TBA} and a_{NBTA} (see Appendix C)

(c) $U^* = [(ZF\Psi_{OHP}/2RT) \sinh (ZF\Psi_{OHP}/2RT)]^{-1}$

Table B.18 Data for plot of σ_T^{-1} *versus* $c^{-1/2}$ $[(ZF\Psi_{OHP}/2RT)^{-1} \sinh (ZF\Psi_{OHP}/2RT)]^{-1}$ for $NBTA^+$ and TBA^+ at a constant $NBTA^+$ activity = 1.50 x 10^{-3} mol/L and a constant TBA^+ activity = 7.68 x 10^{-5} mol/L. Data are plotted in Figure 5.14.

c (mol/L)	$C_{m,TBA}$ x 10^4 (mol/L)	Γ_+ x 10^{11} (mol/cm^2)(a)	$C_{m,NBTA}$ x 10^3 (mol/L)	Γ_{NBTA} x 10^{12} (mol/cm^2)	Ratio	$\Delta\Gamma_{NBTA}$ x 10^{11} (mol/cm^2)	Γ_+ x 10^{11} (mol/cm^2)(b)	σ_T x 10^6 ($Coulomb/cm^2$)	Ψ_{OHP} (mV)	U*(c)
0.05	0.954	1.96	1.86	2.80	-	0	1.96	1.92	34.8	0.927
0.07	0.981	2.12	1.91	3.21	1.02	0.01	2.13	2.08	32.2	0.937
0.10	1.02	2.30	2.04	3.39	1.06	0.02	2.32	2.26	29.7	0.946
0.30	1.15	2.90	2.55	4.88	1.25	0.12	3.02	2.92	22.6	0.968
0.50	1.21	3.26	2.92	5.56	1.37	0.21	3.47	3.35	20.2	0.974

(a) Constant a_{TBA} (see Appendix C)

(b) Constant a_{TBA} and a_{NBTA} (see Appendix C)

(c) $U^* = [(ZF\Psi_{OHP}/2RT) \sinh (ZF\Psi_{OHP}/2RT)]^{-1}$

Table B.19 Data for plot of σ_T^{-1} *versus* $c^{-1/2}$ $[(ZF\Psi_{OHP}/2RT)^{-1} \sinh (ZF\Psi_{OHP}/2RT)]^{-1}$ for NBTA$^+$ and TBA$^+$ at a constant NBTA$^+$ activity = 1.50 x 10^{-3} mol/L and a constant TBA$^+$ activity = 3.84 x 10^{-4} mol/L. Data are plotted in Figure 5.14.

c (mol/L)	$C_{m,TBA}$ x 10^4 (mol/L)	Γ_+ x 10^{11} (mol/cm^2)(a)	$C_{m,NBTA}$ x 10^3 (mol/L)	Γ_{NBTA} x 10^{12} (mol/cm^2)	Ratio	$\Delta\Gamma_{NBTA}$ x 10^{11} (mol/cm^2)	Γ_+ x 10^{11} (mol/cm^2)(b)	σ_T x 10^6 (Coulomb /cm^2)	Ψ_{OHP} (mV)	U*(c)
0.05	4.77	2.94	1.86	1.87	-	0	2.95	2.88	48.8	0.864
0.07	4.90	3.13	1.91	2.11	1.02	0.01	3.14	3.06	44.8	0.883
0.10	5.11	3.40	2.04	2.28	1.06	0.01	3.41	3.32	41.3	0.900
0.30	5.73	4.14	2.55	3.38	1.25	0.09	4.23	4.09	30.8	0.942
0.50	6.03	4.67	2.92	3.83	1.37	0.14	4.81	4.66	27.5	0.954

(a) Constant a_{TBA} (see Appendix C)

(b) Constant a_{TBA} and a_{NBTA} (see Appendix C)

(a) $U^* = [(ZF\Psi_{OHP}/2RT) \sinh (ZF\Psi_{OHP}/2RT)]^{-1}$

Table B.20 Data for plots in Figures 5.18 and 5.19. The values for the following parameters were used: $C_{m,NBTA} = 1.86 \times 10^{-3}$ mol/L and $A_T = 1.03 \times 10^5$ cm^2. The following values were from previous tables: $n_{NBTA,ADS}$ came from column 7 of Table 5.3, $n_{TBA,ADS}$ came from column 8 of Table 5.3, Ψ_I came from column 6 of Table 5.6 and $\overline{A}'_{TBA}$ came from column 2 in Table 5.8.

c (mol/L)	γ_{NBTA}	$n_{NBTA,ADS}$ x 10^6 (mol)	$\frac{n_{NBTA,ADS}}{A_S C_{m,NBTA} \gamma_{NBTA}}$ x 10^9 (L/cm^2) (a)	$\exp\left(-\frac{ZF\Psi_I}{RT}\right)$
0.050	0.805	0.534	3.23	0.509
		0.494	2.89	0.449
		0.369	1.95	0.311
		0.315	1.58	0.256
		0.225	0.988	0.148
0.070	0.783	0.598	3.81	0.525
		0.555	3.46	0.470
		0.416	2.44	0.338
		0.359	2.03	0.283
		0.249	1.29	0.173
0.100	0.733	0.636	4.38	0.548
		0.599	4.07	0.495
		0.447	2.90	0.367
		0.390	2.48	0.312
		0.273	1.63	0.173
0.300	0.587	0.986	8.94	0.604
		0.934	8.53	0.563
		0.722	6.75	0.459
		0.642	6.08	0.410
		0.450	4.43	0.295
0.500	0.513	1.22	12.9	0.630
		1.14	12.2	0.593
		0.886	9.95	0.496
		0.798	9.19	0.449
		0.554	6.92	0.336

(a) $A_S = A_T - \overline{A}'_{TBA} \cdot n_{TBA,ADS}$

Appendix C

Calculation of Γ_+

Experimentally, it is a relatively simple matter to measure Γ_{TBA}, Γ_{NBTA} and Γ_+ under conditions where the concentrations [TBA$^+$] and/or [NBTA$^+$] are held constant while the ionic strength is varied by changing the concentration of NaCl. However, in order to utilize equation 5.25 to obtain Ψ_0 and C_1 it is necessary to employ values of surface excess that prevail at constant *activities*, a_{TBA} and/or a_{NBTA}, while the ionic strength is varied. A problem arises from the fact that activity coefficients change with ionic strength so that the *same activity* corresponds to *different concentrations* of PDI at different ionic strengths. An unattractive way of meeting this constant activity criterion would be to measure surface excesses at a much larger number of concentrations of PDI. However, when there is only one type of PDI present, such as NBTA$^+$ alone, it is easier to fit a curve to the sorption isotherm, as in Figure 5.11. Each isotherm corresponds to a different ionic strength. It is then a simple matter to interpolate between the experimental points on each isotherm to obtain values of surface excess at the concentrations of PDI which correspond to the same activity at each ionic strength.

The problem is more formidable when there are two different PDIs present, such as NBTA$^+$ and TBA$^+$, and when it is desired to vary their activities independently of one another and to evaluate Γ_+ at several ionic strengths with both a_{NBTA} and a_{TBA} held constant. One approach to this problem would be to vary the solution concentrations of both TBA$^+$ and NBTA$^+$ in the mixture and to plot curves of Γ_+ *versus* [TBA$^+$] using one curve for each combination of [NBTA$^+$] and ionic strength. The number of curves required would be the number of curves that presently appear in Figure 5.13 times the number of different concentrations of [NBTA$^+$] that it is necessary to use. Then, in order to find the value of Γ_+ corresponding to a given combination of a_{TBA}, a_{NBTA} and ionic strength for use with equation 5.25, it would be possible, first, to interpolate within a given curve in the set of curves of Γ_+ *versus* [TBA$^+$] at a given combination of [NBTA$^+$] and ionic strength; and then to interpolate *between* the curves in that set which have the same ionic strength but different [NBTA$^+$]. The number of experiments required to generate such a large number of curves is unattractive. Therefore an alternative approach has been taken in the present thesis.

In this study [NBTA$^+$] has been held constant throughout all of the experiments in which both NBTA$^+$ and TBA$^+$ are present. The following steps have been used to calculate Γ_+ at any combination of constant a_{NBTA} and a_{TBA}:

(i) At a constant a_{TBA}, values of Γ_+ are first interpolated from each of the five curves in Figure 5.13 as if only one PDI (*i.e.* TBA$^+$) is present. Since [NBTA$^+$] is the same for all of these measurements but the ionic strength varies among the curves, the value of a_{NBTA} will not have been constant among this set of measurements, even though a_{TBA} is constant. The interpolation just described yields the correct values for Γ_{TBA} corresponding to the selected a_{TBA}. However, the values of Γ_{NBTA} obtained are not the desired ones because they correspond to several different values of a_{NBTA}. Thus the measured value of Γ_+, which is the sum of Γ_{TBA} and Γ_{NBTA}, is not accurate because Γ_{NBTA} is not accurate.

(ii) For each point described above, an estimate is made of the *difference*, $\Delta\Gamma_{NBTA}$, between the value of Γ_{NBTA} obtained and the value of Γ_{NBTA} that would have been obtained if a_{NBTA} had been at the value of interest. To calculate each $\Delta\Gamma_{NBTA}$ the following steps are performed: (a) The concentration, [NBTA$^+$]$_2$, which would be needed to give the desired a_{NBTA} at a particular ionic strength is calculated from the expression [NBTA$^+$]$_2$ = $a_{NBTA}\cdot(\gamma_{NBTA})^{-1}$. (b) From the isotherm measured for NBTA$^+$ alone at the appropriate ionic strength (see Figure 5.11) the following ratio is calculated:

$$f = \frac{\Gamma_{NBTA,2}}{\Gamma_{NBTA,1}} \qquad (C.1)$$

where $\Gamma_{NBTA,1}$ is the surface excess of $NBTA^+$ sorbed at the concentration $[NBTA^+]_1$ that was actually used in the $NBTA^+/TBA^+$ mixture experiment (*i.e.* read from Figure 5.11 at $[NBTA^+] = 1.86 \times 10^{-3}$ mol/L) and $\Gamma_{NBTA,2}$ is the surface excess of $NBTA^+$ sorbed at the concentration $[NBTA^+]_2$ that would be needed given the desired a_{NBTA}. (There will be a different value of "f" for each a_{NBTA} at each ionic strength). (c) Plots of Γ_{NBTA} *versus* $[TBA^+]$, at each of the five ionic strengths, are made using the data obtained in the $NBTA^+/TBA^+$ mixture experiments (see Figure 5.17). (d) The correction terms are calculated from the expression:

$$\Delta\Gamma_{NBTA} = \Gamma_{NBTA}(f - 1) \qquad (C.2)$$

where Γ_{NBTA} is the surface excess of $NBTA^+$ which is read off the appropriate Γ_{NBTA} *versus* $[TBA^+]$ plot at the value of $[TBA^+]$ which corresponds to the desired a_{TBA}.

(iii) Finally, for each point of interest on the Γ_+ *versus* $[TBA^+]$ curve in Figure 5.13 the appropriate calculated value of $\Delta\Gamma_{NBTA}$ is added to Γ_+ in order to obtain the corrected value of Γ_+ corresponding to the specified combination of a_{TBA} and a_{NBTA}.

In this scheme for correcting Γ_+ it is assumed, in combining step (d) with step (b), that $NBTA^+$ and TBA^+ do not compete significantly with one another for space in the ODS bonded phase. Evidence that this is a good approximation comes from the results in Section 5.3.4.2 where it is shown that, at the surface excesses involved, the mutual effect of $NBTA^+$ and TBA^+ on one another arises mostly from their contribution to the potentials Ψ_0 and Ψ_I rather than from a competition for space. Furthermore the relative magnitude of the correction, $(\Delta\Gamma_{NBTA}/\Gamma_+)$, is generally small, being in no case greater than 18%.

Therefore small errors in the estimated values of $\Delta\Gamma_{NBTA}$ will cause negligible errors in Γ_+.